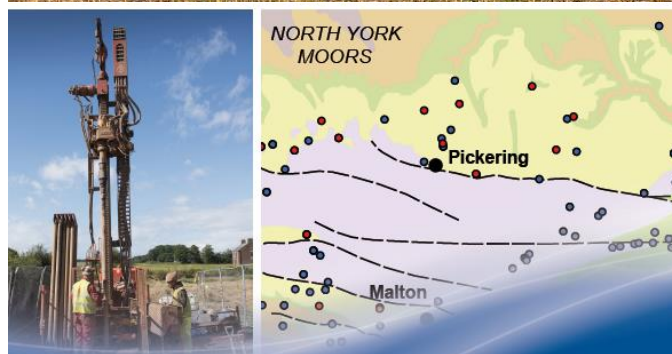**British Geological Survey**

Expert | Impartial | Innovative

Environmental Baseline Monitoring: Phase III Final Report (2017-2018)

Groundwater Programme

Open Report OR/18/026

www.bgs.ac.uk/valeofpickering

Environmental Baseline Monitoring: Phase III Final Report (2017-2018)

R.S. Ward (1), P.L. Smedley (1), G. Allen (2), B.J. Baptie (1), M.R. Cave (1), Z. Daraktchieva (3), R. Fisher (5), D. Hawthorn (1), D.G. Jones (1), A. Lewis (4), D. Lowry (5), R. Luckett (1), B.P. Marchant (1), R.M. Purvis (4) and S. Wilde (4)

With contributions from:

E.J. Bradley (3), M. Bowes (1), M. Coleman (5), A. Horleston (6), C.H. Howarth (3), R. Fisher (5), M. Lanoisellé (5), T.R. Lister (1), C.A. Miller (3), C.J. Milne (1), J. Pitt (2), M.O. Rivett (7), A.K.A.P. Barkwith (1) and J.M. Wasikiewicz (3)

(1): British Geological Survey
(2): University of Manchester
(3): Public Health England
(4): University of York (National Centres for Atmospheric Science)
(5): Royal Holloway University of London
(6): University of Bristol
(7): GroundH2O Plus

Keyworth, Nottingham   British Geological Survey   2018

BRITISH GEOLOGICAL SURVEY

The full range of our publications is available from BGS shops at Nottingham, Edinburgh, London and Cardiff (Welsh publications only) see contact details below or shop online at www.geologyshop.com

The London Information Office also maintains a reference collection of BGS publications, including maps, for consultation.

We publish an annual catalogue of our maps and other publications; this catalogue is available online or from any of the BGS shops.

The British Geological Survey carries out the geological survey of Great Britain and Northern Ireland (the latter as an agency service for the government of Northern Ireland), and of the surrounding continental shelf, as well as basic research projects. It also undertakes programmes of technical aid in geology in developing countries.

The British Geological Survey is a component body of UK Research and Innovation.

British Geological Survey offices

Environmental Science Centre, Keyworth, Nottingham NG12 5GG

Tel 0115 936 3100

BGS Central Enquiries Desk

Tel 0115 936 3143
email enquiries@bgs.ac.uk

BGS Sales

Tel 0115 936 3241
email sales@bgs.ac.uk

The Lyell Centre, Research Avenue South, Edinburgh EH14 4AP

Tel 0131 667 1000
email scotsales@bgs.ac.uk

Natural History Museum, Cromwell Road, London SW7 5BD

Tel 020 7589 4090
Tel 020 7942 5344/45   email bgslondon@bgs.ac.uk

Cardiff University, Main Building, Park Place, Cardiff CF10 3AT

Tel 029 2167 4280

Maclean Building, Crowmarsh Gifford, Wallingford OX10 8BB

Tel 01491 838800

Geological Survey of Northern Ireland, Department of Enterprise, Trade & Investment, Dundonald House, Upper Newtownards Road, Ballymiscaw, Belfast, BT4 3SB

Tel 01232 666595
www.bgs.ac.uk/gsni/

Natural Environment Research Council, Polaris House, North Star Avenue, Swindon SN2 1EU

Tel 01793 411500   Fax 01793 411501
www.nerc.ac.uk

UK Research and Innovation, Polaris House, Swindon SN2 1FL

Tel 01793 444000
www.ukri.org

Website www.bgs.ac.uk
Shop online at www.geologyshop.com

Acknowledgements

Contents

FIGURES

TABLES

Summary

High-quality environmental baseline monitoring data are being collected in areas around two proposed shale gas sites near Kirby Misperton, North Yorkshire and Little Plumpton Lancashire. Monitoring has now been on-going for over two years and has produced an internationally unique data set that will allow any future changes that arise from industrial activities at either or both shale gas sites to be detected and characterised, as well as providing a significant resource for future research. The monitoring includes: water quality, air quality, seismicity, ground motion, soil gas and radon in air.

This report presents the results of monitoring in the Vale of Pickering, within which the Kirby Misperton shale gas site (KM8) is located, for the period April 2017–March 2018. It also includes the results of atmospheric composition measurements made near the Little Plumpton (Preston New Road) site. Earlier results and other monitoring in Lancashire are reported elsewhere and can be accessed from the British Geological Survey's website[1].

As well as providing valuable insight into the importance of establishing robust information on the conditions before shale gas operations start, it also highlights the challenges in establishing effective monitoring and producing reliable results. For groundwater, this includes the importance of: developing and flushing newly installed boreholes; the spatial variation in water quality and; the selection of monitoring and measuring techniques. Having two years of data has allowed comparison between years. The preliminary analysis reported here has shown that sample populations were not significantly different between the two years. This is directly relevant to the duration of monitoring required by legislation, with the evidence supporting a baseline monitoring period of at least 12 months before any site operations start.

The seismic monitoring network installed for measuring background seismicity has operated successfully throughout the reporting period. All but one station show levels of data completeness over 90% which represents a high-quality dataset. There has been no significant change in recorded noise levels at any of the stations in the network. This combined with instrument performance means the network is capable of detecting seismic events with magnitudes of 0.5 ML or less around Kirby Misperton.

The monitoring has detected successfully a number of earthquakes around both the Vale of Pickering and the Fylde peninsula. However, all of these are at some distance from the shale gas sites. The Vale of Pickering network has also detected a number of other seismic events that have been attributed to quarry blasts. The magnitudes of these events range from 0.7 ML to 1.6 ML.

We have also developed and applied a new magnitude scale to correct for overestimation of magnitudes at small epicentral distances. This results in a significant reduction of the magnitudes of quarry blasts in the Vale of Pickering by over 0.5 magnitude units in some cases. The variance in the magnitude estimates is also slightly reduced. This issue is critical for correct estimation of the magnitudes of any earthquakes that might be induced by hydraulic fracturing.

The greenhouse gas monitoring continues to reinforce the conclusion that a baseline at one location is not applicable to other locations. However, the consistency of the baseline measurements (and baseline variability within each year) at both sites clearly suggests that 12 months of baseline monitoring is sufficient to establish a meaningful climatology to compare with analogous climatologies during the operational lifetime of the shale gas sites. Twelve months of data allow differentiation of local and long-range sources of greenhouse gases. At both sites, local (<10 km) sources dominate the contribution to statistically elevated concentration observations.

---

[1] www.bgs.ac.uk/research/groundwater/shaleGas/monitoring/home.html

We conclude that: the consistency of the baseline statistics year-to-year at each site separately, strongly validates the utility of these statistics in future comparative work; repeatability and similarity in both mean and statistical variability at each individual site across both annual periods suggests that 12 months of monitoring is sufficient to characterise the baseline at future sites usefully and; the large differences between the baselines at both sites, due to influence of local sources, demonstrate that careful thought and further work may be required to assess the spatial scale over which baselines can be usefully applicable.

The baseline distribution of air pollutants measured at the Lancashire site has been broadly similar in 2017 to previous years, but there have been substantial changes observed at Kirby Misperton. There was a noticeable increase in NO_x from Autumn 2017 as the site was prepared for hydraulic fracturing operations to begin. The high level of vehicle movements and operation of equipment during this period led to enhanced local NO_x emissions. The equipment was removed after operations were suspended and the NO_x concentrations returned to broadly the same concentrations seen previously during the baseline period. This highlights the importance of measuring the whole shale-gas operational cycle for air quality as the preparative operations can have a substantial impact on air pollution.

In the Vale of Pickering, 133 households volunteered to have detectors for measuring indoor radon concentrations. The results were consistent with the usual log-normal distribution for indoor radon and reflected the locations of the monitoring with respect to whether they were in Radon Affected Areas or not, i.e. radon levels above 200 Bq/m^3 were measured in homes in Malton which confirmed the PHE/BGS classification of this location as a Radon Affected Area.

Outdoor radon was also measured. There is no indication of elevated outdoor radon concentrations in either the Pickering or Malton Radon Affected Areas, or elsewhere. Results from an active monitor and passive detectors, placed on the Kirby Misperton well site were in good agreement with the average outdoor radon concentrations for the area around Kirby Misperton. The active monitoring showed significant short-term variations over time. However the annual average was consistent, whichever of the techniques was used.

Seasonal variability in baseline soil gas and flux values continues to be observed as well as shorter-term diurnal changes and event-driven variations, for example related to the passage of weather systems. The longer-time-series data and the preliminary geostatistical appraisal of selected data suggest that any emissions related to shale gas operations will be easiest to detect in the autumn when baseline biological activity is lower and the soil remains dry. Saturation of the ground in the winter months precludes free gas measurements.

A further component of the study is to characterise ground motion (subsidence and/or uplift) in the study areas using satellite data. The objective being to determine what the current situation is, so that any changes that might be caused by hydraulic fracturing, if it takes place, can be identified. The baseline conditions have previously been reported (Ward et al, 2018) and as now hydraulic fracturing has yet taken place, no further analysis has been carried out during this reporting period.

Other reports in this series:

Smedley, P.L., Ward, R.S., Allen, G., Baptie, B, Daraktchieva, Z., Jones, D.G., Jordan, C.J., Purvis, R.M. and Cigna, F. 2015. *Site selection strategy for environmental monitoring in connection with shale-gas exploration, Vale of Pickering, Yorkshire and Fylde, Lancashire.* BGS Report, OR/15/067.

Ward, R.S., Allen, G.; Baptie, B.J., Daraktchievea, Z., Jones, D.G., Jordan, C.J., Purvis, R.M., Smedley, P.L. 2016. *Environmental baseline monitoring - Vale of Pickering: Phase I - Final Report (2015/16).* BGS Report, OR/16/002.

Ward, R.S., Smedley, P.L., Allen, G., Baptie, B.J., Daraktchieva, Z., Horleston, A., Jones, D.G., Jordan, C.J., Lewis, A., Lowry, D., Purvis, R.M., Rivett, M.O. 2017. *Environmental Baseline Monitoring Project. Phase II, Final Report*. BGS Report, OR/17/049.

1 Introduction

This report details the results of activities carried out during the period April 2017 to March 2018 in compliance with the conditions set out in the grant awarded to the British Geological Survey (BGS) to support the jointly-funded "Science-based environmental baseline monitoring" project. Results are presented of monitoring/measurement and ongoing interpretation of environmental data that together contribute to characterisation of the baseline conditions in the Vale of Pickering, North Yorkshire and, for air quality, the Fylde in Lancashire. This database is gathered ahead of any shale-gas development in the area(s) of investigation. At the time of writing, ministerial approval is awaited for initiation of shale-gas exploration including hydraulic fracturing at the Kirby Misperton site (KM8), Vale of Pickering. For background to the monitoring programme, the reader is referred to previous reports detailed on the BGS website: www.bgs.ac.uk/research/groundwater/shaleGas/monitoring/home.html. The website also contains additional background information, summary data and near real-time data for air and water quality and for seismic monitoring.

It is widely recognised that there is a need for good environmental baseline data and establishment of effective monitoring protocols ahead of any shale-gas/oil development. This monitoring will enable future changes that may occur as a result of industrial activity to be identified and differentiated from other natural and man-made changes that are influencing the baseline. Continued monitoring will then enable deviations from the baseline, should they occur, to be identified and investigated independently to determine the possible cause(s)and significance to the environment and public health.

Credible and transparent monitoring is key to gaining public acceptance of the evidence base on the industry's environmental and public-health impact. With this remit, BGS and its partners in early 2015 initiated a coordinated programme of environmental monitoring in Lancashire that was then extended to the Vale of Pickering after BEIS awarded a grant to the British Geological Survey (BGS). The monitoring programme has continued, anticipating that the baseline condition may have transitioned to operational monitoring over the grant period. This did not happen and so the activities carried out during April 2017 to March 2018 have continued to augment the robust databases that are contributing to characterisation of the environmental baseline. The exception is air quality, where preparations for hydraulic fracturing (plant movement/installation) in Autumn 2017 resulted in changes in air quality. The monitoring has also enabled development of monitoring procedures and techniques, as well as building experience and expertise of wider application in the UK unconventional hydrocarbons context. The monitoring includes: water quality (groundwater and surface water), seismicity, soil gas, atmospheric composition (greenhouse gases and air quality) and radon in air; the interdisciplinary approach is internationally unique.

2 Water Quality

2.1 INTRODUCTION

Monitoring of both surface water and groundwater in the Vale of Pickering has continued over the grant period from April 2017 to March 2018. The water monitoring network (Smedley et al., 2015) was initially set up for sampling in September 2015 and augmented with sampling sites provided by new BGS purpose-drilled boreholes from March 2016. We have also been sampling Third Energy's boreholes at KM8 since April 2016 (Figure 1). New multi-level samplers for groundwater sampling, installed some 2 km east of KM8, have also been monitored frequently since May 2017. Two multi-level samplers have been installed: one with a depth range of 4–20 m (Quaternary extends to depth 7 m) and another with a range of 8–75 m (Kimmeridge Clay extends from 7 m to ca. 200 m). The sampler ranges overlap slightly but are designed to sample mainly from the Quaternary and mainly from the Kimmeridge Clay respectively.

The monitoring network aims to establish baseline chemical characteristics of groundwater and surface water, the former from a Superficial aquifer (Quaternary ± topmost Kimmeridge Clay; depicted as Upper Jurassic clays in Figure 1) and the Corallian Limestone aquifer; the latter from low-order streams dispersed across the Vale of Pickering. The monitoring infrastructure and sampling protocols have been described in detail by Ward et al. (2017). At the time of reporting (March 2018), monitoring of the initial network has been carried out 21 times (with additional samples at other times), the BGS boreholes 21 times, Third Energy Boreholes 20 times and the BGS multi-level samplers 7 times. Frequency of sampling of the network sites and BGS boreholes was initially monthly for 12 months, according to the requirements (for methane) of the 2015 Infrastructure Act. Thereafter, sampling reduced to quarterly, until the point where hydraulic fracturing looked likely to start (October 2017). Monthly sampling was conducted in each from October 2018–January 2018, with a final sampling for the reporting period in March 2018. Laboratory data are here reported mostly up to January 2018.

In addition, summary data from the five sondes, installed to collect real-time quality and physical-properties data in the BGS monitoring boreholes, are reported for the period up to March 2018.
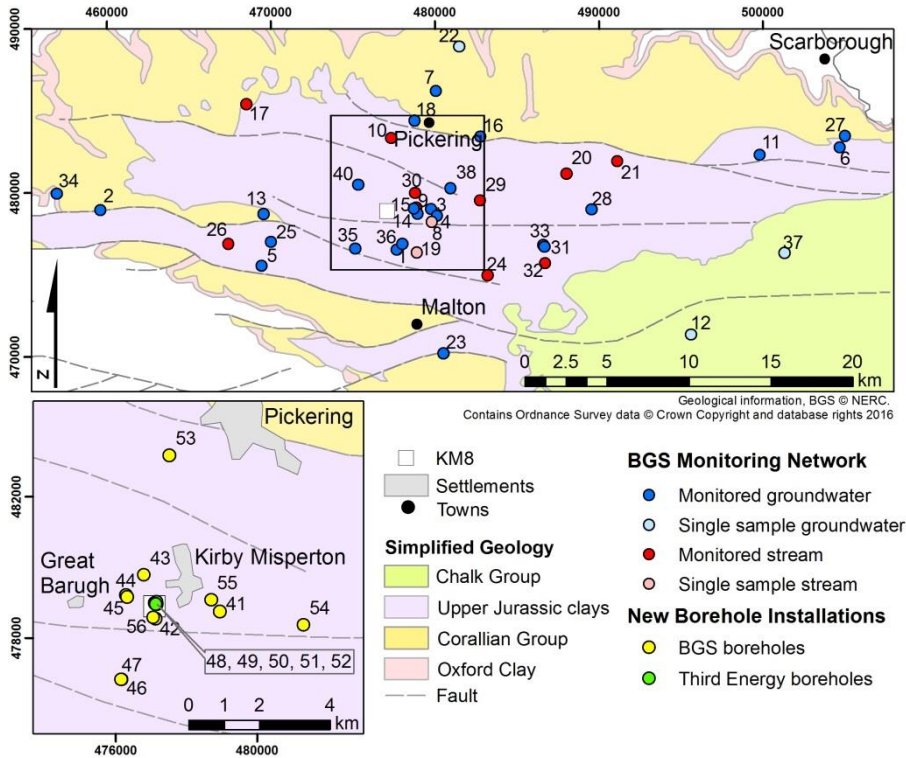
Figure 1. Water monitoring network for the Vale of Pickering (from Ward et al., 2017)

2

2.2 MONITORING NETWORK DATA

Data for the sites in the monitoring network from the Superficial aquifer are shown in Figure 2–Figure 4. Groundwater pH varies spatially from 7.0–8.8 with broad consistency in values for individual sites over time. Redox potential is dominantly between -200–+200 mV, indicating the mildly to strongly reducing conditions across the Superficial aquifer. Specific electrical conductance (SEC) shows a large range spatially from 500–3000 µS/cm but with a notable consistency at individual sites over time. Groundwater temperature commonly reflects a dampened response to ambient air temperature but with greatest response tending to be in the shallowest boreholes. In the boreholes with the most extreme temperature fluctuations, some artefact from the sampling procedure is possible, including changes in water level and flow induced by pumping.
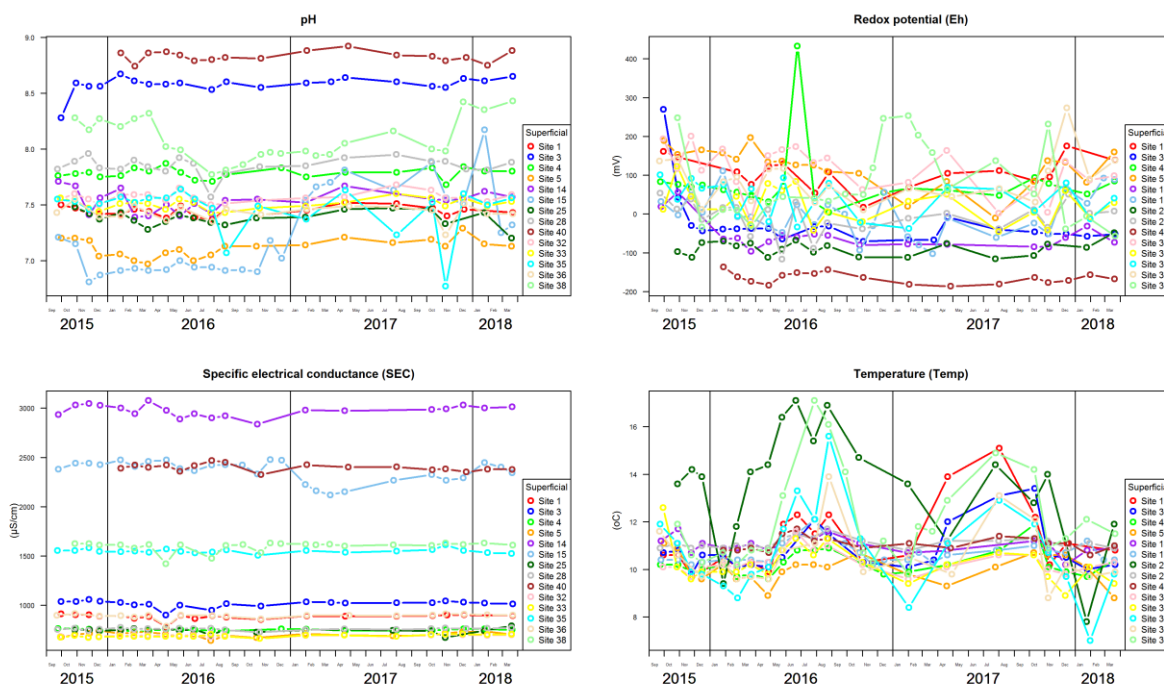
Figure 2. Physico-chemical parameters monitored in groundwater from the Superficial aquifer

Data for major and minor ions (Figure 3, Figure 4) also indicate a range of compositions in the groundwater from the Superficial aquifer but most have a notable consistency over time. The data confirm the Na-HCO$_3$ dominance of the water types in the aquifer, with reducing conditions supported by high concentrations of dissolved NH$_4$, Fe and Mn in many. By far the largest variability is seen in groundwater sampled from Site 15. This borehole is on a site with numerous nearby boreholes and was disused before being incorporated into the monitoring network. Changes over time could reflect changes induced by pumping of the borehole itself, effects of pumping neighbouring boreholes, or a combination of the two. The borehole was pumped more regularly during February–March 2016, November–December 2016 and January 2017 (pump rates unknown). The changes in water chemistry at Site 15 over time imply some stratification of water with depth, with draw-in from different horizons depending on local pumping rates and regime. These observations highlight the care required in designing/selecting and operating groundwater monitoring points. It also illustrates the need for multiple monitoring points to ensure that results are representative of groundwater quality in the area and that future changes that might arise from shale gas site operations can be detected.

Concentrations of dissolved CH$_4$ are repeatedly high in groundwater from many of the boreholes (Figure 4), several exceeding 1 mg/L and two showing groundwater with consistently greater than 5 mg/L and maxima to 50 mg/L, albeit with substantial variation between sampling visits. Data for dissolved CO$_2$ show a strong inverse relationship with CH$_4$ in Site 15 (Figure 4),

suggesting varying redox status over time, in further response to changing pumping rates and inflow horizons. In combination with observations for the major/minor this site is displaying very unusual behaviour, when compared to other nearby sites. This will be investigated further and the outcomes used to inform future site selection, operation and sampling guidance.
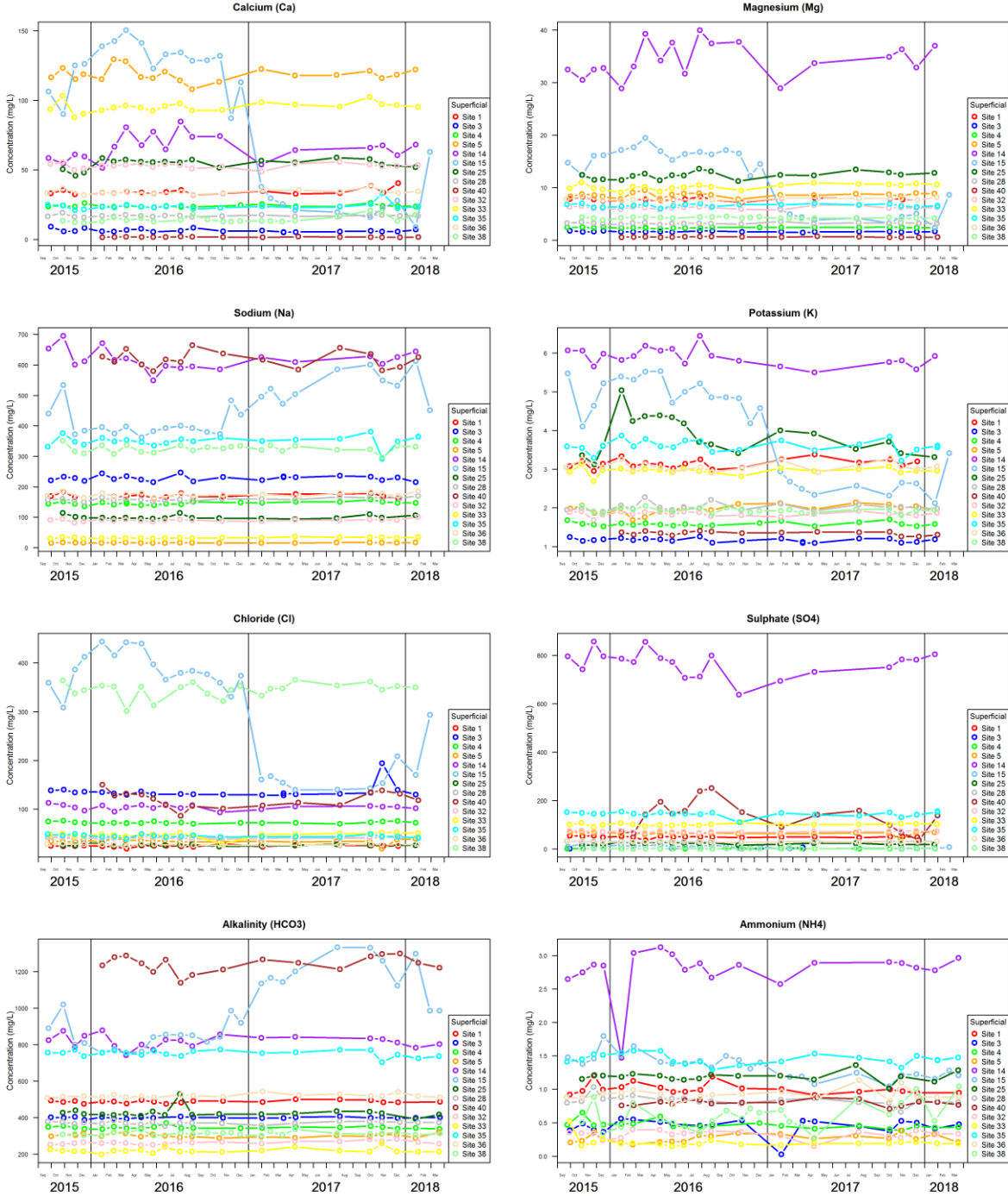
Figure 3. Data for selected major ions and ammonium in groundwater from the Superficial aquifer

Data for groundwater from the new BGS boreholes in the Superficial aquifer (Figure 5–Figure 7) show similar features to the pre-existing boreholes, with Na-HCO$_3$ dominance, pH varying from 6.5–8.5, Eh -100 to +200 mV, SEC 1000–3500 µS/cm, and temperature varying seasonally. The data show a greater temporal variability but still with broad consistency in chemical composition. This reflects the greater number of monitoring points and data now available.

Groundwater in the BGS boreholes is reducing with respect to Fe, Mn, NH_4 and CH_4, and CH_4 concentrations reach up to 40 mg/L in line with values observed in the Superficial aquifer groundwater monitoring network.
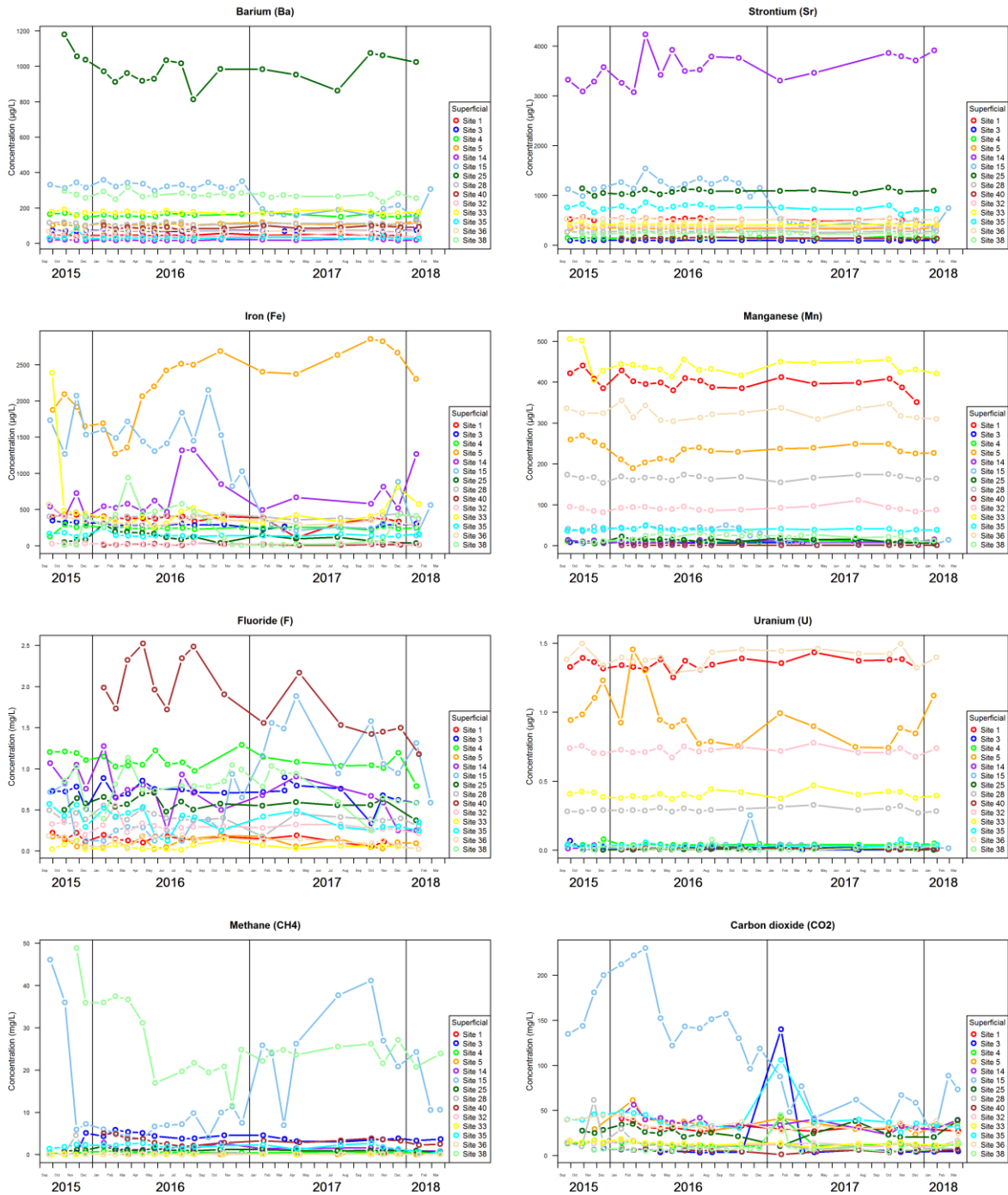
Figure 4. Data for selected minor ions and dissolved gases in groundwater from the Superficial aquifer
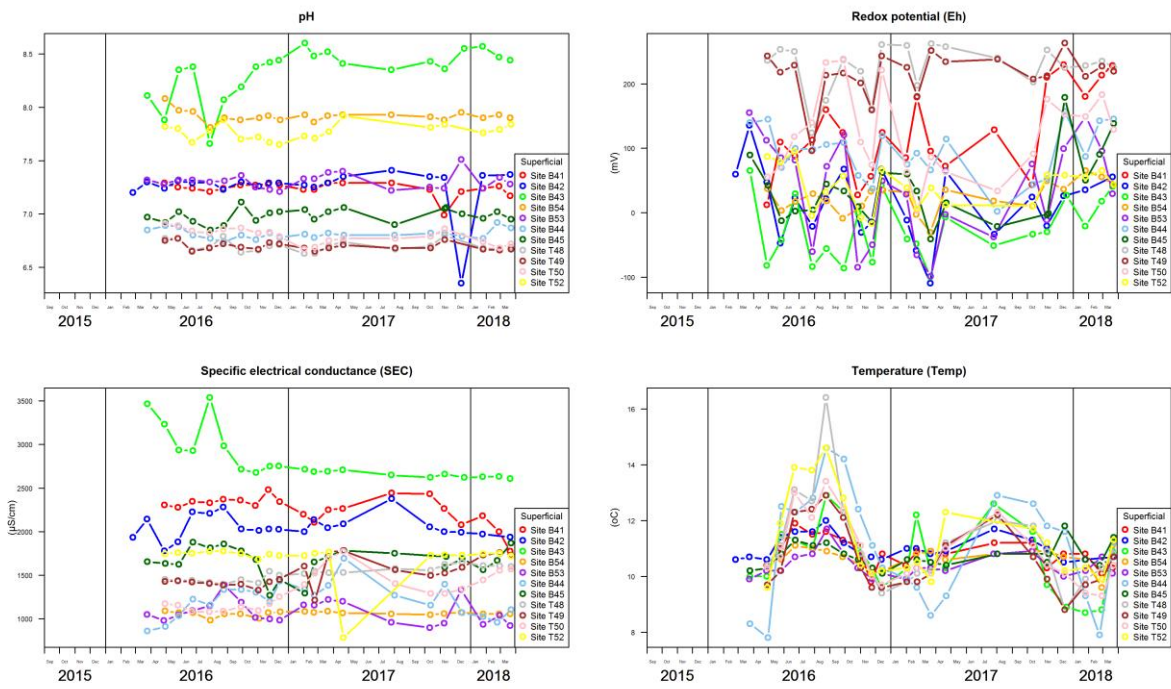
Figure 5. Physico-chemical parameters in groundwater from the BGS boreholes in the Superficial aquifer

Figure 6. Major ions and ammonium in groundwater from BGS boreholes in the Superficial aquifer
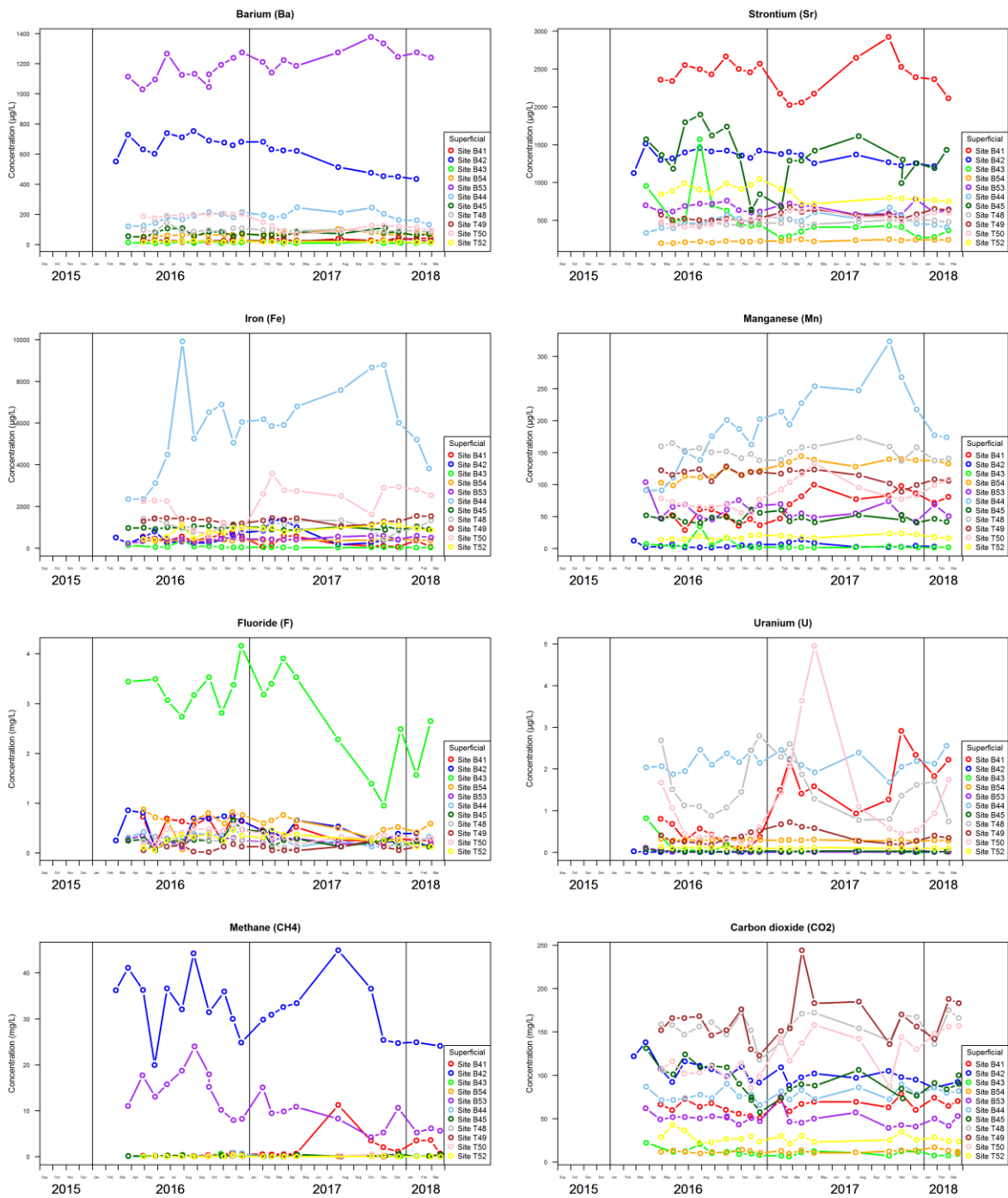
Figure 7. Minor ions and dissolved gases in groundwater from BGS boreholes in the Superficial aquifer

Groundwater in the Corallian Limestone aquifer from the margins of the Vale of Pickering (Figure 1) contrasts with that from the Superficial clay-dominated aquifer, being of Ca-HCO$_3$ composition, with a pH range of 7.2–8.0, Eh from 0–500 mV reflecting a large range of redox conditions from oxic to anoxic, and SEC values of 300–750 µS/cm (lower than in the Superficial aquifer). Temperature is mainly in the 10–11°C range, although temperatures for Sites 7 and 16 are more variable (Figure 8). Redox-sensitive minor-element concentrations reflect the range of redox conditions, with some showing high Fe and Mn concentrations and NH$_4$ usually <0.2 mg/L but reaching up to 0.5 mg/L (Figure 9, Figure 10). These very occasional peaks may reflect incomplete purging of boreholes before sampling. Trends in CH$_4$ concentration over time are spiky, but with much lower concentrations (and range) than observed in the Superficial aquifer (up to 0.7 mg/L in the Corallian; Figure 10). Compositions of many of the solutes in the

8

Corallian groundwater are relatively stable over time compared to observations from the new BGS boreholes in the Superficial aquifer.
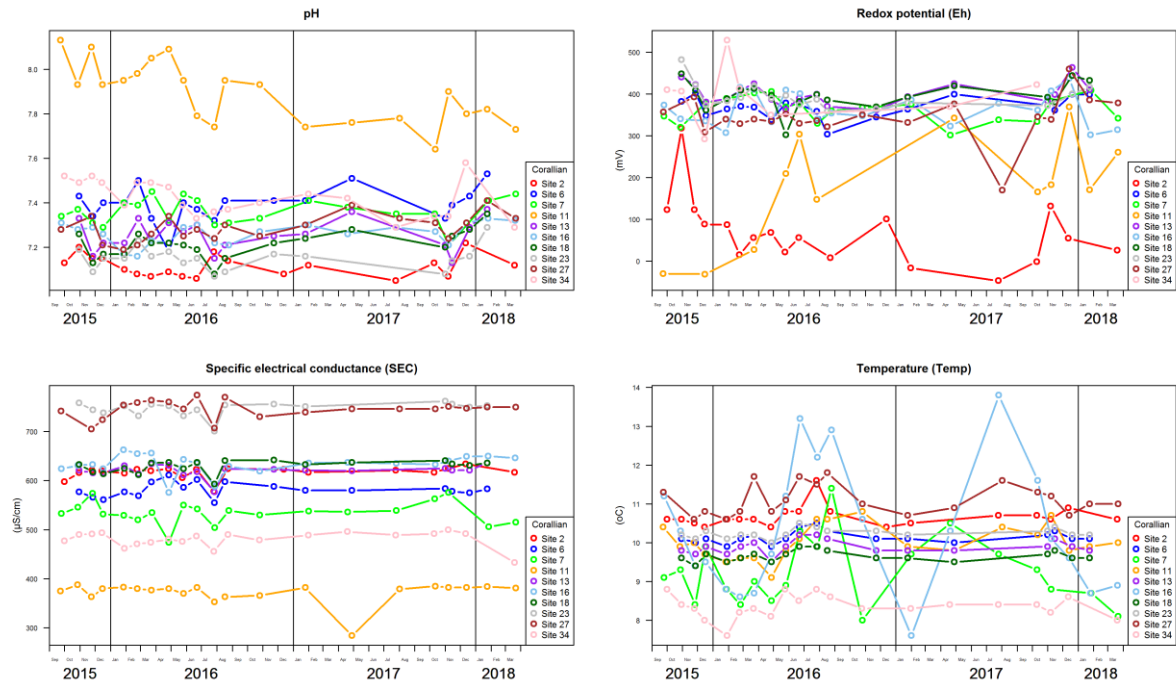
Figure 8. Variation in physico-chemical compositions of groundwater from the Corallian aquifer around the margins of the Vale of Pickering
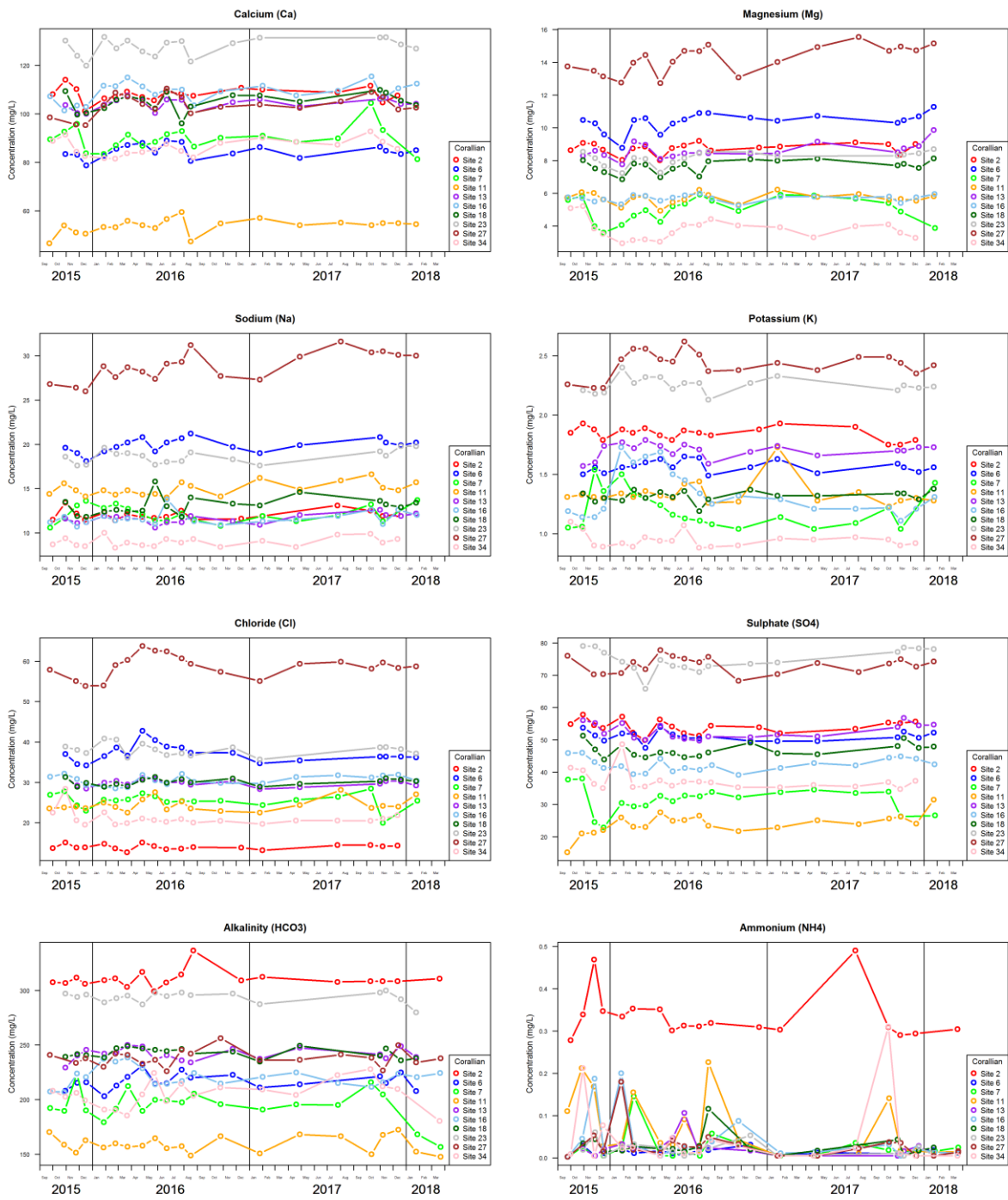
Figure 9. Variation in major-ion and NH4 concentrations in groundwater from the Corallian aquifer around the margins of the Vale of Pickering
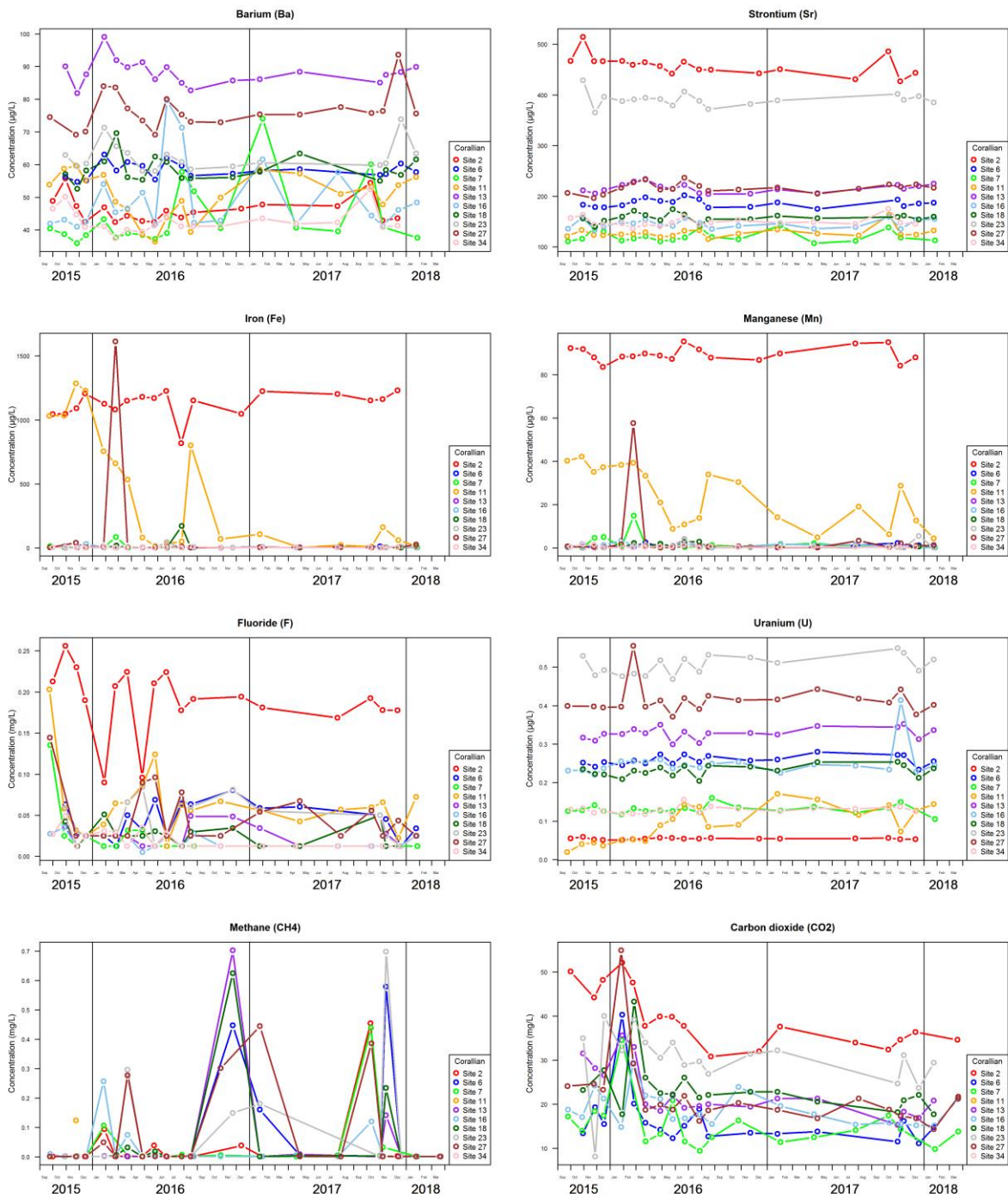
Figure 10. Variation in minor-ion and dissolved-gas concentrations in groundwater from the Corallian aquifer around the margins of the Vale of Pickering

In the monitored streams, pH values are typically 7.0–8.5 with SEC mainly between 200 and 800 µS/cm and occasionally up to 1400 µS/cm (Figure 11, Figure 8). The stream site with the highest SEC values (Site 29) also periodically has the highest concentrations of Na and Cl as well as the greatest variability in these ions over time (Figure 12). For other major ions and many of the minor ions, compositions are less variable. Occasional spikes in concentrations of Fe may be from material present as a fine colloidal suspension reflecting higher flow rates.

11
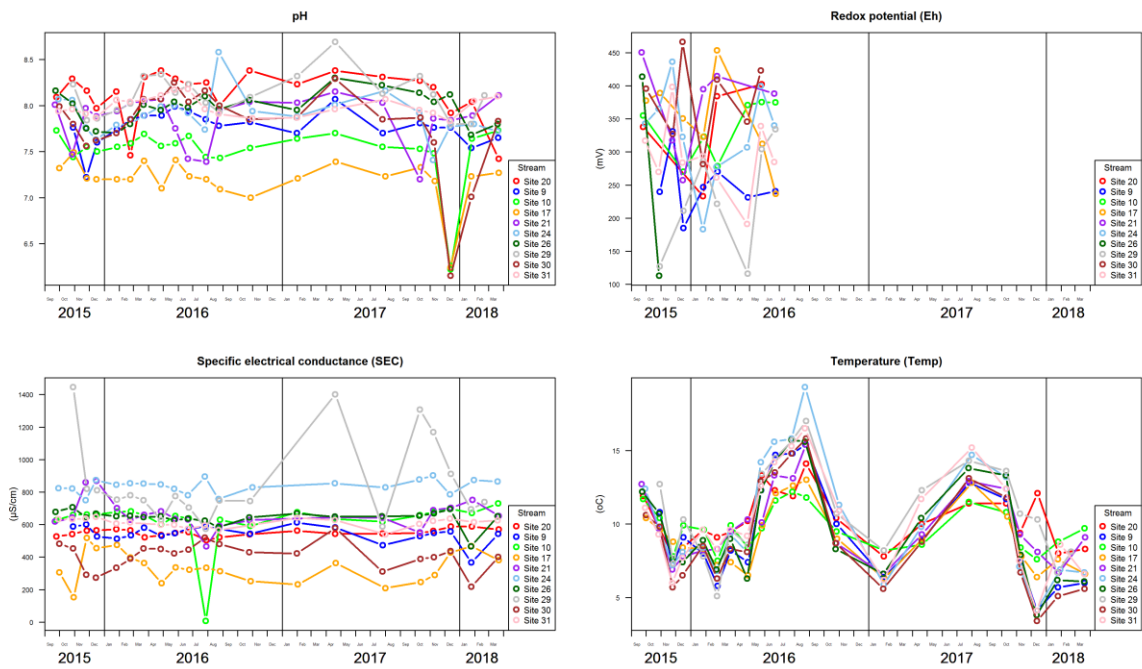
Figure 11. Variation in physico-chemical compositions of streams in the Vale of Pickering (Note: redox potential (Eh) only measured for a short period to cross-check electrode performance and confirm oxidising condition)
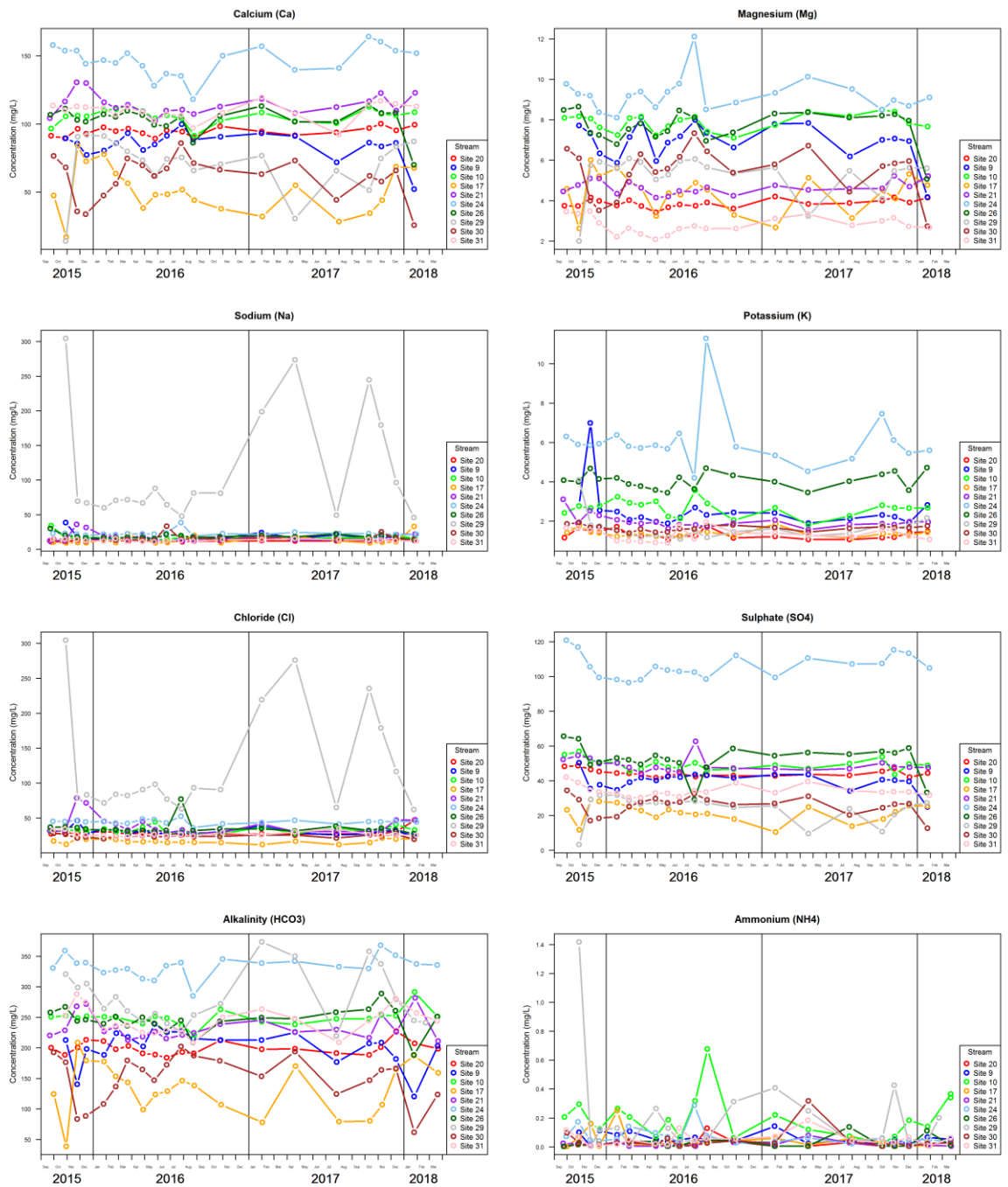
Figure 12. Variation in major-ion and NH₄ concentrations in streams from the Vale of Pickering
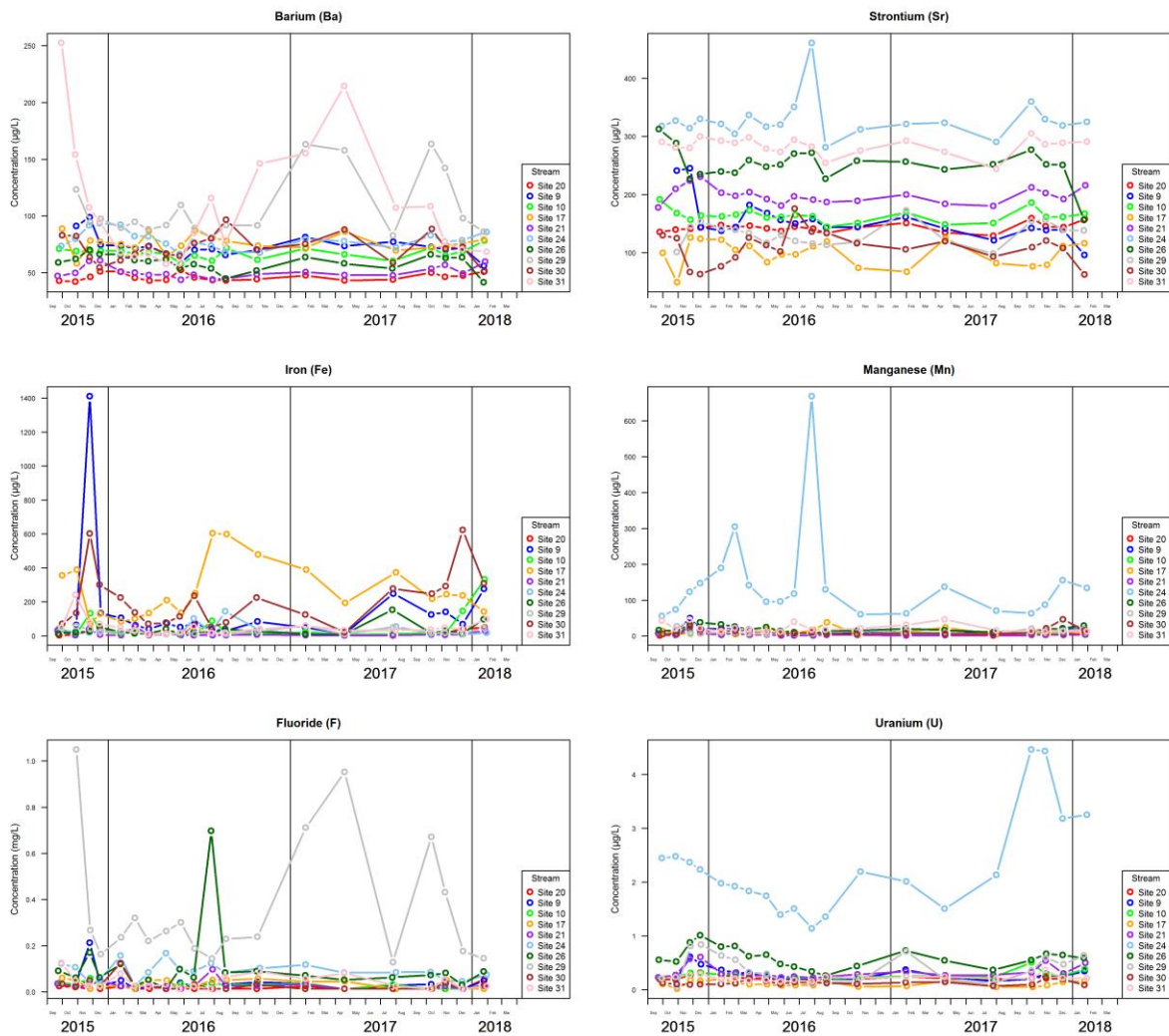
Figure 13. Variation in minor-ion concentrations in streamwater from the Vale of Pickering

2.3 MONITORING STATISTICS

Statistical summary data for selected important analytes in groundwater from the Superficial aquifer and for streams, each collected between September 2015 and January 2018, are provided as violin plots in Figure 14, Figure 15 and Figure 16. These display median, interquartile range and range in the box plots as well as probability density functions (the outer envelope showing relative likelihood of a concentration occurring). The data are divided into: all groundwater data for the period; data in a defined API ('area of potential impact', categorised as within an approximate 2 km radius around KM8), control area outside this zone; data for 2016; data for 2017. Data for streams also include all data for the period as well as 2016 and 2017 data. The divisions investigate baseline chemical distributions both spatially and temporally; the time differences have been included to investigate similarities and differences between the distributions for two separate 12-month intervals of monitoring. The summary distributions for groundwater are given in Table 1 and for streams in Table 2. Once a complete baseline dataset is available, the statistics will be re-run and a range of thresholds identified, above which any detection in groundwater will suggest that a deviation from baseline has occurred with an associated level of confidence.
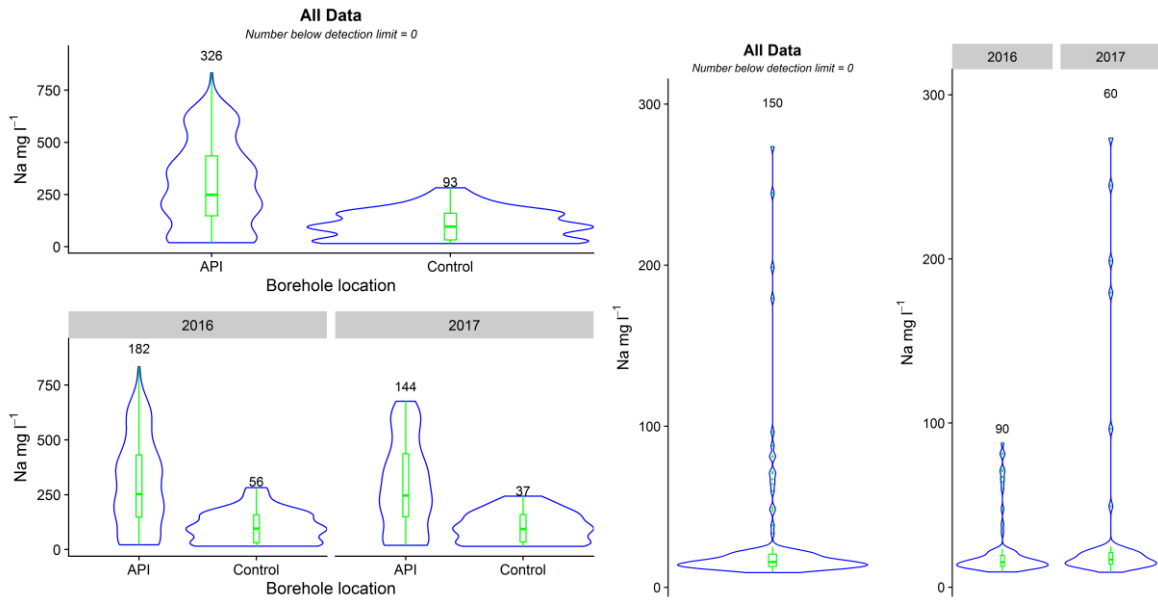
Figure 14. Violin plots (box plots with kernel density estimation) for Na in samples collected between September 2015 and January 2018 left: groundwater; right: streams. API: area of potential impact
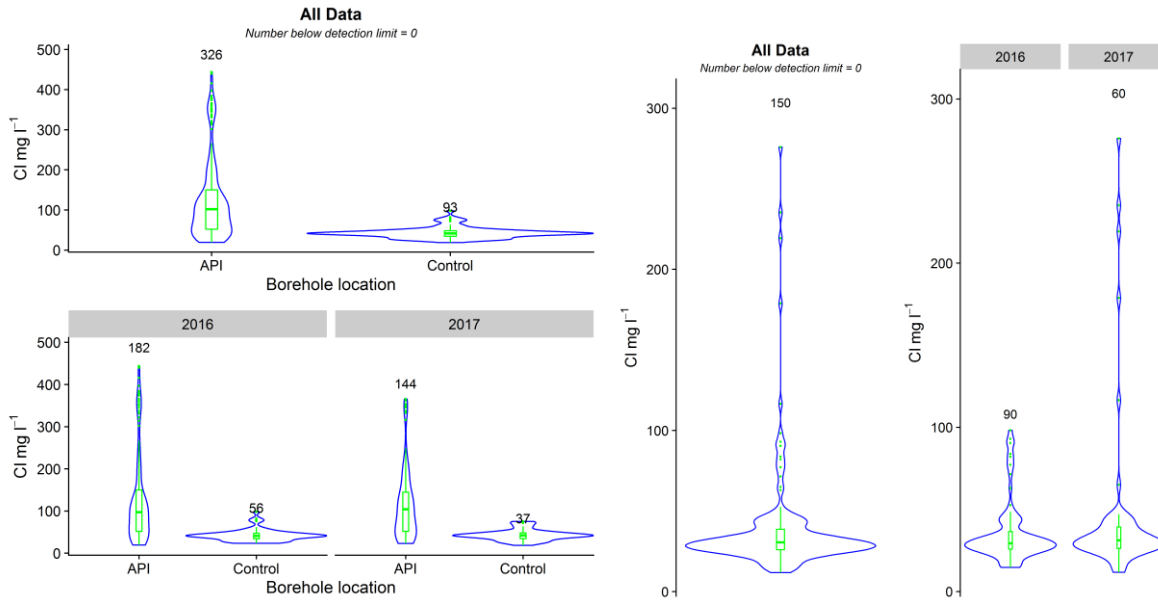
Figure 15. Data for Cl for samples collected between September 2015 and January 2018; left: groundwater; right: streams. API: area of potential impact
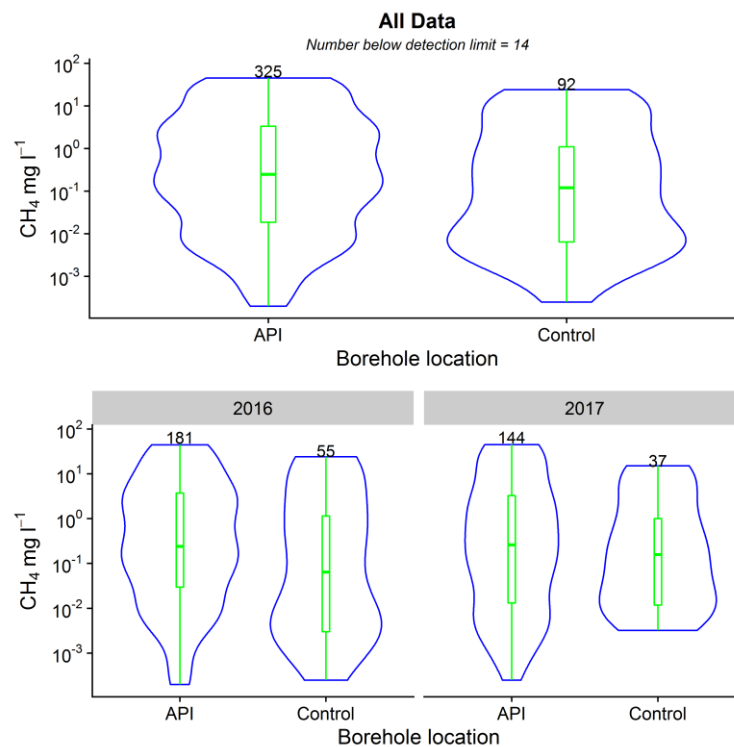
Figure 16. Data for CH$_4$ for groundwater samples collected between September 2015 and January 2018. API: area of potential impact

Table 1. Statistical summary of groundwater-chemistry data from the Superficial aquifer of the Vale of Pickering.

Notes: All data: samples collected September 2015 to January 2018; API: area of potential impact (ca. 2 km radius of KM8); control: Superficial aquifer beyond 2 km radius; data for 2016 and 2017 only are also given. Min, max: minimum and maximum observed values; sd: standard deviation; mad: median absolute deviation. Values for mean, standard deviation, range and skew are not computed for data with non-detects to avoid assumptions about their distributions

Analyte	Units	Group	n	mean	sd	median	mad	min	max	range	skew
Ca	mg/L	All data	493	80.4	86.8	45.7	46.1	1.40	370	369	1.57
Mg	mg/L	All data	493	9.91	7.95	7.85	5.44	0.50	40.0	39.5	1.71
Na	mg/L	All data	493	249	195	190	227	14.9	834	819	0.69
K	mg/L	All data	493	2.88	1.30	2.56	1.04	0.96	6.72	5.76	0.88
Cl	mg/L	All data	493	104	94.2	71.8	53.9	18.7	443	425	1.76
SO$_4$	mg/L	All data	493			63.0	91.5	<0.25	857		
NH$_4$	mg/L	All data	473	0.95	0.71	0.83	0.73	0.010	3.12	3.11	0.87
Ba	µg/L	All data	493	198	293	90.0	92.8	7.60	1380	1370	2.44
Sr	µg/L	All data	493	737	759	499	340	86.0	4230	4145	2.43
Li	µg/L	All data	493	35.7	27.3	30.0	26.7	3.00	120	117	0.73
CH$_4$	mg/L	All data	474			0.20	0.30	<0.001	48.8		
Ca	mg/L	API	375	84.8	97.4	34.0	36.2	1.40	370	369	1.34
Mg	mg/L	API	375	10.39	8.90	7.60	6.12	0.50	40.0	39.5	1.46
Na	mg/L	API	375	296	199	248	201	19.6	834	814	0.34
K	mg/L	API	375	3.01	1.41	2.87	1.47	0.96	6.72	5.76	0.65
Cl	mg/L	API	375	124	100	101	74.2	19.2	444	424	1.42
SO$_4$	mg/L	API	375			67.0	99.0	<0.25	857		
NH$_4$	mg/L	API	361	1.04	0.75	0.88	0.78	0.010	3.12	3.11	0.75
Ba	µg/L	API	375	127	146	70.9	69.1	7.60	753	745	2.29
Sr	µg/L	API	375	808	845	514	418	86.0	4230	4140	2.09
Li	µg/L	API	375	41.1	27.8	36.0	31.1	5.00	120	115	0.55
CH$_4$	mg/L	API	361			0.29	0.43	<0.001	48.8		
Ca	mg/L	Control	118	66.5	33.3	57.3	47.1	15.9	129.5	114	0.20
Mg	mg/L	Control	118	8.36	3.03	9.00	3.12	2.95	13.6	10.7	-0.45

Analyte	Units	Group	n	mean	sd	median	mad	min	max	range	skew
Na	mg/L	Control	118	99.3	67.7	94.3	92.7	14.9	283	268	0.49
K	mg/L	Control	118	2.47	0.72	2.14	0.39	1.69	5.04	3.35	1.29
Cl	mg/L	Control	118	42.3	12.8	41.4	9.41	18.7	97.7	79.0	1.39
SO$_4$	mg/L	Control	118			50.3	35.1	<0.25	108		
NH$_4$	mg/L	Control	112	0.69	0.47	0.46	0.45	0.15	1.76	1.61	0.43
Ba	µg/L	Control	118	427	472	124	97.0	36.2	1380	1340	0.81
Sr	µg/L	Control	118	512	274	384	119	252	1160	905	1.21
Li	µg/L	Control	118	18.4	16.4	10.0	8.90	3.00	50.4	47.4	0.74
CH$_4$	mg/L	Control	113			0.10	0.15	<0.01	24.0		
Ca	mg/L	2016	238	80.6	79.6	51.7	52.5	1.50	299	297	1.31
Mg	mg/L	2016	238	10.1	7.71	8.39	5.52	0.53	40.0	39.4	1.67
Na	mg/L	2016	238	252	197	199	234	15.2	834	818	0.68
K	mg/L	2016	238	2.97	1.35	2.69	1.22	0.96	6.44	5.48	0.71
Cl	mg/L	2016	238	110	101	72.3	53.7	19.2	443	424	1.69
SO$_4$	mg/L	2016	238	139	184	61.3	89.9	<0.25	855		
NH$_4$	mg/L	2016	218	1.00	0.74	0.84	0.78	0.01	3.12	3.11	0.78
Ba	µg/L	2016	238	212	298	94.2	103	8.00	1270	1270	2.14
Sr	µg/L	2016	238	780	777	505	381	87.6	4230	4140	2.25
Li	µg/L	2016	238	39.3	29.5	33.5	30.4	4.00	120	116	0.63
CH$_4$	mg/L	2016	236			0.20	0.30	<0.01	44.2		
Ca	mg/L	2017	181	88.1	101	40.4	40.3	1.40	370	369	1.44
Mg	mg/L	2017	181	9.84	8.18	7.70	5.43	0.50	40.0	39.5	1.69
Na	mg/L	2017	181	251	196	213	246	14.9	676	661	0.60
K	mg/L	2017	181	2.79	1.21	2.55	0.99	1.09	6.72	5.63	1.07
Cl	mg/L	2017	181	100	80.8	73.3	54.9	18.8	365	347	1.62
SO$_4$	mg/L	2017	181			66.8	97.2	<0.25	783		
NH$_4$	mg/L	2017	181	0.91	0.68	0.83	0.72	0.02	2.90	2.88	0.83
Ba	µg/L	2017	181	189	295	85.1	82.3	7.60	1380	1370	2.69
Sr	µg/L	2017	181	690	705	494	309	86.0	3860	3770	2.64
Li	µg/L	2017	181	33.5	23.7	32.0	28.2	3.00	87.0	84.0	0.55
CH$_4$	mg/L	2017	181			0.19	0.28	<0.01	44.9		

Table 2. Statistical summary data for stream samples collected September 2015 to January 2018

Analyte	Units	n	mean	sd	median	mad	min	max	range	Skew
Ca	mg/L	205	95.4	31.0	98.3	21.7	13.8	219	205	0.07
Mg	mg/L	205	5.89	2.22	5.63	2.56	1.99	16.8	14.8	0.66
Na	mg/L	205	25.8	37.7	15.9	5.34	9.10	304	295	5.20
K	mg/L	205	3.54	11.8	1.86	0.86	0.89	169	168	13.3
Cl	mg/L	205	42.1	42.6	30.8	8.19	11.8	340	329	4.64
SO$_4$	mg/L	205	45.3	23.7	43.1	15.8	3.23	121	118	1.45
NO$_3$	mg/L	205			26.9	17.8	<0.15	63.3		
NH$_4$	mg/L	195			0.04	0.04	<0.004	3.73		
Ba	µg/L	205	75.8	32.6	70.4	17.9	41.5	311	269	3.42
Sr	µg/L	205	189	79.8	161	67.7	48.6	467	418	0.71
Li	µg/L	205			3.00	1.48	<1	36.0		

For groundwater from the Superficial aquifer, data from the API and control areas (all dates) have been compared using the non-parametric Wilcoxon signed rank test of significance (Table 3). Statistically significant differences are observed for Na, Cl, SO$_4$, NH$_4$ and Li between the API and control data sets. Significant differences are not observed for Ca, Mg, K, Sr and CH$_4$. For several indicators of salinity therefore, baseline concentrations in the groundwater closer to KM8 (i.e. in the central part of the Vale of Pickering Superficial aquifer) are significantly higher than in the control area (median and maximum values respectively for Na in the API being 248 mg/L/834 mg/L, for control area being 94.3 mg/L/283 mg/L; median and maximum values respectively for Cl in the API being 101 mg/L/444 mg/L, for control area being 41.4 mg/L/97.7 mg/L). It is important to have established this distinction under baseline

conditions before considering regional variations in chemistry that may occur under post-baseline (operational) conditions.

Table 3. Wilcoxon signed rank test of significance for selected analytes from the API and control areas, Superficial aquifer (S: significant; NS: not significant, 99% confidence level)

Test	Ca	Mg	Na	K	Cl	SO_4	NH_4	Ba	Sr	Li	CH_4
Two-sided	NS	NS	S	NS	S	S	S	S	NS	S	NS
One-sided	NS	NS	S	NS	S	S	S	NS	NS	S	NS

Table 4 and Table 5 show the comparison of results for 2016 and 2017 data from groundwater in the Superficial aquifer and from streams respectively. For the analytes considered, no statistically significant differences (at 99% confidence level) were observed. From the sample sites and the analytes investigated, there is no indication that significant differences occurred in the water chemistry from the two 12-month intervals of sampling. This suggests that a 12-month period of monthly monitoring ahead of any site operations may be sufficient to characterise the baseline.

Table 4. Wilcoxon signed rank test of significance for selected analytes from groundwater in the Superficial aquifer, for the years 2016 and 2017 (NS: not significant, 99% confidence level)

Test	Ca	Mg	Na	K	Cl	SO_4	NH_4	Ba	Sr	Li	CH_4
Two-sided	NS	NS	NS	NS	NS	NS	NS	NS	NS	NS	NS
One-sided	NS	NS	NS	NS	NS	NS	NS	NS	NS	NS	NS

Table 5. Wilcoxon signed rank test of significance for selected analytes measured in streams, for the years 2016 and 2017 (NS: not significant, 99% confidence level)

Test	Ca	Mg	Na	K	Cl	SO_4	NH_4	Ba	Sr	Li	CH_4
Two-sided	NS	NS	NS	NS	NS	NS	NS	NS	NS	NS	NS
One-sided	NS	NS	NS	NS	NS	NS	NS	NS	NS	NS	NS

2.4 REAL-TIME GROUNDWATER DATA

Results for hourly monitoring of groundwater quantity and quality (pH, SEC, temperature and groundwater level) from five sondes over the last year of monitoring (March 2017 to March 2018) are displayed in Figure 17. Short-term spikes in the time series indicate intervals when sondes were removed for maintenance or calibration and have been retained in the record to indicate frequency of intervention. We experienced significant problems with EBM8 over the monitored interval despite attempts to rectify. For this sonde, some values for pH, SEC and temperature from September 2017 to March 2018 are spurious. The sonde has since been repaired. The pH electrode in EBM9 also gave spurious data in early September 2017, since repaired. Other fluctuations over the year are believed to be real variations; pH shows variations typically of 0.5 pH units (up to 1 pH unit), SEC of up to 1000 µS/cm and water level of <1 m (Figure 17). Temperature has been the most stable parameter, varying between 10–11°C for the boreholes observed. Hourly monitoring is continuing.
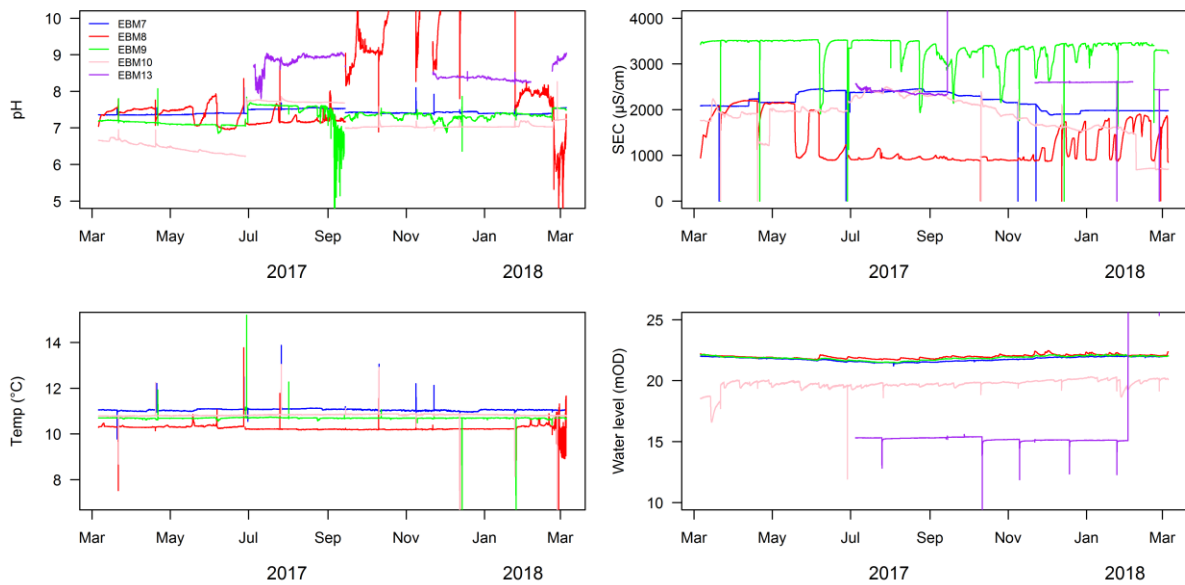
Figure 17. Real-time monitoring data (pH, SEC, temperature and groundwater level) from five sondes within boreholes in the BGS groundwater monitoring network
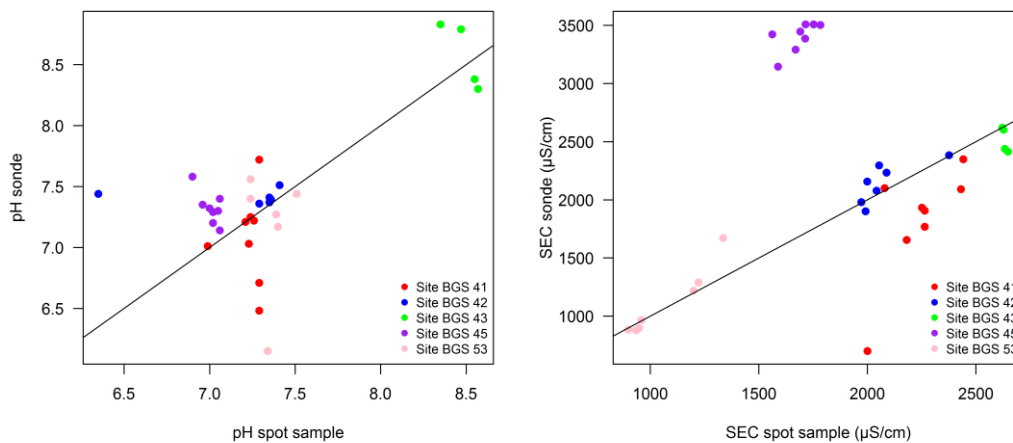
Figure 18. Comparison of pH and SEC values for groundwater collected during the monitoring rounds with values determined by sondes in real-time (1:1 lines also shown)

Figure 18 shows a comparison of pH and SEC values determined during spot sampling in the monitoring rounds from the BGS boreholes (Superficial aquifer) with values determined downhole from the installed sondes at the approximate time of sampling. Values are broadly comparable for each parameter and provide confidence in the data produced. Data for Site BGS 45 (EBM9) are an exception, with both pH and SEC showing systematically higher values in the sonde data than the monitoring samples, albeit only by 0.5 units for pH. Spot sampling involves recording of field readings while pumping until stable values are obtained. In the case of Site BGS 45, on most sampling occasions, SEC values started at around 3500 µS/cm but dropped during the course of monitoring (periods of up to 1 hour). This suggests that low-flow pumping of the borehole over time induces flow with a differing composition from different horizons in the aquifer sediments. This may point to salinity stratification with depth in this borehole, and will be investigated further using depth profiling. Measurements of SEC made during spot sampling are reported after stable readings have been obtained and therefore reflect the lower SEC values.

19

2.5   PROFILES FROM MULTI-LEVEL SAMPLERS

Profiles of groundwater from the two multi-level samplers indicate some notable consistency over the successive sampling rounds between June 2017 and February 2018 (Figure 19). Where depths of the two sampler systems overlap, differences at a given depth are likely in part due to spatial heterogeneity. However, systematic differences in redox status are also apparent, with more oxidising conditions indicated (higher SO_4, CO_2, lower CH_4) in the shallower CMT system and more strongly reducing conditions in the Waterloo MLS system.

Low SO_4 concentrations in the MLS groundwater, accompanied by a notable sulphide smell, are consistent with dissimilatory SO_4 reduction. The strongly reducing conditions in the MLS system are also indicated by high concentrations of CH_4 and C_2H_6 in the groundwater (up to 80 mg/L and 800 µg/L respectively). The simplest explanation is that these hydrocarbons are generated in situ within the Kimmeridge Clay, rather than deriving from extraneous sources.
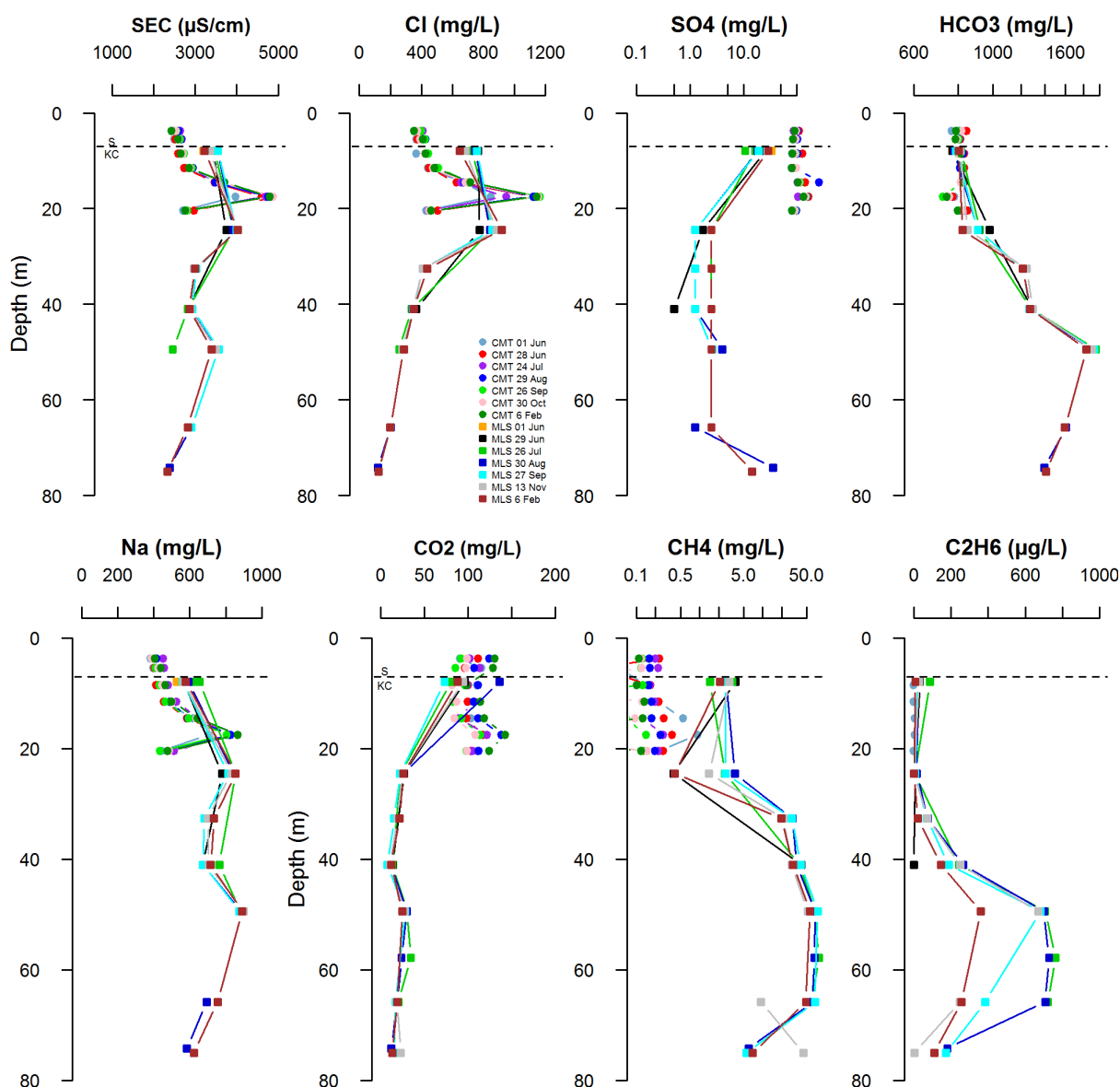
Figure 19. Profiles of selected analytes from a multi-level sampler array sited some 2 km east of KM8; CMT: Solinst Continuous Multichannel Tubing; MLS: Solinst Waterloo multi-level sampler; S: Superficial (Quaternary) aquifer; KC: Kimmeridge Clay

20

2.6 SUMMARY

A high-quality groundwater baseline dataset is being compiled. It is providing important insights into the importance of establishing robust information on the conditions before shale gas operations start and also some of the challenges in achieving it. Monthly/quarterly monitoring has shown the greatest consistency in chemical compositions occurring in groundwater from sites in the original monitoring network (both Superficial and Corallian aquifers). Streams also showed a broad consistency over time. Greatest variability was seen in groundwater from the BGS new borehole sites. This suggests that these boreholes, which have only been pumped under low-flow conditions due to the small water yields, may not yet have been flushed and reached a steady state. This is an important finding for future monitoring borehole design and operation.

Wilcoxon signed rank tests indicate that for groundwater from the Superficial aquifer, salinity (Na, Cl, SO_4) as well as NH_4 and Li differ significantly between the aquifer around KM8 (API) and that in the control area. This could be due to differences in e.g. Quaternary lithology (clay representation) and thickness, groundwater flow regimes and redox conditions between the central part of the vale and the more peripheral areas. Comparing statistical summary data for 2016 versus 2017 for groundwater from the Superficial aquifer and for streams showed that sample populations were not significantly different in either case. These statistical distributions will continue to be investigated as more baseline monitoring data become available.

Real-time sensor data for five boreholes monitored hourly over the year of reporting show greatest fluctuations for pH and SEC. Although some of the variability has been due to analytical artefacts, underlying fluctuations are likely due to real variability in flow and chemistry within the boreholes. Fluctuations have been greater in EBM8 and EBM9 than the other boreholes. EBM9 in particular is found to vary significantly in its discharge chemistry over a period of pumping. The real-time data are providing a further measure of baseline groundwater chemistry in the Vale of Pickering at times not sampled by the monitoring campaigns and will continue to provide evidence of any material change in water chemistry should the state of monitoring change from baseline to operational conditions.

Groundwater data from multi-level samplers installed into both Quaternary and Kimmeridge Clay formations provide much greater spatial resolution on groundwater chemical compositions. Groundwater from the Kimmeridge Clay is strongly reducing (sulphate-reducing and methanogenic). In-situ formation of methane (and ethane) within this shallow formation can explain the high concentrations of these gases observed in the shallow groundwater elsewhere in the Vale of Pickering.

2.7 REFERENCES

Smedley, P.L., Ward, R.S., Allen, G., Baptie, B, Daraktchieva, Z., Jones, D.G., Jordan, C.J., Purvis, R.M. and Cigna, F. 2015. Site selection strategy for environmental monitoring in connection with shale-gas exploration, Vale of Pickering, Yorkshire and Fylde, Lancashire. BGS Report, OR/15/067.

Ward, R.S., Smedley, P.L., Allen, G., Baptie, B.J., Daraktchieva, Z., Horleston, A., Jones, D.G., Jordan, C.J., Lewis, A., Lowry, D., Purvis, R.M., Rivett, M.O.. 2017. Environmental Baseline Monitoring Project. Phase II, final report. BGS Report OR/17/049.

3 Seismicity

3.1 BACKGROUND

The primary aim of the seismicity work package is to deploy a network of seismic sensors to monitor background seismic activity in the vicinity of proposed shale-gas exploration and production near Kirby Misperton, North Yorkshire and the Fylde, Lancashire. The data collected from these sensors will then allow characterisation of baseline levels of natural seismic activity in the region, and subsequently facilitate discrimination between any natural seismicity and induced seismicity related to shale-gas exploration and production. A further aim is to use the results of the monitoring to make recommendations for a suitable traffic-light system to mitigate earthquake risk.

The initial design requirement for the seismic monitoring network was reliable detection and location of earthquakes with magnitudes of 0.5 and above within a 20 km by 20 km area around the two proposed exploration sites at Preston New Road, Lancashire and KM8, Vale of Pickering.

3.2 NETWORK PERFORMANCE

The seismic monitoring network around KM8 consists of seven near-surface sensors (red squares in Figure 20) and four sensors installed in boreholes (orange squares in Figure 20). The latter comprise three downhole geophones and a downhole broadband seismometer.
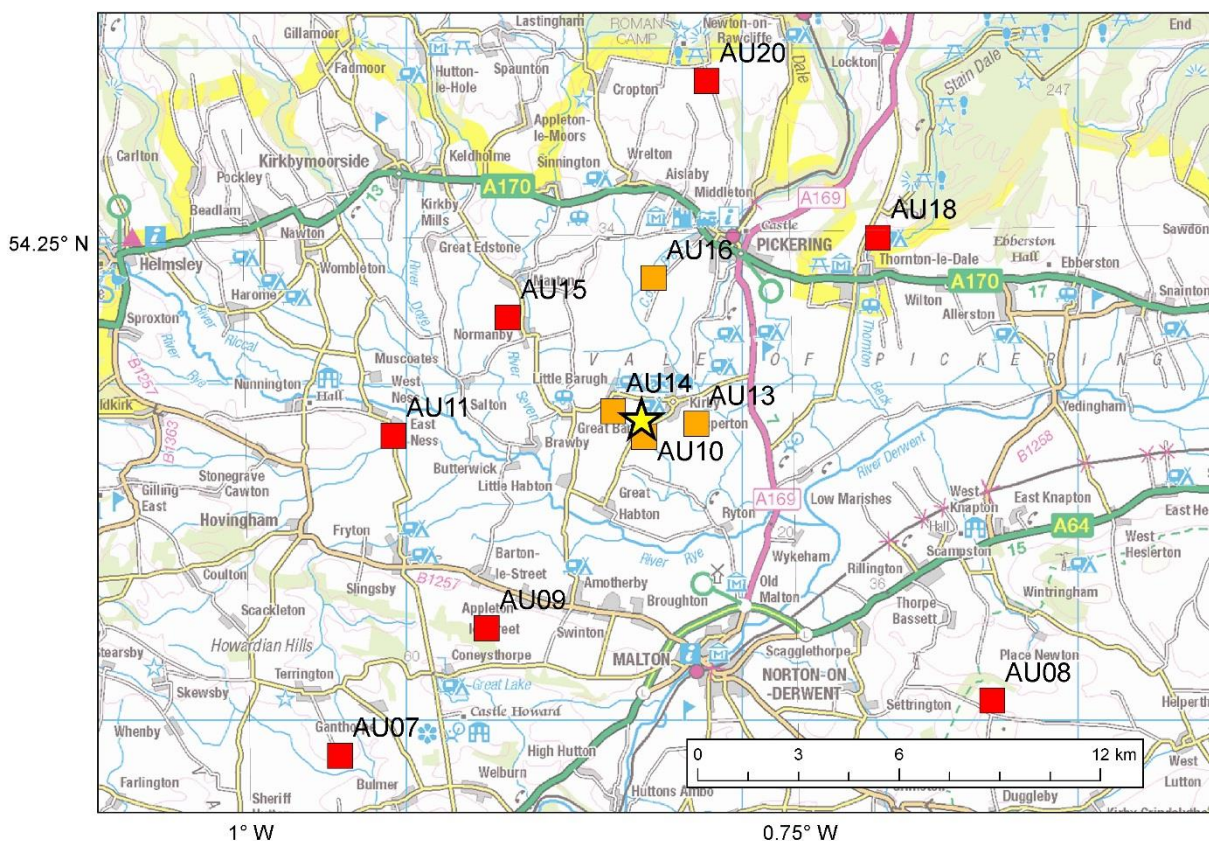
Figure 20. Ordnance Survey map of the Vale of Pickering. Red squares show the surface sensors and the orange squares show the locations of the borehole sensors. There are also surface sensors co-located with some of the borehole sensors. The yellow star shows the location of the drill site. © Crown Copyright and/or database right, 2018. Licence number 100021290 EUL
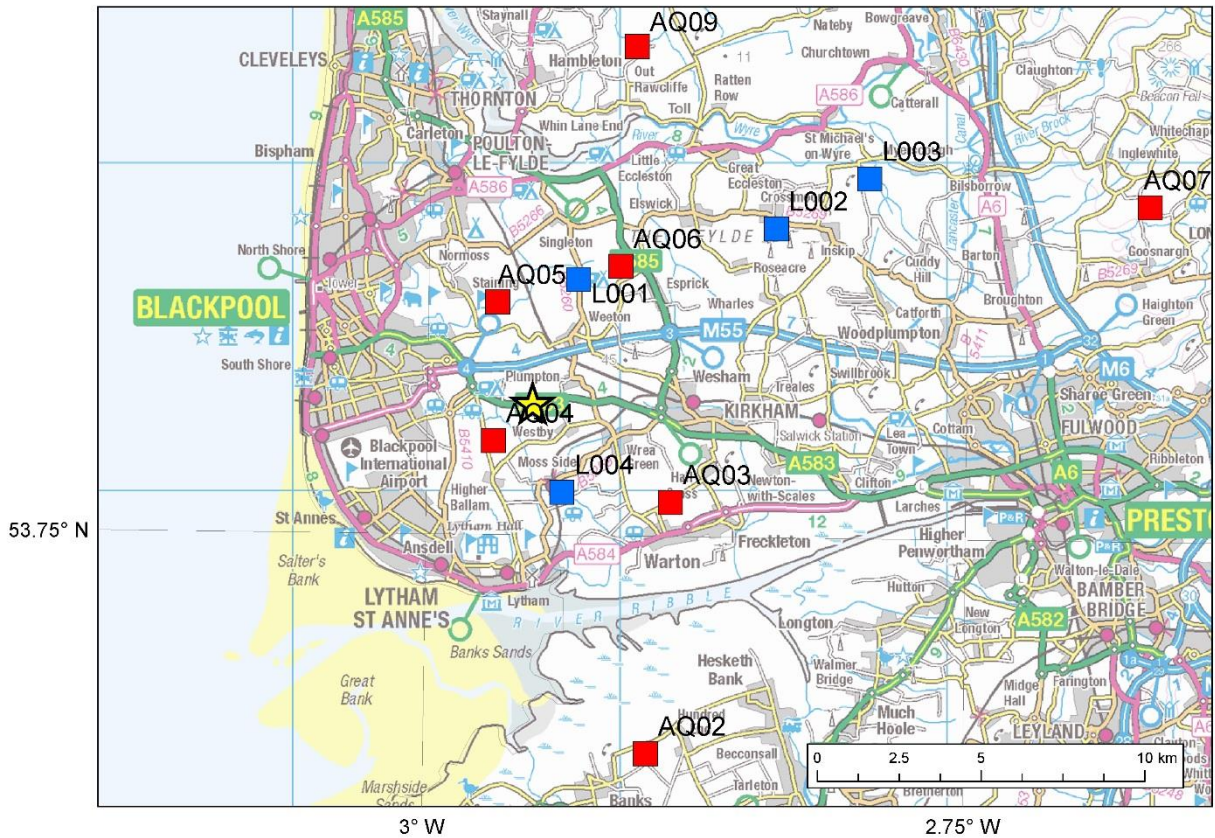
Figure 21. Ordnance Survey map of the Fylde peninsula. Red squares show BGS sensors and the blue squares show the locations of Liverpool University sensors. The star shows the location of the site of possible hydraulic fracturing at Preston New Road. © Crown Copyright and/or database right, 2018. Licence number 100021290 EUL

The borehole sensors are situated at a depth of approximately 30 m below the surface and are all close to KM8. Installing instruments in boreholes is intended to improve the signal-to-noise ratio of the recorded data and allow smaller events to be detected and located.

The seismic monitoring network across the Fylde consists of eight near-surface sensors (red squares in Figure 21). Stations AQ05 and AQ06 were installed in March 2018 and September 2017, respectively. We also receive real-time data from four stations (blue squares in Figure 21) installed and operated by Liverpool University. The latter were installed independently of this project and data acquisition from these is therefore not guaranteed.

Continuous data from all stations are transmitted in near real-time to the BGS office in Edinburgh, where the data are processed and archived[2]. The completeness of these data can be easily checked to gain an accurate picture of network performance.

The completeness levels for the seismometers in the two areas are shown in Figure 22. All stations in the Vale of Pickering show high levels of data completeness for the time period 1st April 2017 to 31st March 2018, with over 95% available from all stations except AU13, AU14 and AU16, which were 94%, 94% and 93% complete, respectively. This means that the detection capability of the network was good over this time period and loss of data was minimal. The level of data completeness is similar to the values obtained between 1st April 2016 and 31st March 2017 as reported in the Phase 2 report (Ward et al, 2017).

---

[2] BGS seismic data archive - http://www.earthquakes.bgs.ac.uk/archive/Archive_home.htm
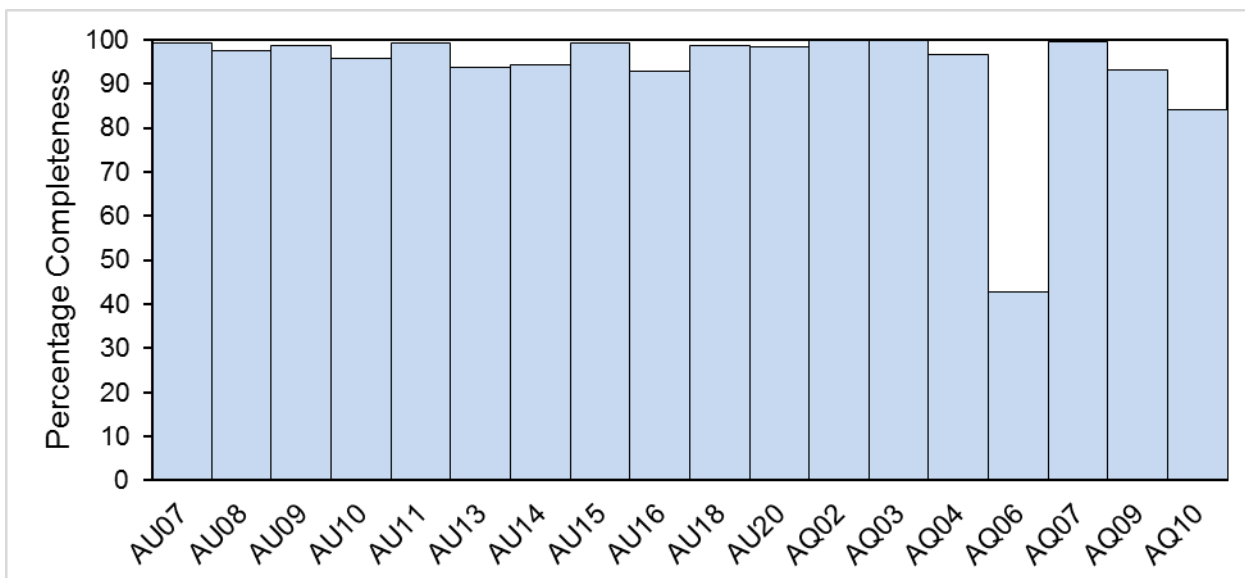
Figure 22. Data completeness for the period 1/4/2017 to 31 /3/2018 for monitoring stations in the Vale of Pickering (AU07-AU20) and Fylde (AQ02-AQ10). AQ05 is not included as it was not installed until the end of the reporting period. AQ06 was installed in September 2017

A value of over 95% is extremely good for data transmitted in near real-time using mobile phone networks and is better than many of the BGS permanent monitoring stations that use similar technology.

Data losses that have occurred result from failure of outstation hardware, data communication problems, or failure of central data processing. The data acquisition is able to recover from short breaks in communications links to outstations by re-requesting missing packets of data from local data buffers, but failure of outstation hardware requires intervention by local operators or maintenance visits.

3.3 STATION NOISE AND PERFORMANCE

We use power spectral density (PSD), calculated from one-hour segments of continuous data, to characterise noise levels at a range of frequencies or periods at each of the installed stations. A statistical analysis of the PSDs yields probability density functions (PDFs) of the noise power for each of the frequency bands at each station and component. Figure 23 compares the median noise levels calculated at three stations in the Vale of Pickering network (AU08, AU13 and AU14) in three different time periods, 1/4/2016 to 31/3/2017 (solid lines), 1/4/2017 to 31/06/2017 (dashed lines) and 1/7/2017 to 30/09/2017 (dotted lines). Although there are clear differences in noise levels at different stations, the noise levels at each station do not change significantly in different time periods, demonstrating that there is no significant degradation in station performance. This is also the case for the other stations in the network.

Comparing the median noise levels at the selected stations in the Vale of Pickering and the Fylde networks, Figure 24 shows that the Fylde stations are noisier than those in the Vale of Pickering and most other stations in the BGS permanent network. This is because the Fylde is more densely populated, with many sources of cultural noise.

24
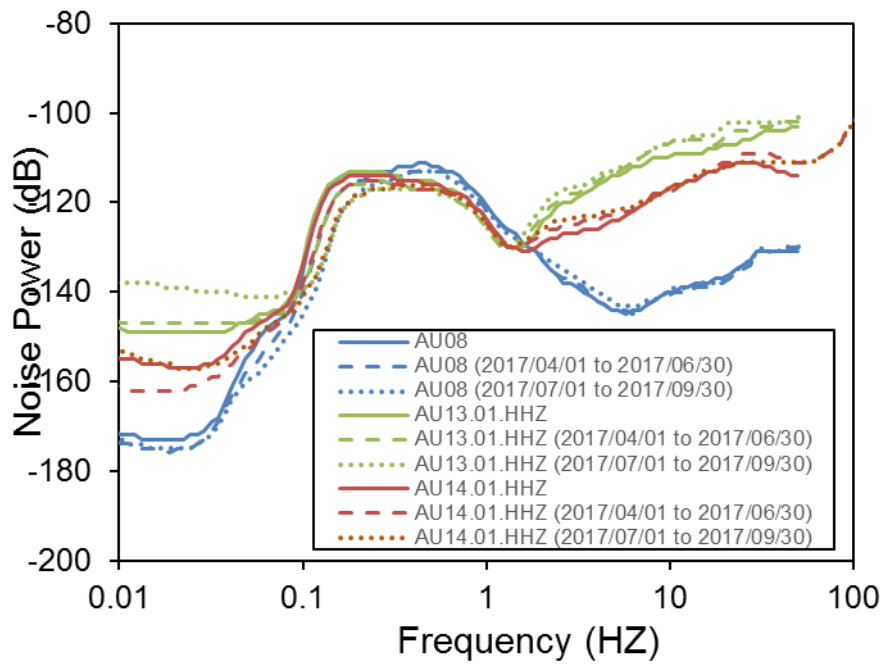
Figure 23. Median noise levels at all stations in the Vale of Pickering network as a function of frequency. AU10, AU13.00, AU14.00 and AU16 are borehole sensors. All other sensors are at the surface
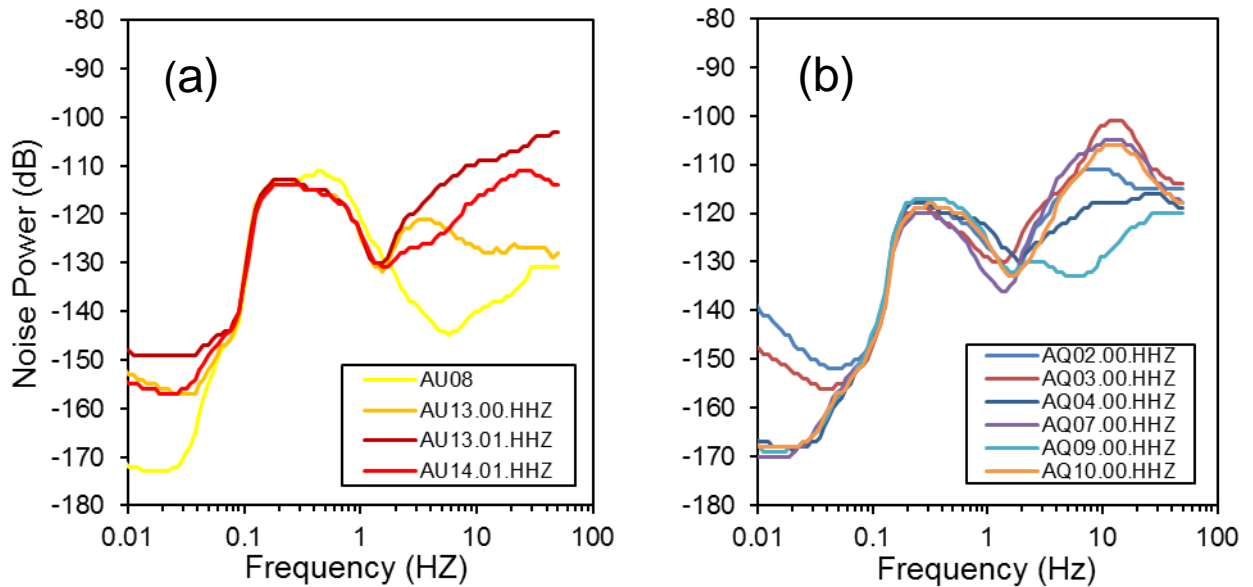
Figure 24. Comparison of the median noise levels at the selected stations in the (a) Vale of Pickering and (b) Fylde networks

We use the median, 5th and 95th percentiles of the observed noise at each station to test the variation in the detection capability of the Vale of Pickering network in different noise conditions. First, we calculate the RMS amplitudes of ground displacement in a constant relative bandwidth of one decade for each station. The resulting RMS amplitudes for each station and for each percentile are shown in Figure 25. As before, we find that noise can vary significantly even for stations that are close together, with variations in RMS displacement amplitudes exceeding two orders of magnitude even in quiet conditions. We also find significant variation between low (5th percentile) and high (95th percentile) noise conditions, which suggests that detection capability will vary strongly with time.

We model the detection capability of the network in different noise conditions as follows:

1. Divide the region into a regular grid of points.
2. For each grid point calculate the distances between the grid point and each station.
3. For each station calculate ground displacement amplitudes for different magnitudes.
4. Find the smallest magnitude value for which the signal amplitude exceeds the noise amplitude by a factor of three at five or more stations.
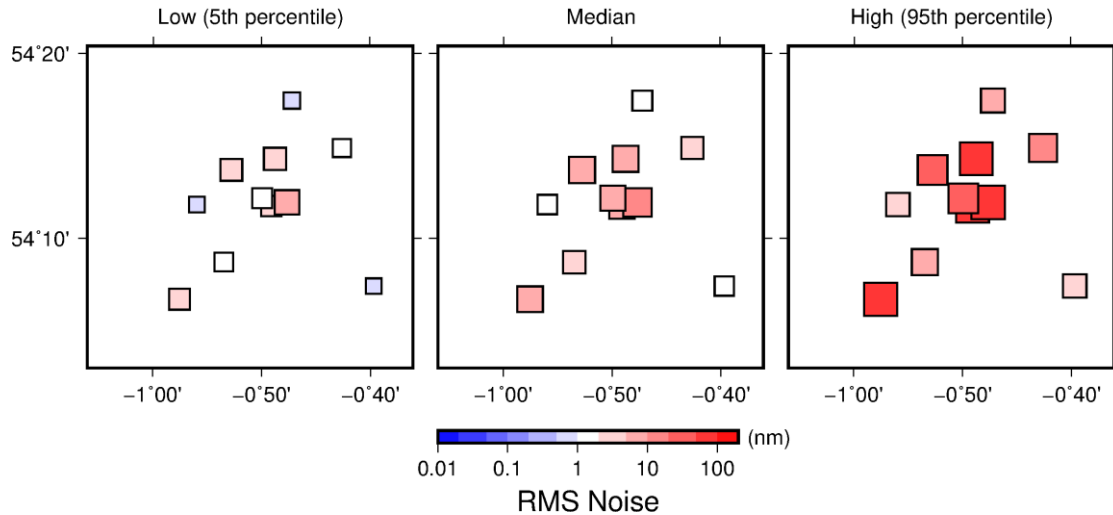
Figure 25. Observed RMS noise levels determined from power spectral density estimates for each day over the time period 01/04/2016 to 31/03/2017

Figure 26 shows the variation in the magnitude of earthquakes that would be detected by the network in different noise conditions. In the quietest conditions (Figure 26b), the network is capable of detecting events with magnitudes as low as -0.5 ML, however, this is only the case 5% of the time. The lowest detectable magnitude increases to just under 0.0 ML in median noise conditions (Figure 26c). For the high noise model (Figure 26d), the network is still able to detect event with a magnitude of 0.5 ML close to the centre of the network.
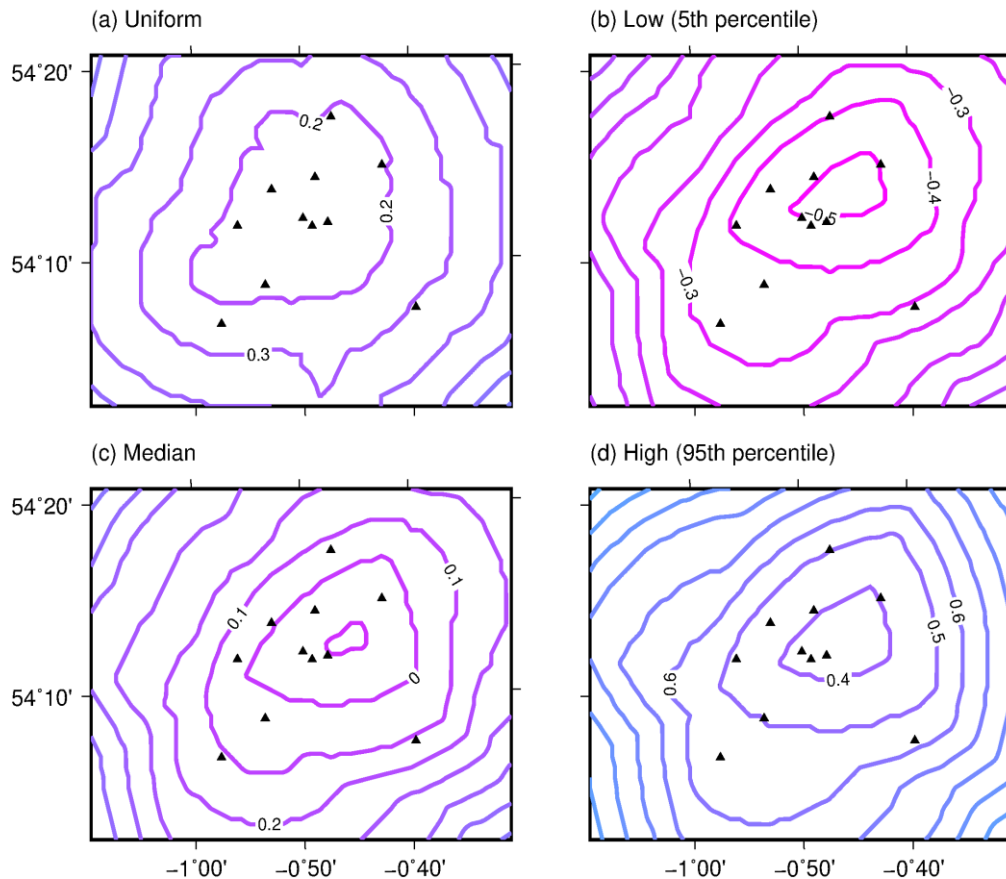
Figure 26. Modelled detection capability using observed noise levels for each station in (a) uniform, (b) low, (c) median and (d) high noise conditions. A signal in excess of three times the noise level is required at five or more stations for an earthquake to be detected

3.4 DATA PROCESSING AND ANALYSIS

Continuous data from all installed stations are transmitted in real-time to the BGS office in Edinburgh and have been incorporated in the data acquisition and processing work-flows used for the permanent BGS UK network of real-time seismic stations. A simple detection algorithm is applied to the data from the Vale of Pickering and the Fylde, including data from permanent BGS monitoring stations, to detect possible events. An experienced analyst has reviewed all detections.

Earthquake activity from the BGS earthquake catalogue in 100 km squares centred on the Kirby Misperton and Preston New Road sites is shown in

Figure 27. Yellow circles show earthquakes in the time period from 1st April 2017 to 31st March 2018. Apart from a magnitude 0.7 ML earthquake close to Kirby Misperton on 22nd September 2015 at the very start of the monitoring project, no other earthquakes have been detected in the immediate locality of the Vale of Pickering, however, a number of other natural earthquakes from the surrounding region, along with quarry blasts have been detected. The closest earthquake to the network was a magnitude 0.7 ML event near Wold Newton, North Yorkshire, on 3rd November 2017, 27 km east of Kirby Misperton. A magnitude 1.9 ML earthquake was detected near Saxton, North Yorkshire, on 16th May 2017. Three earthquakes with magnitudes of 1.3 and 0.7 ML were detected near Hinderwell, North Yorkshire, on 20th March 2017, 35 km north.

A number of earthquakes were detected in the Fylde peninsula in the period from 1st March 2017 to 31st March 2018. The closest of these to Preston New Road was a 1.7ML earthquake in the Irish Sea on 10th August 2017, approximately 30 km northwest of the Preston New Road site. All the other detected earthquakes were at greater distances either to the north or south.
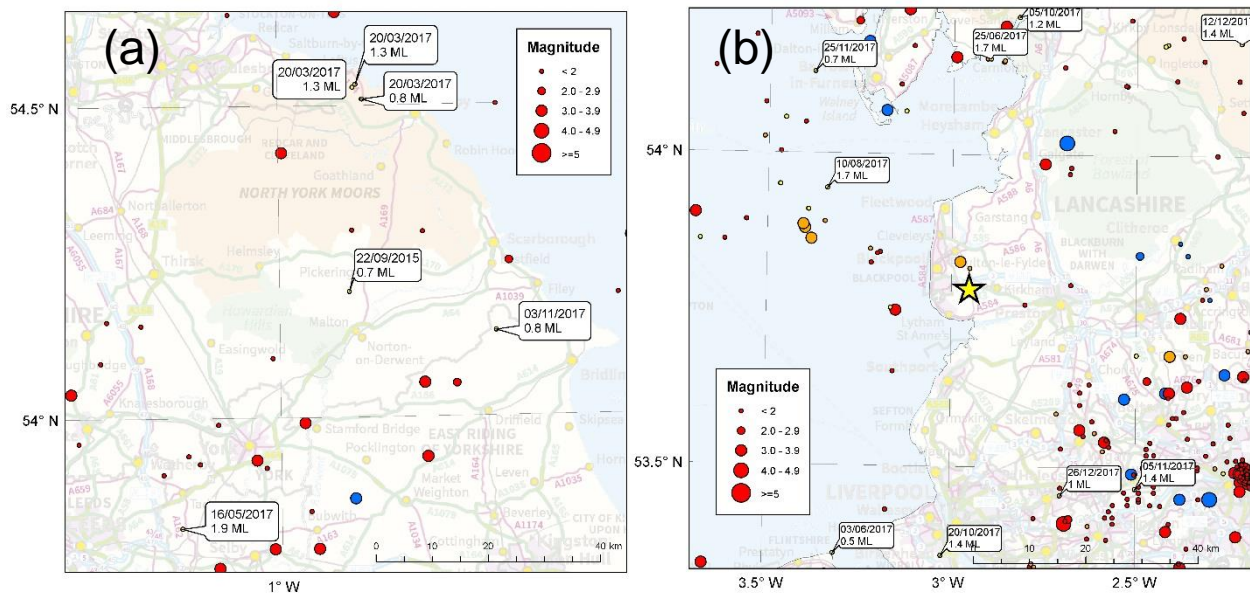
Figure 27. Earthquake activity in 100 km squares centred on Kirby Misperton (a) and Preston New Road (b). Earthquakes in the time period from 1/4/2017 to 31/3/2018 are marked by yellow circles. Circles are scaled by magnitude. © Crown Copyright and/or database right, 2018. Licence number 100021290 EUL
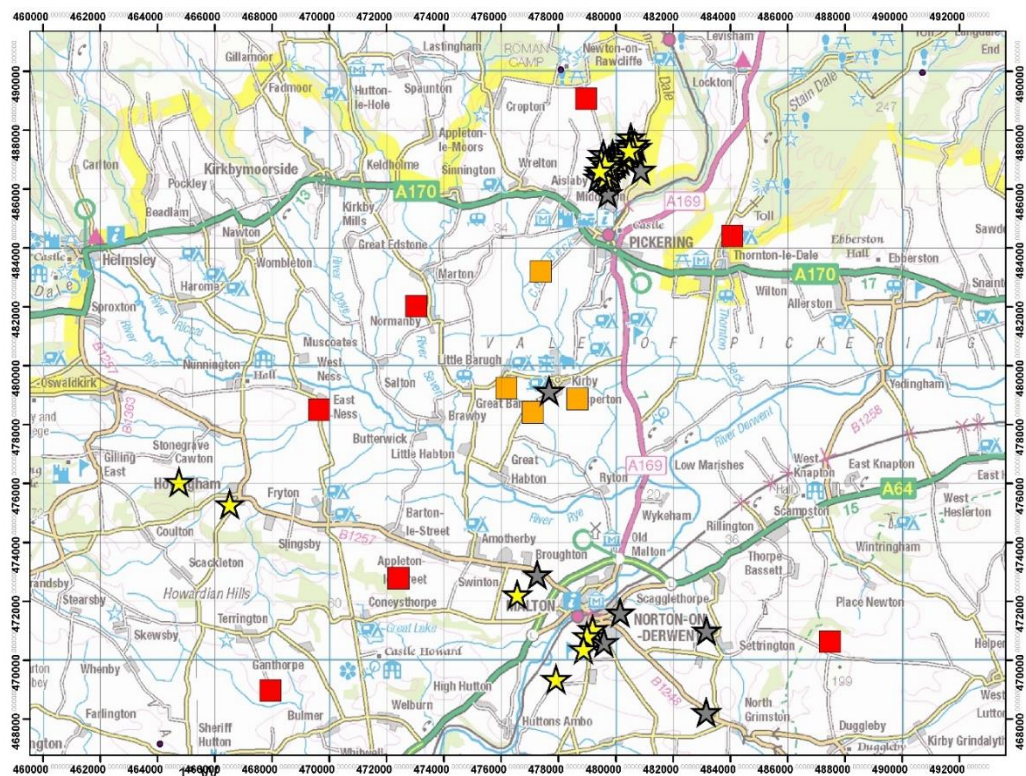
Figure 28. Seismic events in the Vale of Pickering region. Yellow stars show events detected between 1/4/2017 and 31/3/2018. Nearly all detected events are of a suspected explosive origin, i.e. quarry blasts. © Crown Copyright and/or database right, 2018. Licence number 100021290 EUL

A number of other events were detected in the Vale of Pickering. These are shown in Figure 28. The proximity of the calculated locations to quarries where blasting is known to take place, along with the recorded waveforms that are characteristic of a shallow source, suggests that all

these events are of an explosive origin, i.e. quarry blasts. Twenty-one events in the time period from 1ˢᵗ April 2017 to 31ˢᵗ March 2018 were located just north of Pickering in close proximity to the Newbridge quarry, where a number of other quarry blasts have been detected in the past two years. The magnitudes of these events range from 0.7 ML to 1.6 ML. Four other blasts were detected close to a quarry south of Malton and two others were located west of Malton, near Hovingham.

All of the suspected blasts occurred during the working week and during the day. Figure 29 shows histograms of the hour, (a), and the day, (b), of occurrence for all seismic events detected in the Vale of Pickering since the start of the project in 2015. Forty-one of the forty-eight detected events occurred between 10am and 2pm, with only two events occurring during the night: the magnitude 0.7 ML earthquake close to Kirby Misperton on 22ⁿᵈ September 2015; and the magnitude 0.7 ML event near Wold Newton, North Yorkshire, on 3ʳᵈ November 2017.

Similarly, all of the detected events occurred during the working week, with most of the events occurring on Tuesday, Wednesday and Thursday. The strong clustering of the events around the middle of the day provides further evidence of the man-made origin of these events, since we might expect natural seismicity to be more evenly distributed throughout the day.
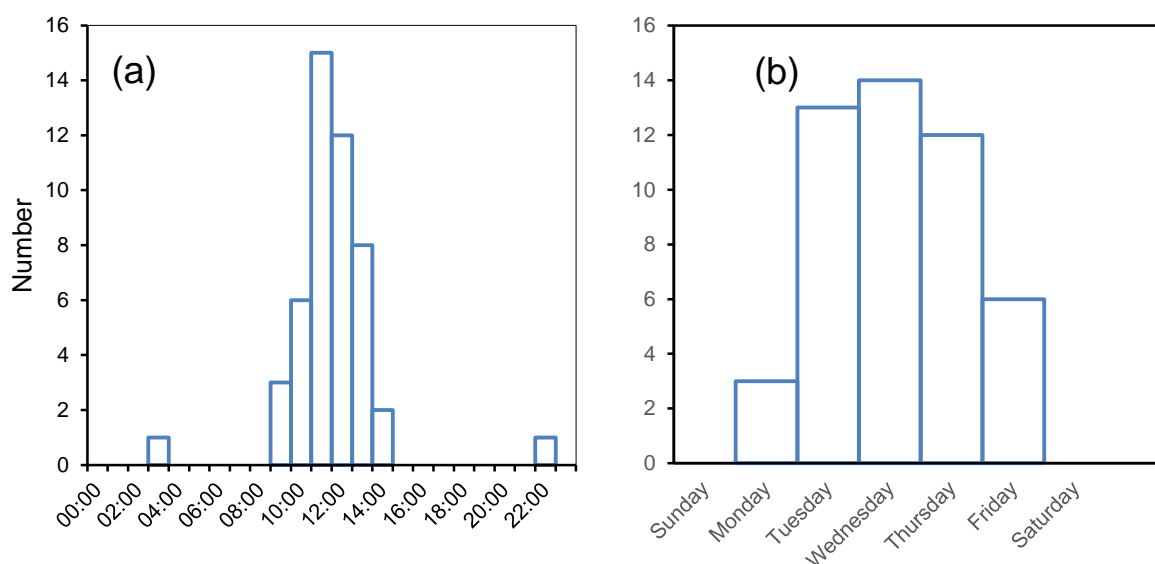
Figure 29. Histograms showing the hour, (a), and the day, (b), of occurrence for all seismic events detected in the Vale of Pickering since the start of the project in 2015

3.5 DATA AVAILABILITY

Helicorder plots showing 24 hours of data from each station are available online and can be found on the BGS Earthquake Seismology Team website and at http://www.earthquakes.bgs.ac.uk/research/BaselineMonitoring.html.

The web pages also contain background information on the baseline monitoring project as well as educational material to explain the scientific context. Recordings of ground motions from all stations are stored in a public open-data archive. These data are available in the standard data format developed in the international seismological community for data exchange. In the future, processed event data (automatically determined and manually revised event parameters) will also be made available through this website.

3.6 IMPROVING DETECTION AND LOCATION OF EVENTS

Very dense networks of seismic stations, such as that in the Vale of Pickering, that are designed to monitor very small earthquakes present a novel set of challenges in earthquake detection. For

example: stations are often very close together, so noise may be coherent on several stations at once; separate phases may be very close together; and the requirement to detect very small earthquakes means that the signal-to-noise ratio may be poor. In addition, earthquakes may occur in rapid succession during hydraulic fracturing, and these need to be located quickly and reliably to make effective operational decisions.

There are many algorithms available to scan a seismic data time series and detect perturbations that could be an earthquake. These are often referred to as 'triggering' algorithms. Here, we describe work carried out to test a number these algorithms and assess their suitability for near real-time detection and location using a dense network.

The algorithms that we test are as follows:

- STA/LTA (Trnkoczy, 2012). The average absolute amplitude of the signal is continuously calculated over two time windows, one long and one short. The characteristic function is simply the short-term average or *STA* divided by the long-term average, the *LTA*.
- Carltrig STA/LTA (Johnson et al., 1995). In addition to the two normal averages (*STA* and *LTA*), corresponding rectified averages (*STAR* and *LTAR*) are calculated. The rectified averages are the absolute value of the difference between the trace and the *LTA*, averaged over the corresponding windows. BGS uses this algorithm routinely for event detection.
- Recursive STA/LTA (Withers et al., 1998). This is a computationally more efficient version of the STA/LTA trigger that also recovers more quickly from large amplitude transients. It has smaller 'shadow zones' where, after a large transient passes the STA, the transient continues to dominate the output by causing a large LTA.
- Z-Detect (Withers et al., 1998). The Z-detector estimates the distance of the data from the mean in units of the standard deviation. It has the advantage of automatic adjustment to variance in the background noise.
- Akaike Information Criterion (Kitagawa and Akaike, 1978). AIC pickers have been used in many P-wave picking algorithms using autoregression (AR) (Leonard and Kennett, 1999). The data are divided into segments, each modelled as an AR process. For the intervals before and after an arrival, the AR coefficients will be of different order (Sleeman and van Eck, 1999). Finding the global minimum of the AR-AIC function gives the most likely position for a pick in the whole seismogram.
- FBPicker. The FBPicker is a modified transient energy method from Lomax et al. (2012). The energy, *E,* of each sample is compared to the *RMS* (root-mean-square) energy in the window before that sample.
- Kurtosis Picker (Saragiotis, 2001). Kurtosis describes a probability distribution; a long-tailed distribution, with many outliers, has high kurtosis. The picker assumes that seismic noise amplitudes have a Gaussian distribution while an earthquake arrival does not.

Each trigger has several parameters that need to be optimised jointly. This was done by trying many different combinations for each trigger and ranking them based on the number of known phases found, with some consideration to the number of false triggers.

In the absence of any induced seismicity in the central part of the Vale of Pickering, we use data from a sequence of mining-induced earthquakes at Thoresby Colliery, New Ollerton (Verdon et al., 2017) to test the different detection algorithms. In February 2014, BGS installed a network of seven seismometers around the mine (Figure 30) after local residents felt a number of earthquakes. This resulted in the detection of over 300 earthquakes, which have been accurately located using a local velocity model (Bishop et al., 1994). We used 63 of these events, with a total of 362 manually picked P-wave arrival times on local stations.
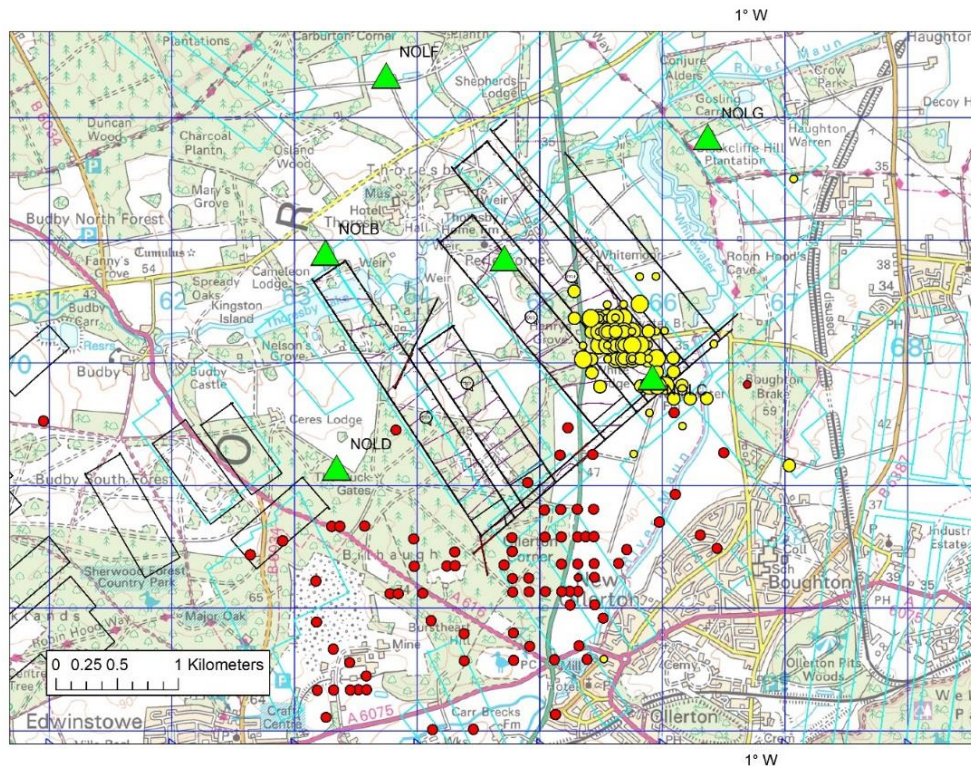
Figure 30. Location calculated for earthquakes at Thoresby Colliery. The red dots are the locations using the national network only. The yellow dots are the locations also using the local network shown by the green triangles. The black rectangles are coal seams at 1 km depth. © Crown Copyright and/or database right, 2018. Licence number 100021290 EUL

We tested each algorithm using only short windows of data around known events, rather than scanning long continuous records. This allowed us to check the accuracy of automatic picks by comparing them against manual picks, as well as to assess the number of missing and false detections. We consider a pick 'good' if it is within 1 second of the manual pick for that station. Picks made more than 1 second from a manual pick were considered 'bad'. We also consider the time taken for the algorithm to scan the data for each. The results are summarised in Table 6.

Table 6. Summary results of testing the different detection algorithms

Algorithm	Number good	Number bad	Time per event
Basic STA/LTA	307	441	0.002 sec
Carltrig STA/LTA	299	154	0.3 sec
Recursive STA/LTA	335	40	0.001 sec
Z-detect	141	239	0.02 sec
AIC picker	312	41	6.5 sec
FBPicker	321	83	0.7 sec
Kurtosis picker	315	48	12.6 sec

Apart from the Z-detect algorithm, all of the pickers detected more than 80% of the picks found for these events manually. This means that, they would have detected all of the events if three station triggers were required for a detection. However, we find significant differences in the number of bad picks and in the time taken to calculate the characteristic function. The latter is an important consideration for real-time detection and location, and both the AIC picker and the Kurtosis pickers are unsuitable for real-time processing for this reason. The number of bad picks is important because too many bad station picks increase the chance of bad event triggers significantly. Both the basic STA/LTA and the Carltrig STA/LTA have many more bad picks

and so are not optimal. This leaves the FBPicker as implemented by Lomax et al. (2012) and the recursive STA/LTA. The latter was quicker for this test and found slightly more good picks and slightly fewer bad ones. The difference is not significant but this algorithm is also very simple to implement and is the algorithm chosen to carry forward to the next step.

3.7   BETTER DISCRIMINATION OF MAN-MADE EVENTS

We have begun to compile a library of waveform templates for known quarry blasts detected by the seismic sensor array. Further work will be carried on this dataset to discriminate events better from operational quarries and background seismicity.

3.8   ENSURING RELIABLE MAGNITUDE MEASUREMENTS

Recent research has shown that amplitude measurements from epicentral distances of less than 15–20 km considerably overestimate event magnitudes compared to more distant observations (Butcher et al, 2017). An example of this is that magnitudes calculated for earthquakes induced by hydraulic fracturing at Preese Hall, Lancashire (Clarke et al., 2014) using ground motions recorded on seismometers distances of a few kilometres away were unrealistically high. A detailed examination of the BGS earthquake catalogue shows that individual station magnitudes for stations within 5 km of an earthquake are up to an order of magnitude higher than magnitudes at other stations (Luckett et al, 2018, submitted). Luckett et al (2018) have also developed a new magnitude scale to correct the overestimation of magnitudes at smaller distances. This scale is designed so that magnitude estimates at greater distances will be the same as when using the previous scale.

We have applied the revised magnitude scale to calculate magnitudes for all the blasts from the Newbridge quarry close to Pickering. Figure 31 shows the original magnitudes plotted against the revised magnitudes. This indicates a clear reduction in event magnitude when the corrected scale is applied. The magnitude change varies, but is over 0.5 magnitude units in some cases. There is also a small reduction in the variance of the magnitude estimates when using the revised scale, as demonstrated by the error bars in Figure 31.
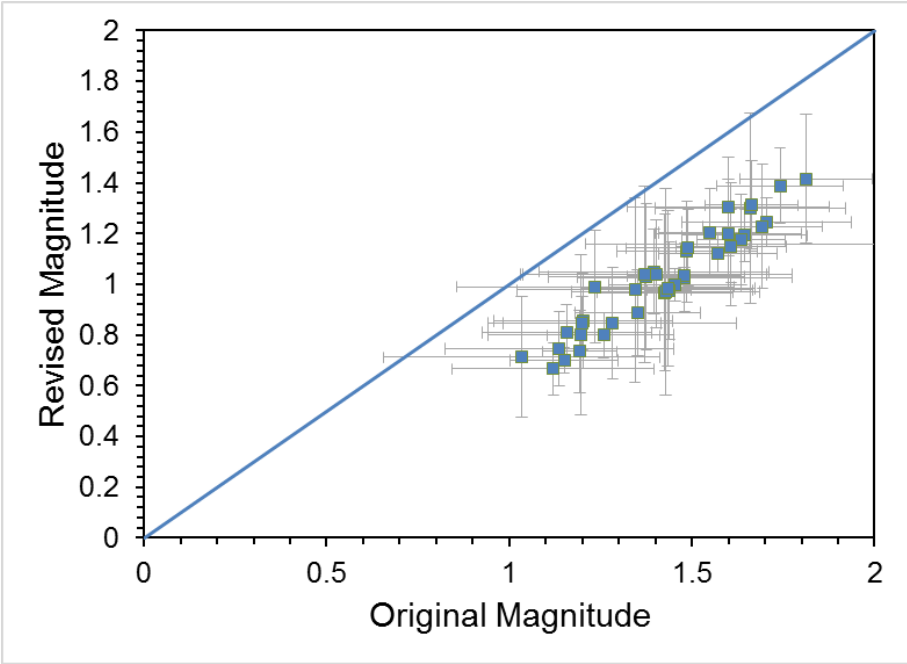
Figure 31. Local magnitudes for Newbridge Quarry events calculated with the Hutton and Boore (1987) scale and a revised scale to correct for overestimation of magnitude at short epicentral distances (Luckett et al, 2018). Error bars show standard deviation in individual station measurements

3.9 SUMMARY

The networks of seismometers installed to monitor background seismicity in both the Vale of Pickering and the Fylde areas have operated successfully throughout the reporting period. Two additional stations were added to the Fylde network to improve detection and location capability. A further station is planned. All but one station show levels of data completeness over 90%. There was no significant change in recorded noise levels at any of the stations in the network.

PDFs of the observed noise at each station have been used to estimate the detection capability of the Vale of Pickering network in low, median and high noise conditions. Although detection capability varies significantly, the network is capable of detecting events with magnitudes of 0.5 ML or less around Kirby Misperton.

The monitoring networks have successfully detected a number of earthquakes around both the Vale of Pickering and the Fylde Peninsula. However, all of these are at some distance from the centres of interest. The Vale of Pickering network has also detected a number of other seismic events closer to the area of interest. The proximity of the calculated locations to quarries where blasting is known to take place, along with the recorded waveforms that are characteristic of a shallow source, suggest that all these events are quarry blasts. All the suspected blasts occurred during the daytime, which adds further evidence to an anthropogenic origin. The magnitudes of these events range from 0.7 ML to 1.6 ML.

A number of phase-picking algorithms have been tested and have been found to give significant improvements in detection against our existing method.

We have begun to compile a library of waveform templates for known quarry blasts that can be used to discriminate better between events from operational quarries and background seismicity.

We have developed and applied a new magnitude scale to correct for overestimation of magnitudes at small epicentral distances. This results in a significant reduction of the magnitudes of quarry blasts in the Vale of Pickering by over 0.5 magnitude units in some cases. The variance in the magnitude estimates is also slightly reduced. This issue is critical for correct estimation of the magnitudes of any earthquakes induced by hydraulic fracturing.

3.10 REFERENCES

Allen, R. V. 1978. Automatic earthquake recognition and timing from single traces. Bulletin of the Seismological Society of America, 68, no. 5, 1521–1532.

Bishop, I., Styles, P. and Allen, M., 1994. Mining Induced Seismicity in the Nottinghamshire Coalfield. Quarterly Journal of Engineering Geology, 26 (4), 253-279.

Butcher, A., Luckett, R., Verdon, J.P., Kendall, J.M., Baptie, B. and Wookey, J. 2017. Local magnitude discrepancies for near-event receivers: implications for the U.K. Traffic-Light Scheme. Bulletin of the Seismological Society of America, 107, 2, 532-541.

Chen, C. and Holland, A. 2016. PhasePApy: A Robust Pure Python Package for Automatic Identification of Seismic Phases. Seismological Research Letters, 87, 6, 1384-1396.

Clarke, H., Eisner, L., Styles, P. and Turner, P. 2014. Felt seismicity associated with shale gas hydraulic fracturing: The first documented example in Europe. Geophysical Research Letters, 41, 23, 8308–8314.

Lomax, A., Satriano, C., and Vassallo, M. 2012. Automatic picker developments and optimization: FilterPicker: A robust, broadband picker for real-time seismic monitoring and earthquake early warning. Seismological Research Letters, 83 (3), 531–540.

Luckett, R., Butcher, A., Baptie, B. and Ottemöller, L. 2018. Correcting Local Magnitudes at for Near-Event Distances. Submitted to Geophysical Journal International.

Peterson, J., Observation and modelling of seismic background noise, U.S. Geol. Surv. Tech. Rept., 93-322, 1-95, 1993.

Kitagawa, G. and Akaike, H. 1978. A procedure for the modelling of non-stationary time series. Ann. Inst. Stat. Math., 30, 351–363, Part B.

Leonard, M. and Kennett, B.L.N. 1999. Multi-component autoregressive techniques for the analysis of seismograms, Physics of the Earth and Planetary Interiors, 113 (2), 247–264.

Saragiotis, C., Hadjileontiadis, L. and Panas, S.M. 2002. Pai-s/k: A robust automatic seismic P phase arrival identification scheme. IEEE Transactions on Geo- science and Remote Sensing, 40(6), 1395–1404.

Sleeman, R., and van Eck, T. 1999. Robust automatic P-phase picking: An on-line implementation in the analysis of broadband seismogram recordings. Physics of the Earth and Planetary Interiors, 113 (1), 265–275, doi: 10.1016/S0031-9201(99)00007-2.

Trnkoczy, A. (2012), Understanding and parameter setting of STA/LTA trigger algorithm, in New Manual of Seismological Observatory Practice 2 (NMSOP-2), IS 8.1, 20 pp.

Verdon, J.P., Kendall, J.M., Butcher, A., Luckett, R. and Baptie, B., 2017. Seismicity induced by longwall coal mining at the Thoresby Colliery, Nottinghamshire, U.K., Geophysical Journal International, 212 (2).

Withers, M., Aster, R., Young, C., Beiriger, J., Harris, M., Moore, S. and Trujillo, J., 1998. A comparison of select trigger algorithms for automated global seismic phase and event detection. Bulletin of the Seismological Society of America, 88 (1), 95–106.

Ward, R S, Smedley, P L, Allen, G et al. 2017. Environmental Baseline Monitoring Project: Phase II – Final Report. Report of the British Geological Survey. OR/17/049. http://nora.nerc.ac.uk/id/eprint/517889/.

4 Atmospheric Composition

4.1 INTRODUCTION

This section of the report discusses ongoing baseline measurements of atmospheric composition (greenhouse gas and air quality indicator concentrations) sampled near to the Little Plumpton and Kirby Misperton drilling sites, and discusses climatological relationships between concentrations and other factors such as time of day, week, year, and prevailing meteorology. For a further detailed discussion of the definition of an atmospheric baseline in this context, see the Phase 1 and Phase 2 project reports (Ward et al, 2017 and Ward et al, 2018: http://nora.nerc.ac.uk/id/eprint/520354/ and http://nora.nerc.ac.uk/id/eprint/517889/), which also detail the scientific measurement rationale, site selection criteria, infrastructure and instrumentation, and details of data provision and access.

The Universities of Manchester and York have been carrying out measurements for air quality and greenhouse gas concentrations for a near-continuous period of 24 months to define intra-annual and annual baselines for Kirby Misperton ("KM"), in the Vale of Pickering and Little Plumpton ("LP") in the Fylde. In the remainder of this report, the analysis of data for greenhouse gases (Sections 4.4 to 4.6) is provided by authors from the University of Manchester. Analysis of air quality data (Section 4.7 to 4.7.8) is provided by authors from the University of York. Mobile survey case studies to characterise local and regional methane sources around each site, using isotopic fingerprinting, were conducted by, and a reported by authors from, Royal Holloway University London.

The analyses in this report draw on high-precision greenhouse gas (carbon dioxide and methane) measurements, key air quality trace gas (ozone, nitrogen oxides and non-methane hydrocarbons) and particulate matter concentrations, alongside meteorological data. The data considered in this report cover the period between February 1 2017 and 31 January 2018 for meteorology and greenhouse gases, and between February 1 2017 and 31 February 28 2018 for air quality parameters. The data reported here is self-consistent in terms of methodology and can be compared between sites and also with the equivalent preceding calendar year, as presented in our Phase 2 report (Ward et al 2017).

From September 2017, mobilisation of equipment for hydraulic fracturing operations began at the KM8 site. This involved significant HGV traffic movement to/from the site and the placement/construction of temporary infrastructure (e.g. sound barrier, work-over rigs, storage tanks etc). These operations continued throughout the winter of 2017/18 and were still continuing at the time this report was prepared. The mobilisation on site has resulted in a change to certain air quality parameters, e.g. NO_x, and these have been highlighted in the report. Detailed analysis has not yet been undertaken as site works were still continuing, but once these have finished the data set will provide opportunity to evaluate the impact of site mobilisation on air quality and the transition from baseline to a pre-operational state. Not all parameters have shown a change. There has been no observed change in greenhouse gas emissions as methane is not yet being extracted from the KM8 site and none of the other equipment transported to site is expected to emit methane or carbon dioxide. We do however note a possible continuing long-term fugitive emission of CH_4 from the KM8 pad infrastructure itself, which is noted in the report.

4.2 MONITORING SITE SELECTION AND SUPPORTING INFORMATION

Site selection is described in detail in the project's Phase 1 report and the site selection strategy for environmental monitoring in connection with shale-gas exploration: Vale of Pickering, Yorkshire and Fylde, Lancashire in Smedley et al. (2015).

4.2.1 Addition of Ethane Measurement to Mobile Monitoring

Royal Holloway University London added a Los Gatos Research Ultraportable Methane-Ethane Analyser (LGR UMEA) to mobile measurement capabilities in October 2017 to allow for quick identification of leaks in the gas distribution system and to gain insight into the usefulness of methane:ethane ratios to identify gas from different sources. This was used in all subsequent mobile surveys around the LP and KM locations.

4.3 MONITORING ACTIVITIES

Data have continued to be collected at both KM and LP over the past year (2017–2018). Any technical or mitigating issues with the monitoring and the associated dataset are highlighted in the following subsections.

4.3.1 Little Plumpton monitoring

Monitoring has continued at the Little Plumpton site, with the additional installation of a hydrogen sulphide instrument (H_2S).

There have been some technical instrument issues throughout the past year: methane, carbon dioxide, particulates and ozone instruments have experienced short-term technical equipment failures, but these were rectified as soon as possible (within days or weeks) and these events are highlighted in the relevant section below. These instrument failures are not atypical of long-term field-based monitoring, and each event has provided additional insight into instrument performance and suitability.

4.3.2 Kirby Misperton monitoring

Monitoring has continued at the Kirby Misperton site, with additional H_2S measurements added to the suite of measurements during this reporting period. From 19th September 2017, Third Energy were permitted to bring equipment on to KM8 wellsite that would be used for hydraulic fracturing and flow testing. From an air quality perspective this meant the measurements at the site after this date could no longer be classed as baseline. Hence, from this point onwards for the reporting period covered by this report, the monitoring is defined as "pre-operational".

A sound barrier was also erected around the wellsite, this was constructed from steel containers, scaffolding above and plastic sheeting. This was not ideal for the atmospheric measurements as it meant the instruments could no longer sample unperturbed airflows in all directions. To alleviate this problem all gas inlets were extended to 9 m above ground level at the top of the scaffold sound barrier. The weather station was also repositioned there. It was not possible to move the Particulate Matter (PM) instrument inlet due to the requirement for a fixed, calibrated, heated inlet. This means that from 19th September 2017, PM measurements were no longer representative of wider region air quality as locally-derived (site) pollutants may be pooled within the area surrounded by the sound barrier at low wind speed.

4.3.3 Calibration and quality assurance

Calibration and quality assurance procedures in the Phase 3 (2017–2018) baseline period have continued to follow those outlined for the Phase 2 (2016–2017) period to ensure consistency and continuity in the dataset. Data from both sites employ quality assurance (QA) and quality control (QC) for air quality and greenhouse gas concentration data covering all aspects of network operation, including equipment evaluation, site operation, site maintenance and calibration, data review and ratification. All instrumental calibrations are traceable through an unbroken chain to international reference standards to ensure high accuracy, comparability with similarly calibrated high-precision instrumentation, and quantified uncertainties in the dataset. Metadata concerning the precision and guidance on use of the data is prepared for each measurement reported and

made available to view publicly on the Centre for Environmental Data Analysis (CEDA) archive (www.CEDA/ac/uk) after final QC approval.

Site visits occurred at 3-weekly intervals to check the condition of instruments and to perform checks on analyser accuracy, precision and response times, as well as calibration. A full list of instrument technical specifications and precision is available in the Phase 2 project report (Ward et al, 2017).

The Picarro G2301 instrument used to measure methane concentrations during mobile surveys has very low long term drift upwards of <0.1 %/yr. It is calibrated to the global WMO scale using 3 standards in the range 1.8–2.1 ppm between mobile surveys and short term variability is <0.05% of the known values. Each survey day of raw data is corrected using the calibration closest in time before utilisation.

4.4   RESULTS

4.4.1   Meteorological baseline

The principal meteorological variable of interest to baseline characterisation and pollution source interpretation is the local wind speed and direction, as an indicator of the local and regional airmass history (i.e. what source(s) of pollution the sampled airmasses may have been influenced by upwind). The instantaneous wind speed and direction can elucidate relatively nearby sources of pollution (within ~ 10 km) where repeated and consistently elevated concentrations of trace gases may be observed to correlate with particular wind direction and wind speed. When considering longer-range sources of pollution (such as may be added over cities many 10s or 100s of km upwind), the timescales of interest to airmass history typically extend to no more than around 5 days. Beyond this time, the uncertainty in the path of air upwind (and the chemical changes in such air) increases and interpretation becomes more speculative. Therefore, we limit our analysis to these timescales of advection only.

In Sections 4.4.2 and 4.4.3 we describe the climatology of winds observed at the sites and discuss their meaning in the context of pollutant gas concentrations and emission sources that have been observed at the measurement stations.

4.4.2   Little Plumpton wind climatology

The wind speed and wind direction statistics observed at the LP site over both the 2016–2017 baseline (left panel) and 2017–2018 baseline period (right panel) for comparison, are shown in

Figure 32 as a conventional wind rose. This type of illustration shows the frequency (in percent of total time) of instances when wind blows from various directions (seen as the vector and radius in

Figure 32). The colour scale in

Figure 32 then illustrates the corresponding proportion of wind directions measured from each direction for a range of surface wind speeds (see colour legend in

Figure 32).

It should be noted that the 2016-17 data (left panel of

Figure 32) presented here differs very slightly to that presented in our Phase 2 report due to a 21-degree bias error in measured wind direction that was detected and corrected in October 2017 at the LP site, and will also be corrected in the final dataset provided to CEDA. This does not materially affect earlier conclusions made in our Phase 2 report (Ward et al, 2017) and does not affect summary climatological statistics regarding trace gas concentrations. However, LP wind data presented here should be considered prime. It should also be noted that due to storm damage there is no wind data between 17/10/2017–31/10/2017.
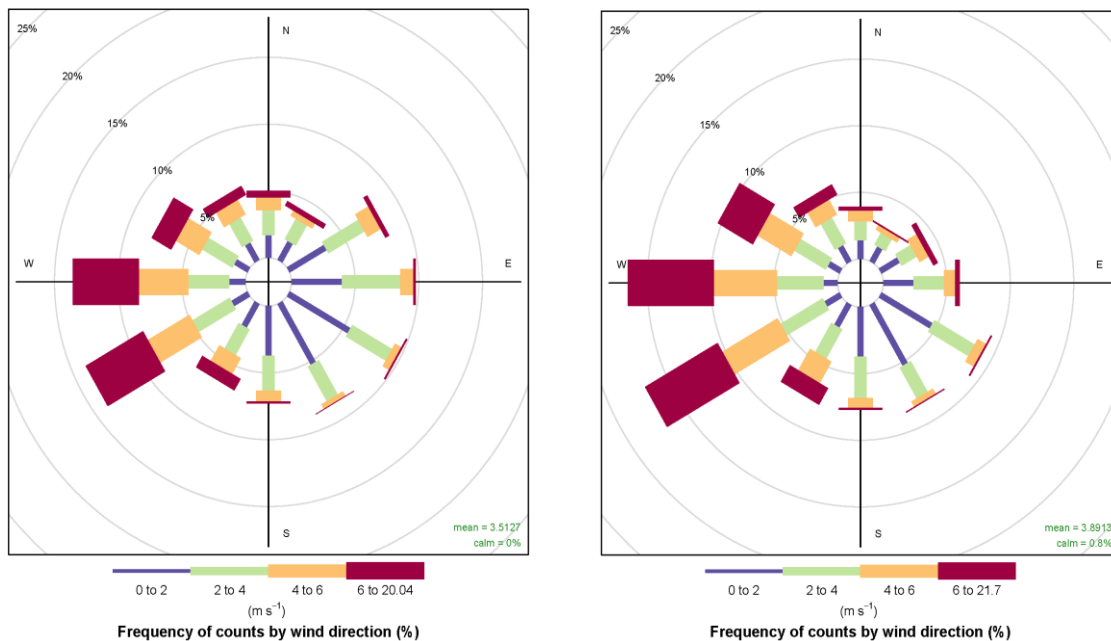
Figure 32. Wind rose for the LP site, showing wind speed and direction statistics for: (left): 1 Feb 2016–31 Jan 2017; (right): 1 Feb 2017–31 Jan 2018. The radius defines the percentage of total time in each of 12 wind direction cones (30 degree span), while the colour scale (see colour legend) defines the wind speed. © University of Manchester, 2018

As expected at the LP site (as for any exposed site in the UK), the dominant wind direction in both periods is from the north-west to south-west quadrant (~30–40% of the time in both years), consistent with the site's location on the west coast of the UK mainland and exposed to flow associated with the Atlantic mid-latitude storm track. This is also the direction from which the strongest winds are observed (red and orange colours in

Figure 32), typically coinciding with the passage of mid-latitude cyclones near to, and over the UK mainland. Within this quadrant, the dominant wind speed is between 6–12 m/s (red colours) in both years, followed by frequent wind speeds between 2–6 m/s, with extremely strong winds peaking up to 20 m/s in very rare storm conditions (<0.5% of the time). The consistency of the wind climatology across both annual periods demonstrates the power and comparability of the statistical baseline approach.

As discussed in the Phase 2 report, this wind climatology has important implications for the local baseline. The position of the LP site near to the Blackpool shoreline means that winds bringing air from the Atlantic may typically be expected to carry relatively well-mixed and background airmasses to the LP measurement site. In this context, a background can be conceived to be an airmass relatively unaffected by local or regional pollution sources, broadly representative of the average composition of Northern Hemispheric air at the time. These airmasses often represent the Northern Hemispheric seasonal average concentrations of greenhouse gases especially well, as these gases are relatively inert on the time and spatial scales of advection across the Atlantic in mid-latitude cyclones. As these airmasses dominate the statistical climatologies at the LP site in a consistent way year-to-year, the baseline for this wind direction provides a very useful background from which to assess future local changes in pollution sources in the immediate upwind vicinity. The position of the LP site just 300 m directly to the east of Cuadrilla's Preston New Road shale gas site makes the dominant westerly wind direction highly favourable for potential future operational comparative assessment.

Winds from the southeast were also frequent, accounting for 22% of the 2016–2017 period, and 18% of the 2017–2018 period while northerly and easterly quadrant wind directions were less frequent, representing <20% in each quadrant over the course of each baseline period. Wind speeds for these quadrants (all other than westerlies) were also typically much lighter (dominated by light breeze winds in the range 2–4 m/s, followed by stagnant winds classified as 0–2 m/s). This is due to a number of factors: 1) that winds from these directions are moderated by passage over the mainland UK land surface, and 2) that winds from these directions typically represent flow in less frequent high pressure regimes to the north and east or from low pressure systems to the south and west. Light winds from these directions will typically carry airmasses that have spent a significant time in dynamic contact with the surface of the UK mainland and may also represent air that has passed over Western Europe. Therefore, these airmasses may be expected to typically contain pollution added to surface air as they pass over a range of anthropogenic (manmade) and natural sources of greenhouse gases and other pollution upwind of the measurement site. Such sources include cities, landfill, industry, transport, agriculture etc. This air may be a mix of both local (<10 km distant), regional (UK mainland) and more distant (Western Europe) pollution sources, making it difficult to quantitatively deconvolve the relative inputs of each. However, the frequency and duration of transient enhancements seen in trace gas concentration data offers important markers of the proximity (and type) of pollution source, as regionally impacted airmasses will typically display broad (longer timescale) and more invariant enhancements relative to background westerly airmasses, while local inputs are often seen as sharper and shorter-lived enhancements. This will be discussed further in the following sections, making use of additional airmass history tools such as back trajectory analysis.

4.4.3   Kirby Misperton wind climatology

The wind speed and wind direction statistics observed at the KM site over the 2016–2017 and 2017–2018 baseline periods are shown in Figure 33, again as a conventional wind rose.
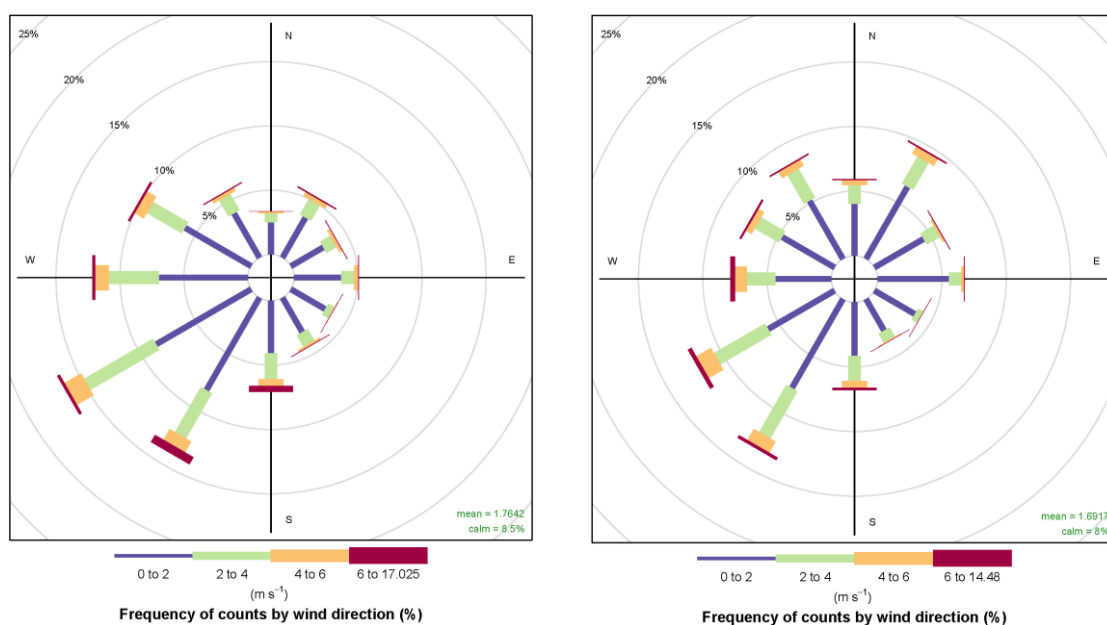
Figure 33. Wind rose for the KM site, showing wind speed and direction statistics for: left: 1 Feb 2016 – 31 Jan 2017; right: 1 Feb 2017-31 Jan 2018. The radius defines the percentage of total time in each of 12 wind direction cones (30 degree span), while the colour scale (see colour legend) defines the wind speed. © University of Manchester, 2018.

The dominant wind directions are from the western and southern quadrants (collectively accounting for 40–45% of the time in both annual periods), with the most frequent winds from a south-westerly direction (>30% of the period in both cases). This is also the direction from which the most frequent strongest winds are observed (red colours in Figure 33), typically

coinciding with the passage of mid-latitude cyclones over the UK mainland. Within this westerly quadrant, the dominant wind speed is between 2–4 m/s in both years, with occasionally strong winds peaking between 15–17 m/s in storm conditions (<0.5% of the time) over both periods. It should be noted that the frequency of strong winds above 6 ms^{-1} (~3% of the time) is much reduced compared with the LP site due to its more inland and easterly location.

Northerly, easterly and southerly quadrant wind directions were less frequent in both years, representing 8–20% in each quadrant over the course of each 12 month baseline. Wind speeds from these quadrants were also dominated by light breeze conditions in the range 0–2 m/s with wind speeds rarely exceeding 6 m/s in either period. This is broadly due to the same factors that define the LP wind climatology: 1) that wind speeds from those directions are moderated by passage over the mainland UK land surface, and 2) that winds from these directions usually represent flow in less frequent high pressure regimes to the north and east or from low pressure systems to the south and west. An important difference between the LP and KM site is seen in the strength of westerly and south-westerly winds, which appear to be significantly moderated by virtue of the position of KM far inland from the western coast of the UK mainland. The dominant wind direction is south-westerly, which is consistent with observations at LP over the course of both baseline periods. This can be expected to be linked to the track of mid-latitude cyclones, which typically follow a direction toward the northeast as they pass over the UK mainland, especially between late autumn and early spring when storm activity (and hence wind speed) is climatologically most intense.

These subtle differences in wind speed and direction between the two sites, but the consistency of the climatology year-to-year at each site separately, suggest that pollution sources contributing to airmasses arriving at the KM site from different wind directions will differ greatly, especially for westerly and south-westerly directions, but that such sources will be internally consistent at each site separately by virtue of the similarity year-to-year. Winds from the west and south will typically represent airmasses that have spent a significant time in dynamic contact with the surface of the UK mainland and may also represent air that has passed over the cities of the midlands and North West England. Such airmasses may be expected to typically contain pollution added to the surface air as they pass over a range of anthropogenic (manmade) and natural sources of greenhouse gases and other pollution upwind of the measurement site, such as cities, landfill, industry, transport, agriculture etc. This air may be influenced by a mix of both local (<10 km distant) and regional (UK mainland) sources.

A further difference at the KM site relates to (albeit infrequent) easterly and south-easterly wind directions, which, unlike LP, represent airmasses that have more recently passed over Europe. To summarise, the position and wind climatology observed at KM preclude the more obvious definition of a "background" wind direction (as is the case for westerlies at LP), that can be assumed to represent a Northern Hemispheric average compositional state. The position of the KM site to the east-south-east of the Third Energy site makes the north-west-westerly wind direction optimal for any future operational comparative assessment with the caveat that the more variable nature of polluted airmasses from this wind direction (due to other regional UK sources upwind) may lead to more variable concentration statistics when diagnosing any future incremental changes due to on-site activity. However, as in the case of LP, the frequency and duration of transient enhancements seen in trace gas concentration data offers important evidence for the proximity (and type) of pollution source, as regionally impacted airmasses will typically display broad (longer timescale) and more invariant enhancements relative to local inputs, which are often seen as shorter-lived but more intense enhancements. The closer proximity of the KM site to the drilling operations (just a few metres) also means that more significant but transient enhancements would be observed compared with those observed at LP due to dilution and dispersion and the quantification of emission flux (for greenhouse gases) is significantly more problematic, due to turbulent flow and an inability to make idealised assumptions implicit to many conventional flux methods such as eddy covariance, Gaussian plume inversion, and mass balancing. This will be discussed further in the following sections.

4.4.4 Greenhouse gas baseline

This Section reports and discusses the greenhouse gas baseline periods for both the LP and KM sites. The analysis of the air quality baseline will be presented separately in Section 4.7.

We present the statistical analysis of the greenhouse gas baseline dataset and mobile vehicle surveys of nearby greenhouse gas sources at each site in turn; and interpret this in the context of sources of emission and background using meteorological (and other) data to aid analysis.

4.4.5 Little Plumpton

4.4.5.1 FIXED SITE CLIMATOLOGY

Figure 34 illustrates the measured ambient CO_2 and CH_4 concentrations at LP as a function of time across the baseline periods sampled at the fixed measurement site positioned ~300 m to the east of the Cuadrilla site perimeter. Figure 35 and Figure 36 go on to illustrate how the measured concentrations relate to their coincidently-measured wind direction for each greenhouse gas, while Figure 37 and Figure 38 show the same information but also display how the relationship between measured concentration and wind direction varies as a function of time.
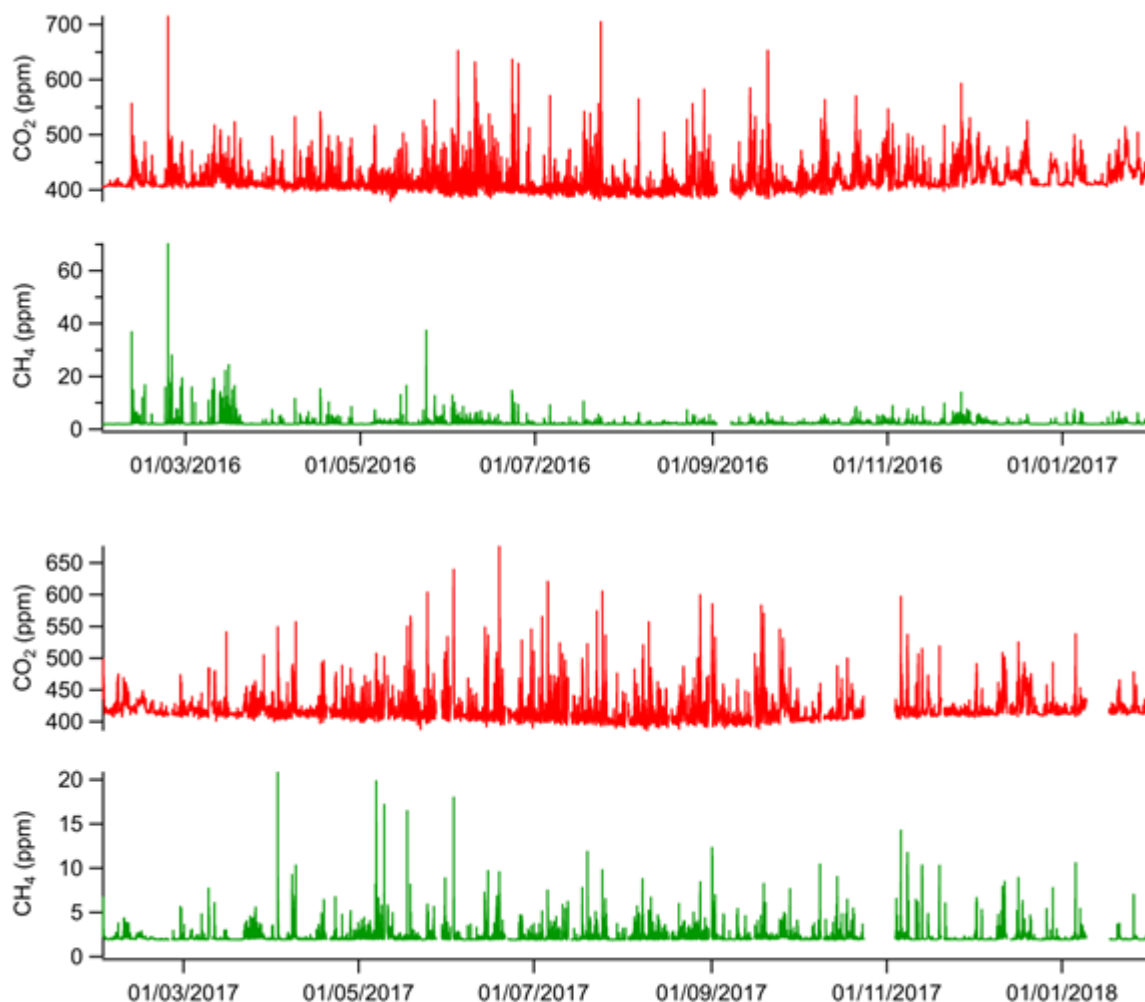
Figure 34. Time series of carbon dioxide (red) and methane (green) in units of ppm measured at LP between: 1 Feb 2016 and 31 Jan 2017 (top panels); 1 Feb 2017-31 Jan 2018 (bottom panels). © University of Manchester, 2018.

Comparing both the CO_2 and CH_4 datasets and the 2016-17 and 2017-18 baseline periods, we can infer key features which can affect measured greenhouse gas concentrations at the site on a range of different timescales. A summary of these features is provided below:

- Both CO_2 and CH_4 datasets exhibit a well-established background concentration for each species. These background concentrations, ~400 ppm for CO_2 and ~2 ppm for CH_4, appear broadly consistent in both baseline periods from Figure 34, but examination of the lower percentiles in Table 11 and Table 12 reveals that both CO_2 and CH_4 concentrations increased in 2017–18 relative to 2016–17. This is consistent with observations at background monitoring sites across the Northern Hemisphere, which reflect the continued annualised global increase in background concentrations of these greenhouse gases, and can also be seen in Figure 35 and Figure 36 as a reduction in the proportion of measurements in the lowest two bins (represented by green and blue colours).

- Both species also exhibit a seasonal cycle in concentration. This is particularly pronounced for CO_2 where increased biospheric uptake during the summer relative to the winter causes background concentrations to be depleted. A similar pattern exists for CH_4, driven by changes in removal processes (largely through reaction with the hydroxyl radical) and emission sources, but this is less significant in the context of typical CH_4 variability at the site due to local and regional emissions (as seen in Figure 34).

- From Figure 35 and Figure 36 it can be seen that periods of enhanced CO_2 and CH_4 above these background concentrations are more frequently associated with wind directions between 0 and 180 degrees. This can also be seen as a function of time from the colour-coded-time-series in Figure 37. As introduced in the previous section, this is expected to result partly from the fact that the majority of CO_2 and CH_4 sources are land-based and partly as a result of the prevalence of lower wind speeds from this sector, which result in larger enhancements being generated per kg of gas emitted.

- Very large enhancements of > 500 ppm CO_2 and > 5 ppm CH_4 are usually associated with local sources and light wind speeds. For CH_4 it can be seen from Figure 35 that this is most commonly associated with easterly wind directions, where there is a strong local agricultural source from nearby farms.
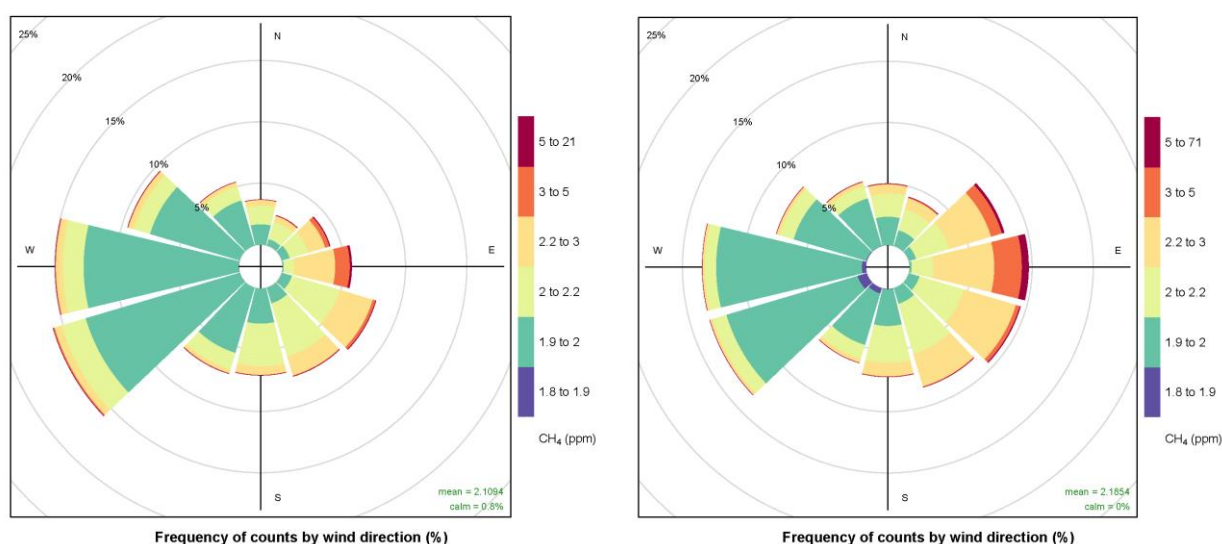
Figure 35. Concentration (as per colour scale) wind roses for methane (units of ppm), as measured at LP for the 2016-17 period (left panel) and 2017-18 period (right panel). © University of Manchester, 2018.
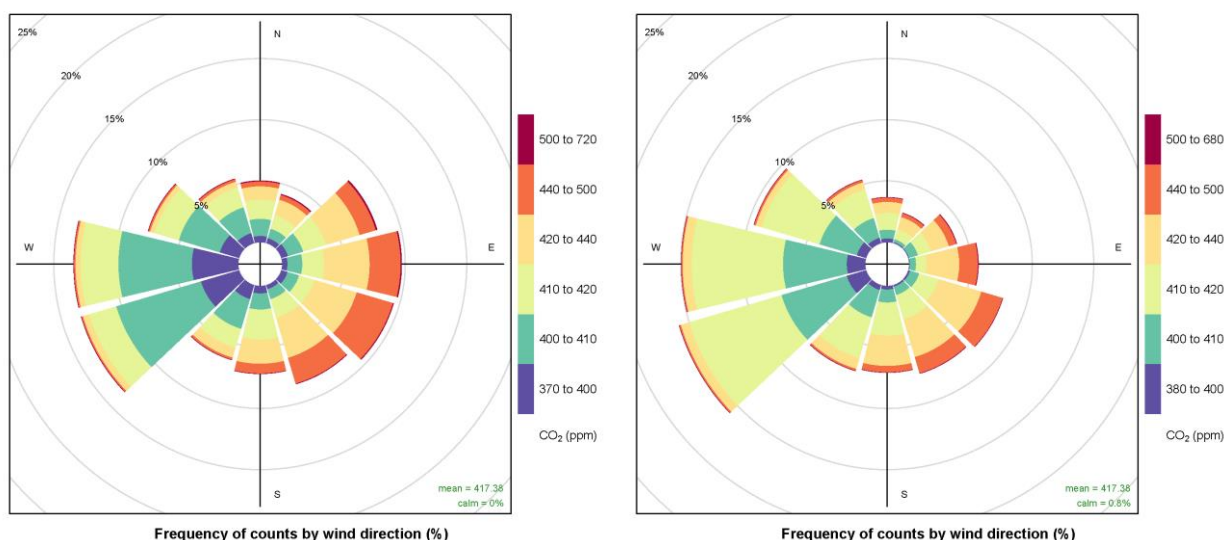
Figure 36. Concentration (as per colour scale) wind roses for carbon dioxide (units of ppm), as measured at LP for the 2016-17 period (left panel) and 2017-18 period (right panel). © University of Manchester, 2018
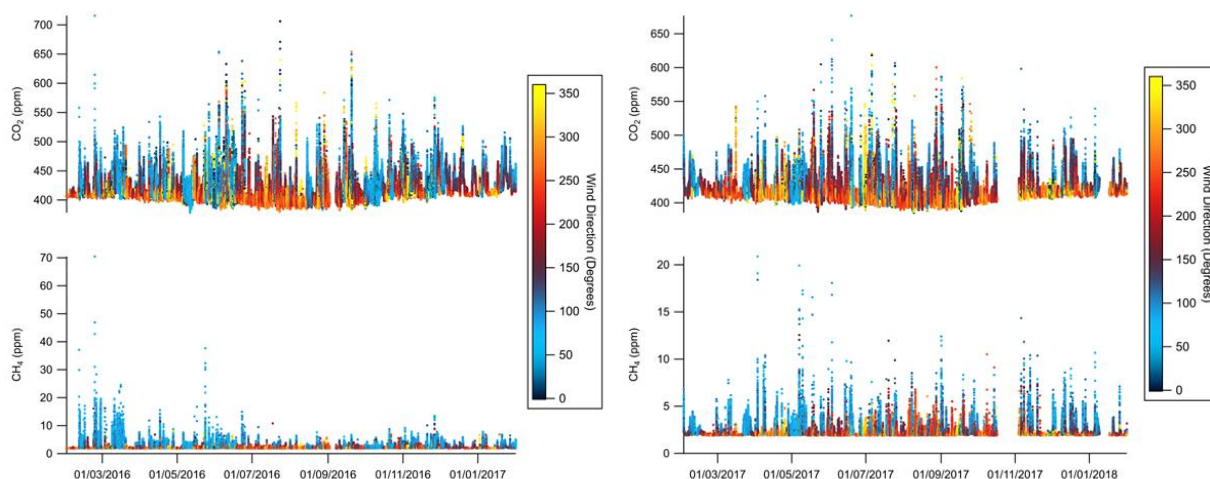
Figure 37. Concentrations (as per colour scale) in air as a function of time (x-axis) and wind direction (colour-coding) for carbon dioxide (top panels), and methane (bottom panels) as measured at LP for the 2016-17 baseline period (left panel) and 2017-18 period (right panel). © University of Manchester, 2018

Figure 38 illustrates the correlation between simultaneously-measured CO_2 and CH_4 concentration in air, colour-scaled for sampling density (each count representing a one-minute data interval). Warmer colours indicate more frequent measurement. Clear correlations between the concentrations of the two greenhouse gases aseen in plots of this type delineate so-called mixing lines or tracer-tracer source relationships. Such correlations (or mixing lines) often correspond to specific airmass types where co-emission from specific sources, or common airmass chemistry, may be active. In Figure 38, we see that there are two broad correlations, which appear remarkably consistent year-to-year, and one dominant feature, seen, as follows:

1. A dominant mixing line (traced by red and yellow colours) with a relationship of $[CO_2]=132.1[CH_4]+386.5$ ppm (in 2016) and $[CO_2]=132.4[CH_4]+388.5$ ppm (in 2017) – representing co-emission (or bulk mixing) of nearby CO_2 and CH_4 sources upwind to the east and north east (based on understanding of how such concentrations relate to wind direction in Figure 37 to Figure 40).

43

2. A weaker and broader mixing line with a relationship of $[CO_2]=7.5[CH_4]+386.5$ ppm – representing co-emission (or bulk mixing) of CO_2 and CH_4 regional UK and longer-range sources upwind to the east and south east.

3. A dominant red cluster centred at ~400 ppm CO_2 and 2 ppm CH_4 in both years – this represents the dominant and frequent background signal seen in westerly Atlantic airmasses (Figure 36 and Figure 37). Note that the darkest red colours in this cluster correspond to >40 total days of measurement each within the baseline period.
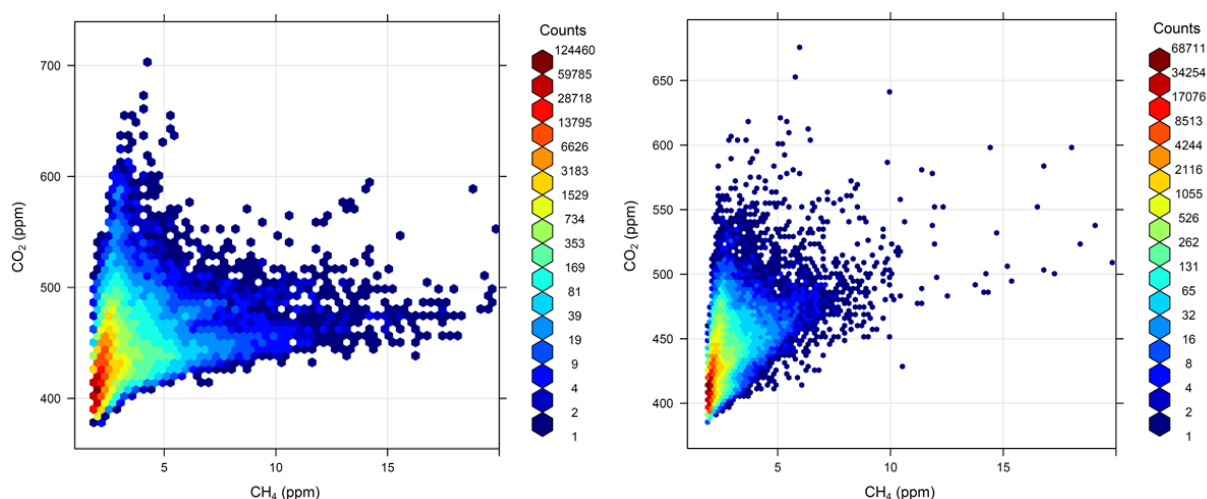
Figure 38. Coincident CO₂ and CH₄ concentrations measured at LP for the 2016-17 period (left panel) and 2017-18 period (right panel). Colours indicate the frequency density of sampling (number of coincident measurements). N.B. One count refers to a one-minute period of data. © University of Manchester, 2018

Mixing lines such as these are a powerful differentiator of source types, especially at the regional and national spatial scale. When temporally averaged (as data in Figure 38 have been), they characterise airmasses that have passed over a large fetch of similar pollution source types and where the airmass has had time to mix internally. The two dominant mixing line modes seen in Figure 38 are seen to correspond to the less frequent easterly, southerly, and south-easterly wind directions. Considering the location of LP, these wind directions represent air that has passed over the Pennines and the cities of Manchester, Leeds and Sheffield in the case of easterlies, and the cities of Birmingham and London in the case of south easterlies. While cities and infrastructure are a principal source of UK pollution (including greenhouse gases), biogenic sources of greenhouse gases, such as the biosphere, landfill and agriculture would also be expected to feature in the fetch of such airmasses when upwind of the LP site. The summative mix of these longer range pollution types upwind for easterly and south-easterly wind directions gives rise to the dominant mixing line observed as the red and yellow trace in Figure 40 and described in summary point 2 above.

To interpret more local sources of pollution (within ~10 km), we must focus in detail on the more transient features in the high temporal resolution dataset. To do this on an event-by-event basis for a year of data would be meaningless (and impractical) in the context of the baseline analysis here, though event-led (case study) analysis may well be advisable during any operational phase monitoring. However, it is possible to interpret the relative role of proximal pollutant sources to the overall baseline by considering short-lived but significant excursions from the average baseline and comparing these with wind speed and direction.

Figure 39 illustrates a polar bivariate representation of the relationship between both wind speed and direction and greenhouse gas concentration for both baseline years. The colour scale in Figure 39 highlights the wind speed and wind direction conditions that dominate the overall concentration average seen at the measurement site (as a weighted mean of concentration x

frequency of occurrence). The red areas seen in all panels (CO_2 and CH_4) in Figure 39 correspond to light winds (0–2 m/s) from the south east indicating a well-constrained local source for both gases. Given the site's location, these local (strong) CH_4 sources to the south east are strongly expected to be associated with the nearby dairy farm and the nearby A583 main road, while the southerly dominance in CO_2 is likely mostly associated with passing traffic on the A583 main road. The fact that the red area does not extend to higher wind speeds in the south east is consistent with an interpretation that longer range sources of pollution may not contribute significantly to periods where the greatest enhancements in concentrations are sampled at the site, i.e. that local sources dominate the strongest enhancements. The role of longer range (regional, national and continental) sources is therefore to add a smaller increment to the much larger local emission sources that dominate periods of enhancement in south-easterly and easterly wind conditions.

The lighter blue areas seen in Figure 39 to the west indicate a long range and diffuse source of the greenhouse gases, which is consistent with longer range transport of moderately enhanced airmasses, from Ireland and in intercontinental transport from North America, although this source's relative contribution to any enhancement over the baseline is very much weaker than those upwind sources when airmasses are received from the south east.
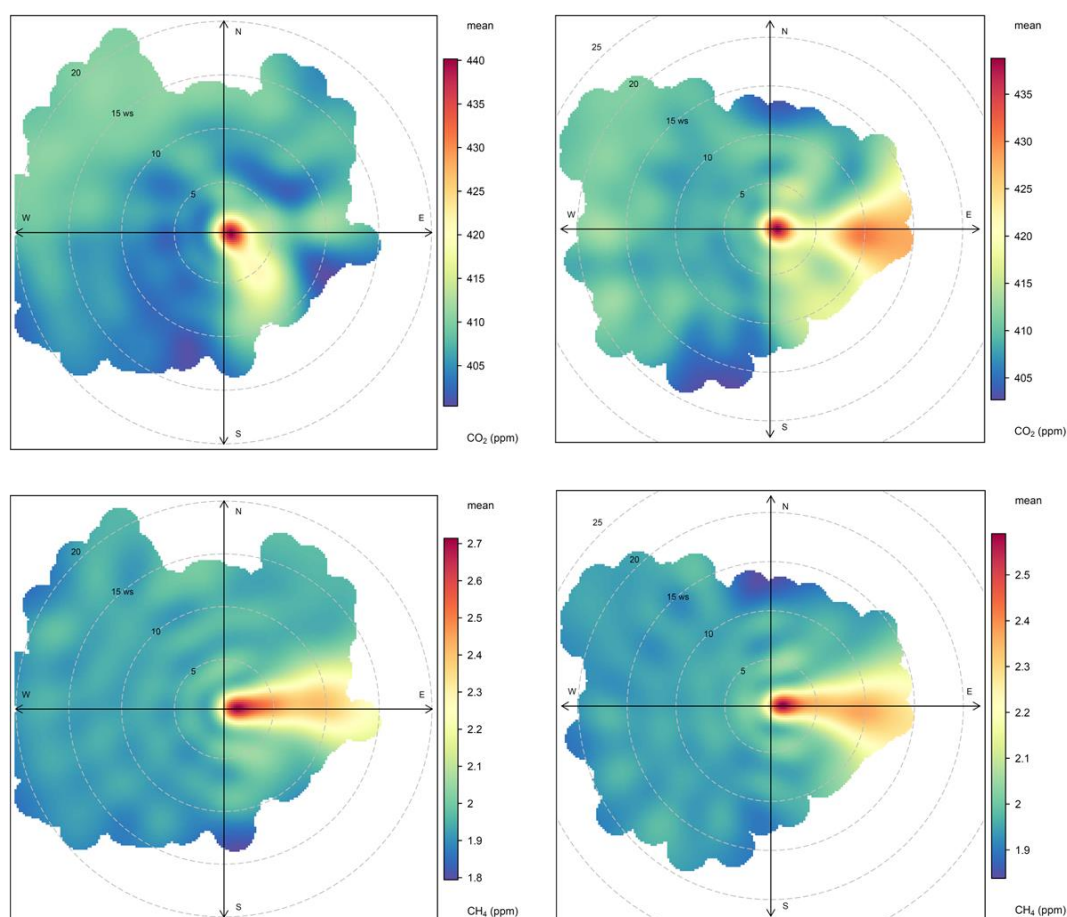
Figure 39. Polar bivariate representation of carbon dioxide (top panels) and methane (bottom panels) as a function of wind direction for the 2016-17 period (left panels) and 2017-18 period (right panels). The colour scale represents the fraction of total measurement time weighted for concentration enhancement relative to the global mean (as scaled for colour in units of ppm) and wind speed (defined by the radial component - each radial increment representing 5 m/s). See text for further details. © University of Manchester, 2018

To further differentiate the role of local, regional and more distant (long range inter-continental) pollution sources, we now examine the airmass history, which can be interpreted using Lagrangian back trajectories. Back trajectories are a useful indicator of the path that air has taken in the atmosphere up to and over the previous 5 days. Beyond this time, the accuracy of hindcasted trajectories degrades rapidly due to numerical and meteorological uncertainty associated with Lagrangian transport models and the accuracy of reanalysis meteorological data. Put simply, back trajectories attempt to trace back the path of neutrally buoyant single particles in the atmosphere as they are carried on the wind (this is known as Lagrangian advection). Back trajectory models use wind fields from meteorological reanalyses (hindcasted winds calculated by forecast models that use assimilated measured data).

In this analysis, we have used the Hybrid Single Particle Lagrangian Integrated Trajectory Model (HYSPLIT) and hourly United States National Centre for Environmental Prediction Global Forecast System reanalysis meteorological data at a spatial resolution of 0.5°x0.5°. We have then calculated 5-day back trajectories with endpoints at the location of the LP site at 6-hourly intervals across the measurement period (~1200 trajectories in total between 1 Feb 2016 and 31 Jan 2017 and the same in the 2017–2018 baseline period).

Figure 40 shows the airmass history of air sampled at LP throughout the baseline periods (2016 in the left panels and 2017 in the right panels). This statistical representation of the history of air can be interpreted as a surface "footprint", illustrating a surface area over which air measured at LP has been influenced by potential surface sources. Figure 40 shows the frequency (as a fraction of total time, in this case as a percentage of each 12-month baseline period) that air has passed near to the surface in a latitude-longitude grid with a 1-degree spacing (or spatial averaging grid) over the Atlantic region (left panels) and a 0.25-degree spacing for the UK region (right panels). The red colours indicate that air received at LP is most characterised by air that has previously passed over Ireland and the Atlantic Ocean. It also shows less frequent contact with the near-surface to the north and east. Most importantly, there is a remarkable degree of similarity between the airmass histories at the LP site year-on-year with very little difference to note, which supports the utility of this statistical approach and the conclusions that can be drawn from examining a dataset in this way.

We now examine the temporal patterns associated with measured concentrations. The diurnal, weekly, and seasonal variability observed can give additional clues as to the nature of sources and their proximity to the receptor site. Figure 41 and Figure 42 show this for methane for each baseline period, respectively, grouped (and coloured) by wind direction. The top panels show the mean diurnal pattern and statistical variability (at the 95% confidence level of sampled variability around the calculated mean) in methane concentration as a function of time of day and day of week, represented as an average over each of the baseline periods. We can clearly see a repeatable diurnal cycle in all wind directions, with a minimum concentration around midday on each day of the week. This pattern is consistent with the ventilation of the local boundary layer, as the height of the planetary boundary layer is lifted by convection in daylight hours (enhanced in summer months relative to winter), further indicating a dominant role for local sources at night, which might be expected to accumulate overnight before being diluted and detrained in daytime. The highest night time concentrations are associated with easterly and north-easterly wind directions, consistent with the earlier conclusion that the nearby dairy farm is a dominant local source. The highest concentrations are also seen in the late autumn and winter months (November to March) in both baseline periods.
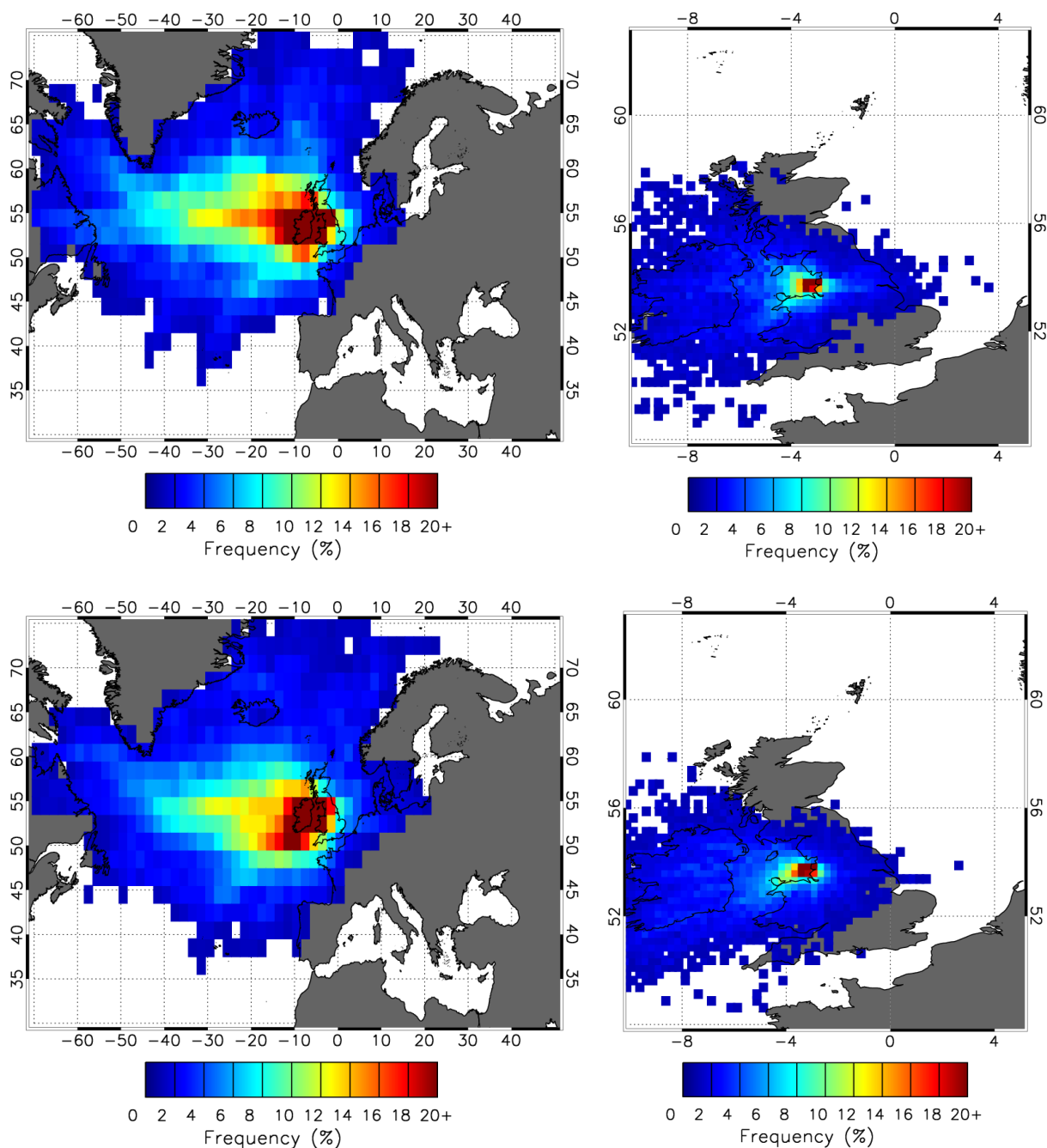
Figure 40. Top panels: 5-day airmass history surface footprint statistics for the period 1 Feb 2016 to 31 Jan 2017 for the Atlantic region (left panels) and UK region (right panels); and bottom panels: 1 Feb 2017 - 28 Feb 2018, as seen from the LP site at a spatial resolution of 1 x 1 degree (Atlantic region) and 0.25x0.25 degree (UK region). Note that frequency refers to the fraction of the total trajectories passing over each spatially-averaged grid cell. © University of Manchester, 2018
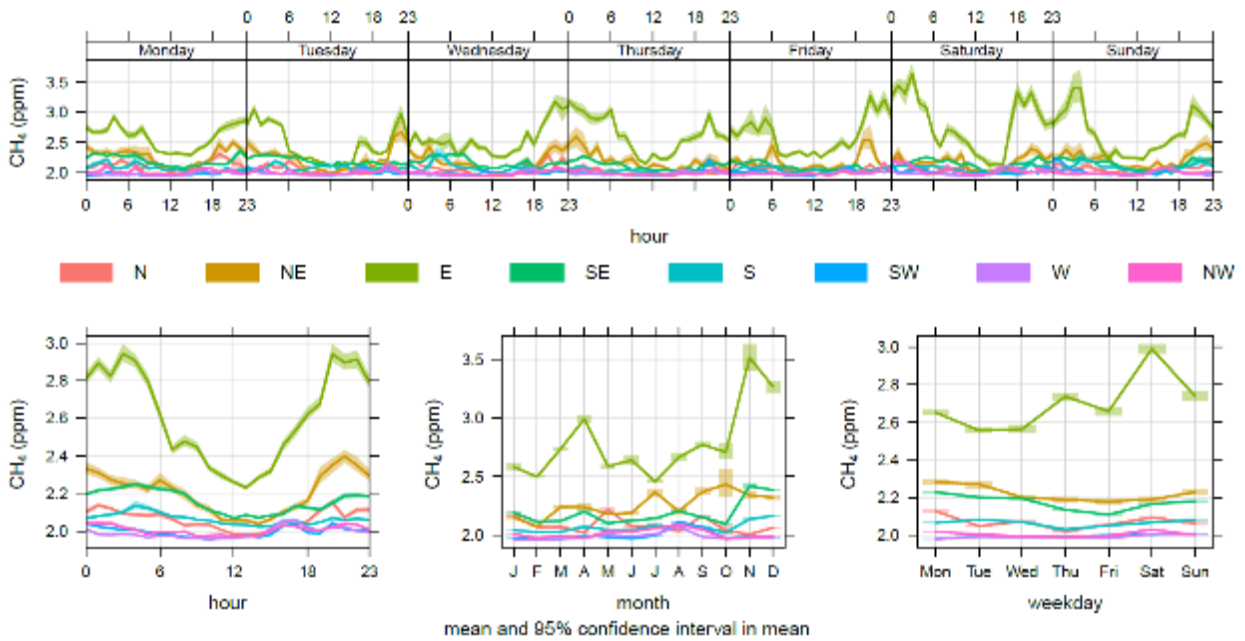
Figure 41. Temporal statistics of methane climatology at LP by time and day of week (top panel), time of day (averaged over all days, bottom left), month of year (bottom middle), and day of week (bottom right) for the 2016-17 period. © University of Manchester, 2018
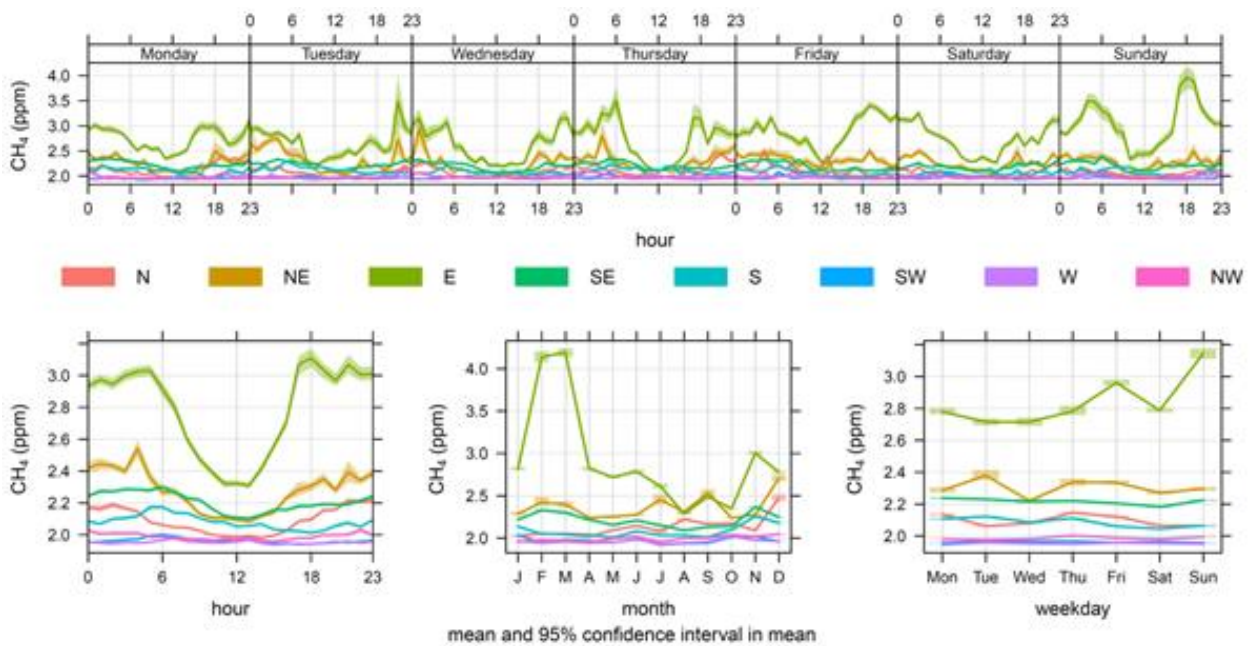
Figure 42. Temporal statistics of methane climatology at LP by time and day of week (top panel), time of day (averaged over all days, bottom left), month of year (bottom middle), and day of week (bottom right) for the 2017-18 period. © University of Manchester, 2018

Repeating this analysis for CO_2 (seen in Figure 43 and Figure 44), we see similar diurnal patterns in both baseline periods, again due to boundary layer ventilation. However, unlike the CH4 pattern, the diurnal variability is very similar for all wind directions. This is expected as the dairy farm is not expected be a source of CO_2 in the local area. Also, a clear seasonal minimum is observed in August in NW and W wind directions. This feature is typical and expected to be due to the summer minimum in northern hemispheric CO_2 concentration due to biospheric respiration (uptake), which peaks in the summer months. This is seen for all but easterly wind directions, simply because the relative change in the seasonal background CO_2 concentration is

48

significant when compared with the signal due to even very nearby CO_2 emission sources, unlike CH_4 (by virtue of the very small absolute mean global concentration of CH_4 around 2 ppm, which means that small mass fluxes of CH_4 can contribute a much greater relative signal on this much lower background).

Figure 43. Temporal statistics of carbon dioxide climatology by time and day of week (top panel), time of day over all days (bottom left), month of year (bottom middle), and day of week (bottom right), averaged for the 2016-17 baseline period. © University of Manchester, 2018
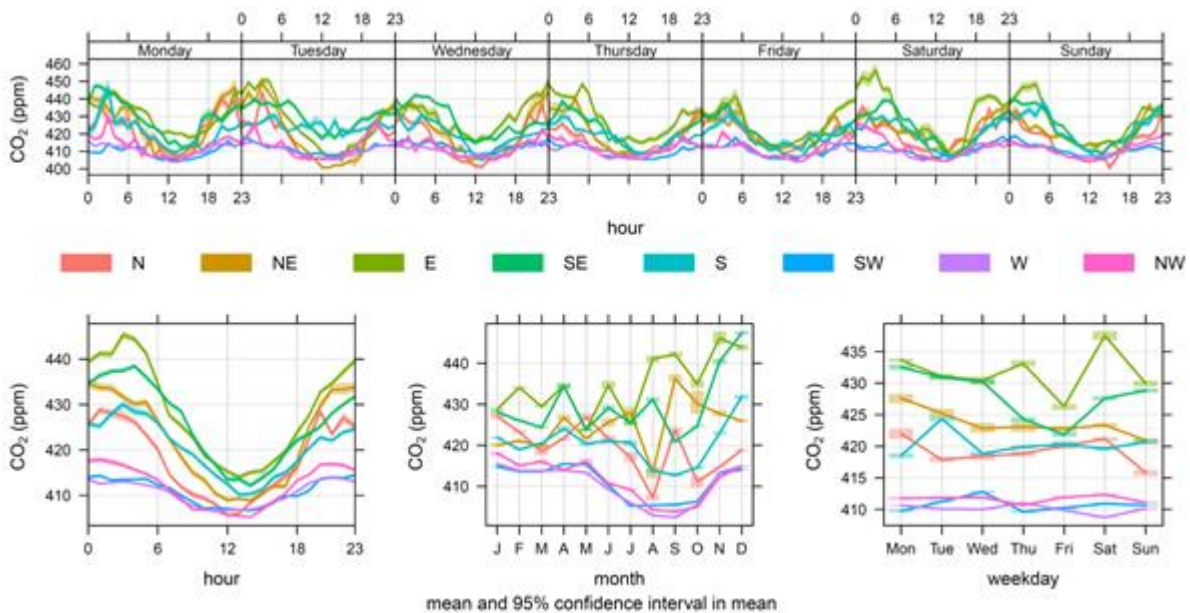
Figure 44. Temporal statistics of carbon dioxide climatology by time and day of week (top panel), time of day over all days (bottom left), month of year (bottom middle), and day of week (bottom right), averaged for the 2017-18 baseline period. © University of Manchester, 2018

Four 2-day surveys were undertaken during this Phase 3 reporting period using the RHUL mobile greenhouse gas laboratory in the Fylde area around the LP site to assess seasonal variation in the distribution and characterisation of methane sources. A total of 79 plume samples and 10 background air samples were collected for subsequent isotopic analysis across the four campaigns. The dates were:

- 27-28 June 2017;
- 24-25 October 2017;
- 23-24 January 2018; and
- 27-28 February 2018.

The main sources of methane identified in the Phase 2 report (Ward et al, 2107) persist with the landfill at Fleetwood giving a consistent $\delta^{13}C$ signature of -58 ±1 ‰ (Table 7). Emissions were greatly reduced during the February 2018 survey when temperatures reached a minimum of -5°C and failed to go above 0°C during the daytime. Identified manure piles from previous surveys were still present, but with no identifiable emission above baseline during this survey.
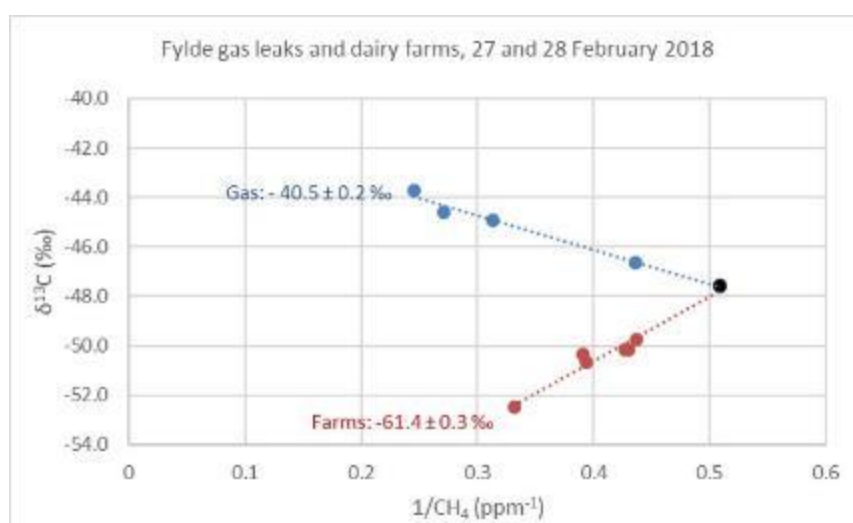
Figure 45. Keeling plot identifying the isotopic source signatures of gas leak and dairy farm methane emissions in the Fylde for samples collected on 27th and 28th February 2018. © RHUL, 2018

Table 7. Isotopic signatures of the main methane sources seen on each campaign in the Fylde

Source	Location (Lat, Long)	$\delta^{13}C$ signature (‰)			
		Jun 2017	**Oct 2017**	**Jan 2018**	**Feb 2018**
Dairy farms	many	-59.1	-60.9	-66.2	-61.0
Manure piles	many	-53.1		-58.6	
Gas leaks	many	-40.9	-42.8	-42.6	-40.6
Clifton Restored Landfill	53.753°, -2.825°			-55.5	
Fleetwood Landfill	53.910°, -3.027°	-58.3			
Anna's Road Landfill	53.775°, -2.976°				-59.8

Gas leaks from the distribution network were identified, the most notable being at the entrance to Anna's Lane (53.773°N 2.975°W), along Peel Road (53.767°N 2.972°W) and in the February 2018 survey only, along Preston New Road (53.786°N 2.956°W) near the LP site during pipe replacement activities. Additional leaks were located in the NE suburbs of St. Annes, including venting from a low-P junction installation. These leaks had consistent isotopic signatures of -41 ±2 ‰ across the survey period (Figure 45 and Table 7).

The isotopic signatures for agricultural sources varied across the seasons. Two end member compositions were defined: cow breath at -70 ±2 ‰ and manure at -51 ±2 ‰. Identified plumes of methane from ruminant husbandry had compositions between these two end members dependent on the activities taking place. Fields of cows with waste partly absorbed by the ground had signatures of -64 ±2 ‰ during the summer months, whereas cow barns emitted methane with the full range of values. If cows were close to the sampling inlet the recorded signatures were closer to the -70 ‰ end member and if there was an empty barn with only waste product emitting the signature was closer to the -51 ‰ end member. Most isotopic signatures calculated for cow barn plumes were in the range -66 to -56 ‰ (Table 7) with some seasonal variation. January 2018 was most consistent with cows indoors at nearly all farms resulting in a common $\delta^{13}C$ signature of -66 ‰. Plumpton Hall farm, 500m east of the Cuadrilla's Preston New Road (PNR2) site, is a consistent emitter of methane from the cow barn with signatures of -66 to -59 ‰, and similarly Moss House Farm, 1km NW of the PNR2 site, with signatures of -64 to -56 ‰.
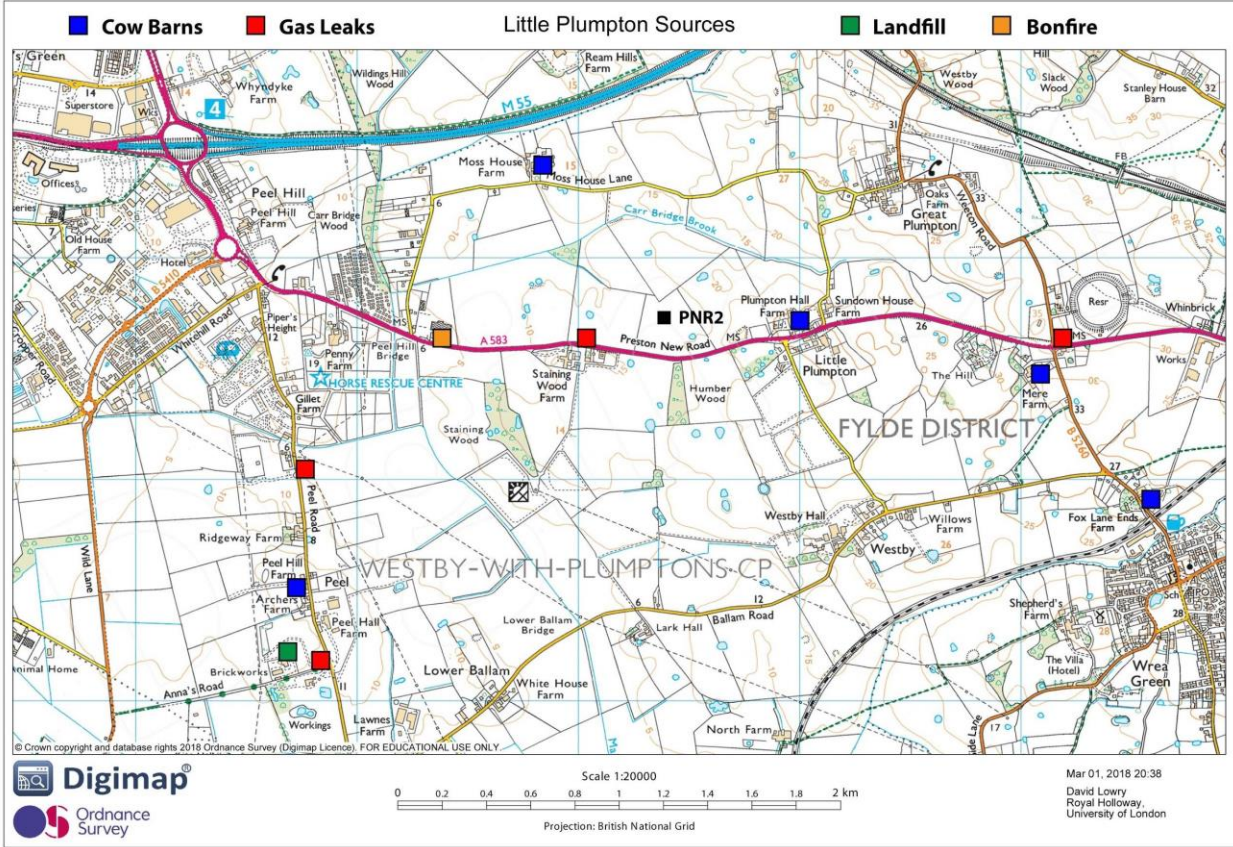
Figure 46. Location of the main methane emitting sources by category within the vicinity of the PNR2 well site. © RHUL, 2018

There was no detectable evidence of significant emissions to atmosphere from the PNR2 well that was being drilled during period covered by this report. The methane sources close to the PNR2 site discussed above are shown highlighted by source category on

Figure 46, then shown in the aerial image with excess methane above baseline plotted for the campaign on 27 February 2018 on Figure 49. The prevailing winds could carry methane from gas leaks, bonfires and cow barns over the PNR2 site. Unless the sources are close enough to

give >100 ppb excess methane, it is likely that ethane will be better than isotopes to distinguish between these sources at the continuous monitoring site. Examples of the GIS maps created to show methane excess over baseline along the survey routes are shown for 27 June 2017 (Figure 47) and 27 February 2018 (Figure 48).
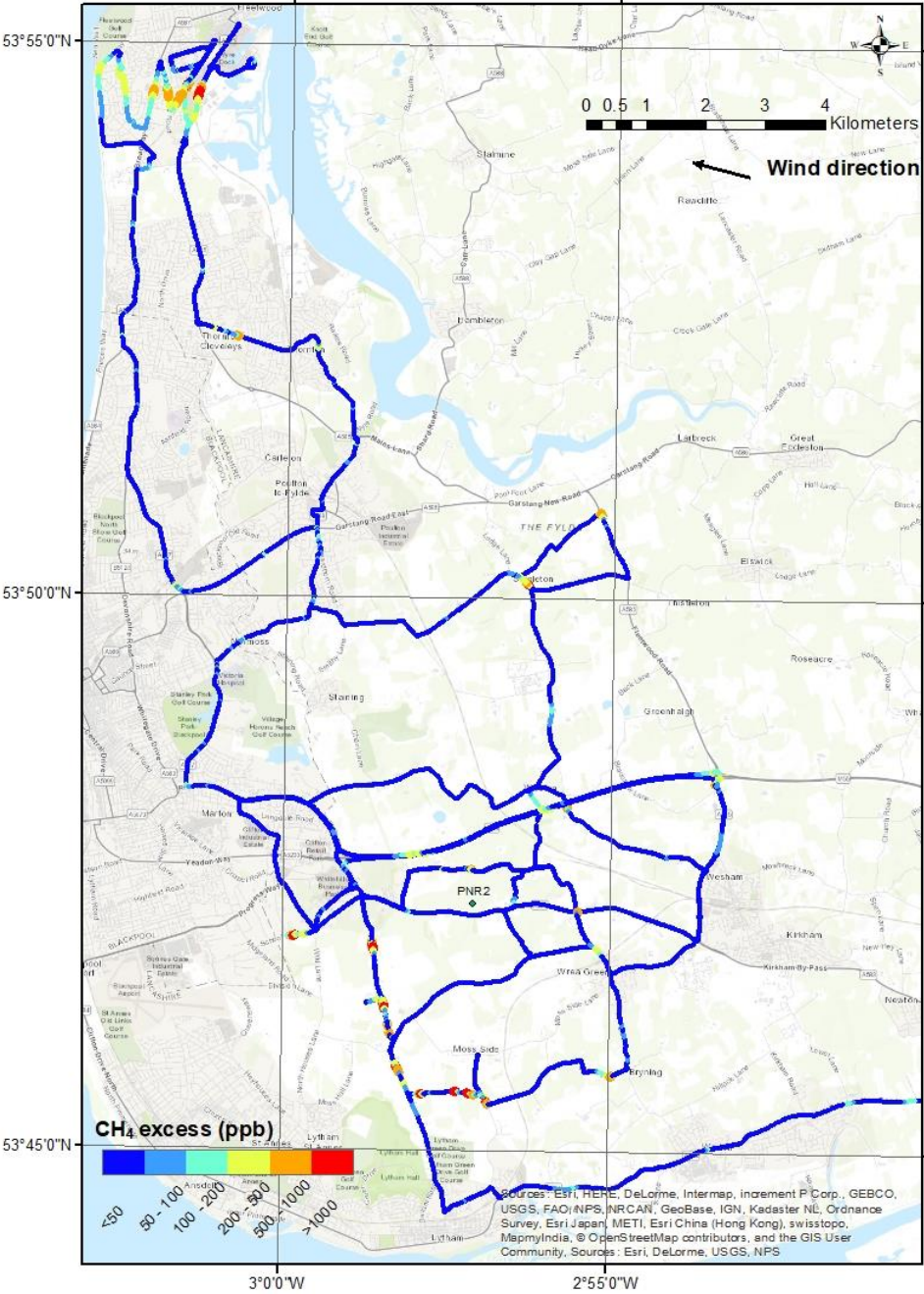
Figure 47. Excess methane mole fraction above baseline for the Fylde survey area, 27 June 2017. The baseline for each survey day is defined as the 2nd percentile of the data. © RHUL, 2018

Measurement of ethane during the more recent survey periods allows the calculation of methane:ethane ratios, which distinguish thermogenic from other gases by having low ratios, mostly <100. Presuming C3 and higher hydrocarbons are not significant components of the gas then this can be represented as a % of ethane in the gas. Consistency of ratios for each 1-second measurement interval within plumes improves with increasing excess over background to a point above 3 ppm excess CH_4 when there is no observed reduction in the standard deviation of the ratio calculated. The instrument has only factory calibration to date and has not yet been finely

calibrated for the high ethane contents measured of 0.1-10 ppm, but the current study is to identify differences between gas leaks and other sources and this is still valid.
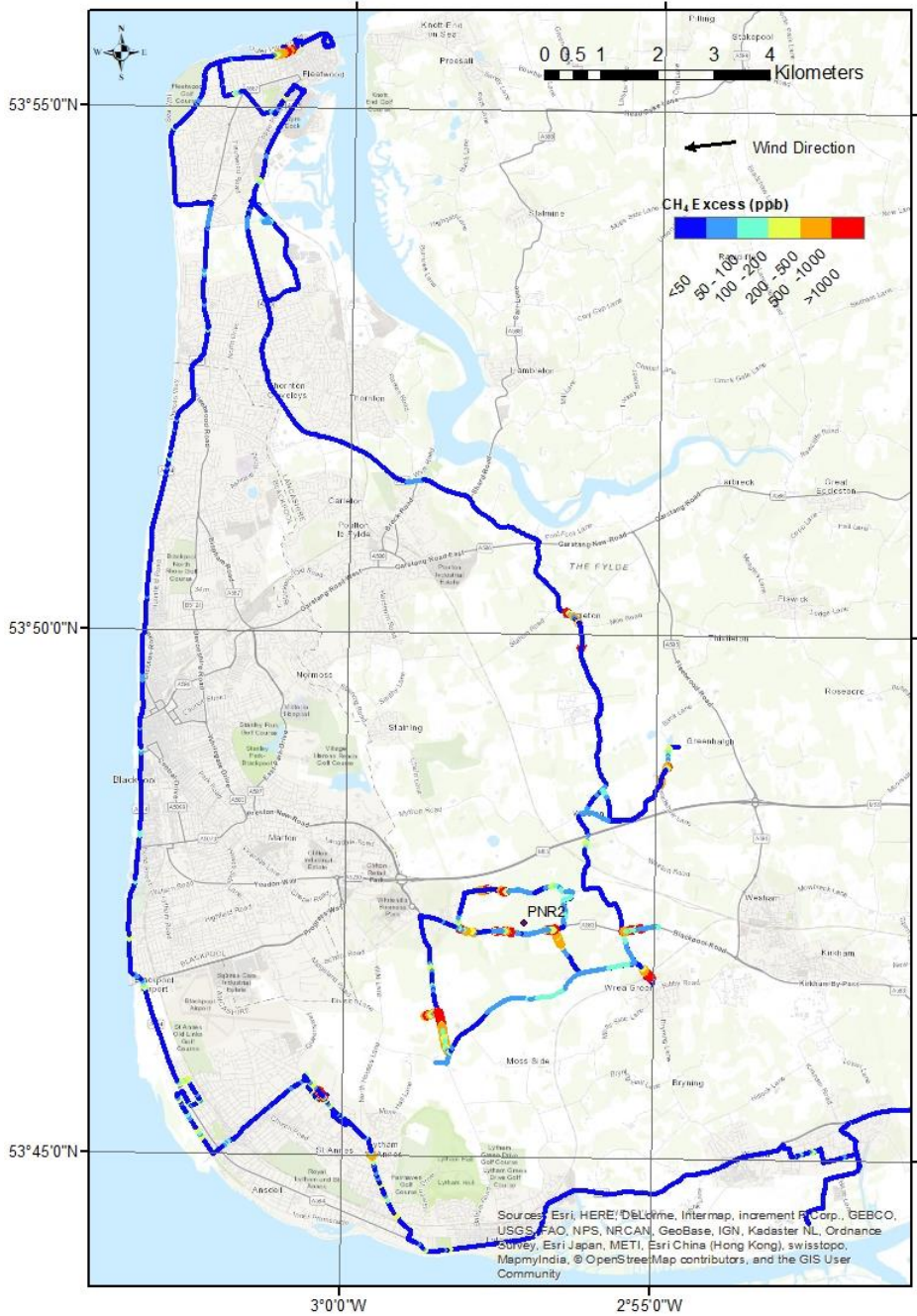
Figure 48. Excess methane mole fraction above baseline for the Fylde survey area, 27 February 2018. The baseline for each survey day is defined as the 2nd percentile of the data. © RHUL, 2018

Ratios of 17-20 (4.9 – 5.6 % ethane, Table 7 and Figure 50) show close agreement for sources considered to be leaks from the national distribution grid within the Fylde area reinforcing the consistency of isotopic signal. This suggests that any new sources of thermogenic gas outwith the distribution network will be identifiable using δ^{13}C and methane ethane ratios. A sampled bonfire plume had a ratio of 3 (25% ethane).
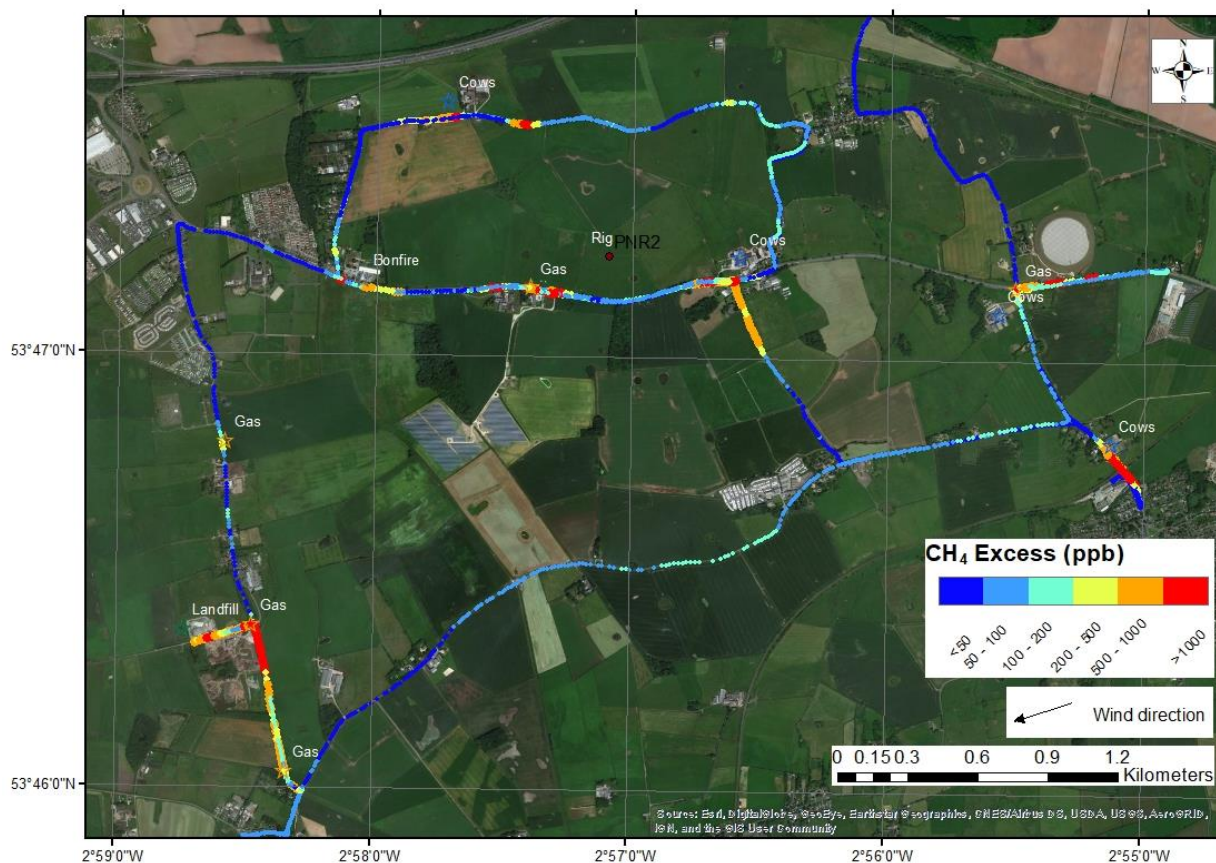
Figure 49. Excess methane mole fraction above baseline for the area around the PNR2 well, Fylde, 27 February 2018 with identified methane sources labelled. The baseline for each survey day is defined as the 2nd percentile of the data. Note in particular methane elevations from dairy farms to the NW and E and gas measured on Preston New Road to the SW of the PNR2 site. (Basemap imagery sources: Esri, DigitalGlobe, GeoEye, Earthstar Geographics, CNES/Airbus DS, USDA, USGS, AeroGRID, IGN, and the GIS User Community). © RHUL, 2018

Table 8**. Methane:ethane ratios and % ethane calculated for fugitive gas emissions identified during the Fylde 27-28 February 2018 mobile survey**

Source	Location	Max CH_4 excess (ppm)	Max C_2H_6 excess (ppm)	CH_4:C_2H_6 ratio (CH_4 excess)	% C_2H_6
St, Annes suburbs B5261	53.760°N 3.006°W	4.33	0.24	17.4 ± 1.7 (>3 ppm excess)	5.4
Fleetwood outside Marine Hall	53.926°N 3.017°W	3.93	0.23	16.8 ± 0.9 (>3 ppm excess)	5.6
Preston New Road	53.786°N 2.956°W	4.32	0.23	19.6 ± 1.0 (>3 ppm excess)	4.9
Anna's Lane / Peel Road junction	53.773°N 2.975°W	3.36	0.20	17.4 ± 1.9 (>1 ppm excess)	5.4
Preston New Road – garden centre bonfire	53.786°N 2.968°W	0.90	0.26	3.0 ± 0.4 (>0.4 ppm excess)	24.7
St. Annes – low- pressure junction vents	53,765°N 3.017°W	1.73	0.11	17.2 ± 3.1 (>1 ppm excess)	5.5
A6 Catterall – Garstang section	53.875°N 2.765°W	4.27	0.25	17.7 ± 1.1 (>3 ppm excess)	5.4
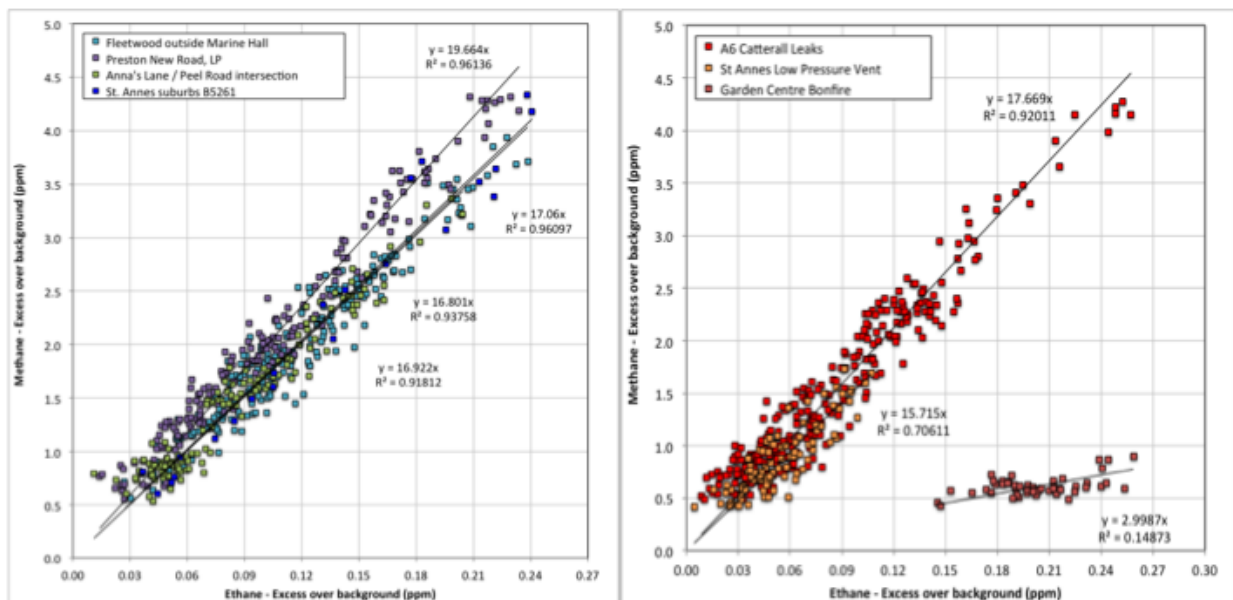
Figure 50. Methane:ethane excess cross plots for fugitive gas emissions emissions identified during the Fylde February 2018 mobile survey. Left: 27th, Right: 28th. The multiplier of x is the ratio for the whole plume with CH₄ excess >0.5 ppm. © RHUL, 2018

4.4.6 Kirby Misperton

4.4.6.1 FIXED-SITE GREENHOUSE GAS BASELINE

Time series of the data collected at the KM site over both baseline periods are shown in Figure 51. A general correlation between variability in CO_2 and CH_4 can be seen, consistent with that seen for the LP site across both periods. Figure 52 illustrates how the measured GHG concentrations relate to wind direction and wind speed. Unlike the LP site, Figure 54 illustrates that all wind directions occasionally display enhanced greenhouse gas concentrations relative to the background – a consistent feature across both years.

When interpreted together, Figure 51 to Figure 54 distil several important and internally-consistent summary features (some quite similar to those discussed for LP), which can be seen in the baseline dataset when comparing salient concentration features with wind direction:

- There are clear periods of what can be defined as a "background" (accounting for ~50% of the period) – where CO_2 and CH_4 concentrations appear relatively constant at around 400–420 parts per million (ppm) and 1.8–2 ppm, respectively (as seen in Figure 51 and Figure 54). These periods coincide with times of westerly winds seen, and as the orange and red colours in the top panels of Figure 54; and represent a typical seasonally-variant Northern Hemispheric average concentration for these greenhouse gases.

- There are prolonged periods (several consecutive days) of marginally enhanced CO_2 and CH_4 (between 410-450 ppm and 1.9–2.5 ppm, respectively. These periods coincide most often with moderate (0-4 m/s) south-easterly winds (see Figure 33), when comparing with Figure 53 and Figure 54 (where blue colours indicate easterly and south-easterly wind directions). These features are consistent with an interpretation that suggests that these episodes represent regional pollution inputs from continental Europe and the cities of Southern England, including London.

- There are short-lived (less than a few hours) but large enhancements (often referred to as "spikes") in the time series data (greater than 2.5 ppm CH_4 and 450 ppm CO_2). These coincide most often with very light (0–2 m/s) easterly and south-easterly and northerly wind directions seen in Figure 53, compared with Figure 54 (where easterly winds are seen in blue colours). These features in the data, often superimposed on the more regional increment describe above, are expected to represent local (<10 km upwind) sources such as nearby

55

agricultural activities, roads, and landfill. It is notable that such transient enhancements at KM typically extend to lower maximal concentrations compared with the much larger enhancements seen at LP due to the increased presence of nearby agriculture and major roads at the LP site.

- For most of the time (>90% of the period), CO_2 and CH_4 display common patterns, in that both gases are often seen at their respective background concentrations, or are mutually enhanced with a scalable linear relationship (as shown in Figure 55 and discussed further below).
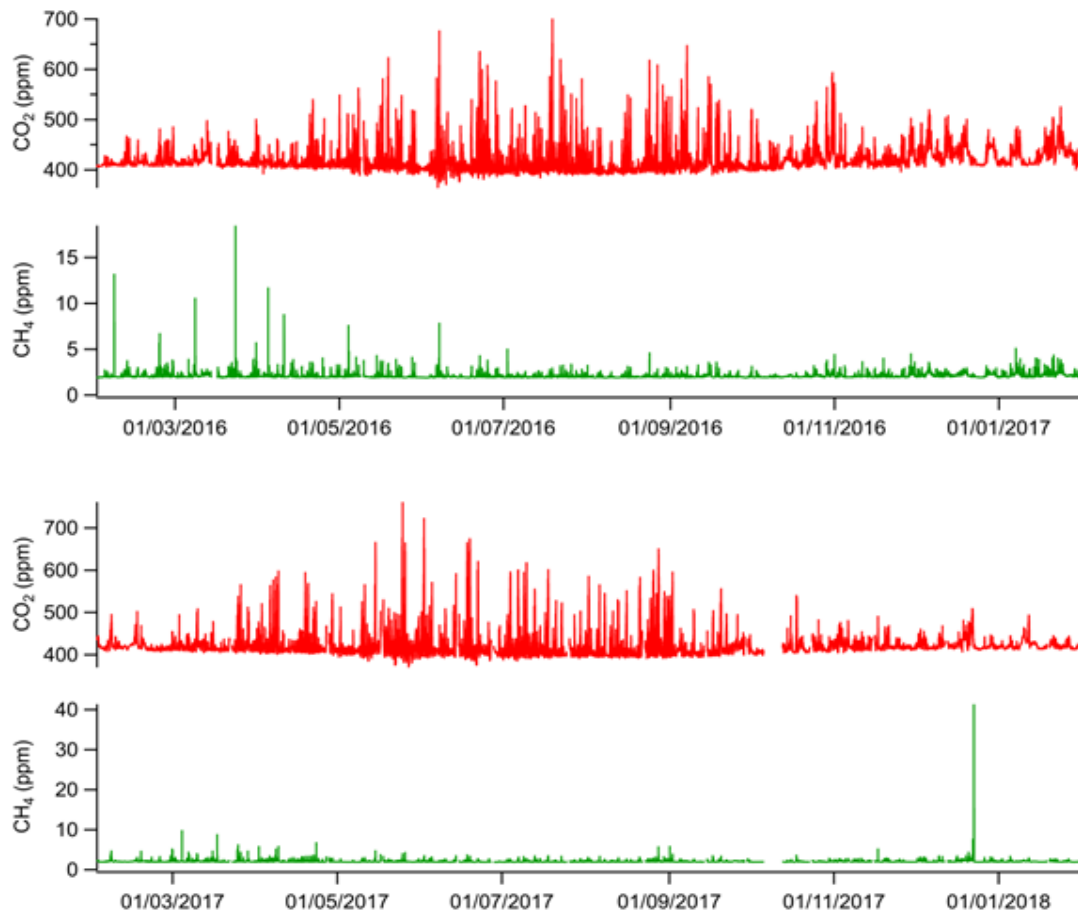
Figure 51. Time series of carbon dioxide (red) and methane (green) in units of ppm measured at LP between: 1 Feb 2016 and 31 Jan 2017 (top panels); 1 Feb 2017-31 Jan 2018 (bottom panels). © University of Manchester, 2018

Interpreting this further, it can be seen that westerly wind directions typically (but not exclusively) bring relatively unpolluted (background concentration) air to the KM site. And, like LP, other wind directions deliver more complex airmasses likely comprising a wide mix of pollutant sources upwind, both local and regional, requiring additional interpretation (see below).

56
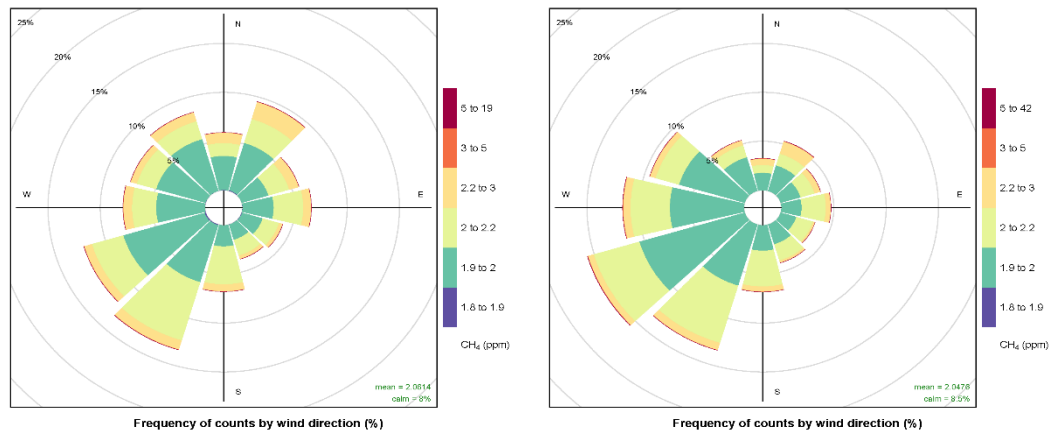
Figure 52. Concentration (as per colour scale) wind rose for methane as measured at KM in the 2016–17 baseline period (left) and 2017–18 period (right). Radial extent contours define 2% frequency intervals. © University of Manchester, 2018
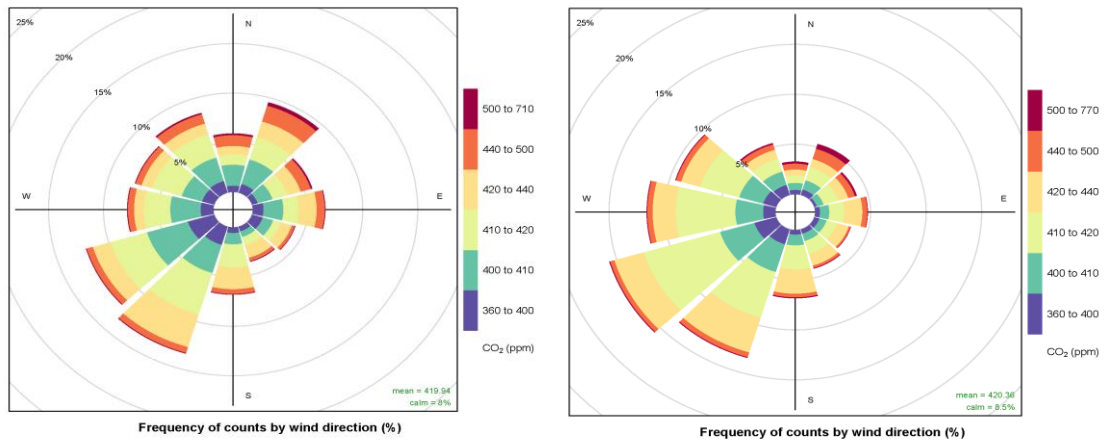
Figure 53. Concentration (as per colour scale) wind rose for carbon dioxide as measured at KM in the 2016–17 baseline period (left) and 2017–18 period (right). Radial extent contours define 2% frequency intervals. © University of Manchester, 2018
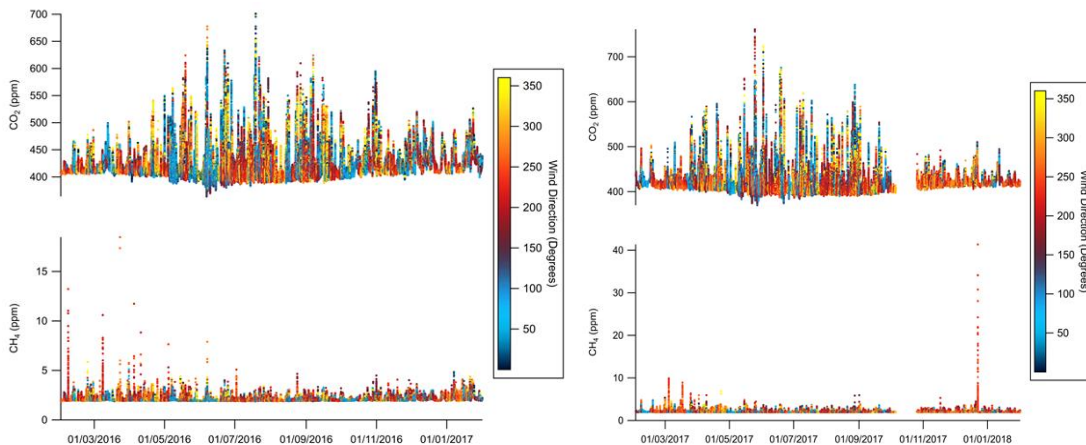
Figure 54. Concentrations (as per colour scale) in air as a function of time (x-axis) and wind direction (colour-coding) for carbon dioxide (top panels), and methane (bottom panels) as measured at KM for the 2016–17 baseline period (left panel) and 2017-18 period (right panel). © University of Manchester, 2018
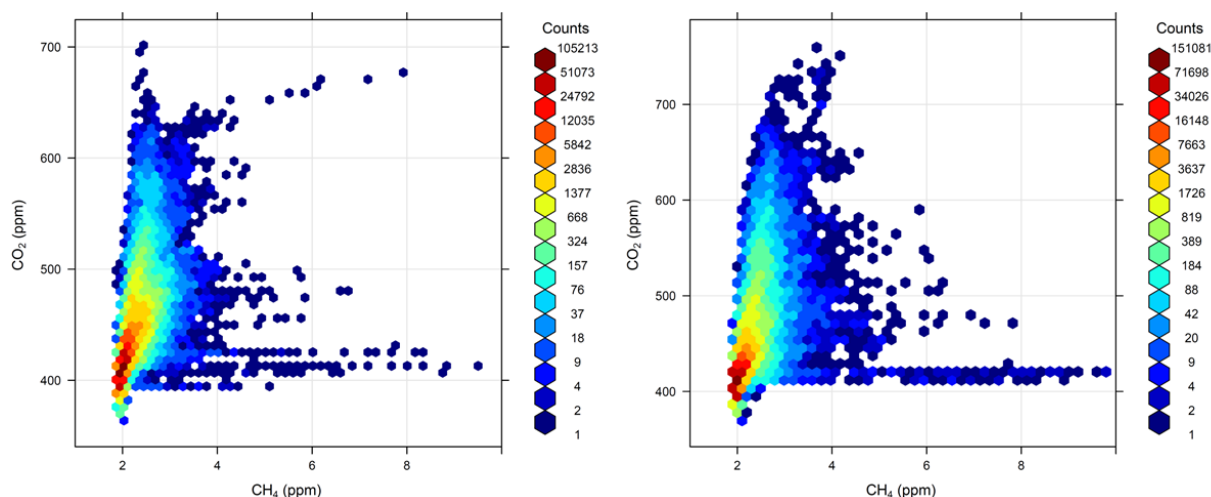
Figure 55. Coincident CO$_2$ and CH$_4$ concentrations measured at KM for the 2016-17 period (left panel) and 2017-18 period (right panel). Colours indicate the frequency density of sampling (number of coincident measurements). Note: one count refers to a one-minute period of data. © University of Manchester, 2018

Figure 55 illustrates the correlation between simultaneously-measured CO$_2$ and CH$_4$ concentration in air, colour-scaled for sampling density (each count representing a one-minute data interval) for each baseline period. Much like LP, we can note the remarkable similarity between the tracer-tracer relationship between CO$_2$ and CH$_4$ year-on-year, with the same very prominent correlation between the two greenhouse gases, and a number of (very infrequent) features where enhancements of CH$_4$ are seen at times when no change is CO$_2$ is observed, as follows:

1. A dominant mixing line (traced by red and yellow colours) with a relationship of [CO$_2$]=215.2[CH$_4$]+386.5 ppm in 2016 and [CO$_2$]=213.1[CH$_4$]+389.6 ppm in 2017 – representing co-emission (or bulk mixing) of nearby CO$_2$ and CH$_4$ sources upwind to the east and south east (based on understanding of how such concentrations relate to wind direction in Figure 54). The gradient at KM is almost twice that seen at LP (Figure 38) suggesting that CO$_2$ sources dominate the relative mix of these two gases in airmasses received at KM (compared to LP).

2. A number of clear (but very infrequent) CH$_4$ excursions (seen as the blue horizontal lines in Figure 55 in both the left and right panels) to relatively high ambient concentrations of up to 10 ppm (>5 times background), where very little change in CO$_2$ concentration is observed. However, these features represent only 635 minutes of sampling (~6.5 hours) in 2016 and ~10 hours in 2017; and are noted to occur mostly in the spring months in light southsoutheasterly wind conditions (see Figure 54). These features are consistent with a methane-only (highly localised) source, associated with wind directions from ~200 degrees (southsouthwesterly – see Figure 54). Given that the existing Third Energy well-head is positioned ~100 m upwind from the measurement site in this direction, we suggest that these enhancements may well represent detection of fugitive emissions of CH$_4$ from the existing conventional gas extraction site, which appear to be a continuous feature across both baseline periods.

3. A dominant red cluster centred at ~400 ppm CO$_2$ and 2 ppm CH$_4$ – this represents the dominant and frequent background signal seen in westerly Atlantic airmasses (Figure 52 and Figure 53). Note that this dominant background cluster corresponds to >210 total days of measurement in both baseline periods.

The dominant mixing line seen in Figure 55 corresponds to frequent easterly and south-easterly wind directions. Considering the location of KM, these wind directions represent air that has passed over continental Europe and the cities of southern England, respectively (including London). As discussed earlier for LP, while cities and infrastructure are a principal source of UK

pollution (including greenhouse gases), biogenic sources of greenhouse gases, such as the biosphere, landfill and agriculture would also be expected to feature in the fetch of such airmasses when upwind of the KM site.

To interpret more local sources of pollution (within ~10 km), we focus on the more transient features in the high temporal resolution dataset. To do this on an event-by-event basis for a year of data would be meaningless (and impractical) in the context of the baseline analysis here, though event-led (case study) analysis may well be advisable during any operational monitoring, especially given the observation of potential fugitive emissions at the existing Third Energy site concerning CH_4 discussed in point 2 above.
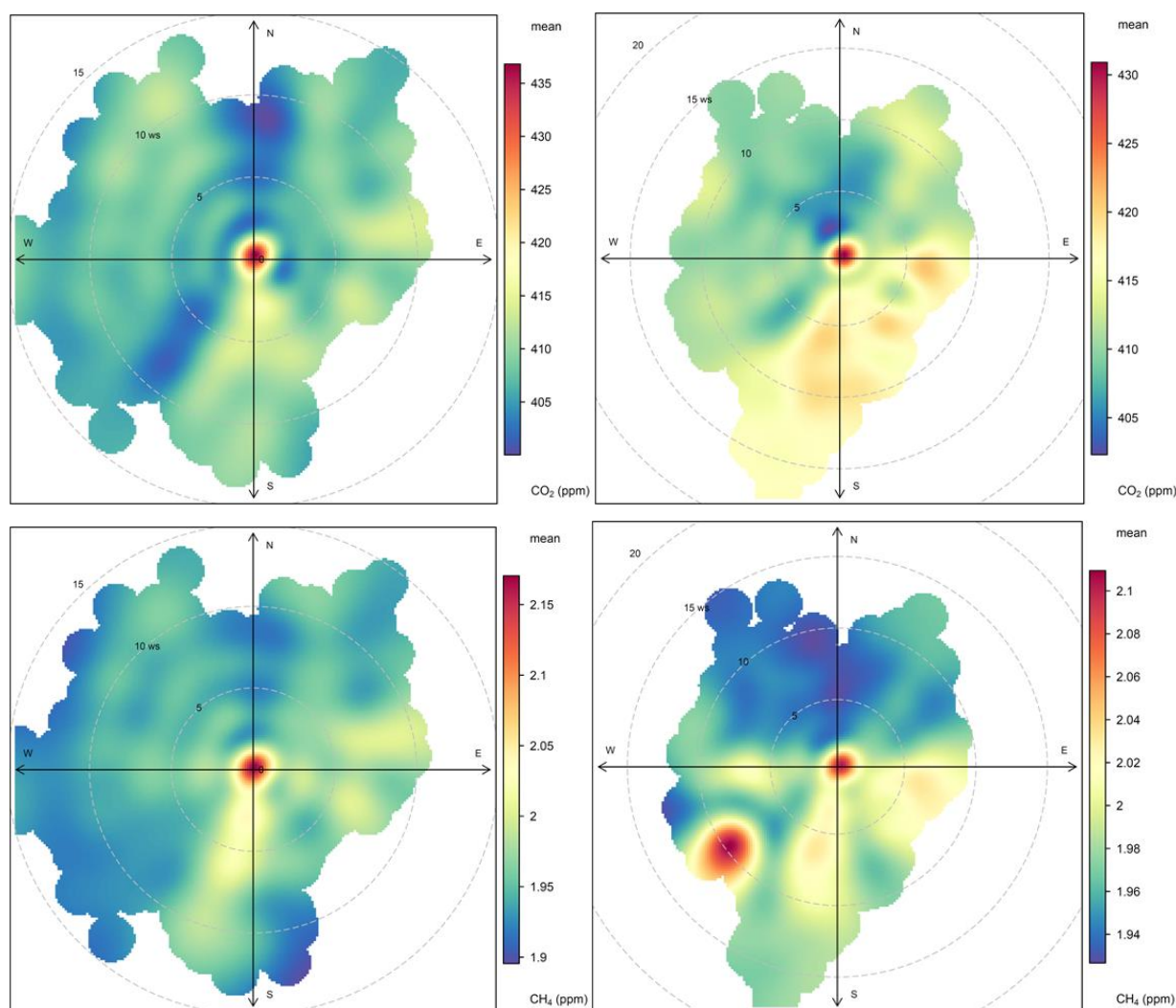
Figure 56. Polar bivariate representation of carbon dioxide (top panels) and methane (bottom panels) as a function of wind direction for the 2016-17 period (left panels) and 2017-18 period (right panels) sampled at KM. The colour scale represents the fraction of total measurement time weighted for concentration enhancement relative to the global mean (as scaled for colour in units of ppm) and wind speed (defined by the radial component - each radial increment representing 5 m/s). © University of Manchester, 2018

Figure 56 illustrates a polar bivariate representation of the relationship between both wind speed and direction and greenhouse gas concentration in both baseline periods. The colour scale in Figure 56 highlights the wind speed and wind direction conditions that dominate the overall concentration average seen at the measurement site (as a weighted mean of concentration x frequency of occurrence). The red areas seen in both panels (CO_2 and CH_4) in Figure 56 correspond to light winds (0-2 m/s) from the south west indicating a well-constrained local source for both gases (suggested to be the existing well-head at the Third Energy site). Figure 56

also shows how the absolute measured concentration relates to wind direction and wind speed, which again shows the dominant southerly, south-easterly and south-westerly origin of more elevated CH_4 and CO_2 concentrations. The fact that the red area does not extend to higher wind speeds in the southwest is consistent with an interpretation that longer range sources of pollution may not contribute significantly to periods where the greatest enhancements in concentrations are sampled at the site, i.e. that local source(s) dominate the strongest enhancements, especially in the case of CH_4.

The role of longer range (regional, national and continental) sources (mainly to the southeast) is therefore to add a smaller increment to the much larger local emission source(s) to the southwest that dominate periods of enhancement in southerly wind conditions. The lighter blue areas seen in Figure 56 in both periods, to the west, indicate a long range and diffuse source of the greenhouse gases, which is consistent with longer range transport of moderately enhanced airmasses, from the fetch to the west, which would include northern UK cities and the Pennines as well as potential longer range emissions from Ireland and in intercontinental transport from the United Stated, although this source's relative contribution to the baseline is very much weaker than those upwind sources when airmasses are received from the south east. In other words, the westerly airmass at KM can be characterised as being broadly similar to the clean westerly airmass seen at LP but with the addition of UK sources over land between the two sites such as the cities of Manchester, Leeds and Sheffield (as well as expected smaller contributions from biogenic emissions over the Pennines such as peat).

To differentiate further the role of local, regional and more distant (long range inter-continental) pollution sources, we again examine the airmass history, which can be interpreted using Hysplit Lagrangian back trajectories over the previous 5 days with endpoints at the location of the KM site at 6-hourly intervals across both baseline periods.

Figure 57 shows the airmass history of air sampled at KM for both baseline periods. This statistical representation of the history of air should be interpreted as a surface "footprint", illustrating a surface area over which air measured at KM has been influenced by potential surface sources. Figure 57 shows the frequency (as a fraction of total time, in this case as a percentage of each 12-month baseline period) that air has passed near to the surface in a latitude-longitude grid with a 1-degree or 0.25-degree spacing for the Atlantic (left panels) and UK (right panels) regions, respectively. The orange and red colours in Figure 57 indicate that air received at KM is most characterised by air that has previously passed over North West England and Wales in both baseline periods, while the light blue and green colours show that a larger area over northern England in general contributes to the annualised footprint, with wider-scale contact with Atlantic and Arctic Ocean and western and northern continental Europe (blue colours).

We can now examine the temporal patterns associated with measured concentrations. The diurnal, weekly, and seasonal variability observed for different wind directions can give additional clues as to the nature of sources and their proximity to the receptor site. Figure 58 and Figure 59 show the temporal statistics for methane in each baseline period. The top panels show the mean diurnal pattern and statistical variability (at the 95% confidence level of sampled variability around the calculated mean) in methane concentration as a function of time of day (and day of week) and coloured according to wind direction.

When illustrated in this way, we can clearly observe highly consistent diurnal behaviour for CH_4 in all wind directions and across both baseline periods. In particular, we see a consistent and repeatable diurnal minimum at around 2 pm on every day of the week across the whole year in both years. We also see a marked increase in winter months for Cluster 2 (centre bottom panels). A similar diurnal and seasonal pattern was seen for LP and linked to local (<10 km) sources. Such a pattern is consistent with the diurnal ventilation of the local boundary layer, as the height of the planetary boundary layer is lifted by convection in daylight hours (enhanced in summer months relative to winter due to solar heating), further indicating a dominant role for local

sources, which might be expected to accumulate overnight before being diluted and detrained in daylight hours.
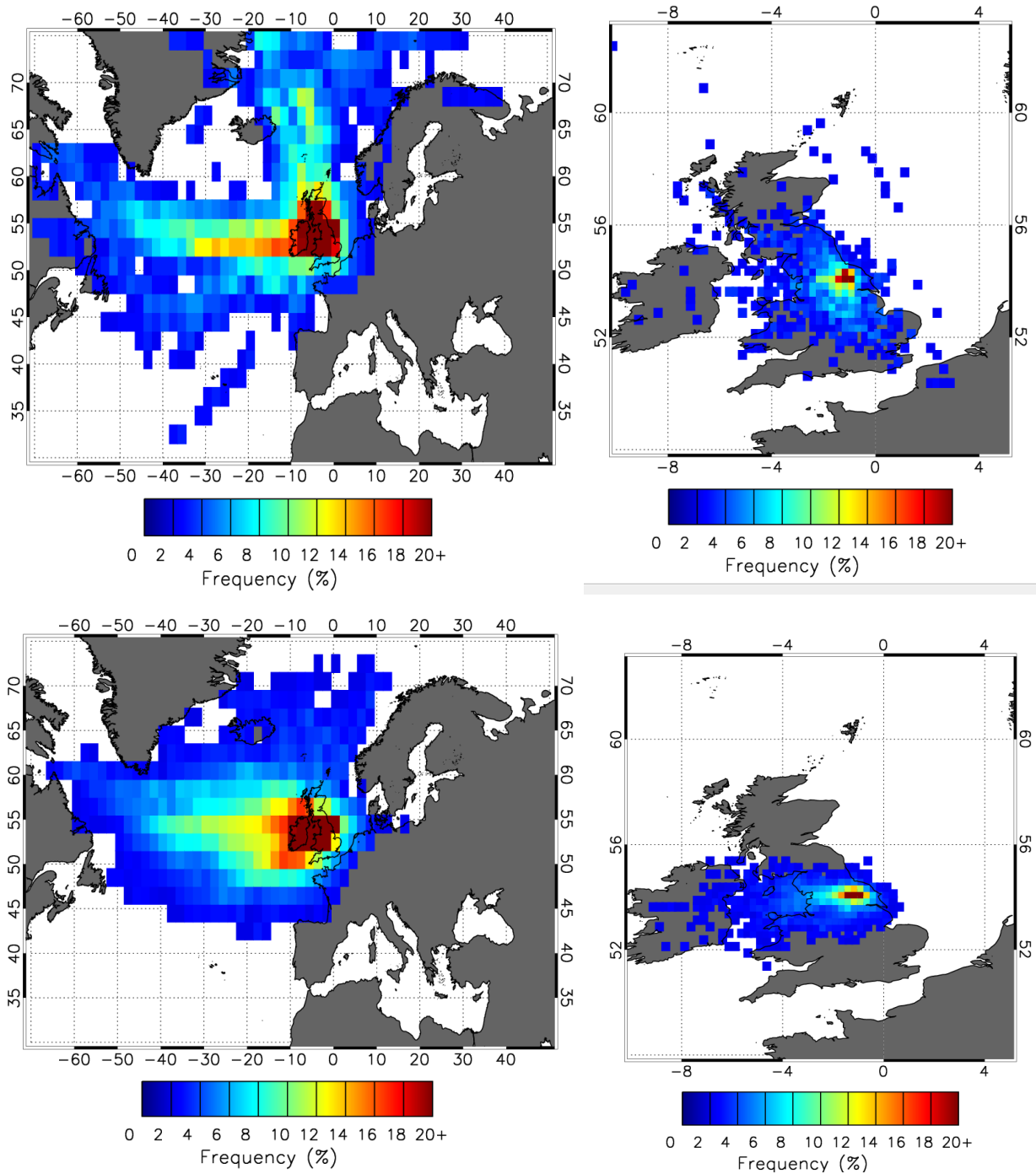
Figure 57. 5-day airmass history surface Lagrangian trajectory footprint statistics for the period 1 Feb 2016 to 31 Jan 2017 (top panels), and 1 Feb 2017 to 31 Jan 2018 (bottom panels) as seen from the KM site at a spatial resolution of 1 x 1 degree (Atlantic region - left panels) and 0.25x0.25-degree resolution (right panels). Frequency refers to the fraction of the total trajectories passing over each lat/long grid cell. © University of Manchester, 2018

There is no statistically significant signal separating days of week from the weekend across both baseline periods. A curious peak at 5 am on Sundays seen in the 2016 period is absent in the 2017 period and the early morning and late evening peaks seen on Fridays in 2017 are not consistently observed in the 2016 period.
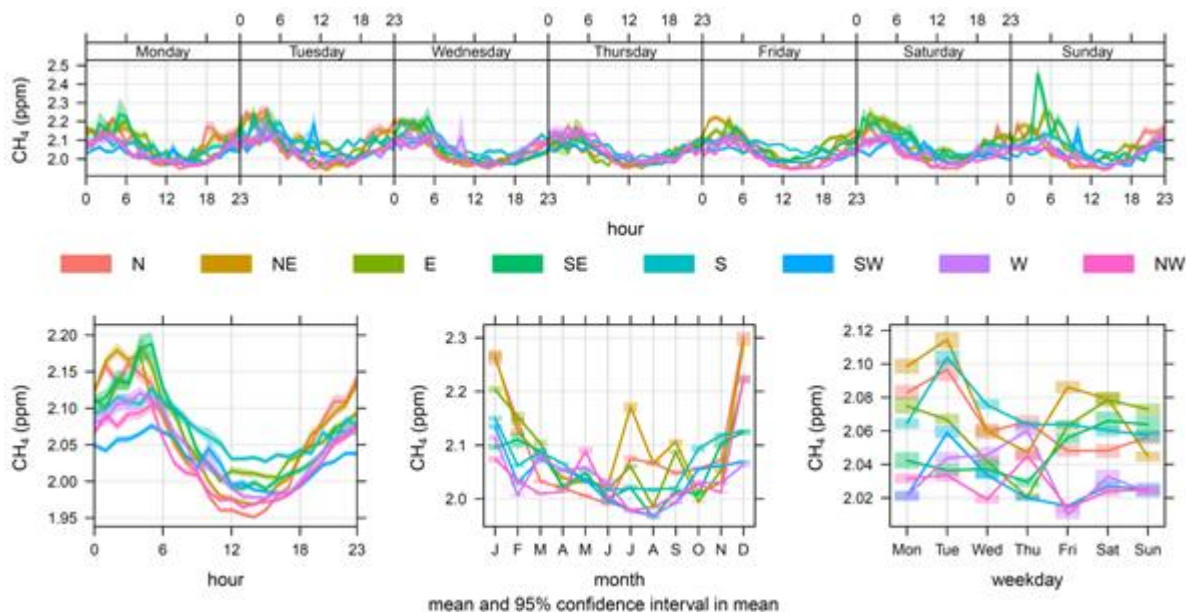
Figure 58. Temporal statistics (for the 2016-17 baseline period) of the methane climatology at KM by time and day of week (top panel), time of day over all days (bottom left), month of year (bottom middle), and day of week (bottom right). © University of Manchester, 2018
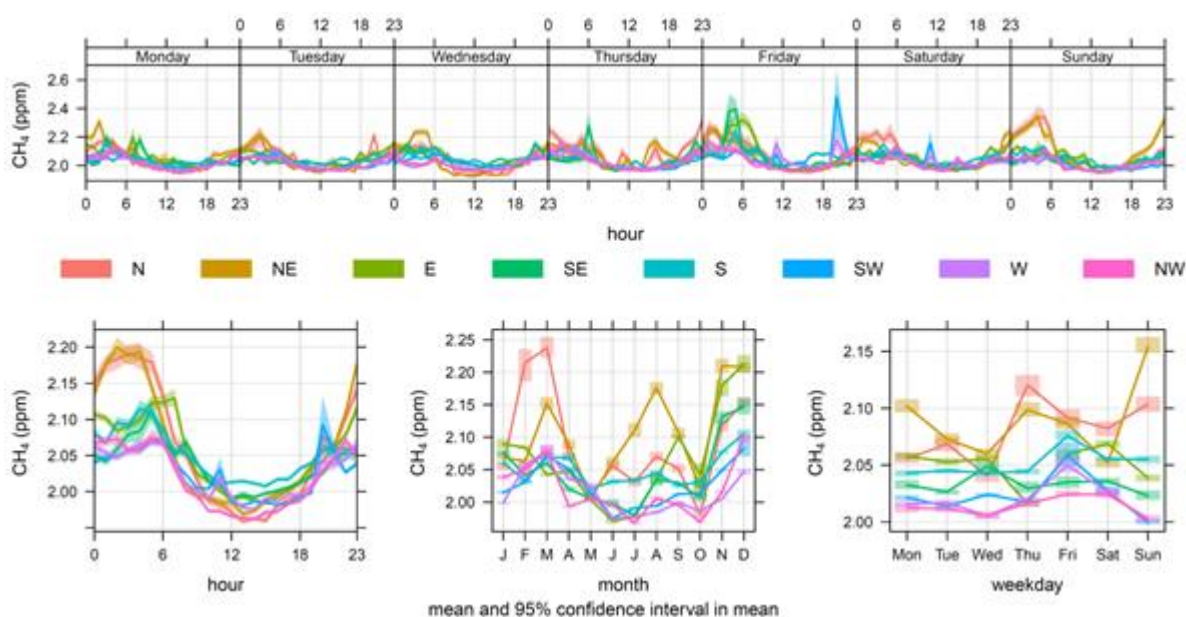
Figure 59. Temporal statistics (for the 2017-18 baseline period) of the methane climatology at KM by time and day of week (top panel), time of day over all days (bottom left), month of year (bottom middle), and day of week (bottom right). © University of Manchester, 2018

Repeating this analysis for CO_2 (seen in Figure 60 and Figure 61), we see very similar diurnal patterns due to boundary layer ventilation (top panels) across both baseline periods. However, unlike methane, a clear seasonal minimum is observed in summer months (JJA) for all wind directions except during northeasterly (both years) and northwesterly (2016-17 only).. This general feature (consistent with that seen at LP) is typical and expected to be due to the summer minimum in northern hemispheric CO_2 concentration due to biospheric respiration (uptake), which peaks in the summer months in the Northern Hemisphere. This is seen for most wind directions simply because the relative change in the seasonal background CO_2 concentration is significant when compared with the signal due to even very nearby CO_2 emission sources, unlike

CH_4 by virtue of the very small absolute mean global concentration of CH_4 around 2 ppm, which means that small mass fluxes of CH_4 can contribute a much greater relative signal on this much lower background. The source(s) of higher CO_2 concentrations observed in summer months associated with northeasterly winds remains unexplained but appears to be dominated by sampling during the hours between midnight and 6am (UT) seen in the top panel of Figures 41 and 42, with higher average concentrations on Mondays and Tuesdays (lower right panels).
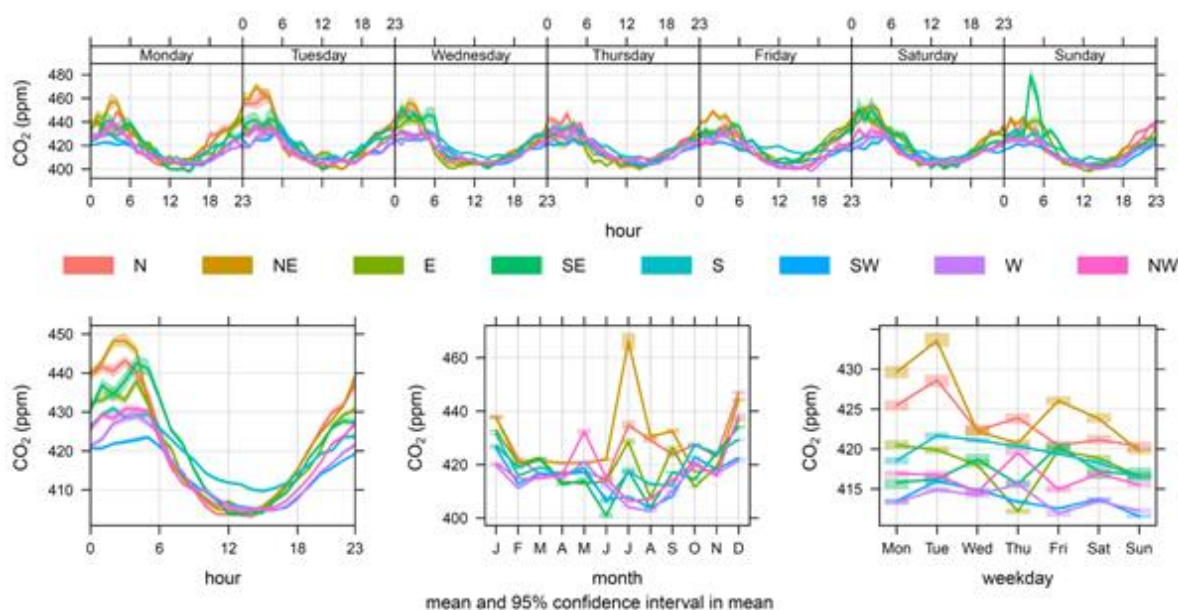
Figure 60. Temporal statistics (for the 2016-17 baseline period) of the carbon dioxide climatology at KM by time and day of week (top panel), time of day over all days (bottom left), month of year (bottom middle), and day of week (bottom right). © University of Manchester, 2018
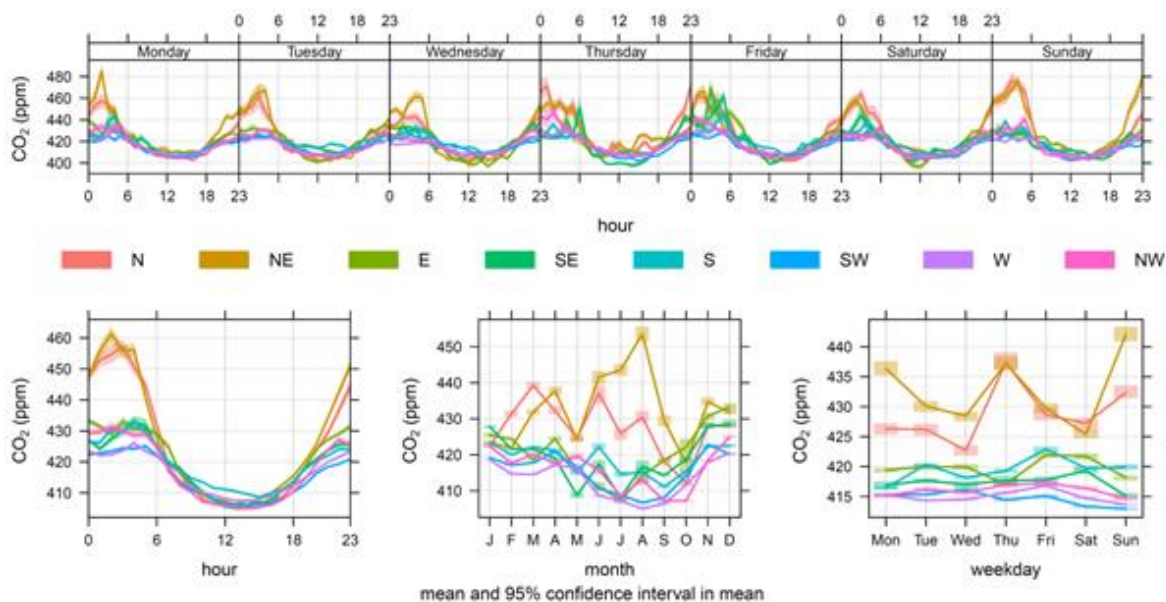
Figure 61. Temporal statistics (for the 2017-18 baseline period) of the carbon dioxide climatology at KM by time and day of week (top panel), time of day over all days (bottom left), month of year (bottom middle), and day of week (bottom right). © University of Manchester, 2018

The peak in night-time hours is explained by reduced boundary layer ventilation of already-enhanced daytime concentrations during hours of darkness. However the reasons for enhancement on Mondays and Tuesdays is less easily explained. The back trajectories (airmass histories) associated with such wind directions have a European continental origin (up to 5 days

prior to measurement), perhaps suggestive of long range transport from combustion sources in western Europe, which may be more active over weekend days. Alternatively, the enhancement may be due to increased local traffic on Mondays and Tuesdays from areas to the north east of the measurement site. However, this cannot be confirmed without case study analysis, beyond the scope of this work, and the ultimate sources of CO_2 contributing to this observation cannot be explicitly ascertained.

4.4.6.2 KIRBY MISPERTON REGIONAL MOBILE VEHICLE SURVEYS OF METHANE EMISSION SOURCES

Four 2-day surveys were undertaken during Phase 3 using the RHUL mobile greenhouse gas laboratory in Ryedale around the KM site to assess seasonal variation in the distribution and characterisation of methane sources. A total of 77 plume samples and 10 background air samples were collected for subsequent isotopic analysis across the four campaigns. The dates were:

- 28-29 June 2017,
- 26-27 October 2017,
- 30-31 January 2018 and,
- 6-7 March 2018.
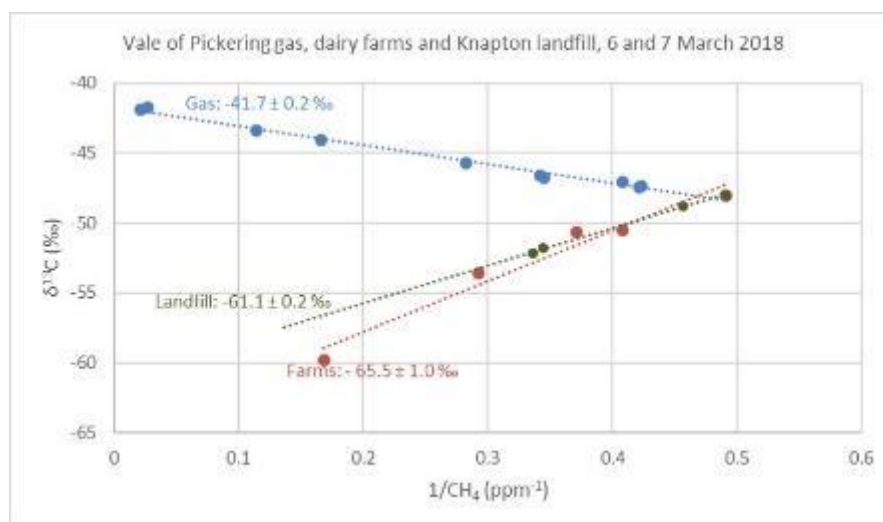
Figure 62. Keeling plot to identify methane $\delta^{13}C$ signature of gas leaks, dairy farms and Knapton landfill site in the Vale of Pickering, 6-7 March 2018. © RHUL, 2018

The main sources of methane identified in the Phase 2 report (Ward et al, 2017) persist with the landfill at Knapton giving a consistent $\delta^{13}C$ signature of -60 ±2 ‰ and the Caulklands landfill at Thornton-le-Dale giving -58 ±1 ‰ when the wind was appropriate for plume intersection (Table 3). The isotopic signatures of methane from the main sources encountered on 6th and 7th March are identified in Figure 62.

Table 9. Isotopic signatures of the main methane sources seen on each campaign to the Vale of Pickering

Source	Location (Lat, Long)	$\delta^{13}C$ signature (‰)			
		Jun 2017	Oct 2017	Jan 2018	Mar 2018
Pickering gas offtake station	54.236°, -0.762°	-40.6	-42.9	-42.0	-42.0
Gas leak, A170	54.264°, -0.905°,		-41.4	-41.5	-41.6
Gas leak, Kirby Misperton Rd.	54.207°, -0.798°	-39.9			-44.2

Knapton Landfill	54.162°, -0.644°	-58.5	-58.6	-59.6	-61.1
Caulklands Landfill	54.242°, -0.711°	-59.0		-57.9	
Dairy farms	many	-64.7	-66.2	-67.3	-65.5
Manure piles	many	-49.7	-56.7		-50.1

The fugitive emissions from the Pickering gas offtake station, 5.5 km to the NE of KM8, have been significant throughout the project with a consistent isotopic signature of -42 ±2 ‰ for up to 30 ppm CH_4 adjacent to the site and up to 10 ppm CH_4 measured across the neighbouring industrial estate to the NE. In this phase of the project (Phase 3), other gas leaks have been located; one in a small layby on the road 0.5 km ENE of Kirby Misperton village, only detected in favourable atmospheric conditions; and 3 leaks along the A170 from Keldholme to Catter Bridge, the largest being from the culvert beneath the road at the entrance to Ox Close (54.264°N, 0.905°W), 9 km to the NW of KM8, with 120 ppm CH_4 recorded from the vehicle roof inlet and distinct odours present. These have persisted throughout mobile surveying carried between June 2017 and March 2018, with a $\delta^{13}C$ signature of -42 ±3 ‰.
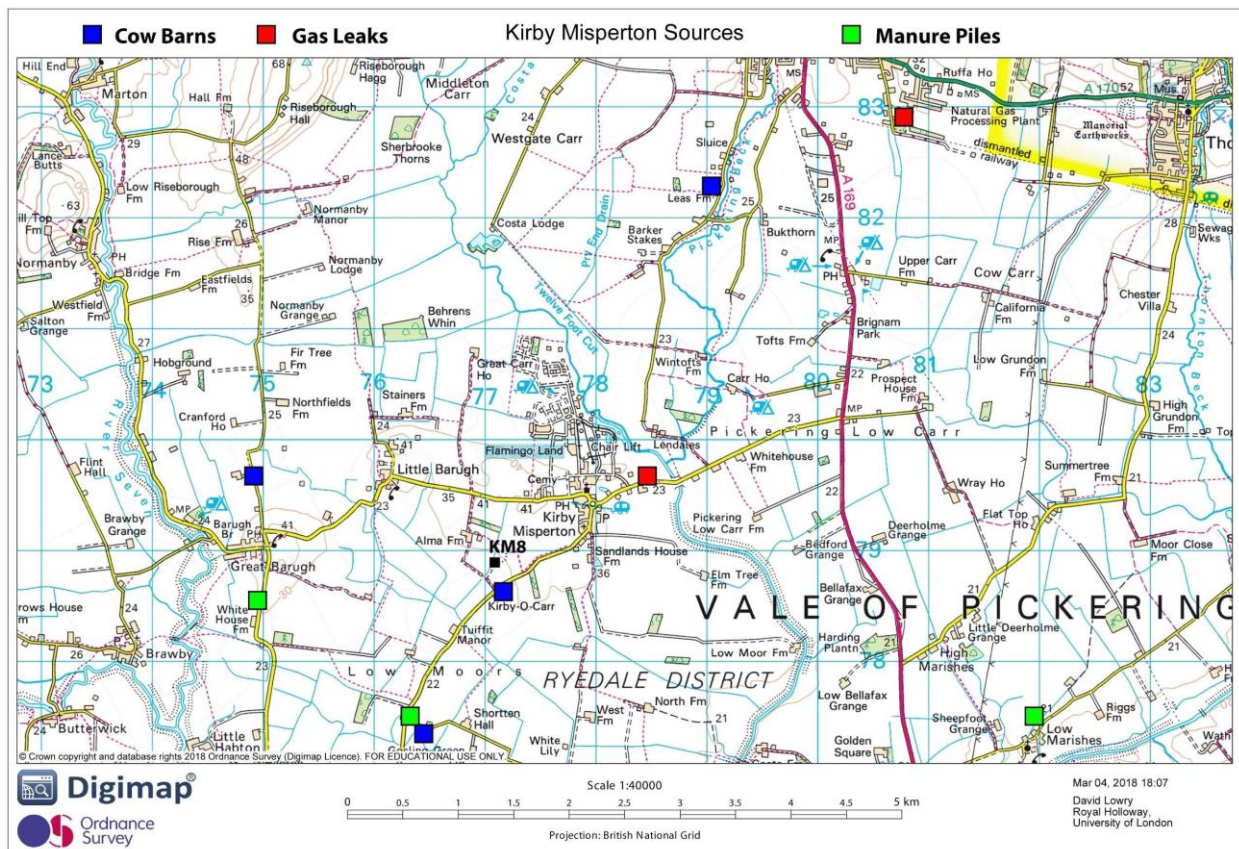
Figure 63. Location of the main methane emitting sources by category within the vicinity of the KM8 well site. © RHUL, 2018

As in the Fylde region the isotopic signatures for agricultural sources varied across the seasons between the ruminant breath (-71 ‰) and waste (manure piles, -50 ‰) end members. The farm at Kirby-o-Carr, opposite the track entrance to KM8 emits methane from the cow barn, but the prevailing westerly winds during the Phase 3 campaigns resulted in a dispersed plume being detected only during the March 2018 campaign and reaching Kirby Misperton village. Further afield, 1.5 km SW of KM8, a 3m high manure pile was located at the Blansby Lane intersection during summer months, with the nearby cow barn (54.187°N, 0.830°W) being a regular emitter of CH_4 plumes. The largest barn plumes were measured from Leas Farm 1.5 km SW of

Pickering. While a range of cow barn signatures from -71 to -56 ‰ have been measured during phase 3, the mean signature recorded is -66 ±2 ‰. This is depleted compared to the Fylde region, but may indicate a better separation of the waste sources from animal groups.
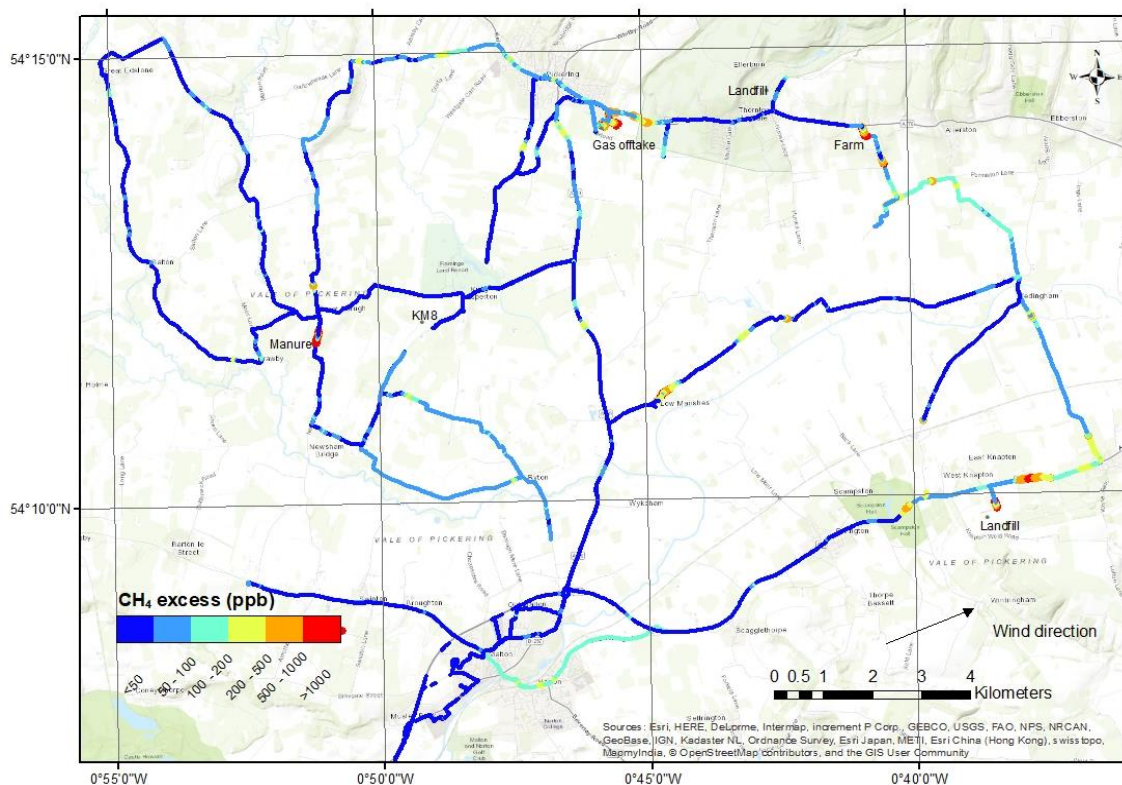
Figure 64. Excess methane mole fraction above baseline for the Vale of Pickering survey area, 26 October 2017. The baseline for each survey day is defined as the average of the 2nd percentile of the data. © RHUL, 2018

No distinct evidence of significant methane emission from the location of the KM8 well was seen on any of the campaign days in the Vale of Pickering. The methane sources close to the KM8 site discussed above are shown highlighted by source category on Figure 63, then shown in the aerial image giving rise to methane mole fractions >500 ppb above the baseline for the campaign on 6 March 2018 as seen on Figure 66. The prevailing winds will carry CH_4 with a depleted isotopic signature over the KM8 site. Only during NE-E winds is there a possibility of isotopically-enriched CH_4 from the gas leak being detected on site. Examples of the GIS maps created to show methane excess over baseline along the survey routes are shown for 26 October 2017 (Figure 64) and 6 March 2018 (Figure 65).

The larger fugitive natural gas sources in the Vale of Pickering have proven to be a good test of the methane-ethane instrument. Despite the isotopic signatures of natural gas in both the Fylde and the Vale of Pickering falling into the $\delta^{13}C$ range of -41 ±2 ‰, there is a significant separation in methane:ethane ratios, being lower at 11–14 in the KM region (Table 10), and therefore having higher ethane at 6.7-8.2 ‰. A vehicle exhaust emission sampled near the centre of Pickering had a ratio of 1.5 (40 % ethane) (Figure 67). This distinction between ratios of regional gas and combustion sources, suggests that any emissions to atmosphere from shale gas operations could be identifiable using this method.
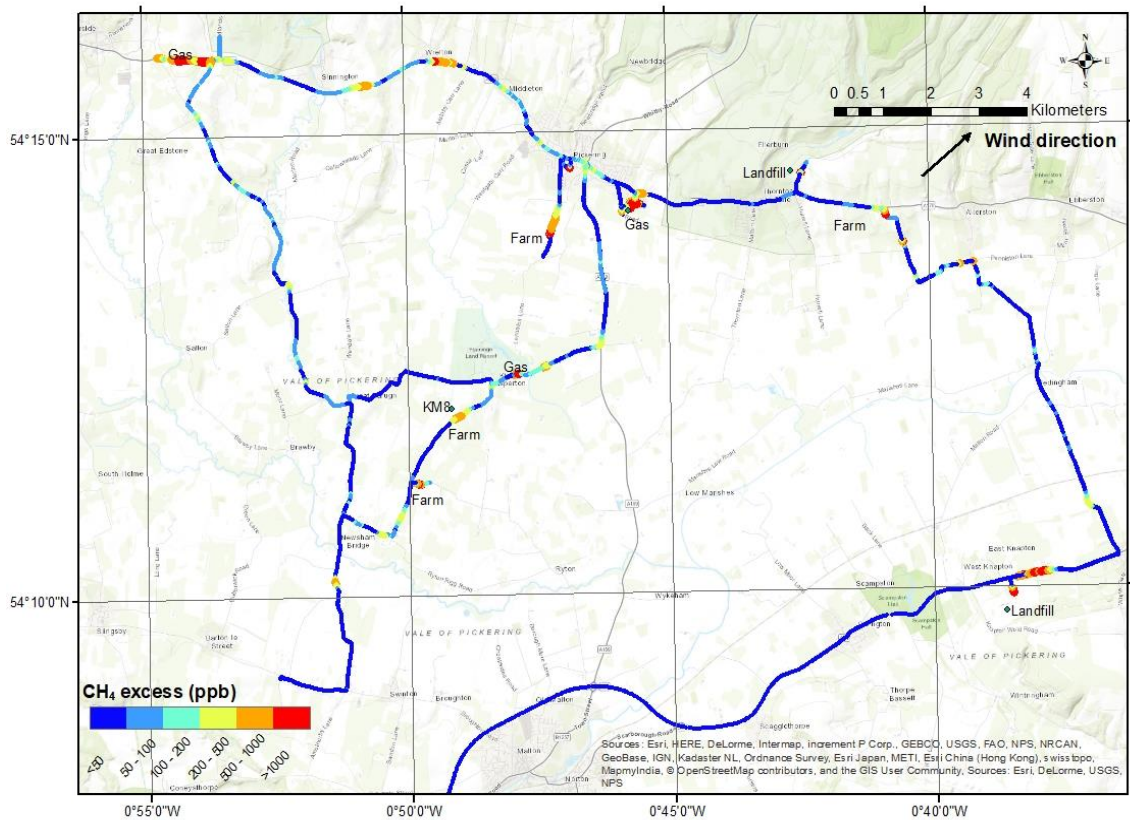
Figure 65. Excess methane mole fraction above baseline for the Vale of Pickering survey area, 6 March 2018. The baseline for each survey day is defined as the average of the 2nd percentile of the data. © RHUL, 2018
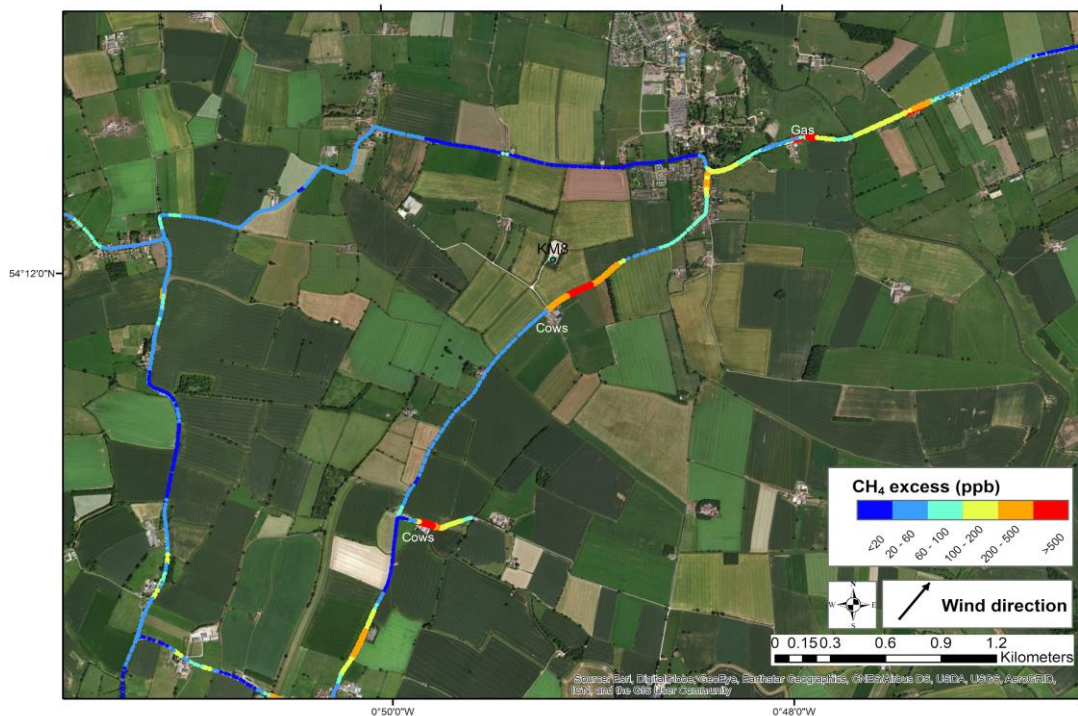
Figure 66. Excess methane mole fraction above baseline for the area around the KM8 well, Vale of Pickering, 06 March 2018. The baseline for each survey day is defined as the average of the 2nd percentile of the data. Note methane elevations from dairy farms to the S and SSW and a gas leak to the ENE of the KM8 site. (Basemap imagery sources: Esri, DigitalGlobe, GeoEye, Earthstar Geographics, CNES/Airbus DS, USDA, USGS, AeroGRID, IGN, and the GIS User Community). © RHUL, 2018

Table 10. Methane:ethane ratios and % ethane calculated for fugitive gas emissions identified during the Vale of Pickering 6-7 March 2018 mobile survey.

Source	Location	Max CH$_4$ excess (ppm)	Max C$_2$H$_6$ excess (ppm)	CH$_4$:C$_2$H$_6$ ratio (CH$_4$ excess)	% C$_2$H$_6$
Day 1 - Pickering Offtake Station plume downwind	54.238°N 0.759°W	6.00	0.49	12.4 ± 0.4 (>3 ppm excess)	7.5
Pickering Offtake Station - adjacent	54.236°N 0.762°W	27.93	2.34	12.9 ± 0.6 (>3 ppm excess)	7.2
A170 Keldholme roadside leak 1	54.264°N 0.905°W	107.77	10.30	12.3 ± 1.0 (>3 ppm excess)	7.5
A170 Keldholme roadside leak 2	54.264°N 0.884°W	6.98	0.52	13.5 ± 0.4 (>3 ppm excess)	6.9
Day 2 - Pickering Offtake Station – adjacent	54.236°N 0.762°W	6.10	0.47	13.3 ± 2.0 (>3 ppm excess)	7.0
Pickering – vehicle emission	54.245°N 0.779°W	0.18	0.11	1.5 ± 0.2 (>0.05 ppm excess)	39.7
Kirby Misperton gas leak	54.206°N 0.798°W	0.96	0.08	13.9 ± 1.9 (>0.5 ppm excess)	6.7
A170 Keldholme roadside leak 1	54.264°N 0.905°W	143.66	14.13	11.2 ± 0.6 (>3 ppm excess)	8.2
A170 Keldholme roadside leak 2	54.264°N 0.884°W	2.06	0.166	12.8 ± 1.1 (>1 ppm excess)	7.3
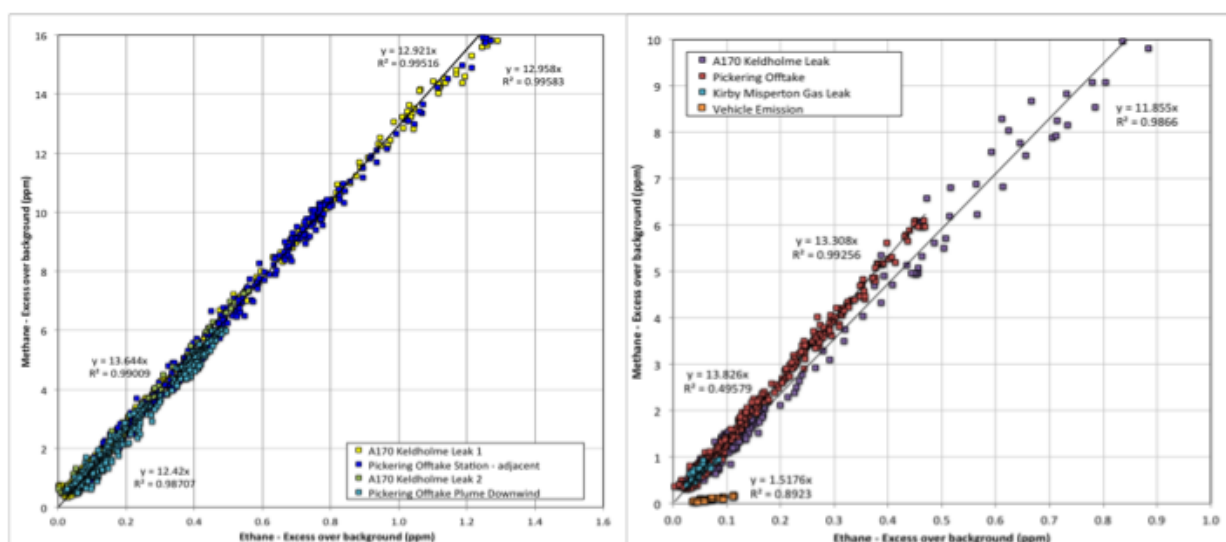
Figure 67. Methane:ethane excess cross plot for fugitive gas emissions identified during the Vale of Pickering March 2018 mobile surveys. Left: 6th, Right: 7th. The multiplier of x is the ratio for the whole plume with CH$_4$ excess >0.5 ppm, except for the vehicle emission, which is >0.05 ppm. © RHUL, 2018

4.5 DISCUSSION OF GREENHOUSE GAS RESULTS AND BASELINE

A summary of the baseline statistical climatology for both sites and for both annual periods is presented in Table 11 and Table 12. We first discuss this climatology for each site separately, before comparing features between both sites.

4.5.1 Little Plumpton – greenhouse gas summary

The summary features of the greenhouse gas baseline climatologies across both baseline periods for the Little Plumpton area can be defined broadly as follows:

- There are clear periods of what can be defined as a "background" (accounting for 50%–60% of the time over both the 2016 and 2017 periods). Background conditions can be conceptualised as conditions where CO_2 and CH_4 concentrations are around 400 parts per million (ppm) and 2 ppm, respectively. These background conditions coincide strongly and exclusively with winds from a direction between 190 and 350 degrees (i.e. from western quadrants), and represent a typical (but seasonally-variant) Northern Hemisphere average concentration.

- There are prolonged periods (several consecutive days) of marginally enhanced CO_2 and CH_4 between 400-450 ppm and 2-4 ppm, respectively, in both baseline periods. These periods coincide most often with moderate south-easterly or easterly winds. These features are consistent year-on-year, with an interpretation suggesting that these episodes represent regional pollution inputs from cities to the south and east such as Manchester, and the cities of Central and Southern England.

- There are short-lived (less than a few hours) but large enhancements (often referred to as "spikes" or "transients") in the time series data, characterised by measured concentrations greater than 4 ppm CH_4 and 500 ppm CO_2). These coincide most often with light easterly and south-easterly and northerly wind directions. These short-lived features in the data, often superimposed on a broader regional increment (enhancement) as described above, are strongly expected to represent local (<10 km upwind) sources such as nearby agricultural activities, roads, and landfill, with the dominant nearby source of methane being a dairy farm 1km to the east of the Cuadrilla site, and, in the case of carbon dioxide, the Preston New Road main road immediately to the south.

- For most of the time (>90% of both periods), CO_2 and CH_4 display common (correlated) patterns, in that both gases are often seen at their respective background concentrations, or are mutually enhanced with a scalable linear relationship. This suggests that most pollution arriving is contained within well-mixed regional airmasses with a mix of common greenhouse gas sources. However, the least frequent, but greatest enhancements, in greenhouse gases are independent of each other and represent a sole (strong and local) source, in this case the dairy farm and Preston New Road traffic emissions.

The climatological annualised GHG statistics for the LP site are given in Table 5 in the following Section, which presents a statistical comparison for both greenhouse gases at both sites and over both baseline periods. The mean concentrations of CO_2 and CH_4 are slightly elevated (4.5% in the case of CO_2, and 18.4% for CH4) compared with the Northern Hemispheric tropospheric average for 2016 (~400 ppm and ~1850 ppb, respectively), with very similar enhancements (4.1% and 11.6%, respectively) in 2017. This is expected due to the position of LP on land and exposed to sources of emission both locally and regionally. The one-standard-deviation variability around the mean is large but highly consistent across both periods: 4.8% for CO_2 and 29.5% for CH_4 in 2016, and 3.8% and 18.5%, respectively, in 2017. The large variability around the mean reflects the variable airmasses that impact the site, while the consistency in variability year-to-year reflects the highly similar overall wind climatology reflected in the back trajectory footprint analysis.

The higher CH_4 variability is expected to be linked to the more variable nature of local sources (such as agriculture and landfill identified in the mobile surveys). Such sources vary with time

and respond to environmental conditions such as temperature, soil moisture and pressure. The interquartile and interdecile ranges for both gases are constrained to 6.5% for CO_2 and 17% for CH_4 relative to the mean, while the extrema (99th percentiles), extend to 16% and 215% of the mean for CO_2 and CH_4, respectively. This demonstrates that for the vast majority of both baseline periods (80%), concentrations do not vary by more than ~20% at most). However, shorter period, extreme events (accounting for 1% of each baseline period), can see concentrations of CH_4 double that of the mean climatological concentration. Such periods are identified with episodic local emissions, lasting for a few hours at most, and appear to be linked predominantly to the nearby dairy farm.

4.5.2   Kirby Misperton – greenhouse gas summary

The summary features of the greenhouse gas baseline at Kirby Misperton can be defined broadly as follows:

- There are clear periods of what can be defined as a "background" (accounting for between 40%-55% of the sampling time across both periods) - where CO_2 and CH_4 concentrations are around 400-420 parts per million (ppm) and 1.8-2 ppm, respectively. These periods coincide mostly with periods of westerly quadrant winds; and represent a typical (but seasonally-variant) Northern Hemispheric average concentration for these greenhouse gases.
- There are prolonged periods (several consecutive days) of marginally enhanced CO_2 and CH_4 between 410-450 ppm and 1.9–2.5 ppm, respectively. These periods coincide most often with moderate (0-4 m/s) south-easterly or southerly winds. These features are consistent with an interpretation that suggests that these episodes represent regional pollution inputs from continental Europe and the cities of Southern and Central England, including London.
- There are short-lived (less than a few hours) but large enhancements (often referred to as "spikes" or "transients") in the time series data in both periods with similar frequency (greater than 2.5 ppm CH_4 and 450 ppm CO_2). These coincide most often with very light (0-2 m/s) easterly and south-easterly and northerly wind directions. These features in the data, often superimposed on the more regional increment describe above, are expected to represent local (<10 km upwind) sources such as nearby agricultural activities, roads, and landfill. It is notable that such transient enhancements in CH_4 at KM typically extend to lower maximal concentrations compared with the much larger enhancements seen at LP due to the increased presence of nearby agricultural activity and major roads at the LP site.
- For most of the time (>90% of the period), CO_2 and CH_4 display common (correlated) patterns, in that both gases are often seen at their respective background concentrations, or are mutually enhanced with a scalable linear relationship. However, infrequent periods of strong CH_4 enhancement, which were not coincident with CO_2 enhancement, were observed at KM suggesting the presence of a non-combusted (fugitive) methane source in the local area.

The climatological annualised GHG statistics for the KM site are given in Table 11. The mean concentrations of CO_2 and CH_4 are very slightly elevated: 5.2% in the case of CO_2, and 11.4% for CH_4, in 2016, and 5.1% and 7.2%, respectively, in 2017, when compared with the Northern Hemispheric tropospheric average for each year. This mean enhancement is expected due to the position of KM on land and exposed to sources of emission both locally and regionally. We note that this mean baseline is lower than that of the LP site in terms of GHGs.

The one-standard-deviation variability around the mean is smaller than LP (at 5.8% for CO_2 and 9.3% for CH_4 in 2016, and 5.8% and 10.8%, respectively, in 2017). However, there is no detectable change in the sampled variability year-to-year. The higher CH_4 variability (compared with CO_2) is suggested to be linked to the nature of local sources, such as thermogenic fugitive emission suggested in the analysis of the mobile surveys. The interquartile and interdecile ranges for both gases are constrained to 3.4% for CO_2 and 6.8% for CH_4 relative to the mean, while the extrema (99th percentiles), extend to 22.6% and 34.0% of the mean for CO_2 and CH_4,

respectively. This extreme variability at KM is far smaller than the equivalent statistics for LP (see Section 4.5.1). This demonstrates that for the vast majority of the period (95%), concentrations do not vary by more than ~20% relative the mean for both these greenhouse gases at most). However, shorter period, extreme events (accounting for 0.1% of the baseline period), can see concentrations of up to ten times CH_4 relative to the mean climatological concentration. Such periods are identified with episodic local emissions, lasting for a few hours at most as discussed earlier, and associated with south-westerly wind conditions. These episodic features are worthy of further case study attention during any operational phase and may represent a local fugitive emission source, such as the existing Third Energy conventional gas site and well-head.

Table 11. Summary climatological statistics evaluated over the baseline period for carbon dioxide concentrations measured at the baseline site at both the LP and KM sites over both baseline periods

	KM CO_2 ppm		LP CO_2 ppm	
	2016/17	2017/18	2016/17	2017/18
Mean	419.94	420.28	417.54	417.38
Std dev	24.62	24.42	20.16	15.82
0.1 %-ile	379.82	381.59	386.85	392.01
1 %-ile	390.28	392.77	390.20	395.38
10 %-ile	397.61	399.57	397.39	402.11
25 %-ile	406.31	407.94	405.31	408.18
50 %-ile	413.08	415.65	411.68	413.66
75 %-ile	426.86	424.37	426.26	422.20
90 %-ile	448.31	441.04	443.88	436.57
99 %-ile	515.42	528.59	485.25	474.61
99.9 %-ile	587.50	617.38	541.96	511.84

4.5.3 Comparison of greenhouse gas baseline at both sites and across baseline periods

Comparing data from both measurement sites offers insight into the potential transferability of baseline datasets. In this section, we briefly compare the measurements at each site in the baseline period.

In our Phase 2 report (Ward et al, 2017), and in Section 4.4 of this report, we examined the data from both sites separately. It was seen that there are many periods where CO_2 is simultaneously enhanced at both sites, occasionally with a short lag of a few hours between transient features. However, there are notable times when this is not the case, or when one site appears to lag the other by up to a day or two. Such lag patterns reflect the advection of airmasses across the UK and also indicate that both sites often sample similarly polluted airmasses in terms of CO_2. However, the picture is much more complicated for CH_4. While some peaks in CH_4 are observed at similar times at both sites, the magnitude of the enhancement compared with the ~2 ppm background is markedly different. Many such periods coincide with light easterly winds at the LP site, and with southerly quadrant wind directions at the KM site. It is interesting to note that LP is broadly upwind of KM in a prevailing north-easterly wind regime and that the enhancements seen at LP might be expected to represent sources of methane in the fetch between the two sites. However, for the largest enhancements in methane especially (at both sites), the wind direction does not connect the two sites, strongly suggesting a dominant role for more local sources of methane gas. In the LP case, this source is dominated by the nearby dairy farm, whereas at KM, the local source remains unidentified and worthy of further study. The wind direction for infrequent but strong deviations from baseline at KM does connect with existing onsite infrastructure. However, the mobile surveys have also identified other strong localised sources such as other natural gas infrastructure and pipelines in the area upwind on such

occasions. Additional measurements immediately upwind of the KM Third Energy site (beyond the fenceline) would be needed to isolate and deconvolve on-site emissions from other local sources that may be contributing to such episodes and this should be a focus of future case study work in potential operational phases.

Table 12. Summary climatological statistics evaluated over the baseline period for methane concentrations measured at both sites over both baseline periods. © University of Manchester, 2018

	KM CH$_4$ ppb		LP CH$_4$ ppb	
	2016/17	2017/18	2016/17	2017/18
Mean	2061.43	2046.19	2187.63	2109.32
Std dev	191.62	220.35	644.60	389.91
0.1 %-ile	1891.54	1907.74	1862.10	1905.25
1 %-ile	1909.84	1918.66	1891.21	1915.51
10 %-ile	1932.87	1939.06	1920.74	1937.26
25 %-ile	1953.26	1957.97	1939.85	1951.89
50 %-ile	1997.76	1993.03	2001.48	1987.18
75 %-ile	2095.12	2062.28	2198.92	2103.99
90 %-ile	2272.71	2201.75	2562.11	2376.85
99 %-ile	2763.12	2719.63	4721.52	3737.94
99.9 %-ile	3453.89	3677.31	9525.69	6230.16

4.5.4 Comparison between mobile surveys in both regions

Both regions show strong similarities of sources within the environs of the drilling sites with sources being dominated by cow barns, gas leaks and a smaller number of manure piles. There are more sources in the LP region than the KM region, but the gas leaks in the Vale of Pickering are bigger emitters than those in west Fylde. The isotopic characterisation of the sources in both regions are strongly comparable with generally tight clustering of signatures for the main sources at -58 ‰ for landfills, -50 ‰ for manure piles and -41 ‰ for gas leaks. Only the ruminant animal husbandry shows a greater spread of values in both region depending on proportions of breathing animals to waste product and their location in barns or dispersed in fields, so this has a seasonal variability. The landfill and animal signatures are consistent with those observed in other areas of the UK, whereas the gas from these regions of northern England are depleted compared to signatures observed in SE England of -36 ± 1 ‰ (Zazzeri et al., 2017), a feature that is undergoing further investigation.

The most significant difference between regions identified to date is in the methane:ethane ratio of the distributed gas in each region, being in the range 11–14 in the Vale of Pickering and 17–20 in the Fylde. As this is new instrumentation there are currently few measurements of gas leak sources from outside of northern England for comparison.

Table 13. Summary comparison of findings from methane mobile surveys between the two regions

Parameter	Little Plumpton & Environs	Kirby Misperton & Environs
δ^{13}C range cow barns	-68 to -56 ‰	-71 to -56 ‰
δ^{13}C range animal waste	-58 to -51‰	-51 to -49 ‰
δ^{13}C range landfill	-60 to -55 ‰	-61 to -56 ‰
δ^{13}C range gas leaks	-43 to -39 ‰	-45 to -39 ‰
CH$_4$: C$_2$H$_6$ ratio	17 - 20	11 - 14
% C$_2$H$_6$	4.9 – 5.6	6.9 – 8.2
Major sources in 2 km	5 cow barns, 4 gas leaks	2 cow barns, 1 manure pile, 1
Major sources in 5 km	11 cow barns, 1 manure pile, 1	4 cow barns, 3 manure piles, 1

4.6 SUMMARY AND OVERALL CONCLUSIONS ON GREENHOUSE GAS BASELINE MONITORING AND OUTCOMES

As raised in our Phase 2 report, the differences between the two sites, especially in terms of CH_4, illustrate the need for local baseline (and directly analogous operational) monitoring. A baseline at one location is clearly not applicable as a set of useful comparable (or contextual) statistics at any other location. However, the consistency of the baseline (and baseline variability within each year) at each site separately does clearly suggest that 12 months of baseline monitoring is sufficient to establish a meaningful climatology from which to compare with analogous climatologies within the operational lifetime of onshore unconventional oil and gas well sites. We recommend that a minimum of 12 months of baseline monitoring is sufficient for future site characterisation concerning greenhouse gases where sites are in rural/semi-rural locations. However, in urban areas, or areas where there are multiple local extraneous and transient sources of gas, a longer period of monitoring might be required

The method of airmass clustering is werful in differentiating the role of local and long-range sources, and the airmass history and meteorological analysis here clearly shows that local (<10 km) sources dominate the contribution to statistically elevated concentration observations. In the case of LP, an absence of significant upwind GHG sources to the west, makes future observations from this wind direction especially useful for characterising future fugitive emission linked to shale gas operations in that area. However, existing signals in the baseline at KM may complicate this, requiring us to isolate specific periods (and airmass histories) in the baseline to provide the correct baseline comparison statistics.

In all cases, it must be stressed that the levels of greenhouse gas concentrations seen at the two sites do not represent any known hazard to human health and are well within the typical range seen for any rural or semi-rural land-based measurement site. Even the largest transient enhancements seen in the collected dataset are in what would be considered to be a normal modern (post-industrial) range and the conclusions drawn in this report on the existing sources of local pollution do not represent any cause for local alarm in this author's opinion.

The statistics defined in the baseline period can be used in the following ways when comparing to analogous datasets collected in the future or during periods of new localised activity:

The background (hemispheric average concentrations) seen in airmasses associated with westerly and south-westerly origins lend themselves optimally to assessment of any incremental signal due to shale gas operations in Little Plumpton. This is because the location of the baseline site is directly to the east of the Cuadrilla's Preston New Road shale gas site, which means that any significant fugitive emission should be readily observable against the otherwise uniform and clean signal seen for this wind direction in the baseline dataset. This will allow future work to positively identify (but not quantify mass flux for) the source of emissions on site as a function of time, linking such emissions (should they exist) to site activity and phases of production.

- The observed statistics concerning pre-existing sources of nearby and regional pollution allow any shale-gas-linked emission (in future, should analogous data be collected for comparison) to be compared numerically with concentration statistics in the baseline for other (more elevated pre-existing) wind directions and emission source origins. This allows for a contextual comparison – where any localised elevations due to shale gas can be quantified statistically, as a fraction of the contribution to atmospheric composition due to non-local emission sources. The consistency of the baseline across both annual periods strongly reinforces this conclusion and validates the statistical climatology as a useful set of data from which to compare the impact of any future activity.

To summarise, the purpose of this analysis was to establish and validate the baseline climatology for the LP and KM sites to allow future comparative interpretation. In the context of greenhouse gases, this concerns the future quantification of greenhouse gas mass flux to atmosphere (fugitive emissions) from shale gas operations.

We conclude with 3 summary conclusions regarding the success of the baseline validation and future guidance:

1. The consistency of the baseline statistics year-to-year at each site separately, strongly validates the utility of these statistics in future comparative work.
2. The remarkable repeatability and similarity in both mean and statistical variability at each individual site across both annual periods suggests that 12 months of monitoring is sufficient to usefully characterise the baseline at future sites.
3. The large differences between the baselines at both sites, due to influence of local sources, demonstrate that careful thought and further work may be required to assess the spatial scale over which baselines can be usefully applicable. The current baselines are internally consistent for the LP and KM sites but may not be extrapolated to future sites proposed in different towns or council areas for example. Further modelling work, or the collection and analysis of future site-specific baseline datasets may be required to understand this. However, monitoring needs should be decided in the context of their use, e.g. for receptor exposure to air pollution, or in the quantification of GHG emissions.

4.7   AIR QUALITY

This section reports the Air Quality (AQ) dataset for both the KM and LP measurement sites.

The statistical analysis of the AQ dataset for both sites is presented and interpreted in the context of sources of emissions using meteorological data to aid analysis. The analysis provides information on the annual climatology of air pollution at both locations along with representative insight into shorter-term variability in air pollution. The baseline analysis is framed specifically with reference to the attainment of European Commission (EC) Directive air quality standards at both locations. This uses a range of metrics including annual, 1 hour and 8 hour mean concentrations.

For KM there was a change from baseline monitoring to pre-operational monitoring on the 19th September 2017 when equipment started to be brought on to site in readiness for hydraulic fracturing operations.

4.7.1   The baseline dataset

The dataset used in this report was collected using surface monitors located at KM and LP and covers the observation period from 1 February 2017 until 28 February 2018. However as identified above the data at KM from the 19th September 2017 will not be considered as baseline but are referred to as "pre-operational".

The dataset includes local meteorology (2 m above ground), nitrogen oxides (NO and NO_2, collectively NO_x), particulate matter (PM) in a number of aerodynamic size ranges, ozone (O_3), speciated non methane hydrocarbons (NMHCs) and from 2017 hydrogen sulphide (H_2S) and sulphur dioxide (SO_2). The data are archived and publically accessible at the NERC Centre for Environmental Data Analysis (CEDA). Measurements are available at 1 minute intervals, except NMHCs which are reported as weekly values, see: http://browse.ceda.ac.uk/browse/badc/env-baseline.

The environment baseline is firstly examined on a site by site basis followed by comparison of the climatologies of pollution at each site and then to other regional UK monitoring sites operated by Defra and other agencies.

4.7.2 Results and discussion

Managing and improving air quality in the UK is driven by European (EU) legislation on ambient air quality standards and also commitments to limit transboundary emissions, through the National Emissions Ceiling Directive and the Gothenburg protocol. The 2008 ambient air quality directive (2008/50/EC) sets legally binding limits for outdoor air pollutants that impact on human health and includes NO_2, O_3, benzene, 1,3 butadiene, PM10 and PM2.5. All these species have been measured as part of the baseline project.

Within the UK, ambient air quality is controlled with the aspiration that all locations meet either the prescribed Limit Values or Target Values depending on the species. EU Limit values are legally binding concentrations that must not be exceeded. There are prescribed averaging times associated with each pollutant and for some pollutants a number of exceedances are allowed in each year. Target values are meant to be attained where possible by taking all necessary measures not entailing disproportionate costs, often reflecting natural impacts on those pollutants that can lie outside of regulatory controls. All EU directive standards are listed here: http://ec.europa.eu/environment/air/quality/standards.htm. The UK air quality objectives for data parameters measured as part of the air quality baseline are shown in Table 14.

Table 14. UK National air quality objectives

Pollutant	Concentration (limit/target)	Averaging period	Legal obligation	Permitted exceedances	Approx conversion to ppb[a]
Fine particles (PM$_{2.5}$)	25 μg/m^3	1 year	Limit value	none	n/a
Nitrogen dioxide (NO$_2$)	200 μg/m^3	1 hour	Limit value	18 per year	104.7 ppb
	40 μg/m^3	1 year	Limit value	none	20.9
PM$_{10}$	50 μg/m^3	24 hours	Limit value	35 per year	n/a
	40 μg/m^3	1 year	Limit value	none	n/a
Benzene	5 μg/m^3	1 year	Limit value	none	1.88ppb
Sulfur Dioxide (SO$_2$)	350 μg/m^3	1 hour	Limit value	24	131 ppb
	120 μg/m^3	24 hour	Limit value	3	45 ppb
Ozone (O$_3$)	120 μg/m^3	Maximum daily 8 hour mean	Target value	25 days averaged over 3 years	60.1 ppb

4.7.3 Summary of annual means of air pollutants at KM and LP

Table 15 shows a summary of the annual means of the measured air pollutants at both KM and LP. An important observation is that, over the period of measurement, there were no exceedances of annual mean limit values. For planning and development purposes, air quality issues must be taken into account when ambient air pollution concentrations approach 75% of the limit values. No air pollutants at either site reached this threshold.

Table 15. Summary of annual statistics for KM and LP locations for various air pollutants and comparison against annual mean limit values

Pollutant	Annual Mean at KM Feb 2017–Feb 2018	Annual mean at LP Feb 2017–Feb 2018	Annual mean Limit value
Ozone	17.8 ppb	22.0	60.1 ppb
PM$_{2.5}$	7.4 μg/m^3	6.9	25 μg/m^3
PM$_{10}$	10.6 μg/m^3	10.8μg/m^3	40 μg/m^3
NO	5.3 ppb	2.0	No limit value
NO$_2$	5.2 ppb	4.9	20.9 ppb

NO$_x$	10.9 ppb	6.9	No limit value
Benzene	0.14 ppb	0.32 ppb	1.88 ppb
H$_2$S from Nov 2017 at KM, Oct 2017 at LP	1.1 ppb	0.1 ppb	N/A as not full dataset
SO$_2$ from Nov 2017 at KM Oct 2017 at LP	0.4 ppb	0.2 ppb	N/A as not full dataset

Table 16. Summary of exceedances over UK national air quality limits

Pollutant	Number of 8-hours exceedances KM	Number of 8-hours exceedances LP	8-hour limit
Ozone	0	0	60.1 ppb
	Number of 24-hours exceedances KM	**Number of 24-hours exceedances LP**	24 hour limit
PM$_{10}$	2	2	50 µg/m^3
	Number of 1-hours exceedances KM	**Number of 1-hours exceedances LP**	
NO$_2$	0	0	200 µg/m^3

Exceedances for the period of monitoring covered by this report (Phase 3) are shown in Table 16. Within this measurement period there were no O$_3$ or NO$_2$ exceedances at either site. The 24 hour mean limit value for PM$_{10}$ was exceeded on 13–14th February, 2017 at KM and 14th Feb at LP. As this was observed at both sites it is likely that this was a UK-wide episode similar to that which occurred in March 2016 and was reported in the Phase 2 report (Ward et al, 2017). Other Automated Urban and Rural Network (AURN) monitoring sites run by DEFRA (Department for Environment, Food and Rural Affairs) show similar values on both the 13th and 14th February, 2017. These data can be viewed at https://uk-air.defra.gov.uk/data/. The second exceedance at LP was on the 6th November 2017 coinciding with Bonfire Night, the previous evening. Multiple open fires and fireworks result in a build-up of particulate matter in the air.

4.7.4 Spatially-resolved air pollution climatologies

The annual mean values for air pollution allow for comparison against national targets. NO$_x$, O$_3$, PM and meteorological data have all been collected at 1 minute time resolution and this is advantageous for data analysis as a more detailed climatology of air pollution can be constructed at the local scale.

The hourly average time-series for parameters measured at both sites are shown in Figure 68 and Figure 69 but these tend to only show synoptic / seasonal scale variability. As in the previous report higher O$_3$ is seen in the spring/early summer at both sites, typical for the UK. Due to instrument problems some of the summer data are missing but there do not appear to be many photochemical O$_3$ production events, a result of a generally cool summer in the UK in 2017. The difference in the O$_3$ measurements at the two sites is notable from Oct 2017 where O$_3$ decreased at KM and not at LP. This correlates with periods of higher NO$_x$ being observed at KM. The NO$_x$ spikes are correlated with lower O$_3$, which is related to atmospheric chemistry. This was highlighted in the previous report but is more noticeable in the data set reported here. In the immediate vicinity of high NO emission, O$_3$ is lost via Reaction 1 (see below), resulting in local O$_3$ depletion and the production of NO$_2$.

$$NO + O_3 \rightarrow NO_2 + O_2 \qquad \text{(Reaction 1)}$$
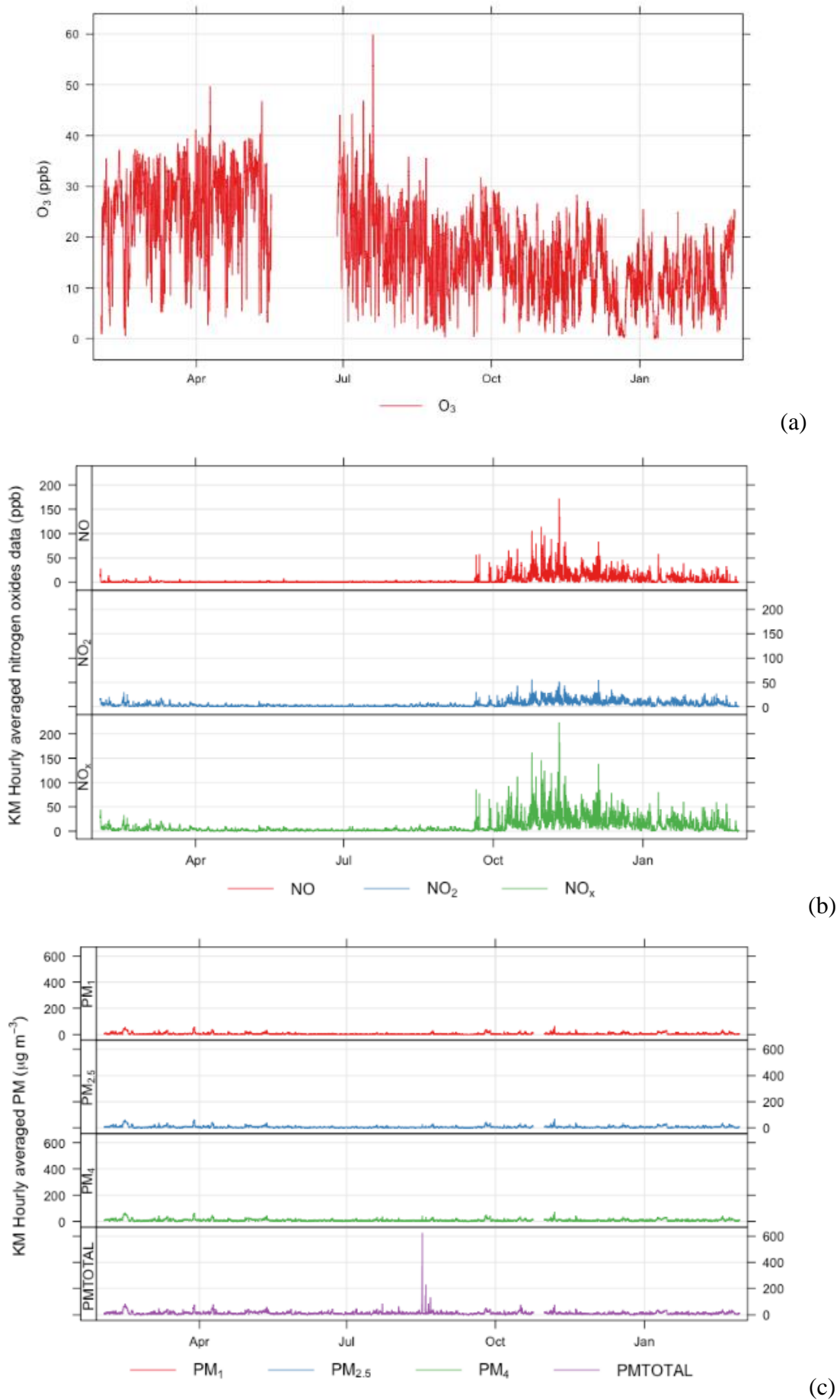
Figure 68. Annual hourly time series at the KM site for (a) O₃, (b) NO, NO₂, NOₓ (c) PM₁, PM₂.₅, PM₄, PM₁₀ and PM_Total between February 2017 and February 2018 © University of York, 2018

77
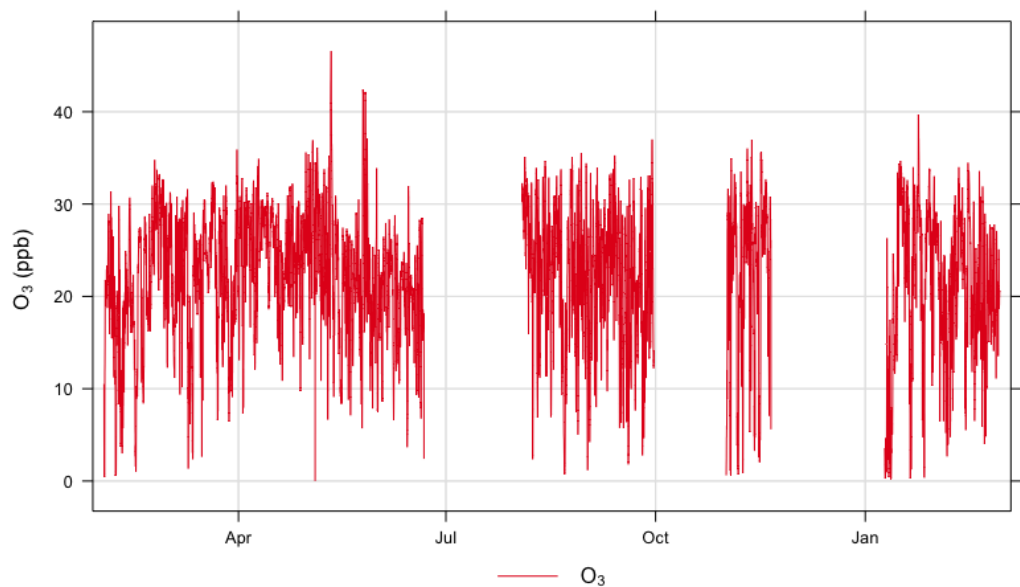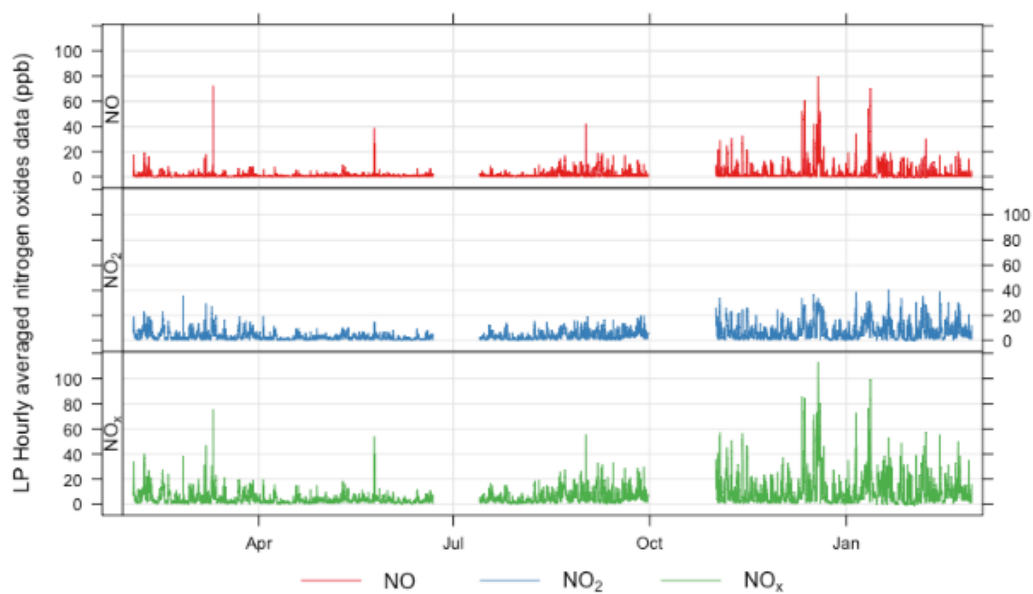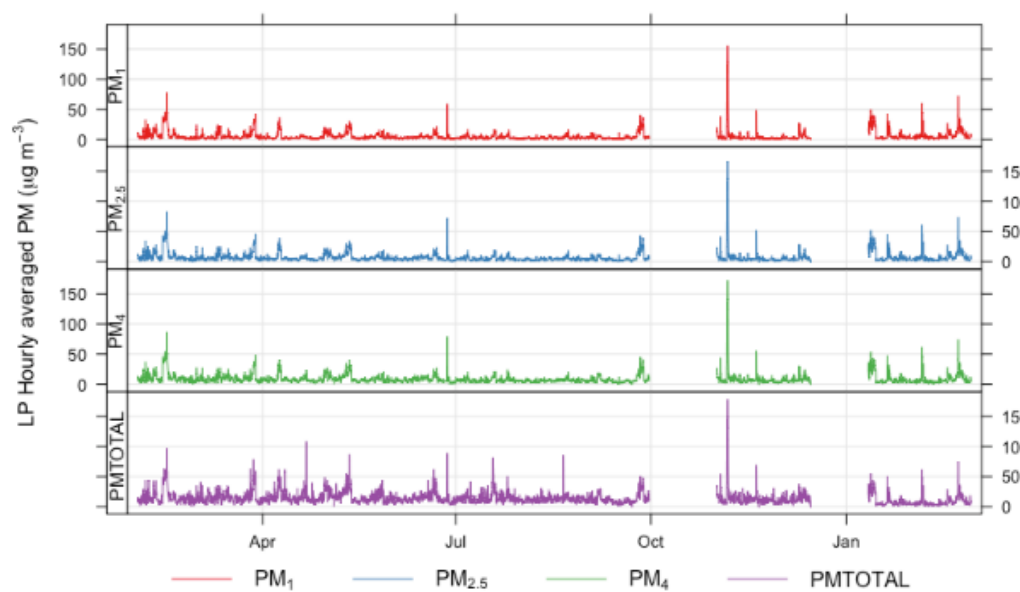
Figure 69. Annual hourly time series at the LP site for (a) O₃, (b) NO, NO₂, NOₓ (c) PM₁, PM₂.₅, PM₄, PM₁₀ and PM_Total between February 2017 and February 2018 © University of York, 2018

An increase in NOx at KM (Figure 68) after September 2017 is evident and will be discussed futher later in the report. There also appears to be an increase at LP (Figure 69), but this has not been discussed as at time at report authors will still awaiting more detail on the operations of Preston New Road well site. Conclusions on additional sources cannot be made until we have this detail.

4.7.5 Kirby Misperton detailed analysis

4.7.5.1 METRICS

To enable a full baseline climatology of air pollution to be established it is important to examine the influence of wind direction. Table 16 reports the annual means for pollutant measured under the EU Air Quality Directive whereas Table 17 reports those metrics by individual wind sector (45 deg). In a similar way to greenhouse gases, it is most common in the UK for air from the East (E) and Southeast (SE) to be most polluted as this often brings air from the SE of England and from continental Europe. The lowest concentrations of air pollution are typically observed during periods of westerly airflow. However, this was not the case for KM during this reporting period for all measurements. Whilst the PM measurements showed maxima in the SE and E wind direction, the NO_x measurements were most enhanced in the West (W) and Northwest (NW) sectors. This is different to that observed in the previous year (Phase 2) where NO_x concentrations were highest in the Southern (S) sector and lowest in the West (W) sector. This change is attributed to the change in activity levels from Autumn 2017 at the KM8 site, when the site entered the 'pre-operational' stage. This is discussed more fully in Section 4.7.5.6.

Percentiles for all the AQ parameters are displayed in the windroses in Figure 84.

Table 17. Annual means for each wind sector for KM site

	N	NE	E	SE	S	SW	W	NW
O_3 (ppb)	14.6	19.9	22.0	19.5	16.1	16.9	18.5	19.3
NO (ppb)	4.3	3.0	1.6	1.2	1.6	7.1	9.4	5.7
NO_2 (ppb)	5.2	4.0	3.7	4.0	5.4	6.6	7.0	5.3
NO_x (ppb)	9.4	7.0	5.2	5.2	6.9	13.7	16.4	11.0
$PM_{2.5}$ ($\mu m/m^3$)	7.5	8.1	13.3	11.6	9.5	6.3	5.0	5.1
PM_{10} ($\mu m/m^3$)	11.0	11.9	17.5	15.6	12.7	9.6	7.5	7.7
H_2S (ppb) Only from 19/11/17	0.9	0.8	1.1	1.2	1.2	1.2	1.3	1.1
SO_2 (ppb) Only from 19/11/17	0.6	0.6	0.5	0.4	0.5	0.4	0.3	0.4

4.7.5.2 DIURNAL VARIATION OF AIR POLLUTION AT KM

The diurnal air quality profiles for KM are shown in Figure 70. The O_3 profile in 2017 is similar to that in 2017 (Ward et al , 2017) with it being lowest at night and peaking just after midday, as expected in the general context of UK oxidative air chemistry. This reflects a combination of boundary layer height and photochemical production during the day and surface loss at night. However the NO_x and PM display different diurnal cycles when compared to the previous year. The fact that these are different is the first indication that the PM and NO_x may have different sources.
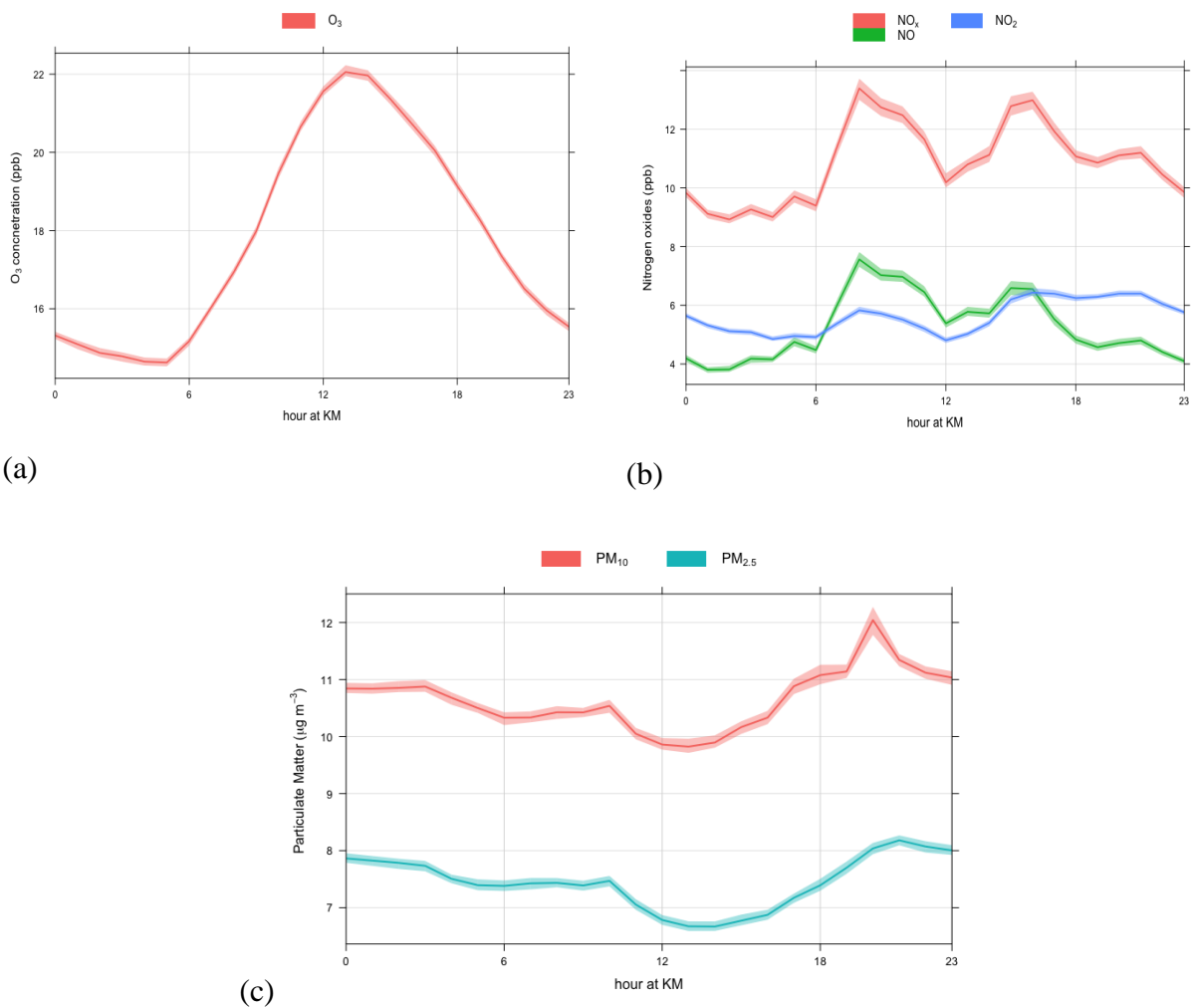
Figure 70. Diurnal variations for (a) O$_3$, (b) NO$_x$ and (c) PM. © University of York, 2018

The NO$_x$ diurnal profile shows NO and NO$_2$ increasing in the morning and again in the afternoon. This is likely to be due to a combination of boundary layer height and local traffic emission sources. The relative distribution of NO to NO$_2$ is different to the previous year (Phase 2). In Phase 2, NO$_x$ was predominately balanced towards NO$_2$, rather than NO indicating that most NO was from regional sources. In Phase 3 (this period) the balance of NO$_x$ has been shifted more towards of NO rather than NO$_2$, a clear signal that there was an increase in local sources of NO$_x$ emission.

4.7.5.3 HEBDOMADAL CYCLES

Hebdomadal cycles are shown in Figure 71. The working week (Mon–Fri) is clear in the NO$_x$ measurements with NO$_x$ being highest during the week and decreasing at the weekend. Associated with this, O$_3$ is highest on the Saturday which may be due to reduced titration from local NO (Reaction 1).
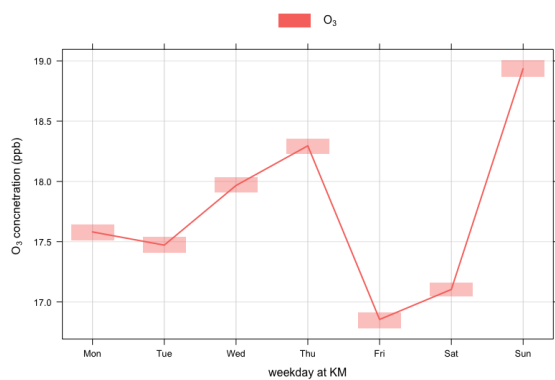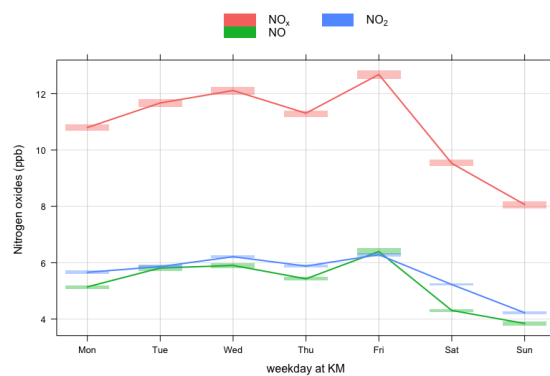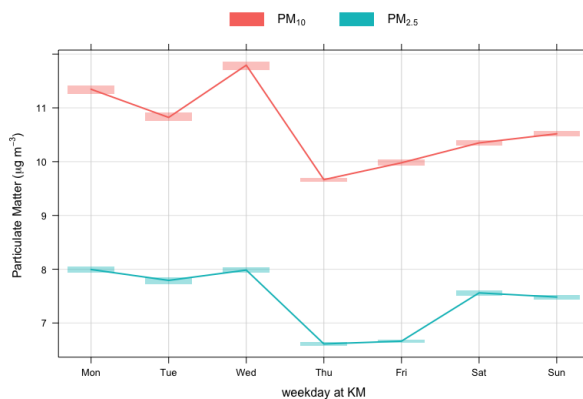
Figure 71. Hebdomadal variations at KM8 for (a) O₃, (b) NOₓ and (c) PM. © University of York, 2018

4.7.5.4 ANNUAL CYCLES AT KM

Before Autumn 2017, the KM site displayed air pollution behaviour that was typical in terms of temporal cycles at other similar locations in the UK (Figure 72). There was however a noticeable change in behaviour from September 2017 onwards, particularly in NOₓ, and this coincided with developments at the KM8 shale gas site in preparation for hydraulic fracturing operations. From this date onwards there were increased vehicle movements to, from and around the site, and the operation of on-site diesel generators. These are believed to account for the majority of increased in emissions locally; these are discussed more fully in the section on pre operational measurements.

4.7.5.5 SOURCE APPORTIONMENT FOR KM8

Figure 73 shows percentiles roses for the *in situ* air quality parameters split by season. A percentile rose places the data into 5 bands (the colour-scale) and then plots each of those by wind direction (radial axis) and concentration. The grey line is the mean for the data set. The plots are separated into season with Spring (March, April, May), Summer (June, July, August), Autumn (September, October, November) and winter (December, January, February). Figure 74 shows polar plots for the same pollutants, with concentrations (colour scale), wind direction (radial scale) and wind speed.
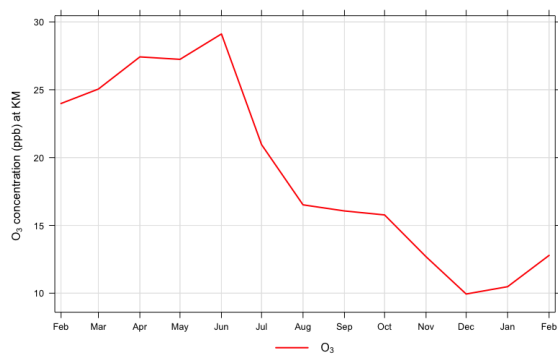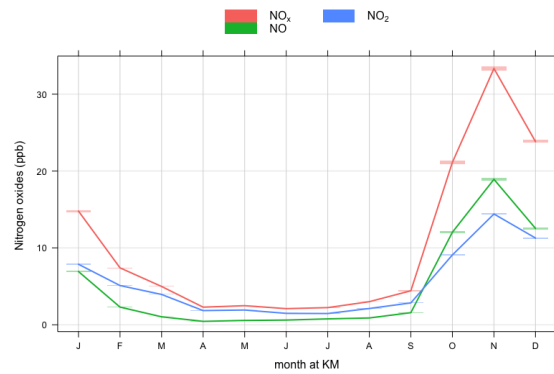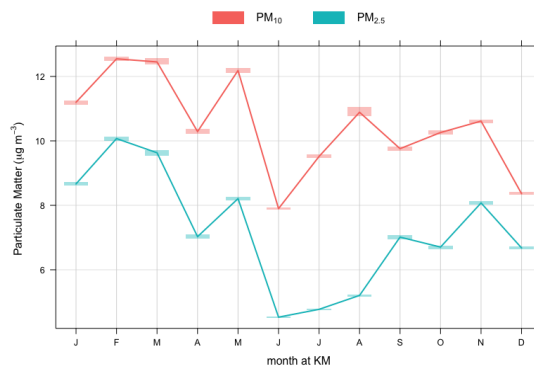
Figure 72. Annual cycles at KM for (a) O$_3$, (b) NO$_x$ and (c) PM. © University of York, 2018

For many situations concentrations would be expected to decrease with increasing wind speed due to increased dilution but there are some instances where this process can lead to increases, for example due to plume grounding or the transport of air over long distances. Combining the two types of data analysis may give some indication of source regions of pollutants, and this is done below.

As in the previous year (Phase 2), O$_3$ concentrations are highest in the spring and winter months from all wind directions except those to the direct south and at the site itself. In the winter months the highest ozone comes from the NE and is highest when wind speeds are higher, this is likely due to the impact of long range transport of this air to the site.

By breaking the analysis down into season it can be seen that the peaks in PM are during the winter and when the wind direction is from the east. This winter-time peak in PM is similar in nature to that seen in the spring of Phase 2 measurements. Wintertime NO$_x$ does not however show the same structure so it can be assumed that the PM peak is not due to road traffic or generator emissions. The increase in PM in winter could be due to low temperature burning sources in the area, for example stoves and open fires from residential properties.

The NO$_x$ measurements show a definite peak in the Autumn (September, October, November) and in wind directions from the west; this is best explained by the NO$_x$ emissions arising from significantly increased traffic and installation of generators on site during the pre-operational phase. The general trend for higher NO$_x$ concentrations from the south in the summer and winter observed in the Phase 2 period, due to extra traffic on the A64, is not as noticeable due to the much higher concentrations from the west in autumn 2017.
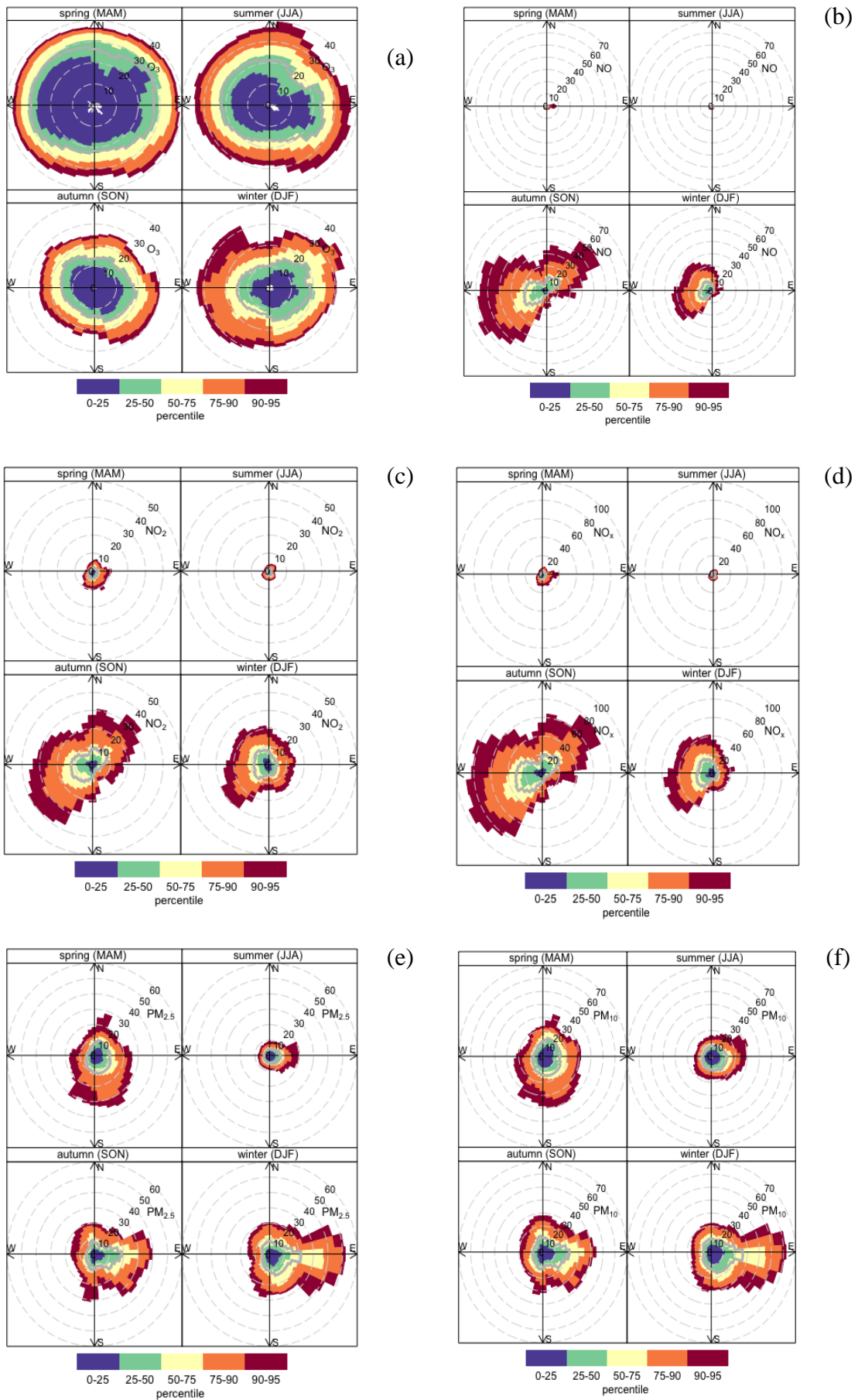
Figure 73. Percentile rose to show the 5th, and 95th percentiles at KM for (a) O_3 , (b) NO, (c) NO_2, (d) NO_x, (e) $PM_{2.5}$, (f) PM_{10}. © University of York, 2018
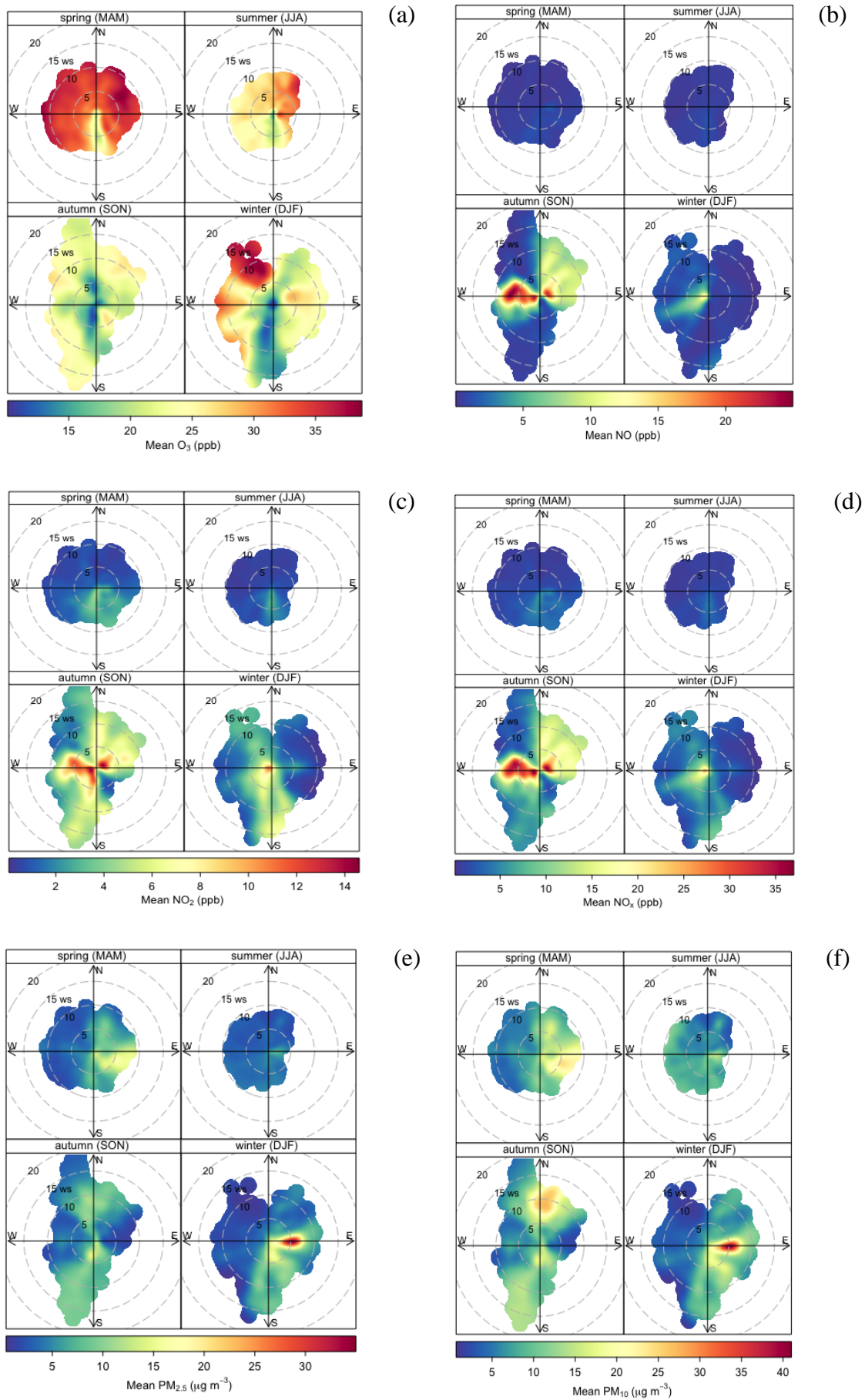
Figure 74. Polar plots for KM for concetrations of (a) O$_3$, (b) NO, (c) NO$_2$, (d) NO$_x$, (e) PM$_{2.5}$, (f) PM$_{10}$. © University of York, 2018

From 19th September 2017, the monitoring changed at the KM8 site as Third Energy started to bring equipment on to site in preparation for hydraulic fracturing. This led to a greater number of vehicle movements to, from and on the site, and in the local area. In addition to equipment being brought to site there was also an increase in traffic associated with the local protests and policing.

These activities changed the emissions at KM8 and marked the end of the baseline period when activities at the KM8 site and locally were relatively benign. Therefore changes in emission from this point forwards could be considered to be associated with the planned hydraulic fracturing (meant its broadest sense to also include local protest activities. From the 19th September 2017 to the 28th February 2018, the measurement dataset was differentiated and renamed the "pre-operational period". From the 1st March 2018, the removal of equipment from the site was commenced as operations were suspended, without hydraulic fracturing taking place, following continued delay in receiving final approval to carry out hydraulic fracturing. As a result of this, patterns in air quality again started to change again as the site returned towards a more benign state as was the case during the baseline period. The mobilisation/de-mobilisation data set will provide a unique opportunity to observe effects on air quality at a site. An analysis of this transition will be included in a future report.
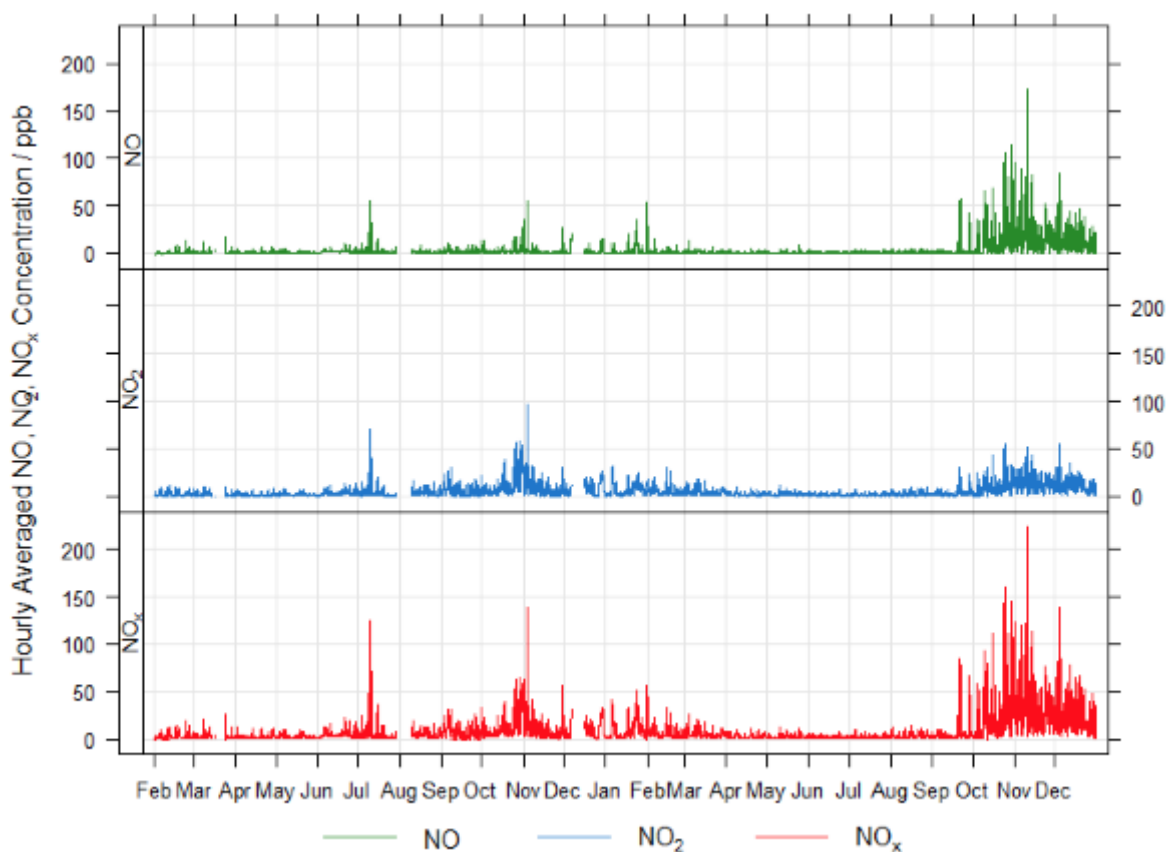
Figure 75. NO$_x$ time series at KM from February 2016 to February 2018. © University of York, 2018

The annual concentration of both NO and NO$_2$ increased significantly in the second half of 2017 and this is evident when looking at the time series of NO$_x$ (Figure 75). Enhancements in NO$_x$, in particular NO, can clearly be seen from Autumn 2017. Road transport is the largest source of NO$_x$ in the UK, nitrogen oxides formed in combustion systems are mainly emitted in the form of NO. NO$_2$ largely exists as a secondary pollutant formed by the oxidation of NO, however there are certain combustion conditions that can lead to higher proportions of NO$_x$ emitted as NO$_2$, for example the oxygen rich environment in a diesel engine aids direct formation of NO$_2$. At KM the

close proximity of the monitoring station to activity on site means increased vehicle activity and addition of diesel generators is reflected in the NO and NO_2 measurements.

A significantly increased peak can be clearly seen in Autumn 2017 when compared to Autumn 2016. Trends at other times of the year are similar across both years. It is expected for NOx concentrations to increase in wintertime and is part of the annual cycle, there tends to be an increase due to more emissions from heating and burning and due to the local metrology and the lower boundary layer. In 2016, the NO_2 concentration was generally greater than NO and therefore made the most significant contribution to NO_x. The monitoring station is some distance away from the nearest major road (Habton Road) meaning the air at KM will be aged. This allows time for primary emissions of NO to be oxidised to NO_2. However, in September 2017 there is a reversal of this trend, where NO begins to dominate NO_x, indicative of the change in the source of these emissions. This coincides with the increased activity known to have taken place on site.
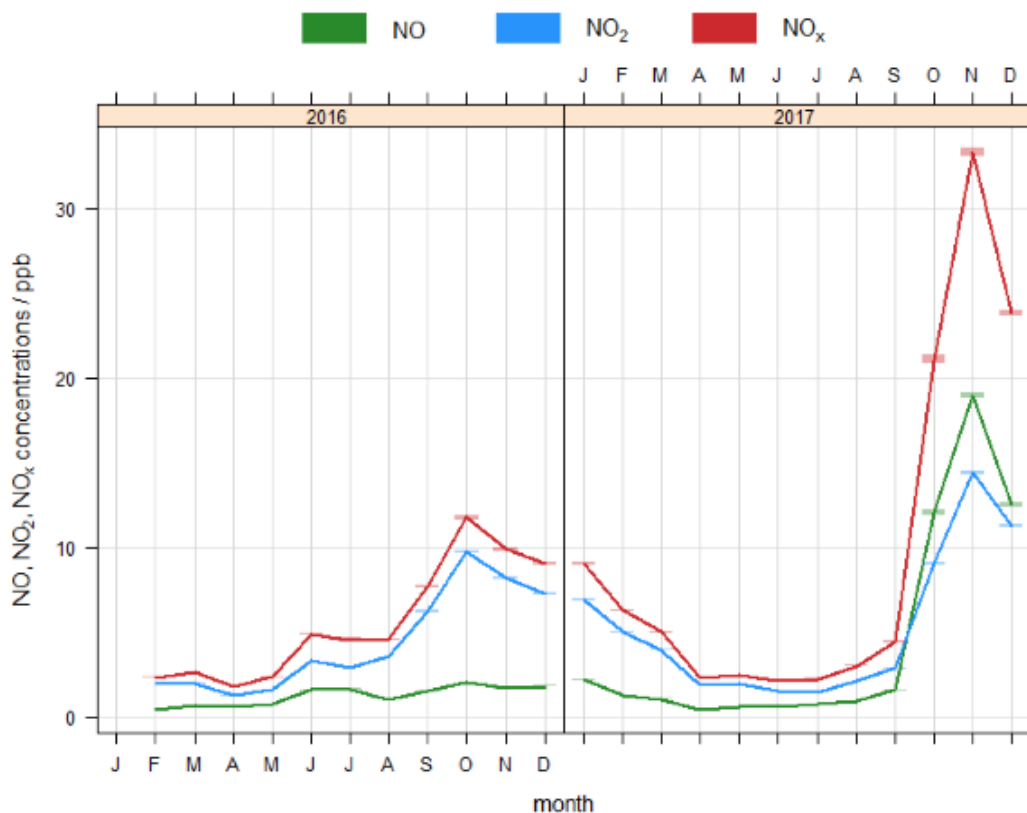
Figure 76. Monthly averages of NO_x at KM. © University of York, 2018

The AURN (Automatic Urban and Rural Network) is the UKs largest monitoring network run by DEFRA (Department of Environment, Food and Rural Affairs) and is used for compliance reporting against Ambient Air Quality Directives. The sites provide high resolution hourly data for a range of pollutants. Each site is given a classification as described in Whilst it does not quite fit all the criteria as specified by DEFRA, KM could be considered as a rural background site. High Muffles is the nearest AURN site to KM and is classified in this category along with Lady Bower (Figure 77).

Figure 78 shows the similarities in the probability distribution function of NO_x between KM during the baseline period and these other similar rural background sites. However, the data for the "pre-operational" period plotted as frequency density plot shows a very different pattern (Figure 79) to the baseline period. For this period, a much wider and higher distribution of concentrations is observed. The distribution in this period is more similar to urban background

sites such as York Bootham and Hull Freetown, which are located within built up urban areas (Figure 77).

Table 18.

Whilst it does not quite fit all the criteria as specified by DEFRA, KM could be considered as a rural background site. High Muffles is the nearest AURN site to KM and is classified in this category along with Lady Bower (Figure 77).

Figure 78 shows the similarities in the probability distribution function of NO_x between KM during the baseline period and these other similar rural background sites. However, the data for the "pre-operational" period plotted as frequency density plot shows a very different pattern (Figure 79) to the baseline period. For this period, a much wider and higher distribution of concentrations is observed. The distribution in this period is more similar to urban background sites such as York Bootham and Hull Freetown, which are located within built up urban areas (Figure 77).

Table 18. Description of AURN site classifications

Site environment	Description
Urban	Continuously built up area
Suburban	Largely built up urban area that may be mixed with non-urbanised areas
Rural	More than 5 km from built up areas and major roads
Traffic	Pollutant levels largely determined by emissions from nearby traffic
Industrial	Pollutant level is predominantly influenced by emissions from nearby industrial source or area
Background	Pollutant levels not influenced significantly by any single source or street but by integrated contribution from all upwind sources

Whilst the change in NO_x concentrations is clear, these are still well within national air quality limits. However, it does indicate that the characteristics of KM site changed significantly as a result of the preparations being made for hydraulic fracturing-related activities. In terms of the impact on residents living in Kirby Misperton, these plots would suggest that after September 2017 (and until end of February 2018) the levels of NO_x pollution at the site were more similar to living in an urbanised area, rather than a rural setting with only a few major roads and industrial sources.
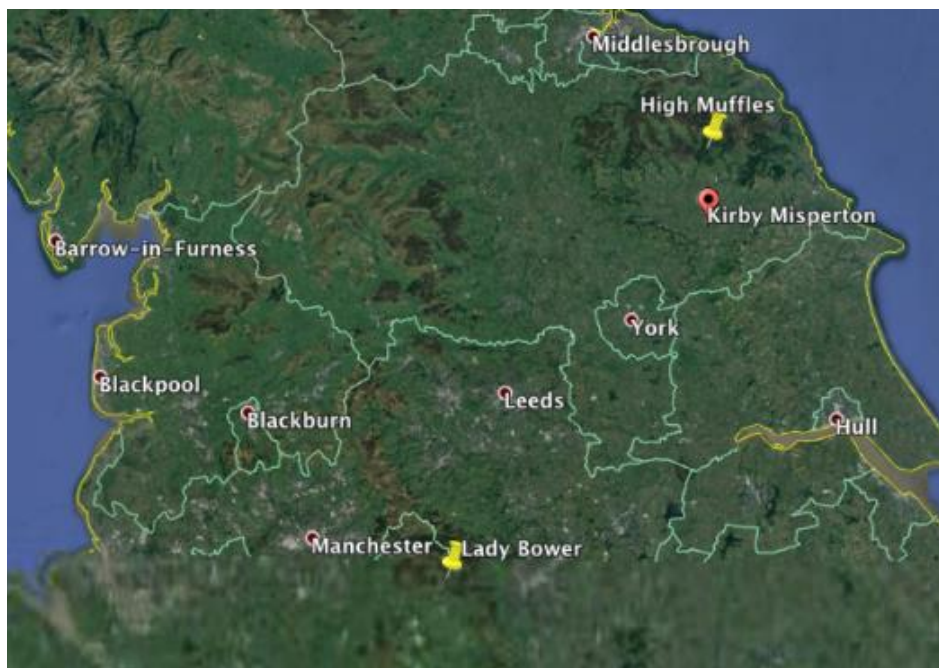
Figure 77. Map of KM site and AURN sites (taken from Google Earth). © University of York, 2018
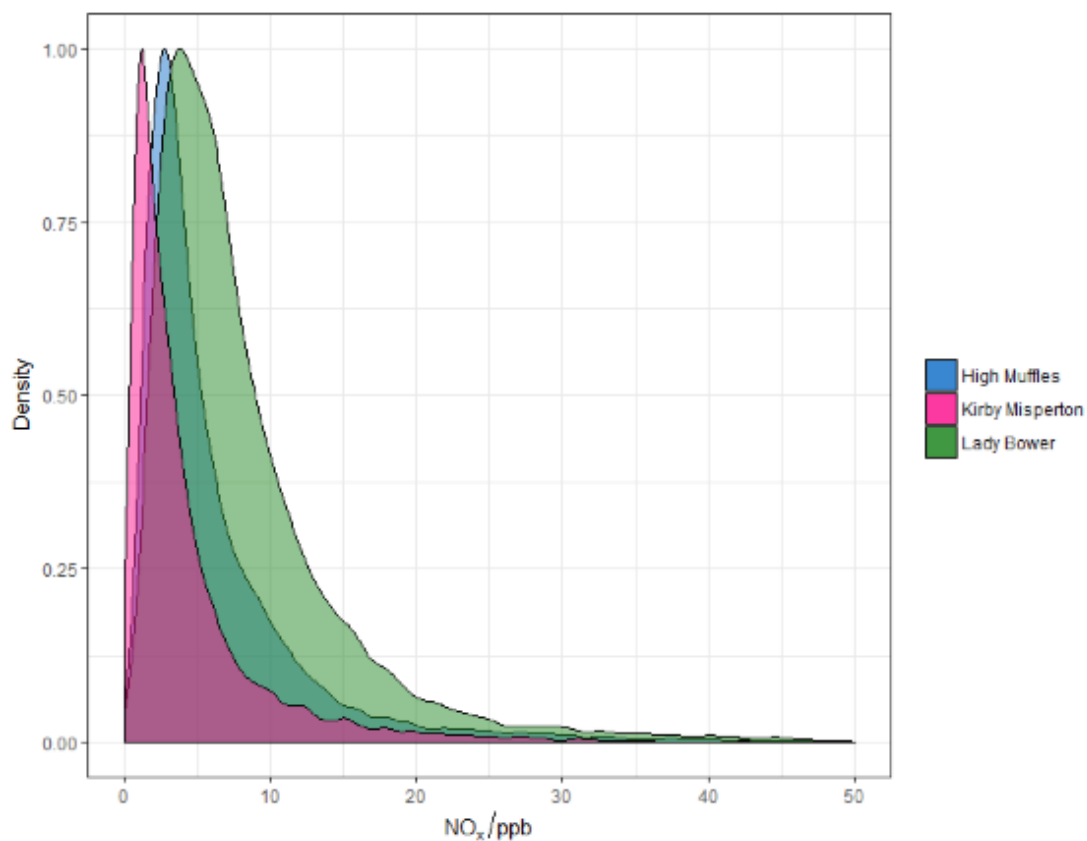
Figure 78. Frequency density plot of rural background sites in the UK, including KM during the baseline period up to beginning Autumn 2017. © University of York, 2018
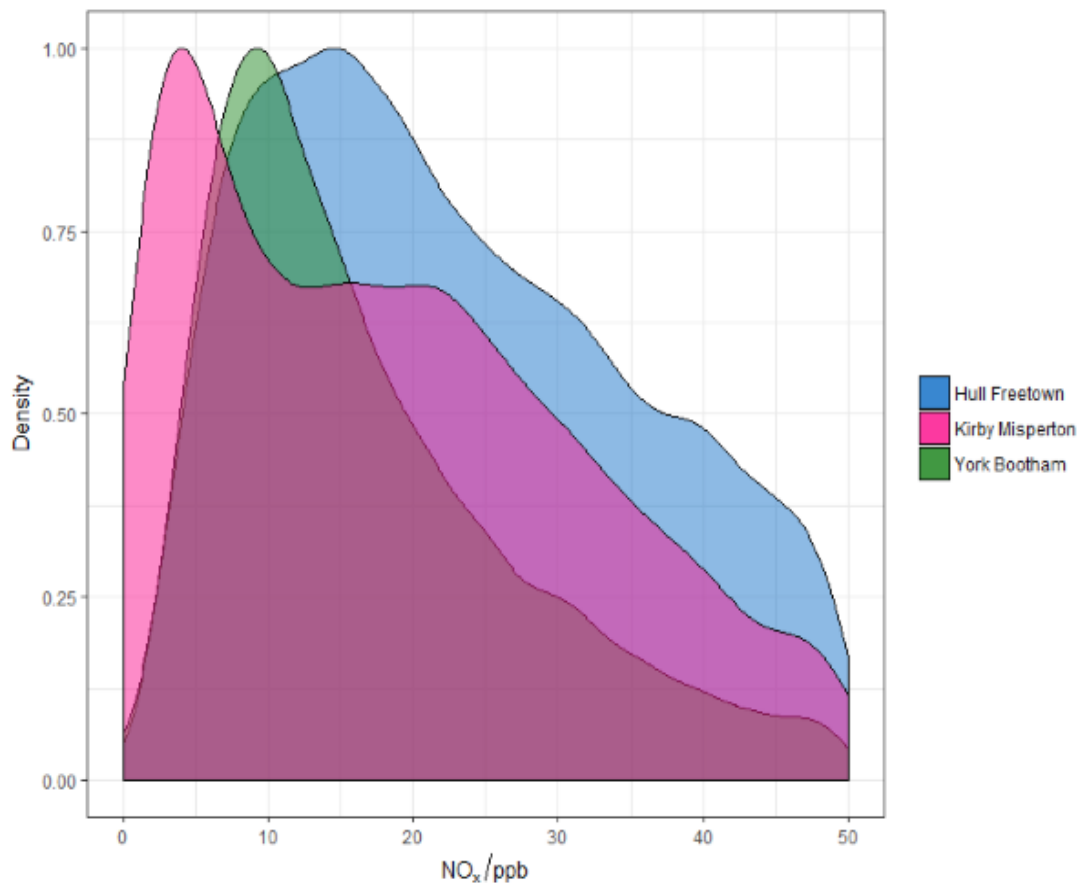
Figure 79. Frequency density plot of urban background sites in the UK, and the KM site during the pre-operational phase in autumn 2017. © University of York, 2018

4.7.5.7 H_2S MEASUREMENTS

Since Autumn 2017, H_2S measurement has been added to the KM8 suite of instrumentation. H_2S has a strong odour associated with it, often described as a rotten egg smell, and this can be detected by humans a low ppb levels. Although the mean value is 1.1 ppb for KM8, there have been occasions where H_2S has been enhanced (maximum in the 1 minute data is 22 ppb). These are well below any health relevant exposure limits (which are at the ppm level). However, odours have been reported in the village. The dataset has therefore been analysed to try and identify any sources of enhanced H_2S, and whether these may explain the reported odour incidents.

Conditional probability functions (CPF) have been used for this analysis. CPF is a useful technique for highlighting which wind directions are dominated by high concentrations and estimating the probability of those events. Figure 80 shows a polar plot of H_2S measured at KM8 based on the CPF function. This plots shows that for most wind directions the probability of H_2S concentrations being greater than the 95th percentile (3.2 ppb) is zero. The exceptions are when the wind speed is low and from the south west sector which indicates a local source. Given the locations of the peak probability and the monitoring site, these peaks may not be due to operations at KM8, but may be due to work being conducted on the conventional gas wells to the south and west of the site. There is also another unidentified source further away in that sector.

There is also a further small source which is NE of the site; this event was detected in the village on the 28th February 2018 and reported to the Environment Agency. Wind direction at the time indicated that airflow was coming from the NE and it was concluded that it was not due to activity on the KM8 well site. CPF analysis confirms this with an increased probability of higher concentrations in the NE. The source of the H_2S still needs to be confirmed but could potentially be from a local landfill site.

89

CPF at the 95th percentile (=3.2)
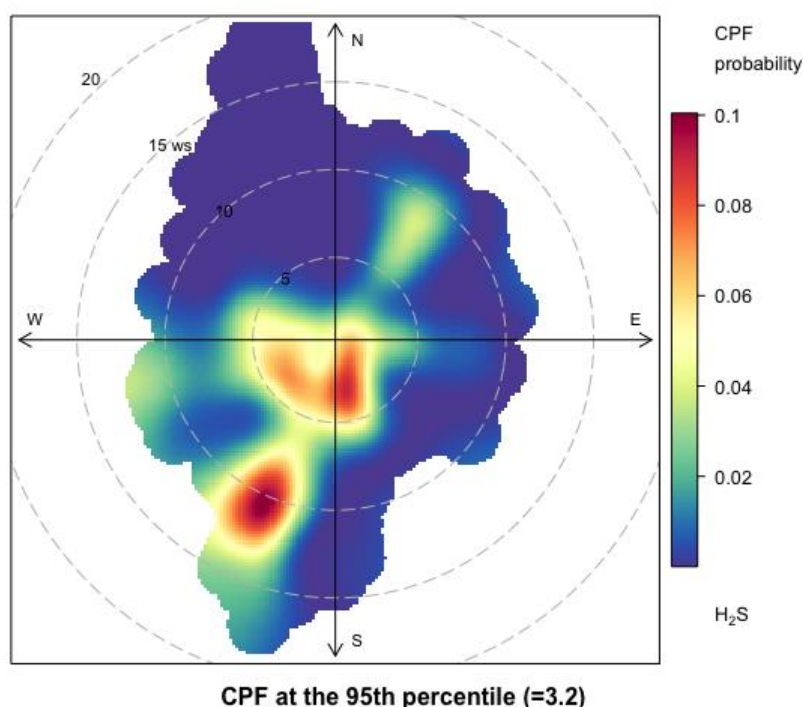
Figure 80. Polar plot of H₂S concentrations at KM8 based on the CPF function.
© University of York, 2018

4.7.6 Little Plumpton (LP) detailed analysis

Table 19 reports the various air pollutant metrics by species and individual wind sector for the Phase 3 reporting period (February 2017 to February 2018). These are very similar to the Phase 2 results and the same conclusions about sources can be applied for this dataset. The mean concentrations for the Phase 3 period are slightly lower than Phase 2. This is despite the drilling having started at the Cuadrilla site at Preston New Road.

As is common in the UK, Easterly and South-easterly air mass are often the most polluted since these bring air from the SE of England and from continental Europe. The lowest concentrations of air pollution are typically observed during periods of westerly airflow. The LP site also has the influence of the major road that is to the south of the site and its influence can be clearly seen in the NO_x and PM measurements from those wind sectors.

Table 19. LP wind sector averages

	N	NE	E	SE	S	SW	W	NW
O_3 (ppb)	21.4	19.6	20.0	16.3	18.6	24.4	25.5	25.9
NO (ppb)	1.0	1.1	2.3	3.7	2.1	1.0	2.3	1.2
NO_2 (ppb)	4.4	5.0	7.1	9.0	6.2	3.0	3.4	2.7
NO_x (ppb)	5.4	6.1	9.4	12.7	8.3	4.0	5.7	3.9
$PM_{2.5}$ ($\mu m/m^3$)	4.5	5.7	12.3	12.9	7.1	5.0	5.1	4.5
PM_{10} ($\mu m/m^3$)	8.0	8.7	16.6	17.0	10.2	8.6	9.2	8.8
H_2S (ppb) October 2017	<LOD	<LOD	<LOD	0.4	0.4	<LOD	<LOD	<LOD
SO_2 (ppb) from Oct 2017	0.2	0.2	0.2	0.2	0.2	0.3	0.2	0.2

90
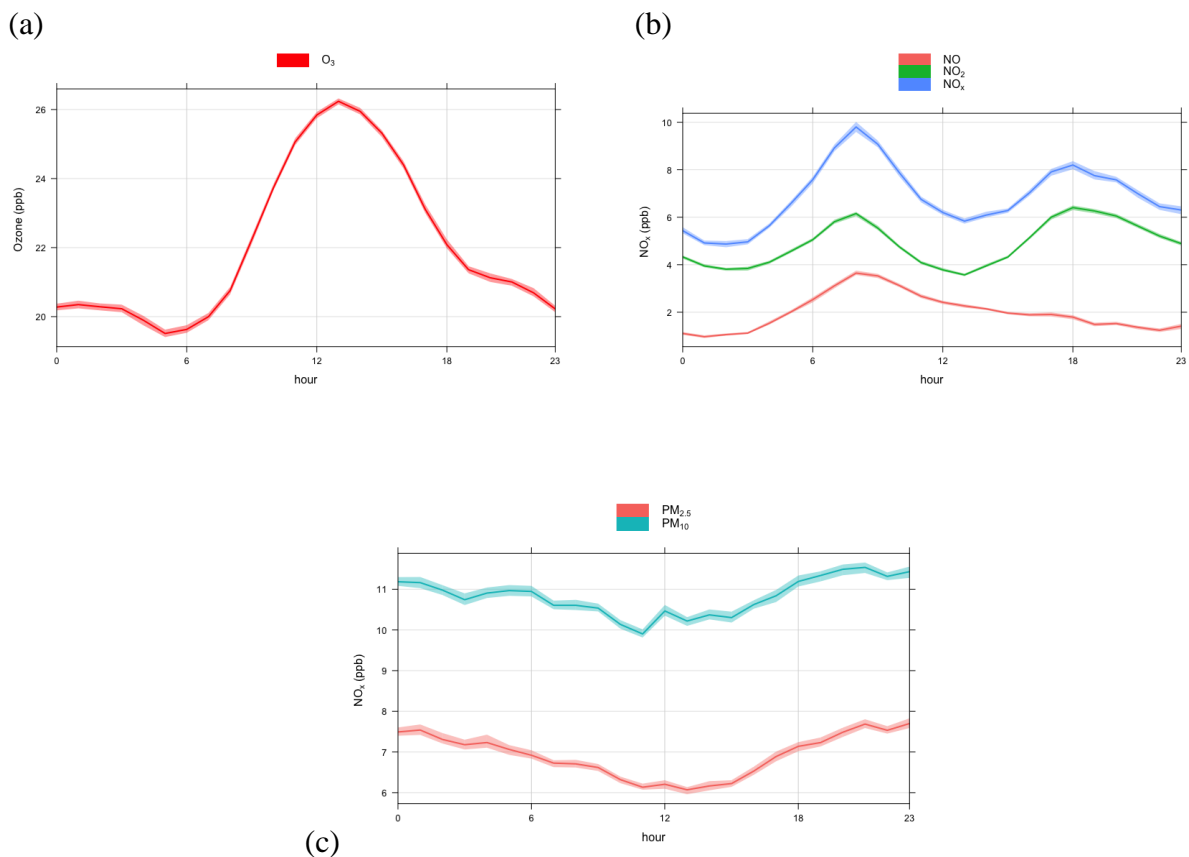
Figure 81. Diurnal variations a LP for (a) O₃ (b) NOₓ and (c) PM. © University of York, 2018

4.7.6.1 DIURNAL VARIATION OF AIR POLLUTION AT LP

LP diurnal cycles are shown in Figure 81. The O_3 diurnal cycle is at its lowest at night and peaks just after midday, as previously discussed this is expected in the context of UK oxidative air chemistry.

The NO_x at LP displays a clear diurnal cycle, but it is different to the KM observations. The PM shows a slight diurnal but this is not as clear as previous measurements. The diurnal cycle at LP is heavily influenced by the larger nearby road traffic source, with NO_x increasing in the morning, due of the boundary layer and heavier local traffic at this time. The early evening peak is again due to the second rush hour. The smoothing of the peaks in the PM diurnal may indicate a further more constant source of PM.

4.7.6.2 HEBDOMADAL VARIATION OF AIR POLLUTION AT LP

LP hebdomadal cycles are shown in Figure 82. The working week is clear in the NO_x and PM measurements with highest daily averages found during the week and decreasing concentrations at the weekend. O_3 is highest on a Thursday; this coincides with a decrease in the NO_x measurements. A similar pattern was observed in the Phase 2 data but on a Wednesday. It is still unclear why this difference should occur as there are no immediate reasons why traffic volumes may be lower at certain times. There have been active protests in the area so it may be that certain road closures have led to this effect being detectable in atmospheric concentrations.

(a)   (b)

91
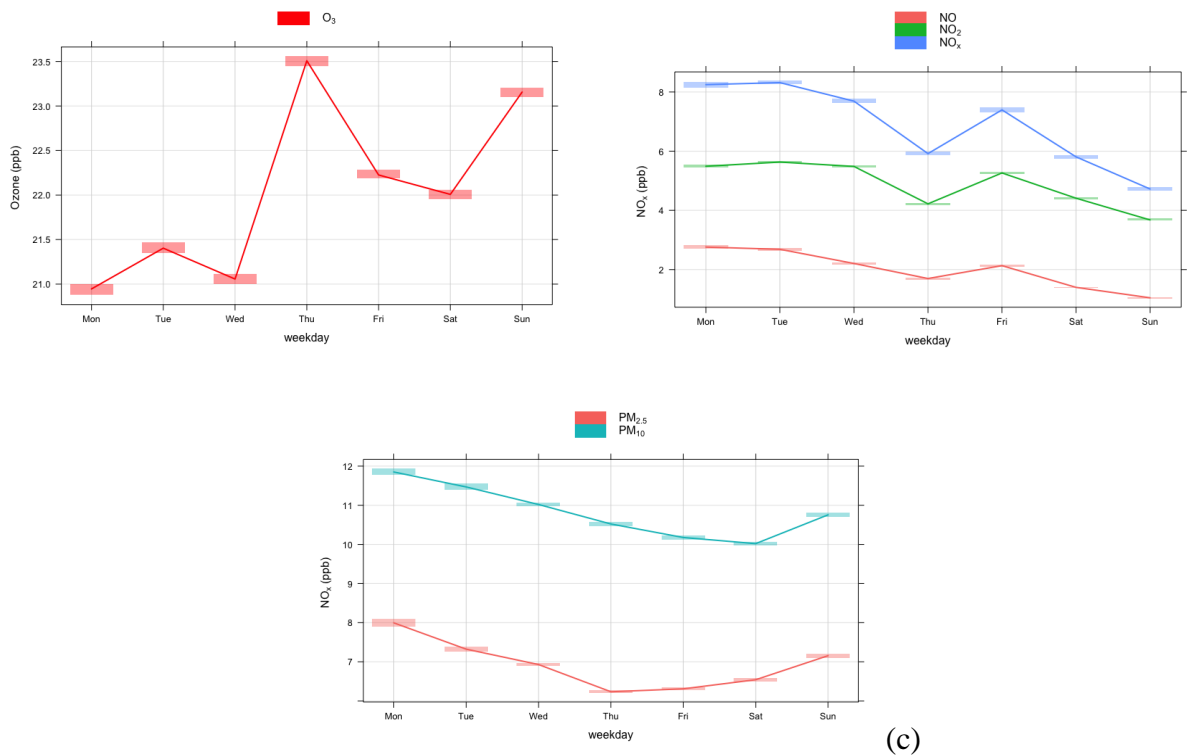
Figure 82. Hebdomadal cycles at LP for (a) O₃ (b) NOₓ and (c) PM. © University of York, 2018

4.7.6.3 ANNUAL VARIATION OF AIR POLLUTION AT LP

The LP ozone instrument underwent maintenance in June–July and December so a full annual cycle was not collected but the data that are available show the expected UK ozone increase in spring, as discussed in the KM section earlier. The other air pollutants, NOₓ and PM also show typical annual cycles in the context of UK air quality and have already been partially discussed previously. Annual cycles for the in situ air quality parameters are shown in Figure 83.
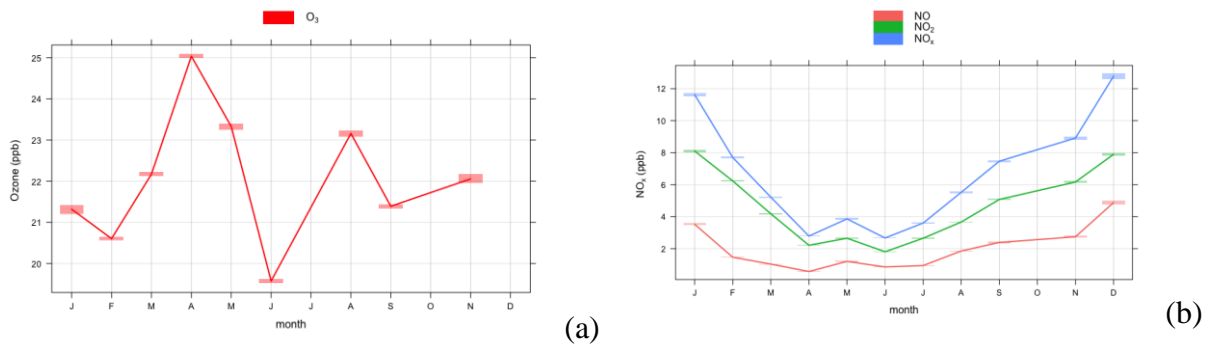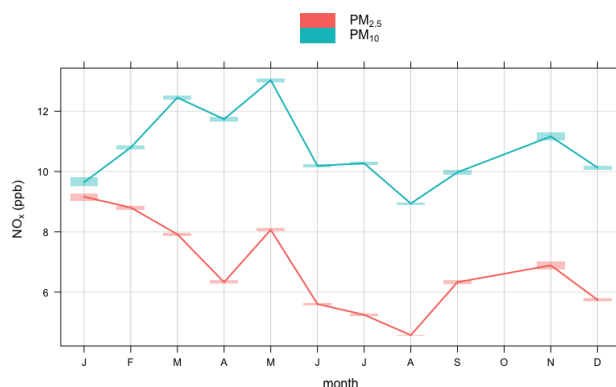
(c)

Figure 83. Annual cycles at KM for (a) O3, (b) NO$_x$ and (c) PM for 2017. © University of York, 2018

4.7.6.4 SOURCE APPORTIONMENT FOR LP

Figure 84 shows percentiles roses for the in situ air quality parameters split by season. A percentile rose places the data into 5 bands (the colour-scale) and then plots each of those by wind direction (radial axis) and concentration. The grey line is the mean for the data set. The plots are separated into season with Spring (March, April, May), Summer (June, July, August), Autumn (September, October, November) and winter (December, January, February).

Figure 85 shows polar plots for the same pollutants, with concentrations (colour scale), wind direction (radial scale) and wind speed.

NO$_x$ sources are seen to the south east of the site which is attributed to road traffic but there is also a strong source directly west of the site. This source was not observed in the previous Phase 2 data and is most likely due to the developments taking place at the Preston New Road site to the direct west of the monitors. Currently this is not having the same scale of effect on concentrations as has been observed at KM in autumn 2017. It should be noted that operations at the two sites are currently very different.

A large source of PM to the south east of the site is visible, recreating a feature seen in previous data from 2016. This has been determined to be a local influence. There are slightly enhanced PM measurements in the westerly air masses, showing the influence of the Atlantic air masses, especially in the coarser fraction arising from atmospheric aerosols.

Enhanced PM in airmass from the SE is related to some general increases also in NO$_x$ in the same wind direction indicating that these higher values are associated with regional transport of air pollution from other UK regions to the site, and in contrast to cleaner Atlantic air masses.

93
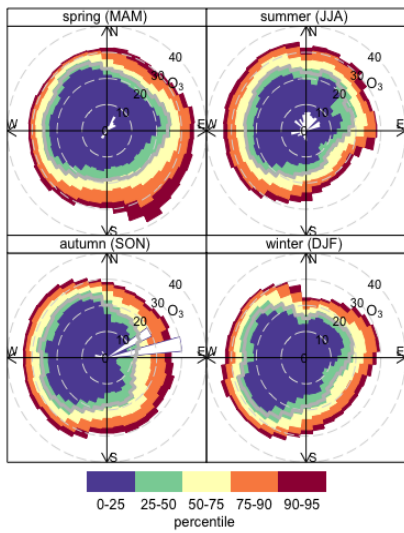
(a)
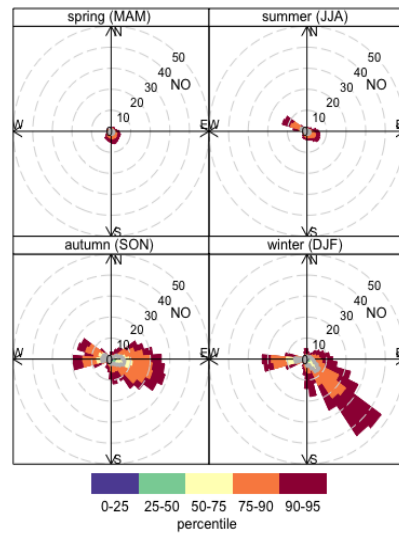
(b)
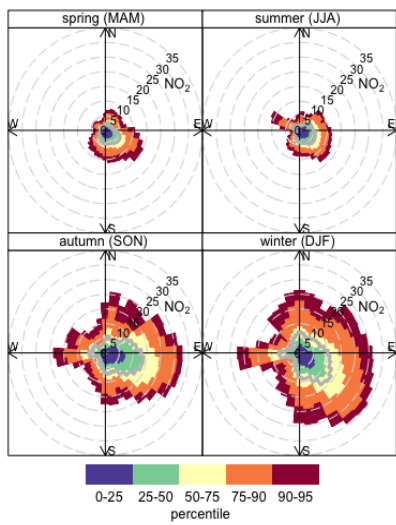
(c)
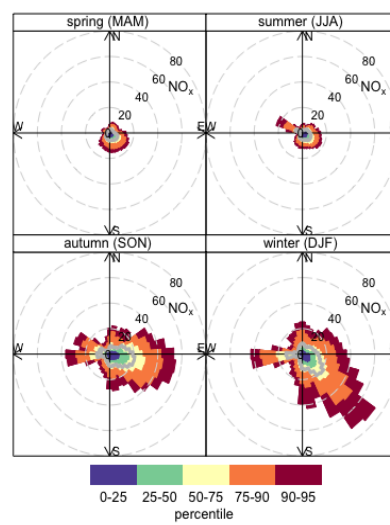
(d)
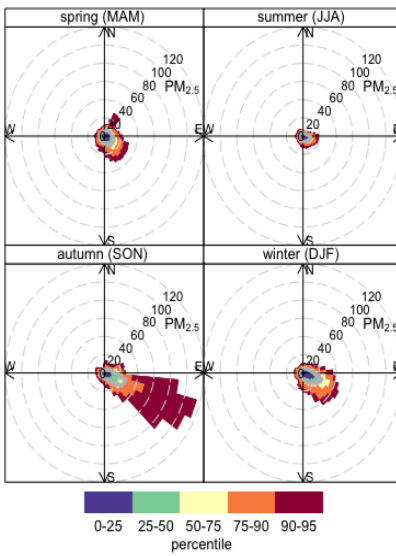
(e)
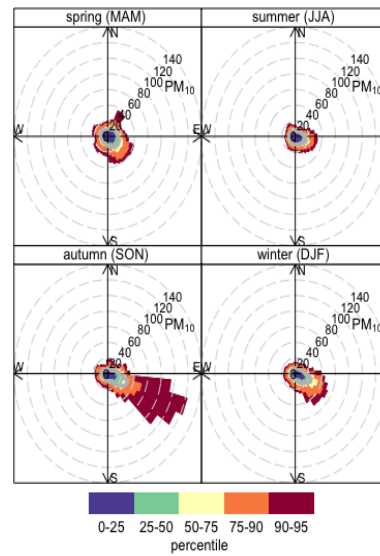
(f)

Figure 84. Percentile rose to show the 5th, and 95th percentiles for (a) O₃, (b) NO,(c) NO₂ (d) NOₓ, (e) PM₂.₅, (f) PM₁₀. © University of York, 2018
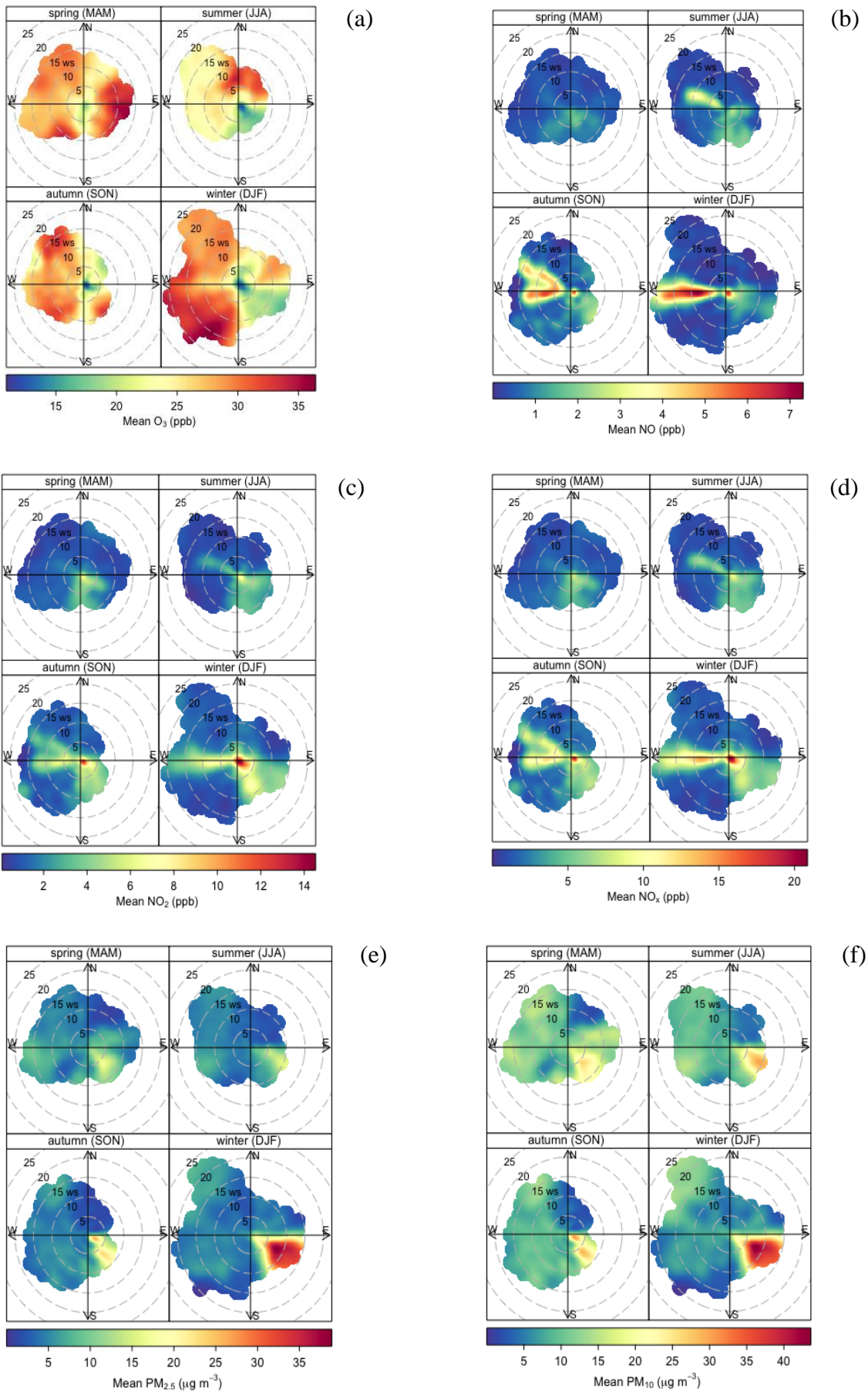
Figure 85. Polar plots for LP (a) O₃, (b) NO (c) NO₂, (d) NOₓ, (e) PM₂.₅, (f) PM₁₀.
© University of York, 2018

4.7.7 Non-Methane Hydrocarbons at KM and LP

Non-methane hydrocarbon (NMHC) measurements have been made weekly at both sites. The NMHC are not continuous but as only one discrete sample a week. This may not be taken when the wind direction is downwind from site, so the results need to be interpreted carefully. A summary of NMHC concentrations for KP and LP is shown in Table 20 and Table 21 respectively. NMHCs are able to give an indication of air mass origin and age since fresh pollution was added; in areas of oil and gas production higher light alkanes such as ethane and propane may be enhanced over typical urban distributions due to fugitive emissions. NMHC data are shown until mid-January 2018. These data are also summarised as box and whisker plots in Figure 86 and Figure 87.

Table 20. Summary of NMHC measurements at KM, N =62. All NMHC have an uncertainty of < 10%

Hydrocarbon	Annual mean (ppb)	Minimum value (ppb)	Maximum value (ppb)
Ethane	2.18	0.68	5.20
Ethene	0.76	0.06	2.52
Propane	1.26	0.20	7.07
Propene	0.15	0.02	0.69
Isobutane	0.41	0.03	5.38
Nbutane	0.80	0.07	11.01
Isopentane	0.29	0.02	3.60
Npentane	0.28	0.02	3.50
Benzene	0.14	0.01	0.43
Toluene	0.18	0.01	2.22

Table 21. Summary of NMHC measurements at LP, N =45. All NMHC have an uncertainty of < 10%

Hydrocarbon	Annual mean (ppb)	Minimum value (ppb)	Maximum value (ppb)
Ethane	2.92	0.50	17.57
Ethene	0.83	0.18	6.43
Propane	1.25	0.07	6.53
Propene	0.13	0.02	0.93
Isobutane	0.41	0.01	4.55
Nbutane	0.77	0.04	5.96
Isopentane	0.23	0.02	1.00
Npentane	0.29	0.02	2.32
Benzene	0.32	0.04	1.10
Toluene	0.37	0.02	7.9
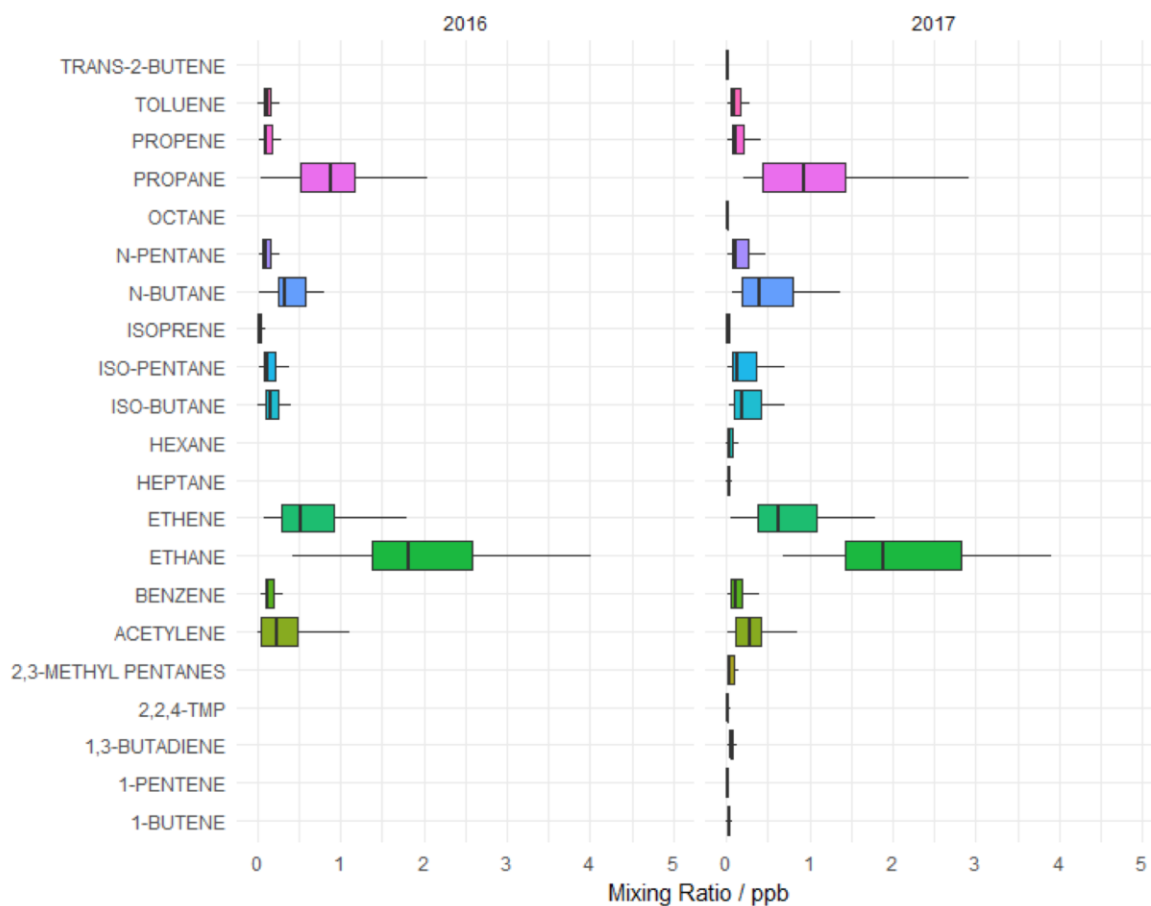
Figure 86. Box and whisker plot of NMHCs measured at KM in 2016 and 2017.
© University of York, 2018
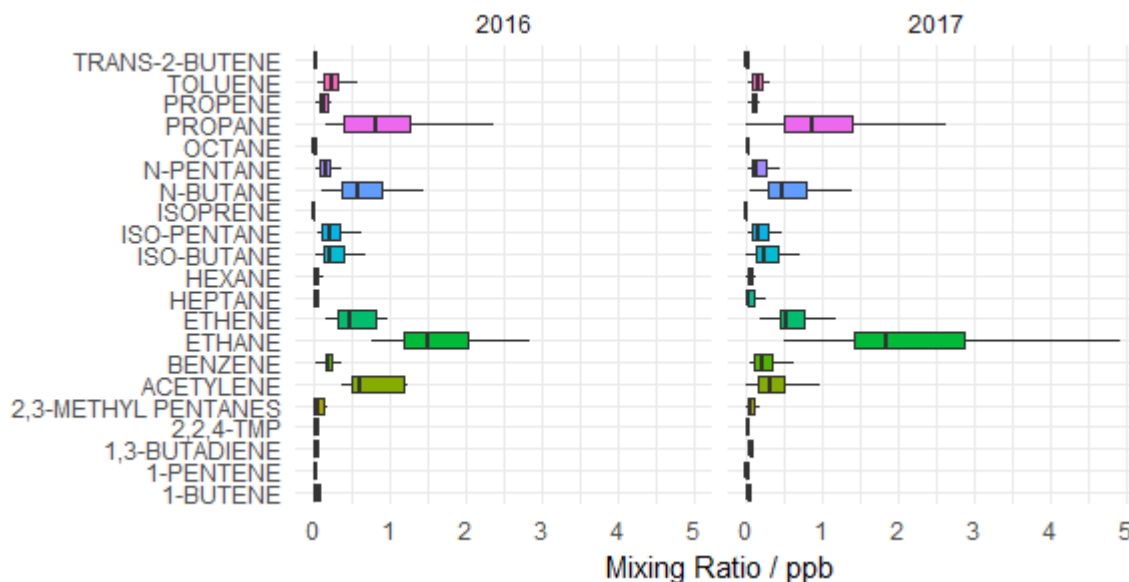
Figure 87. Box and whisker plot of NMHCs measured at LP in 2016 and 2017.
© University of York, 2018

Figure 88 shows the annual means of the non-methane hydrocarbons measured at KM. Ethane and propane are the most abundant compounds measured throughout both years at both sites. There were no significant differences between the means for 2016 and 2017 for both locations.
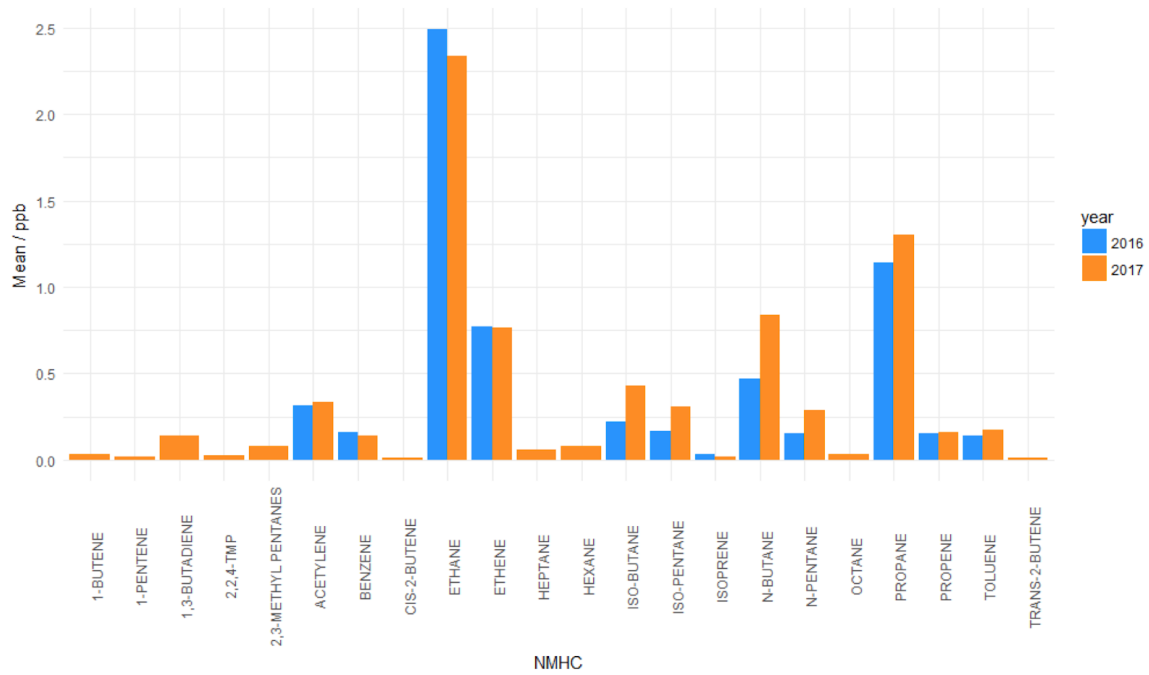
Figure 88. Mean mixing ratios of NMHCs at KM for 2016 and 2017. © University of York, 2018
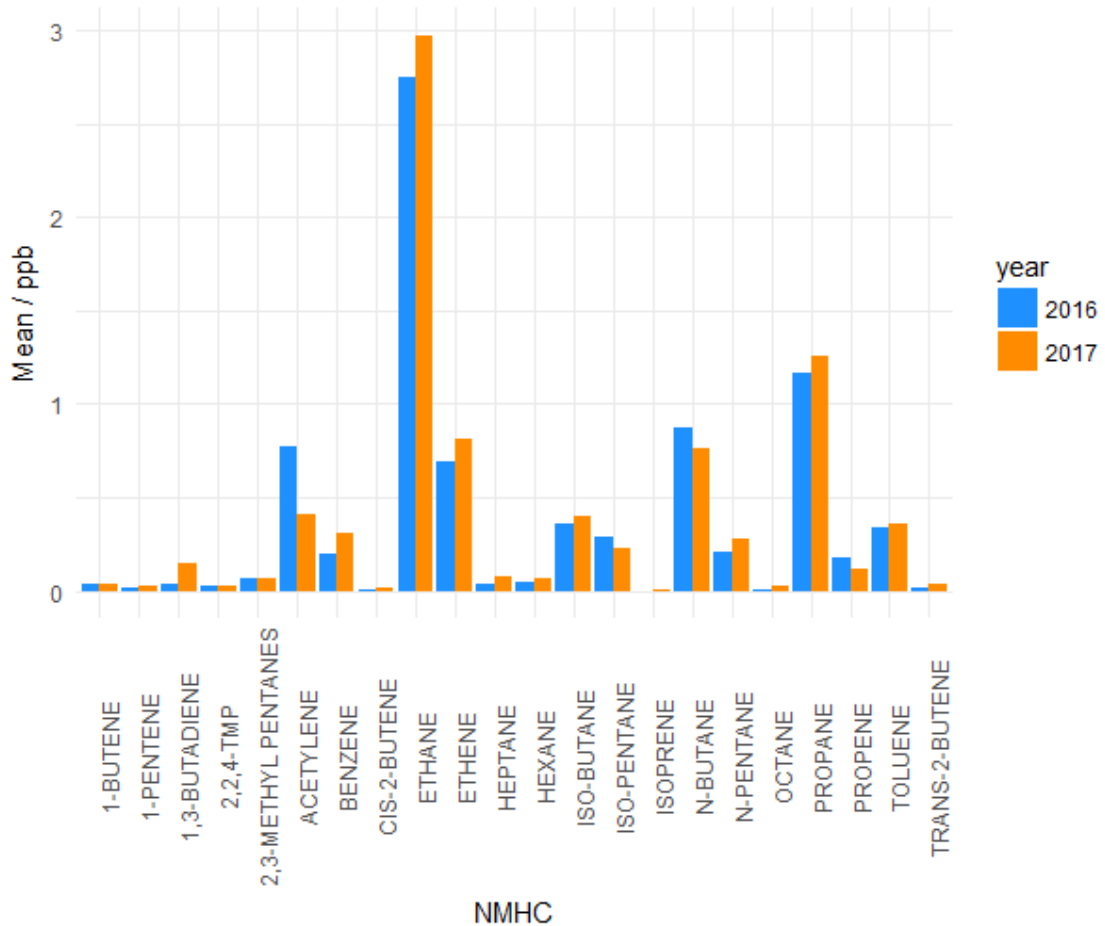
Figure 89. Mean mixing ratios of NMHCs at LP for 2016 and 2017. © University of York, 2018
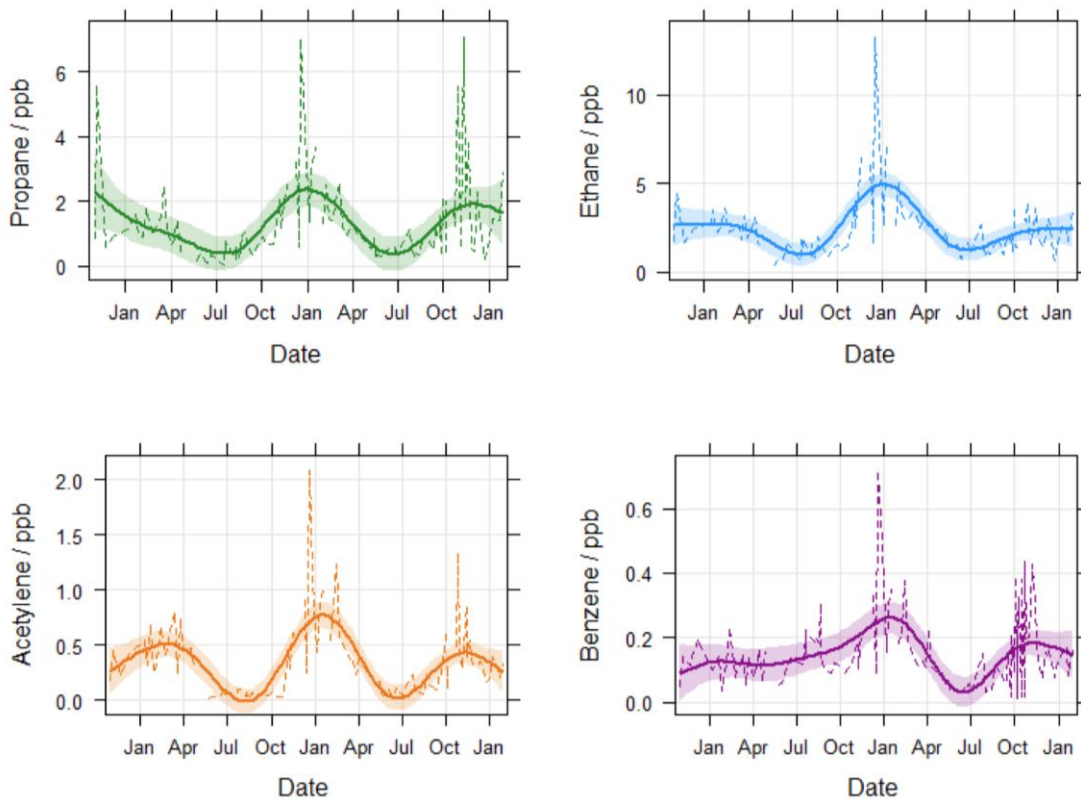
Figure 90. Seasonal variation in selected NMHCs at KM from December 2015 to January 2018. The dotted lines show the actual concentrations measured, the smooth line is the trend. © University of York, 2018
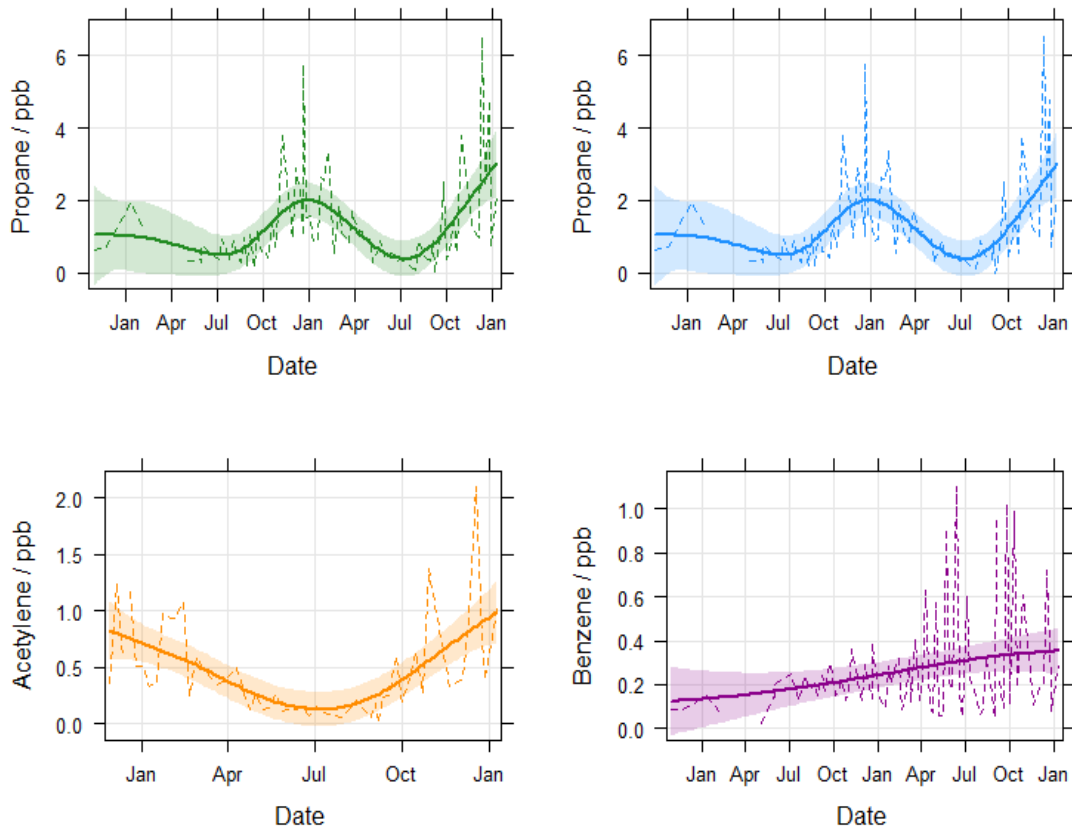
Figure 91. Seasonal variation NMHCs at LP from February 2016 to January 2018. The dotted lines show the actual concentrations measured, the smooth line is the trend. © University of York, 2018

The seasonal profiles for ethane, propane and acetylene are shown in Figure 90 for KM and Figure 91 for LP. A clear annual cycle is visible in the data with a summer minimum and a winter maximum. The reduction of concentration in the summer is predominantly due to the enhanced oxidation of NMHCs as a result of the reaction with the hydroxyl radical (OH). In winter, concentrations are also affected by boundary layer depth and atmospheric stability, where the boundary layer can more frequently be lower, resulting in the higher concentrations of NMHCs.

The only two NMHCs which are currently legislated with limit values are benzene and 1,3 butadiene. The annual mean values at both sites are well below the limit value for the UK.

4.7.8 Summary of air pollution measurements

The baseline distribution of air pollutants measured at LP has been broadly similar in 2017 to previous years, but there have been substantial changes observed at KM. Although hydraulic fracturing has no taken place at KM, there was a noticeable increase in NO_x as the site was prepared for operations to begin. From the Autumn 2017, when equipment was allowed on to the site, local NO_x emissions were enhanced due to additional vehicle movements (on site and off site) and the operation of diesel generators. The most clear evidence for these being local sources of NO_x was the shift in NO_2:NO ratio away from NO_2 and towards more direct NO.

Once equipment was removed from the KM site the NO_x concentrations returned to broadly the same concentrations seen previously during the baseline period. This highlights the importance of measuring the whole shale gas operational cycle for air quality as the preparative operations can have a substantial impact on air pollution. The process of equipment being brought to site, and the operation of additional support equipment (e.g. pumps, generators, etc) leads to additional air emissions. The "pre-operational" phase at the KM site changed the atmospheric characteristics of the location. The monitoring data shifted from having concentrations and behaviours typical of a rural background location, to behaviours more similar to an urban background location. It should be noted however that whilst the preoperational phase at KM led to increases in some air pollutants, no air quality limits were exceeded.

5 Radon

5.1 INTRODUCTION

Radon, [222]Rn, a radioactive, colourless and odourless gas with a half-life of 3.82 days is the largest source of radiation exposure for most of the UK population and is the second highest cause of lung cancer after smoking (Darby et al, 2005).

Public Health England (PHE) reviewed the potential public health impact of possible chemical and radiological pollutants resulting from shale gas activities in 2014 (PHE-CRCE-009). The PHE review recognised that radon would be released to air but expected this to be at low level. PHE could not envisage a plausible mechanism in which shale gas extraction processes could significantly change radon entering properties from the ground but also recognised that people might measure radon in their home after such activities start and mis-attribute any high levels to the shale gas activities rather than from existing natural sources. Radon measurement in outdoor air and in homes was recommended to assess the baseline and provide evidence on radon distributions before shale gas extraction commenced.

The Vale of Pickering is an area which has been selected for shale gas extraction. Whilst the majority of the Vale does not have naturally elevated radon potential, there are areas of naturally elevated radon potential called Radon Affected Areas, at around 5 to 8 km to the north and south of the shale gas exploration site (KM8). In Radon Affected Areas, at least 1% of homes are expected to have radon levels at or above the UK Action Level of 200 Bq/m^3.

To determine the effect (if any) of shale gas extraction on levels of radon, baseline monitoring of radon levels within these radon Affected Areas as well as outside Affected Areas is required prior to commencement of shale gas extraction in order to compare with results at the same locations after shale gas extraction has begun.

PHE has been monitoring indoor and outdoor radon levels at various locations in the Vale of Pickering since October 2015. The results of the monitoring from October 2016 to December 2017 are included in this report. Earlier data are reported in the Phase 2 report (Ward et al, 2017).

Indoor radon concentrations exhibit diurnal, monthly and seasonal variation (Miles and Algar, 1988), thus long term testing gives a better estimate of the annual average radon concentration. PHE has recruited householders who have agreed to receive standard packs of passive detectors by post for several consecutive periods of 3 months. In addition each home has been issued a further two passive detectors for householders to carry out monitoring over a longer period of up to a year. Some 133 properties in the Vale of Pickering were included in the third phase of the monitoring from April 2017 to March 2018. Measurements in this study follow the PHE Validation scheme (Howarth C B and Miles J C H, 2008) for handling, placement and reporting of results for homes.

Outdoor radon levels have been assessed using passive radon monitors very similar to those used routinely in homes. The detectors have been placed in small aluminium-wrapped weatherproof plastic pots in discreet but open-air positions for several consecutive periods of 3 months or longer in a number of locations in the Vale of Pickering and also around Oxfordshire (acting as a control) to measure the radon concentrations in the open air.

An active radon monitor (AlphaGUARD) and passive detectors were placed in the air quality monitoring instrument enclosure at the KM8 site to assess the short term variation and long term average radon concentration at the site.

5.2 INDOOR RADON MONITORING

5.2.1 Results from the four consecutive 3-month tests (December 2016 to December 2017)

Four areas were selected for indoor radon monitoring in the Vale of Pickering: Kirby Misperton and Little Barugh, Yedingham, Pickering and Malton. Pickering and Malton are both areas of established elevated radon potential.

Results from the four 3-month tests covering the period from December 2016 to December 2017 are presented in Table 22. The annual average radon concentrations were calculated employing seasonal correction factors as outlined in the PHE Validation scheme (Howarth and Miles, 2008). The distribution parameters assuming log-normality confirm that homes in Kirby Misperton and Little Barugh are situated in areas with low radon potential while Pickering is situated in an area with higher radon potential (a Radon Affected Area). For Malton, the probability assessment was inconclusive due to a reduced statistical power; results from only a dozen properties were available. Malton is classified as a Radon Affected Area from previous studies (Miles et al, HPA-RPD-033, 2007).

The monitoring identified that a single result for the period June to September 2017 for one house in Yedingham (an area with low radon potential) was above the UK radon Action Level of 200 Bq/m^3. The results for the same house were below the Action Level for all other periods including the eighth 3-month period. It should be noted that there is a small possibility of houses having radon levels above the UK radon Action Level even when they are in the lowest radon probability areas. Year-to-year variability of indoor radon of up to 40 % has also been observed (Hunter et al, 2005).

Table 22. Range and distribution of estimated annual average indoor radon measurements from December 2016 to December 2017.

Area (number of homes)	Fifth 3-month reported results (Dec 16-March 17), Bq/m^3			Sixth 3-month reported results (March 17-June 17), Bq/m^3			Seventh 3-month reported results (June 17-Sep17), Bq/m^3			Eighth 3-month reported results (Sep 17-Dec17), Bq/m^3		
	Range	GM	GSD	Range	GM	GSD	Range	GM	GSD	Range	GM	GSD
Kirby Misperton and Little Barugh (26/30/24/24)	9–60	22	1.6	11–80	26	1.6	11–110	39	1.7	7-80	30	1.7
Yedingham and surrounding (29/31/25/24)	8–80	25	1.9	10–130	29	1.9	12–240	41	2.3	9-130	32	2.1
Pickering (38/41/38/37)	7–400	41	2.8	9–350	47	2.7	9–410	52	2.9	7-450	49	2.9
Malton (13/14/10/11)	13–60	29	1.7	10–80	27	1.7	8–60	26	1.8	11-50	31	1.7

GM = geometric mean; GSD = geometric standard deviation

5.2.2 Seasonality of indoor radon

Seasonality of indoor radon was studied using the eight 3-month consecutive measurements in each home, without seasonal correction. Data were only included from the 73 homes where results were available for all of the measurement periods (November/December 2015 to December 2017).

The average radon concentrations were calculated by combining the results for homes in each of the areas of Kirby Misperton and Little Barugh (KM-LB), Yedingham, Pickering and Malton for each of the measurement periods. The results are presented in Figure 92. From the plot it is

evident that homes in Kirby Misperton and Little Barugh, and also in Yedingham showed rather small seasonal variation. The seasonality in Pickering in contrast is well pronounced as it is in an area with elevated indoor radon concentrations (radon Affected Area), however all areas follow the normal UK seasonal pattern with a minimum in summer and maximum in winter (Miles et al, 2012). The number of results for Malton is rather small (see Table 22) compared to the other areas where results were assessed and hence the uncertainty in the results is higher. It should be noted that the average values for each 3 month measurement period for the first year (November /December 2015 to December 2016) show good agreement with the values for the second year (December 2016 to December 2017.
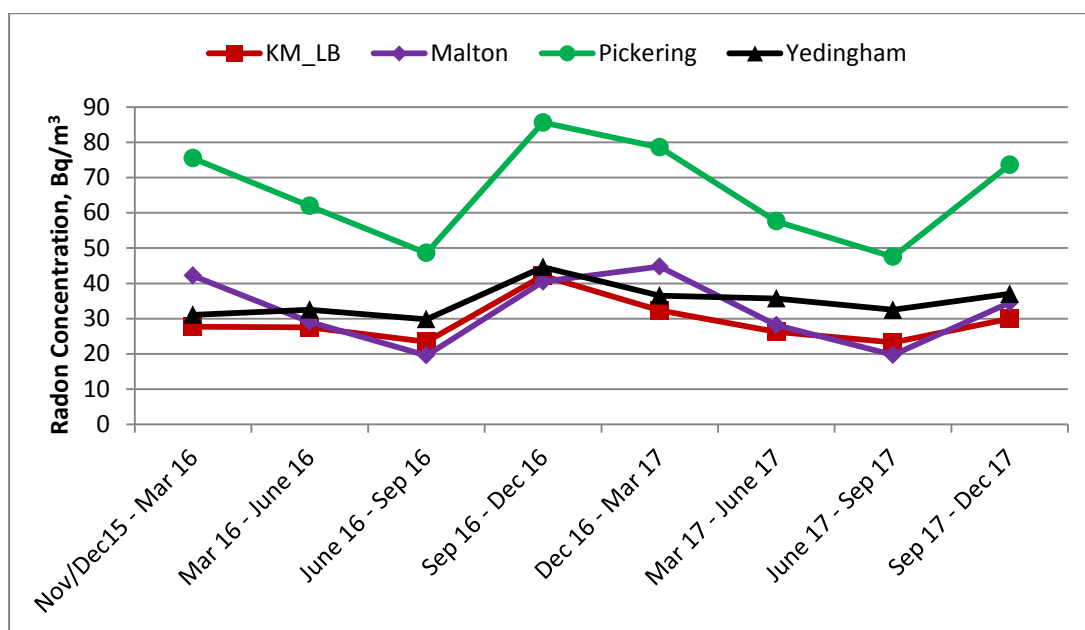
Figure 92. Seasonal variation of average indoor radon concentrations in the area of Kirby Misperton (KM_LB) and Little Barugh, Yedingham, Pickering and Malton

5.3   OUTDOOR RADON MONITORING

Four sites were selected for outdoor radon monitoring in the Vale of Pickering around Kirby Misperton (the area closest to the KM8 site), Yedingham (control site), Pickering and Malton (sites in Radon Affected Areas). One site in Oxfordshire was selected as an additional control. Four 3-month and two 1-year passive detectors were used to record radon concentrations at each monitoring point. The locations of the monitoring points in the Vale of Pickering are shown in Figure 93.

5.3.1   Results for outdoor measurements - January 2017 to October 2017

The 3-month monitoring period in the Vale of Pickering was replaced by a 6-month monitoring period in April 2017. The results from the second year of monitoring (fifth 3-month, sixth 3-month and first 6-month monitoring periods) were plotted and compared with the result obtained from the 1-year test (October 2015 to October 2016), where these are available. The information for each sampling point in the area around Kirby Misperton, Yedingham (control area), Pickering and Malton are shown in Figure 94 to Figure 98, respectively. The results for each detector at each location for each period were averaged and plotted. It was not possible to obtain results for all sites as some of the detectors were removed or damaged during the measurement period due to vandalism. This was most evident in the Malton area. Some sites where this damage occurred early on in the programme were re-located; for these monitoring points the 1-year monitoring results were not available.
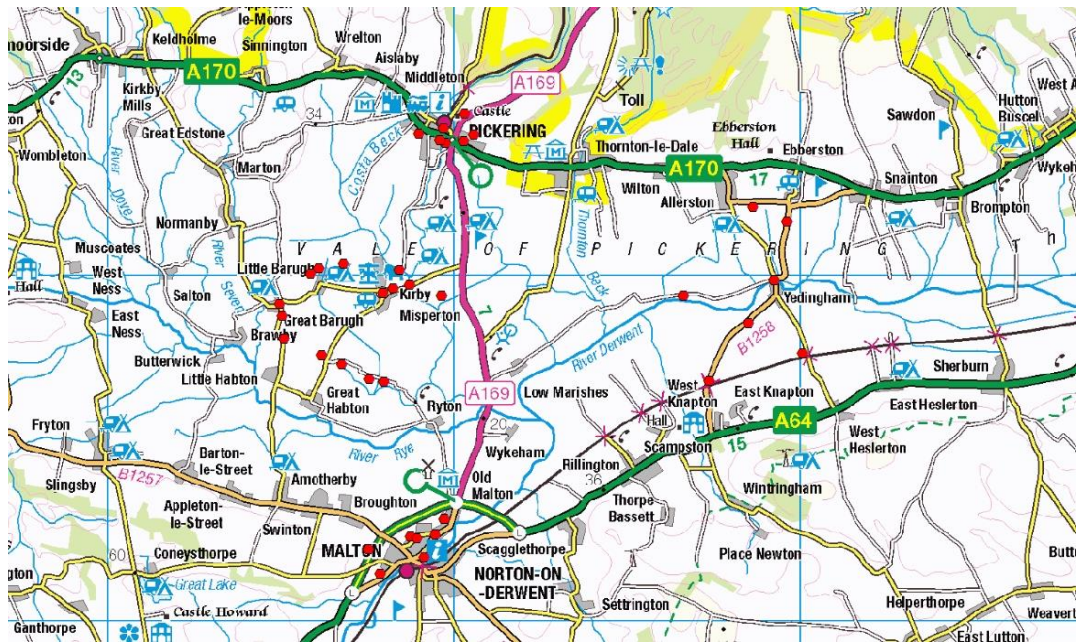
Figure 93. Outdoor radon sampling points in the Vale of Pickering. © Crown Copyright and/or database right, 2018. Licence number 100021290 EUL

The results from the control area in Oxfordshire are shown in Figure 98. The points were located in private gardens. Monitoring was carried out for 15 months from October 2015 to January 2017. In January 2017 one participant left while 3 new participants joined the programme. Where available the averaged results from the four 3-month monitoring periods at each sampling point in the control area from January 2017 to January 2018, were plotted and compared with the 1-year test carried out previously from October 2015 to October 2016.
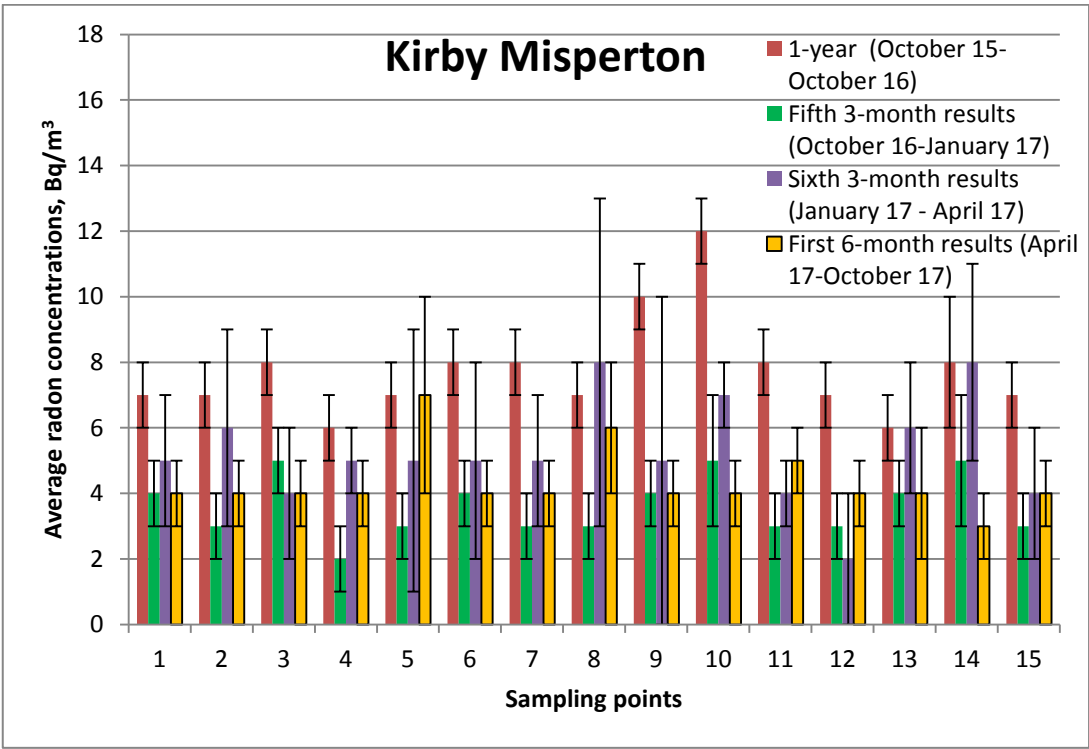
Figure 94. Average radon concentrations at the sampling points around Kirby Misperton
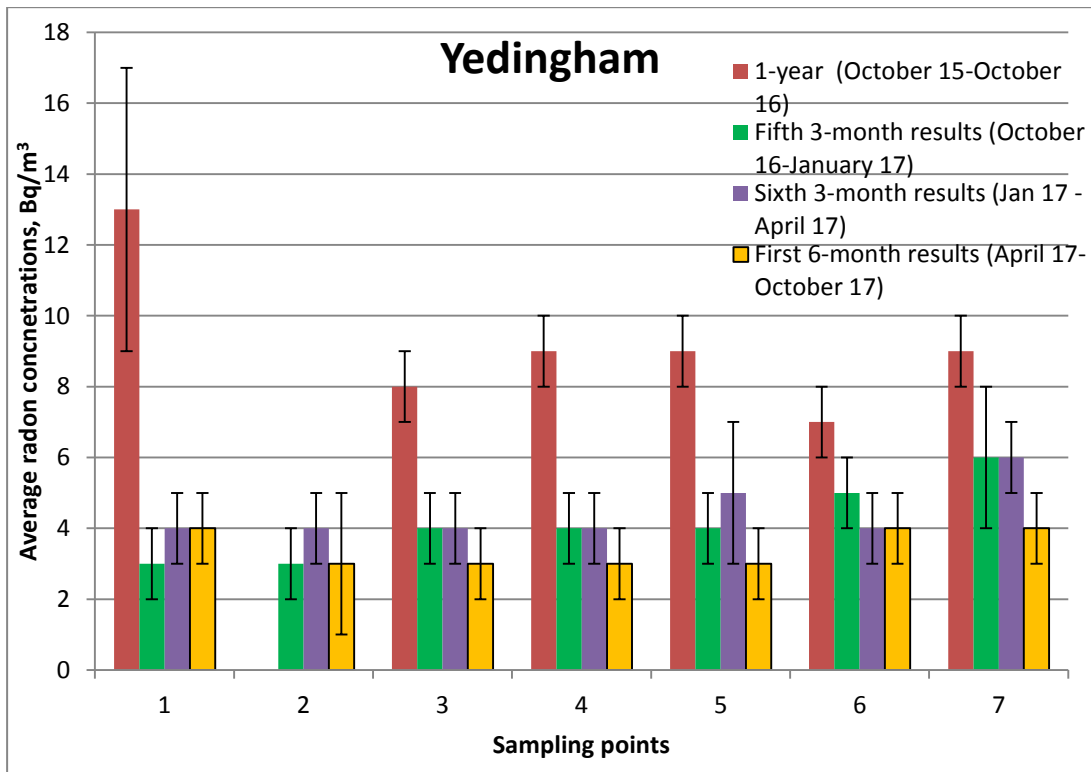
Figure 95. Average radon concentrations at the sampling points around Yedingham
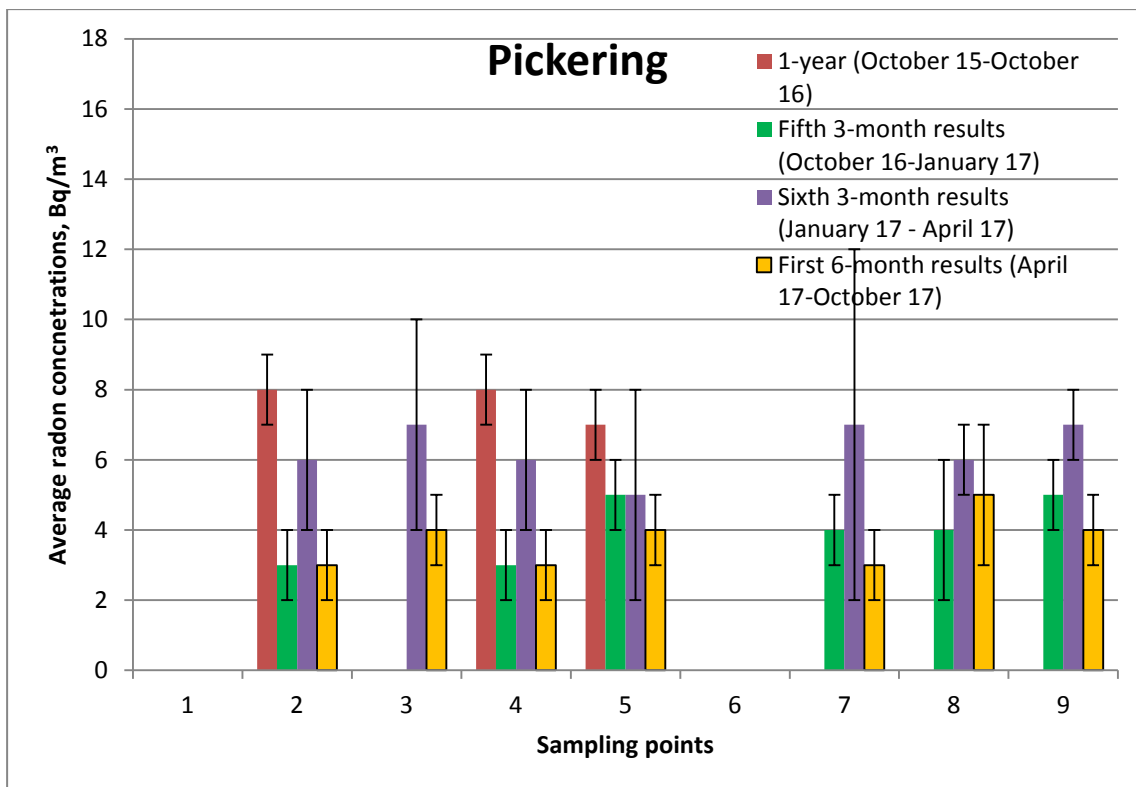
Figure 96. Average radon concentrations at the sampling points around Pickering
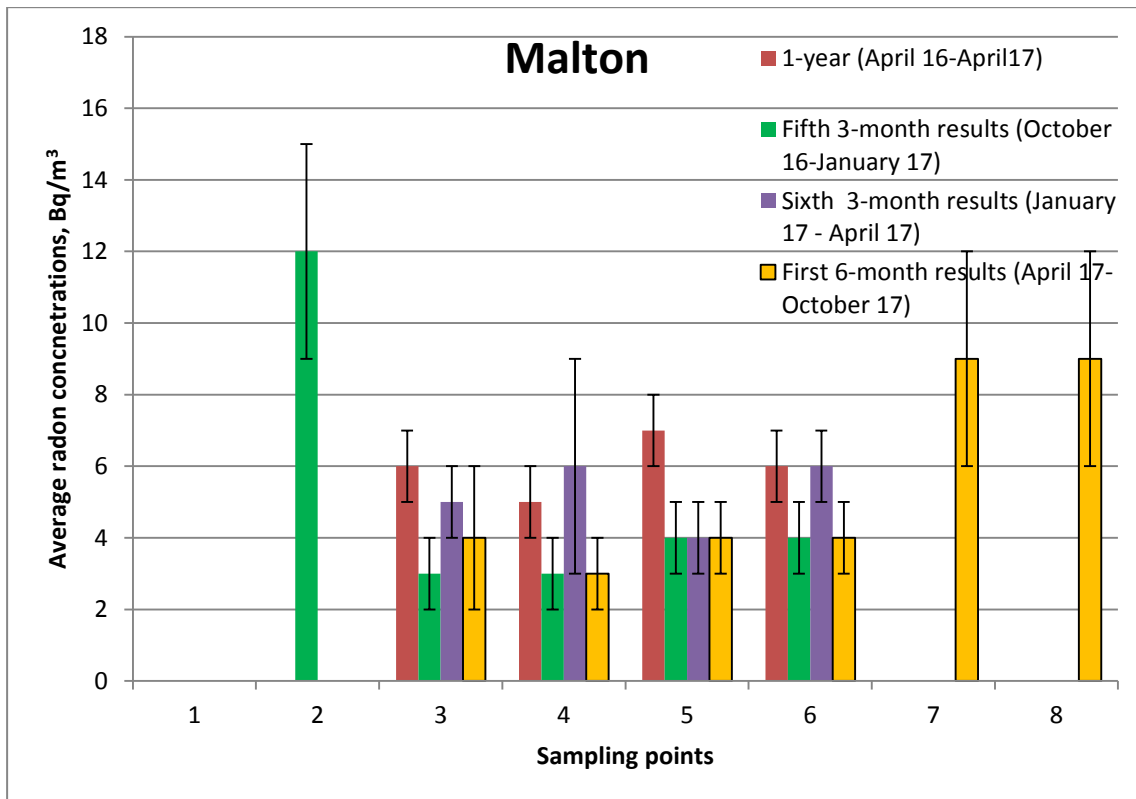
Figure 97. Average radon concentrations at the sampling points around Malton
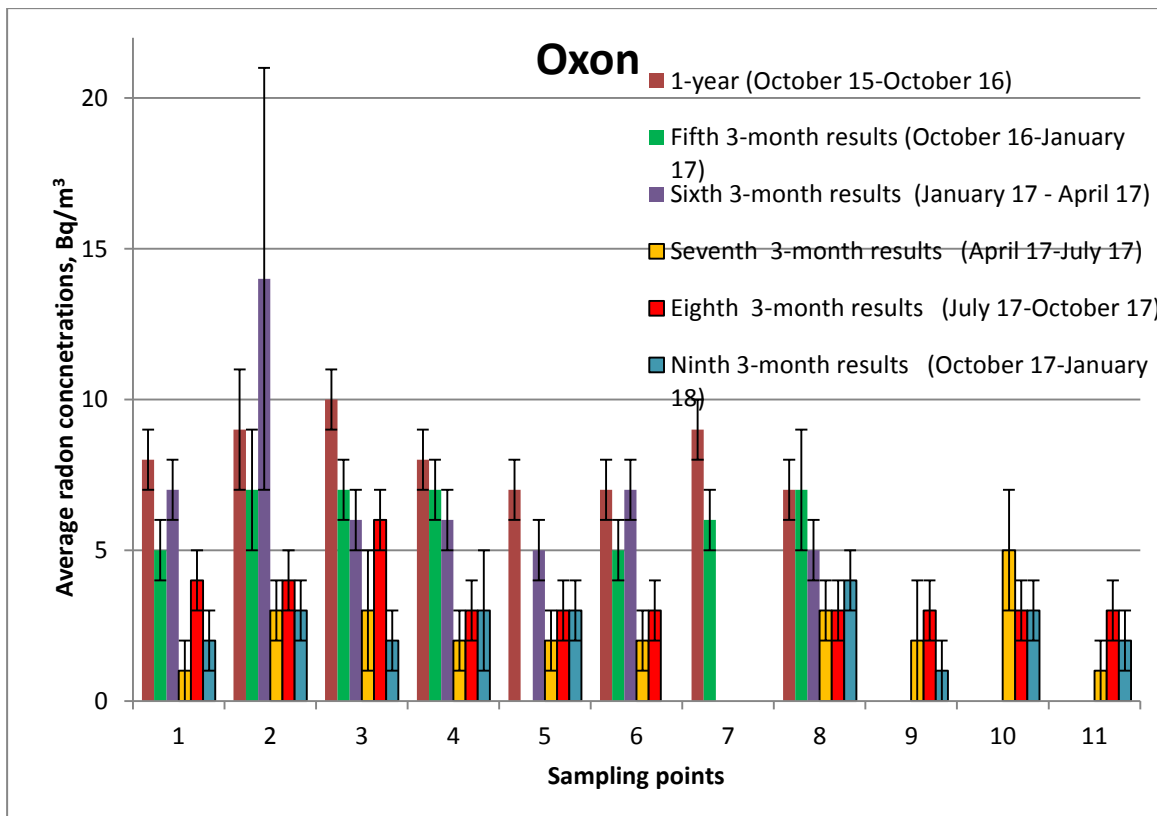
Figure 98. Average radon concentrations at the sampling points in Oxfordshire

5.3.2 Seasonality of outdoor radon

Seasonal variation of outdoor radon was studied using 3-month consecutive measurements over two consecutive years. The average radon concentrations were calculated for the areas around

Kirby Misperton and Little Barugh (15 sampling points) and for Oxfordshire where 8 sampling points monitored from October 2015 to April 2017 and 7 sampling points monitored from April 2017 to January 2018. The data for the other areas were not used because various sampling points were moved or lost due to vandalism and a consistent set was not available, the results are shown in Figure 99.

From the data it is evident that the patterns of outdoor radon in the two areas, which are situated in different parts of England, are very similar. There are also indications that the seasonal pattern of outdoor radon is different to that observed for the indoor radon results for the same periods, with results in the summer (April 2016 to July 2016) being higher than the results in spring (April 2016 to July 2016) and autumn (October 2016 to January 2017). The factors affecting radon concentrations outdoors are different to those indoors. Outdoors the concentrations are likely to be linked to environmental factors. Indoor levels are influenced by human lifestyle factors such as heating and ventilation of the home in addition to environmental factors. It is not surprising that the seasonal pattern for radon is different for indoor compared to outdoor concentrations.

The seasonality was studied further with data for Oxfordshire only; the monitoring in Yorkshire was changed to 6-month periods from April 2017. In Figure 99, which presents values at 3-month intervals, the 6-month monitoring period from April 2017 to October 2017 for Kirby Misperton is presented as two points with the same value. The outdoor radon levels in both Kirby Misperton and in the control area of Oxfordshire were approximately halved in the second year (October 2016 to October 2017) compared to the first year of monitoring (October 2015 to October 2016). This indicates a potential year-to-year variability of outdoor radon.
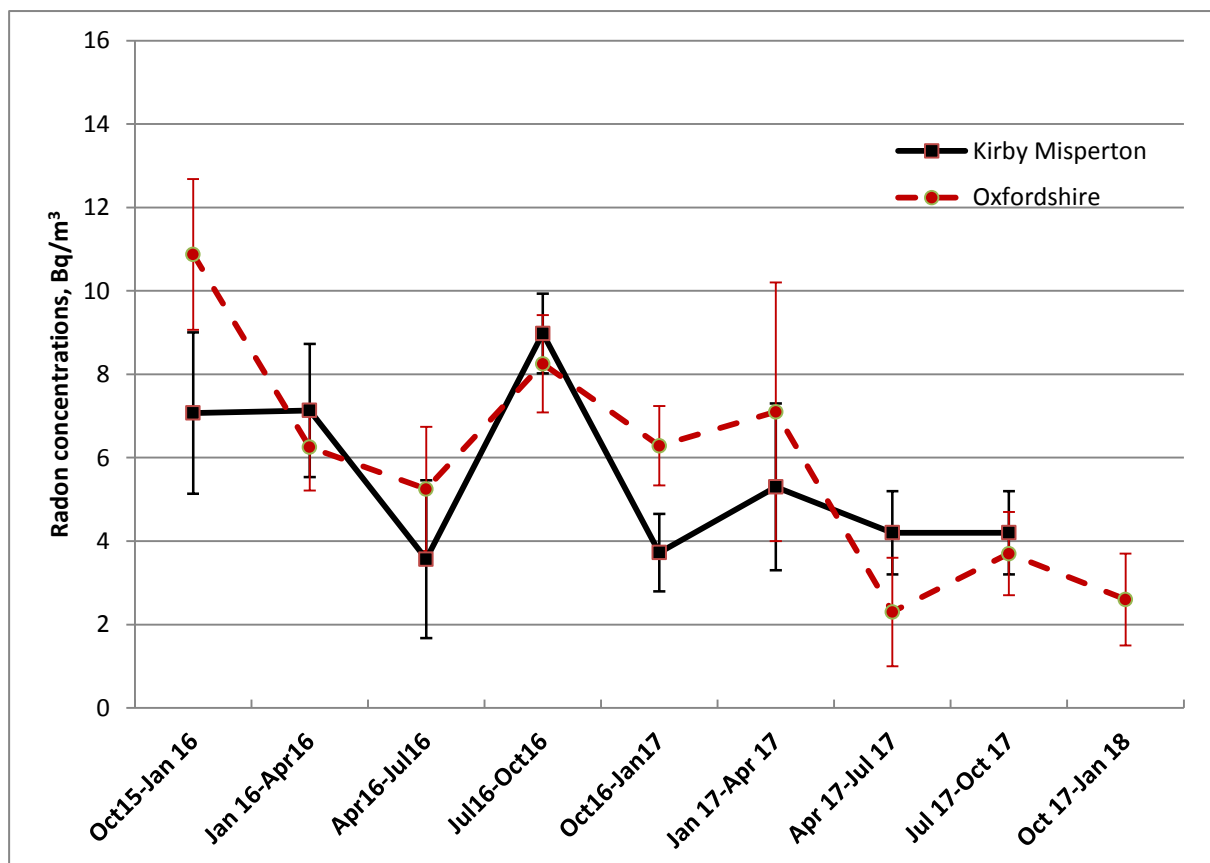
Figure 99. Seasonal variation of outdoor radon concentrations in the area of Kirby Misperton and Oxfordshire

5.4 MONITORING AT THE KM8 ENCLOSURE

The data from the AlphaGUARD continual radon monitoring instrument, placed in the enclosure at the KM8 site for the six 3-month periods between April 2016 and October 2017 were analysed. The inherent background of the instrument of 3 Bq/m^3, resulting from the longer half-life alpha emitting radionuclides (from environmental exposure and materials within the instrument), was taken into account when data were processed. The radon data, taken at 1 hour intervals, are log-normally distributed. The distribution parameters for the above monitoring periods are given in Table 23. The average radon concentrations measured over the six monitoring periods were in the range 4 to 6 Bq/m^3. In order for a comparison to be made between the outdoor radon concentrations measured with the instrument and the other outdoor results, passive monitors were also placed in the enclosure at the KM8 site.

Table 23. Range and distribution of radon measurements made with AlphaGUARD and passive detectors in the KM8 enclosure.

Period of monitoring	Range	AlphaGUARD Bq/m^3			Passive detectors Bq/m^3	
		Arithmetic Mean (AM)	Geometric Mean (GM)	Geometric Standard Deviation (GSD)	Arithmetic Mean (AM)	Standard Deviation (SD)
April 16-July16	1–46	5	5	2.0	4	1
July16-October16	1–81	6	4	2.4	8	1
October16-January 17	1–50	6	4	2.5	7	1
January 17-April 17	1–29	4	3	2.3	5	1
April 17-July17	1–47	5	3	2.4	-	-
July 17-October17	1–38	5	3	2.4	7	1

The average radon concentrations measured using 10 passive detectors are similar to the arithmetic means (AM) of the distributions measured with the AlphaGUARD for these periods as shown in Table 23. This demonstrates a good agreement between the two different measurement techniques.

A graph showing the raw data obtained from the AlphaGUARD, without background correction, is given in Figure 100. No data were collected for a short period in July 2016 when the instrument was removed and returned to PHE Chilton for downloading of data.

5.5 COMPARISON OF YEAR 1 AND YEAR 2 RESULTS

Year to year variation of indoor radon was studied with measurements from 73 homes where results were available for all eight measurement periods. The indoor radon levels did not show any obvious difference between the first year (November/December 2015–December 2016) and the second year (December 2016- December 2017) of monitoring (see Figure 92).

The seasonal and annual variation of outdoor radon concentrations were studied in the area of Kirby Misperton and in the control area in Oxfordshire. The results presented in Figure 99 displayed a difference between the radon levels measured in the first year (October 2015 to October 2016) and the second year of monitoring (October 2016 to October 2017). This is an indication of a year-to-year variability of outdoor radon.
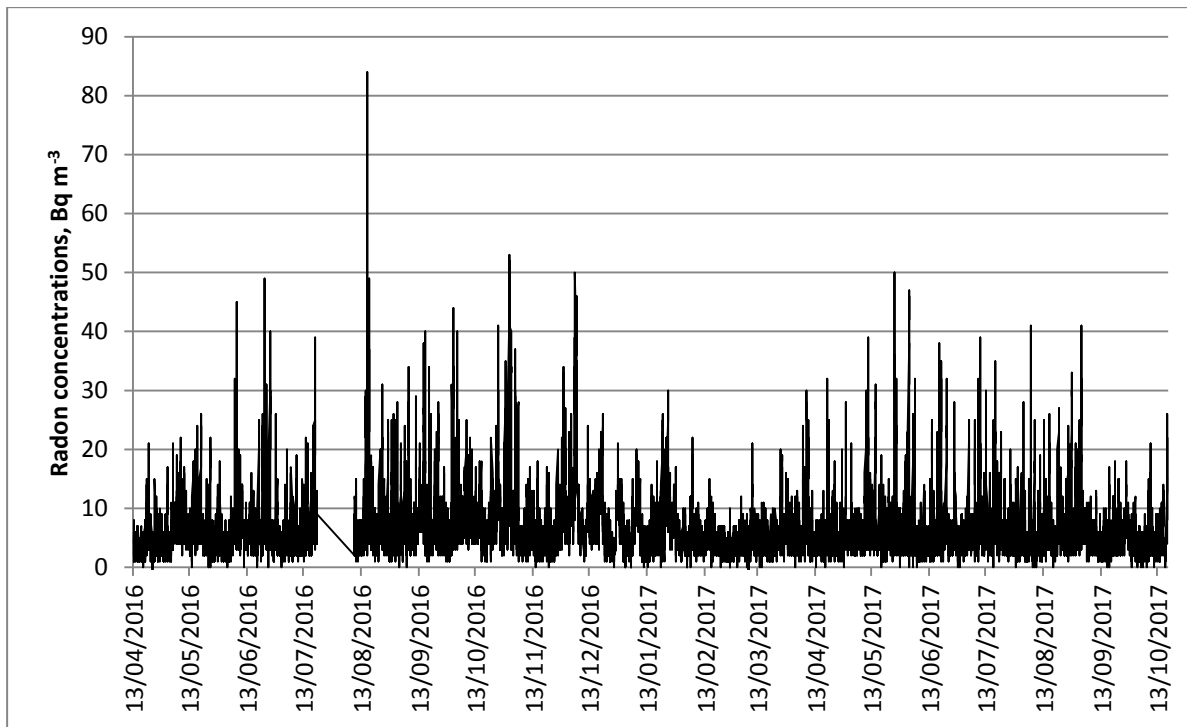
Figure 100. Time series of radon concentrations recorded by AlphaGUARD between April 2016 and October 2017

5.6 SUMMARY

5.6.1 Indoor radon

The analysis of the results for 133 homes measured in the Vale of Pickering showed distributions of indoor radon concentrations consistent with the usual log-normal distribution for indoor radon.

The results for Kirby Misperton and Little Barugh area are consistent with their status as not being Radon Affected Areas.

Results for Yedingham (an area with low radon potential) are also below the Action Level with the exception of one result for the seventh 3-month period which was measured at 240 Bq/m^3. This result demonstrates the variability of radon when measured over a period. We are aware that year-to-year variability of indoor radon of up to 40 % (Hunter et al, 2005) is possible. The other results for this house including the annual average radon results for the eighth 3-month period are lower and below the UK radon Action Level of 200 Bq/m^3.

The results for Pickering confirmed the prior status as a radon Affected Area with radon concentrations spread over a wider range from about 10 to 450 Bq/m^3 and several homes were found to have results exceeding the Action Level. Each householder was given standard advice on any action required; those with high radon levels were given additional information on reducing their radon concentrations.

Radon levels above 200 Bq/m^3 were measured in homes in Malton at the beginning of this study which confirmed our classification as a Radon Affected Area; standard advice to reduce radon levels were issued to these homes. Due to the reduction in available results as householders withdrew from the study over time, the statistical power was also reduced. Hence the probability assessment for December 2016 to December 2017 was inconclusive. To increase the sample for this area, 100 householders were contacted by post and invited to take part in the monitoring. As a result of this mailshot, a further 17 householders in Malton agreed to take part and PHE standard packs of passive detectors were sent to them by post in November 2017.

Seasonal variation of indoor radon was also studied for all areas. Results indicated that there is little seasonal variation in measurements made in homes in the areas of Kirby Misperton and Little Barugh, and in Yedingham. The seasonal variation observed in Pickering was higher, although this may be linked to better statistics (larger sample size and a higher average radon level). All areas follow the normal seasonal pattern in the UK with the highest radon concentrations in winter and lowest radon concentrations in summer. It should be noted that the number of results for Malton is rather small (see Table 22) compared to the other areas where results were assessed.

5.6.2   Outdoor radon

The results from the first year of monitoring (October 2015 to October 2016) of 3-month back to back measurements of outdoor air are about 1.5 times higher than the radon concentrations observed previously in the UK of 4 Bq/m^3 (Wrixon et al). In contrast the results from the second year of the monitoring (October 2016 to October 2017) indicated levels closer to those previously measured. There is no indication of elevated outdoor radon concentrations in the Pickering or Malton Radon Affected Areas. The analysis of results for another control site in Oxfordshire showed similar concentrations.

Seasonal variation of outdoor radon was studied for areas around Kirby Misperton and Oxfordshire. Results showed similar patterns in these geographically distant areas. The study of seasonal variation of outdoor radon is continuing using 3-month back to back measurements in Oxfordshire.

5.6.3   Monitoring at KM8

Results from an AlphaGUARD active monitor and passive detectors, placed in the KM8 enclosure are in good agreement with the average outdoor radon in the area of Kirby Misperton. The active monitoring showed significant variations over time, however the annual average measured at the KM8 site was consistent whichever of the techniques was used.

5.7   REFERENCES

Darby S, Hill D, Auvinen A, Barros-Dios J M, Baysson H, Bochicchio F. et al. (2005) Radon in homes and risk of lung cancer: collaborative analysis of individual data from 13 European case-control studies. BMJ, 330 :223.

Miles J C H and Algar R A (1988) Variations in radon-222 concentrations. Journal of Radiological Protection 8 (2), 103-106.

Miles J C H, Appleton JD, Rees DM, Green BMR, Adam KAM, Myers AH (2007) Indicative Atlas of Radon in England and Wales, Chilton, HPA-RPD-033.

Miles J C H, Howarth C B and Hunter N (2012) Seasonal variation of radon concentrations in UK homes. J. Radiol. Prot. 32, 275-287

Howarth C B and Miles J C H (2008) Validation scheme for organisations making measurements of radon in dwellings: 2008 revision. Chilton, HPA-RPD-047

Hunter N, Howarth C B, Miles J C H, Muirhead C R (2005) Year-to-year variations in radon levels in a sample of UK houses with the same occupants. Seventh International Symposium on the Natural Radiation Environment (NRE-VII). In: Radioactivity in the Environment Book Series, vol. 7. Elsevier, 438-447.

Kibble A, Cabianca T, Daraktchieva Z, Gooding T, Smithard J, Kowalczyk G, McColl N P, Singh M, Mitchem L, Lamb P, Vardoulakis S and Kamanyire R (2014) Review of the Potential Public Health Impacts of Exposures to Chemical and Radioactive Pollutants as a Result of the Shale Gas Extraction Process, Chilton, PHE-CRCE-009.

Wrixon A D, Green B M R, Lomas P R, Miles J C H, Cliff K D, Francis E A, Driscoll C M H, James A C and O'Riordan M C (1988) Natural Radiation Exposure in UK Dwellings. Chilton, NRPB-R190.

Ward R S, Smedley P L, Allen G et al. 2017. Environmental Baslein Monitoring Project: Phase II – Final Report. Report of the British Geological Survey. OR/17/049. http://nora.nerc.ac.uk/id/eprint/517889/.

6 Soil Gas

6.1 INTRODUCTION

The soil gas element of the project sought to establish baseline conditions for the concentrations of gases in the soil, flux of key gases from the soil to the atmosphere and near-ground atmospheric levels of gases. There is therefore some overlap with the atmospheric monitoring (Section 4). Since radon was measured at a subset of the surveyed locations there is also some linkage to the radon work (Section 5).

Baseline soil gas measurements, like those for the other elements of the project, provide a basis against which to assess any future changes that might result from shale gas-related activities. Although of low probability, there is the potential for gas to escape from depth along geological pathways (faults, fractures and other higher permeability zones) or man-made features, especially wells (either pre-existing or drilled for oil/gas exploration, evaluation or development). The more extensive monitoring carried out in the previous phase of the project (Phase 2) is described in Ward et al. (2017).

The soil gas monitoring was restricted during this phase of the project to continuous monitoring. This included measurements with automated flux chambers and a scanning methane laser system located at the shale gas well site (KM8), a soil gas monitoring station at a farm to the east of Kirby Misperton and the operation of an eddy covariance (EC) system near Little Plumpton (the Fylde).

Site selection was based on a mixture of scientific and pragmatic considerations and the general principles are described in more detail elsewhere (Smedley et al., 2015). At KM8 and Little Plumpton the equipment was located close to the air quality and greenhouse gas atmospheric monitoring instrumentation and measurement points. Thus equipment was sited at, or very close to, the proposed shale gas wells. The farm site is close to groundwater monitoring boreholes where high baseline methane concentrations have been measured.

The eddy covariance system has operated throughout the year with data downloaded during monthly site visits by Manchester University staff. Monitoring has been more or less continuous with only very rare loss of measurements resulting from downloading or data corruption issues.

The flux system at KM8 had to be removed on 27th September 2017 as Third Energy were making major changes at the site and planned to move the air monitoring cabinet in which the flux analyser and multiplexer units were installed. One of the flux chambers was found to be faulty and the opportunity was taken to carry out repair and general servicing of the system. The equipment was re-installed on 23rd January 2018.

The soil gas station has operated over most of the period from May 2017 with some downtime for servicing and repair. Telemetry of the data was implemented allowing regular checks on the system and remote data downloads.

There have been major problems with the scanning laser system. It has been returned to the manufacturer in Canada for servicing and repair. The major changes on the KM8 site in the autumn of 2017 precluded the re-installation of the equipment and so the opportunity was taken to carry out a major upgrade of the equipment. It will be available, in a significantly improved form, from April 2jj018 and can be re-installed at the KM8 site now that it is more easily accessible. While not ideal, establishing the CH_4 baseline is not solely reliant on the scanning laser system, as we also have supporting methane data from atmospheric monitoring. The scanning laser system is expected to be back in operation well in advance of renewed site activities taking place.

6.2 RESULTS AND DISCUSSION

### 6.2.1 Continuous CO_2 flux monitoring at KM8

Continuous CO_2 flux data have been acquired from the KM8 well site near Kirby Misperton during the period 14 October 2016 to 27 September 2017, almost a full year of measurement.

Data for the period 01 April 2017 to 27 September 2017 (Figure 101 (combined data) and Figure 102 (individual cells)) are described below and compared with measurements made during the previous year.
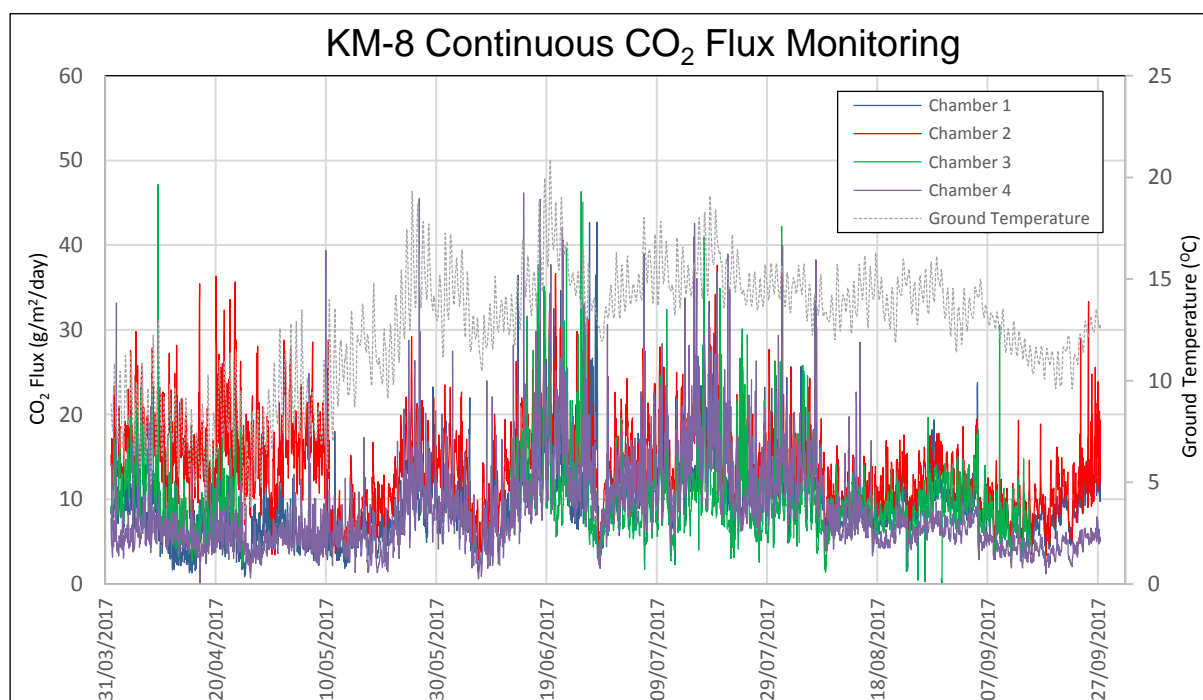
Figure 101. Continuous time series plot of CO_2 flux from chambers 1, 2, 3 and 4, along with ground temperature

Data are continuous for chambers 1, 2 and 4. There is a break in data recorded from chamber 3 between 25/04/2017 and 12/06/2017 and also from 15/09/2017 until the end of data acquisition on 27/09/2017. This was due to water ingress through a faulty seal around the chamber actuator mechanism housing which caused damage to the internal electrical circuit.
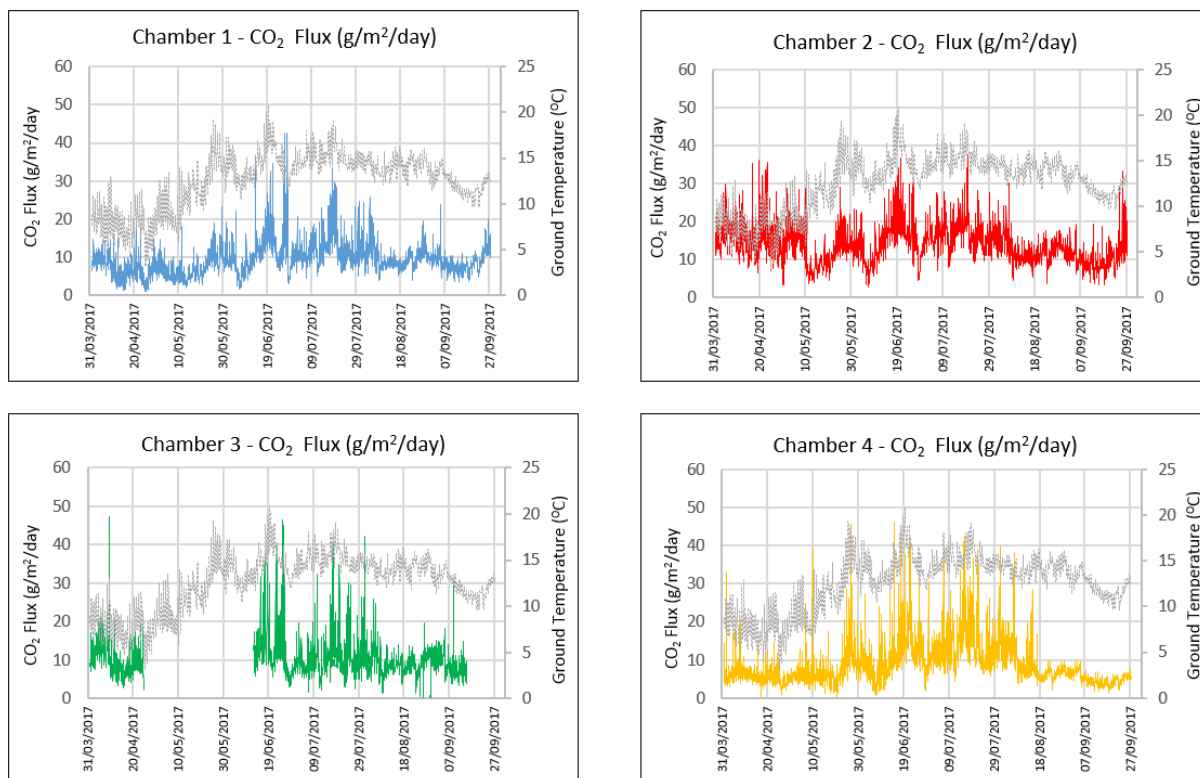
Figure 102. Individual continuous time series plots of CO_2 flux from chambers 1, 2, 3 and 4, along with ground temperature

The overall trends from all four chambers are very similar, generally displaying lower CO_2 flux during the colder months of March, April and September, when plant growth and microbial activity is reduced, thus producing less biogenic CO_2. Data for all four chambers show higher fluxes during May, June, July and August, corresponding with elevated ground temperatures and associated plant growth and microbial activity.

The data show discernible diurnal components and also longer lasting features which likely reflect weather conditions, particularly rainfall. Heavy rain can cause the ground to become saturated, resulting in water 'sealing' the surface and preventing the migration of gas to the atmosphere. This effect is seen in all four chambers between 28th and 29th June 2017 where a sharp decrease in flux can also be related to a coincident drop in both atmospheric pressure and ground temperature.

A slight rise in flux values is seen in chambers 1, 2 and 4 towards the end of the period of continuous data recording, and is concurrent with an increase in ground temperature. Data were not recorded from chamber 3 at this time due to the water-damaged circuit board.

As with the data recorded up to 31st March 2017, the measured fluxes are relatively low, with chamber 2 typically displaying slightly more elevated values, particularly in the period from 1st April to 10th May. The reason for this is unclear, however the heterogeneous nature of the site and the proximity of the chamber to recently planted saplings may be influential.

Flux concentrations from chambers 1 and 3 are very similar and are again consistent with those previously measured at the same locations. Similarly with chamber 4, which, whilst displaying a very similar overall trend to the other three chambers, generally shows slightly lower flux values, particularly when ground temperatures are colder. The relative flux relationships between chambers were the same in 2017-18 as seen in 2016-17. Absolute flux levels were lower in 2016-17 as the data cover October to March, largely the autumn-winter period of lower biological activity rather than the April to October period measured in 2017-18 (Figure 103).
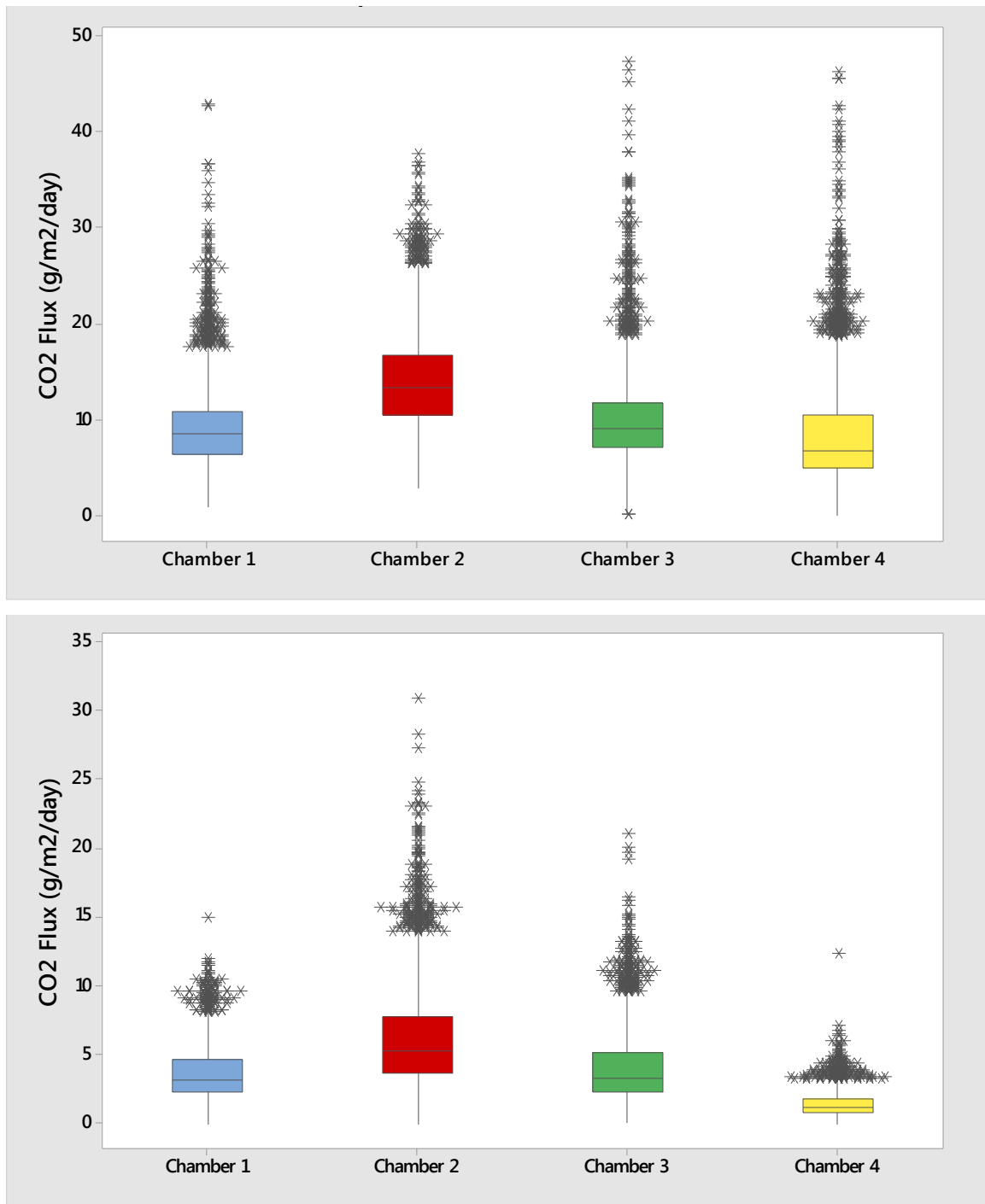
Figure 103 Summary of CO$_2$ flux data at KM8 during 2017-18 (top) and 2016-17 (below)

The flux values measured continuously at the KM8 site are in good agreement with those measured during discrete surveys at nearby farms A and B over a previous, but similar, time period. This illustrates the increase in CO$_2$ flux during the summer months where crop and surface vegetation growth, and accompanying microbial activity, are at their highest rate, resulting in a greater contribution of biogenic CO$_2$ from the soil to the atmosphere. Peak values observed at KM8 are typically between 35g/m^2/day and 45g/m^2/day during the months May – August, which is similar to the bulk of data from farms A and B, shown as boxplots below (Figure 104).
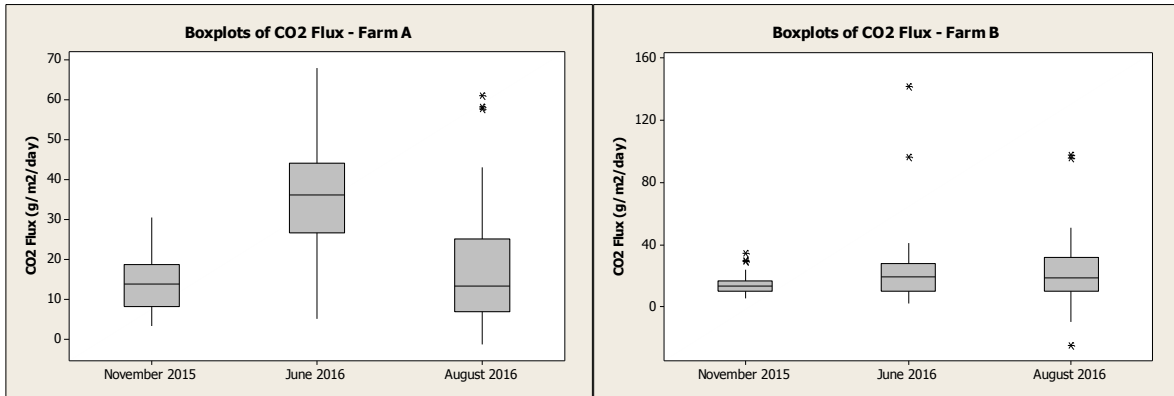
Figure 104. Summary of data (boxplots) from survey flux measurements at two farms east of Kirby Misperton
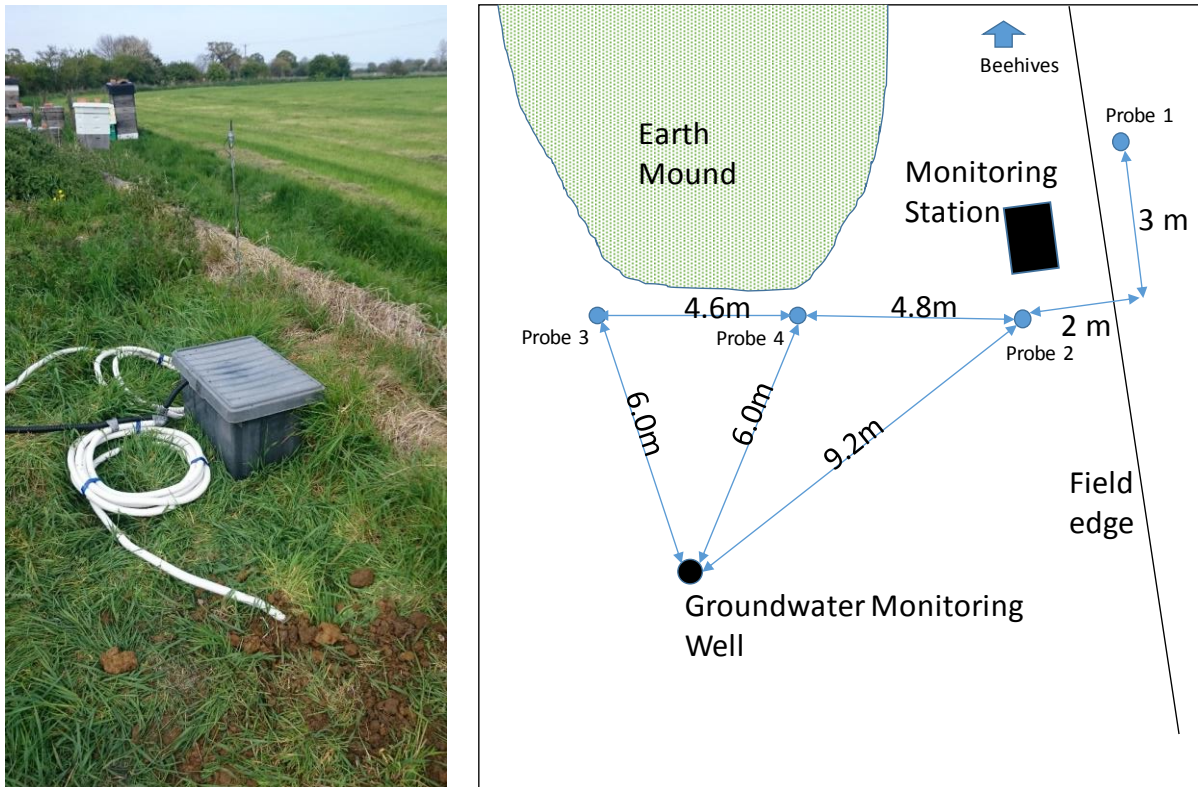
6.2.2 Soil gas monitoring

The soil gas monitoring station east of KM8 was operational from the beginning of September 2016 until 3 March 2017 with a gap for maintenance and repair in November 2016 (Figure 105).

After a period of routine maintenance it was reinstalled in a slightly different configuration in early May 2017 (Figure 106) and has operated since then, although one probe has been out of commission since December 2017. This has now been repaired and can be redeployed. The other three probes have functioned for almost a full year (Figure 107) with much less down-time than in 2016-17 (Figure 105).
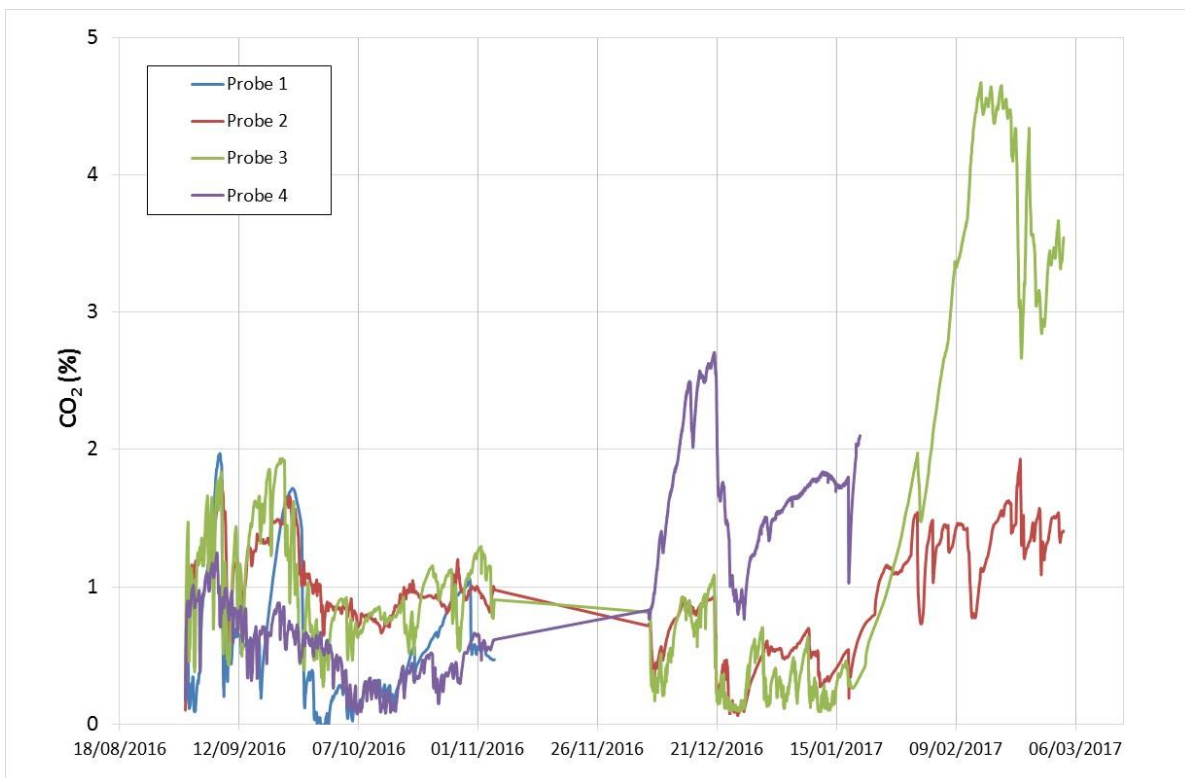
Figure 105. Summary of all continuous soil gas data for the monitoring station east of Kirby Misperton during 2016-17

Figure 106. Soil gas monitoring station appearance (left) and layout in 2017-18 (right)
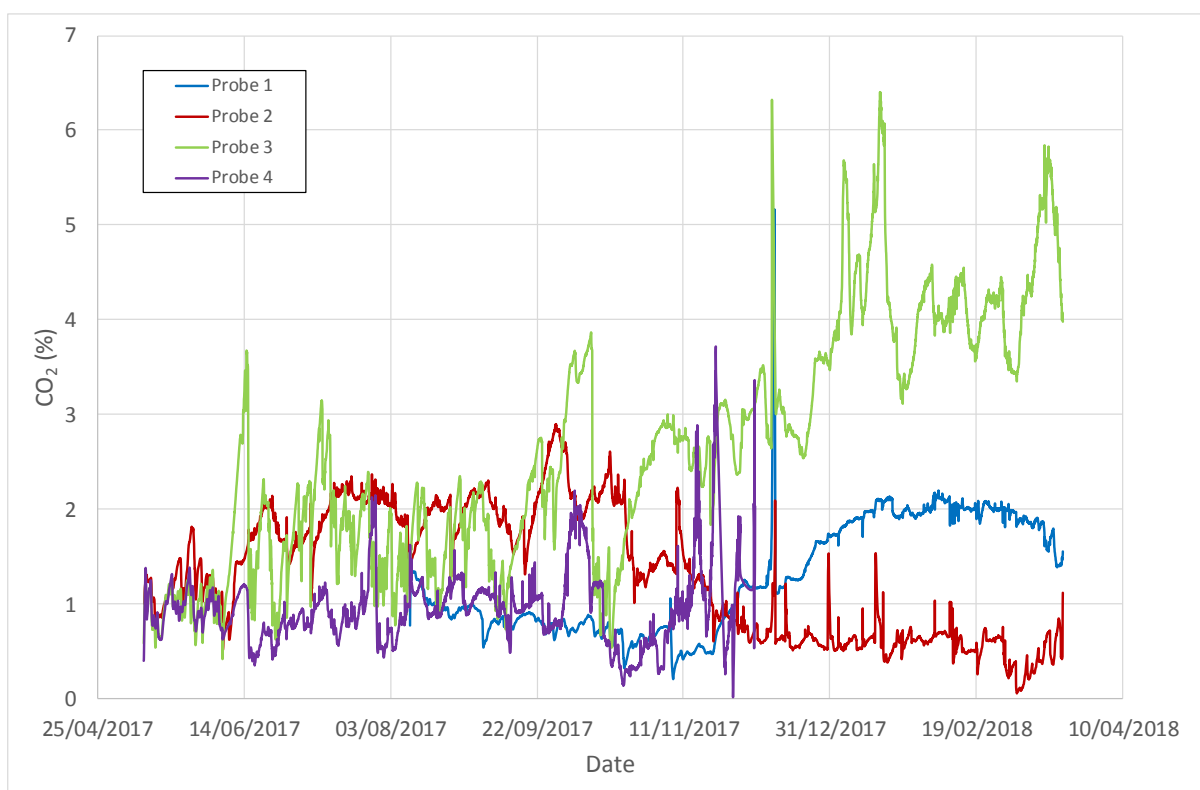
Figure 107. Summary of all continuous soil gas data for the monitoring station east of Kirby Misperton during 2017-18

The highest CO_2 values in both years were recorded by probe 3 in the winter months of January to early March. Relatively higher values were also measured by probe 1 at this time, although probe 2 gave relatively low concentrations during this interval. Wet surface layers can impede the flux of gas from the ground and lead to a build-up of gas in the soil. Saturation of the soil

may also explain the subdued response of probe 1 during this winter period. Differences between the probes likely reflect small-scale variability in ground conditions in the monitored area. This may also explain different patterns of response between the probes. Conversely there are also coincident peaks and troughs of CO_2 concentration seen in the different probes and a fuller analysis with meteorological information could probably tie these to specific events such as rainfall accompanying the passage of weather systems.

6.2.3   Eddy covariance (EC)

Continuous EC data have been acquired from the Little Plumpton site during the period 19/01/2016 to 02/03/2018. There were two periods where data was corrupted and could not be recovered. These are 04/05/2016 to 19/05/2016 and 21/06/2017 to 13/07/2017 and are represented by the flat lines in the time-series data. To allow easier comparison and remove diurnal variation, where a time series is presented the data has been smoothed using a 48h moving average. Overall the range of data from each year is comparable to the other years. This gives us greater confidence that the values being observed are representative of the background for the site.

As expected, air temperature for each year (Figure 108) shows the seasonal trends of cooler temperatures in the winter months and warmer summer months, where there is less variation. The CO_2 flux (Figure 109) mirrors the temperature data, with higher fluxes observed during the cooler months when there is less biological activity. The broadly negative flux observed between day 75 and day 200 is representative of the ground is acting as a CO_2 sink. The positive values during the rest of the year suggest the ground surface represents a source of CO_2.

The peak in CO_2 concentration (Figure 110) also broadly mirrors the temperature, with the greatest concentrations occurring during the summer months. The minimum CO_2 concentration stays broadly the same (c.370 ppm) throughout the year. Wind speed (Figure 111) ranges between 1 and 7 m/s[1] throughout the year with similar values observed for all years. When plotted against CO_2 concentration the fully mixed concentration can be derived (Figure 112). This represents the regional/background CO_2 concentration and is in alignment with that calculated from the time series of concentration (ca. 375 ppm).

Finally, seasonal CO_2 concentration is plotted against wind direction (Figure 113). Since the site is close to the west coast of the UK, CO_2 concentrations are more tightly grouped at lower concentrations when the wind is from a westerly direction when relatively clean air is reaching the instruments from the Irish Sea.
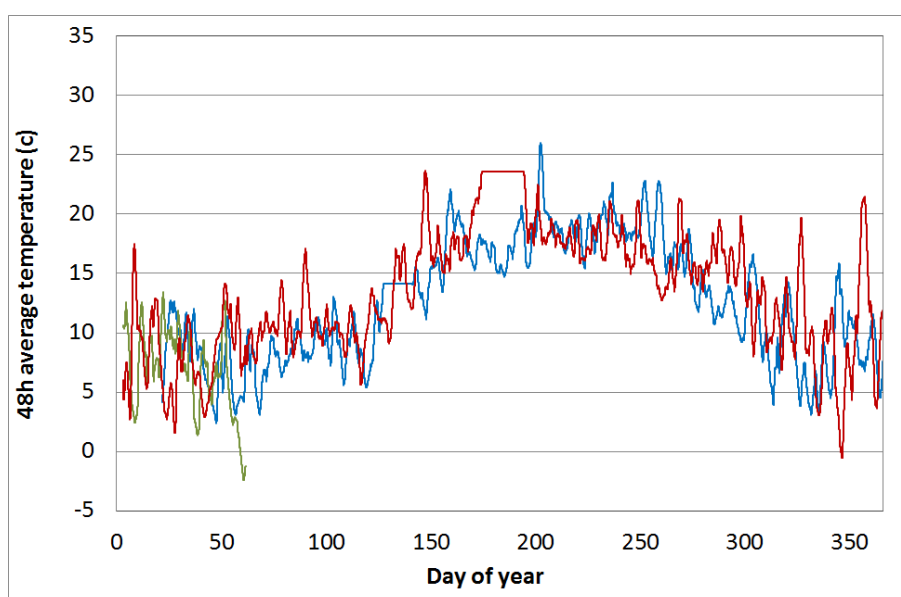
Figure 108. Yearly time series plot of air temperature for 2016 (blue), 2017 (red) and 2018 (green)

118
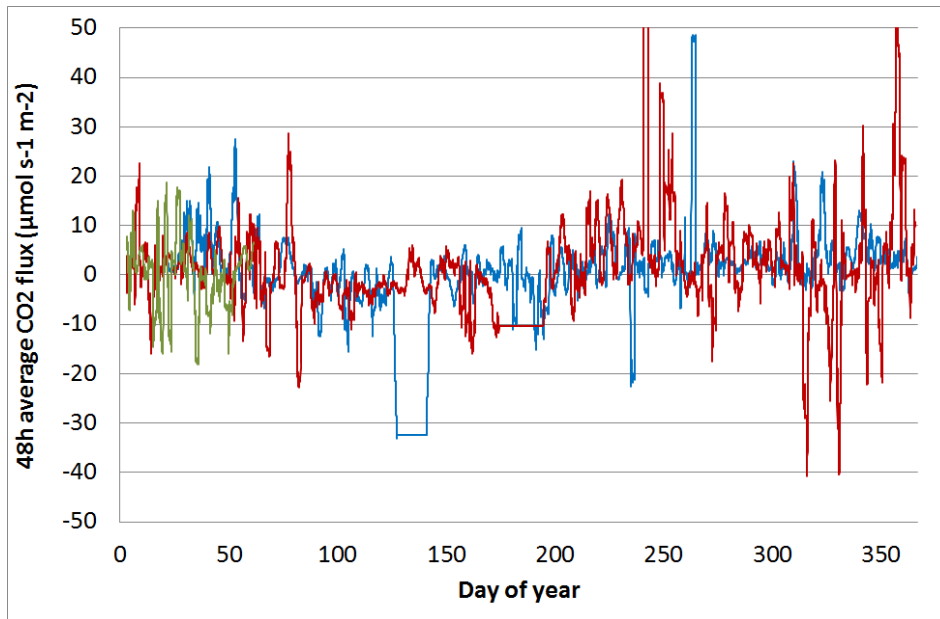
Figure 109. Yearly time series plot of CO_2 flux for 2016 (blue), 2017 (red) and 2018 (green)
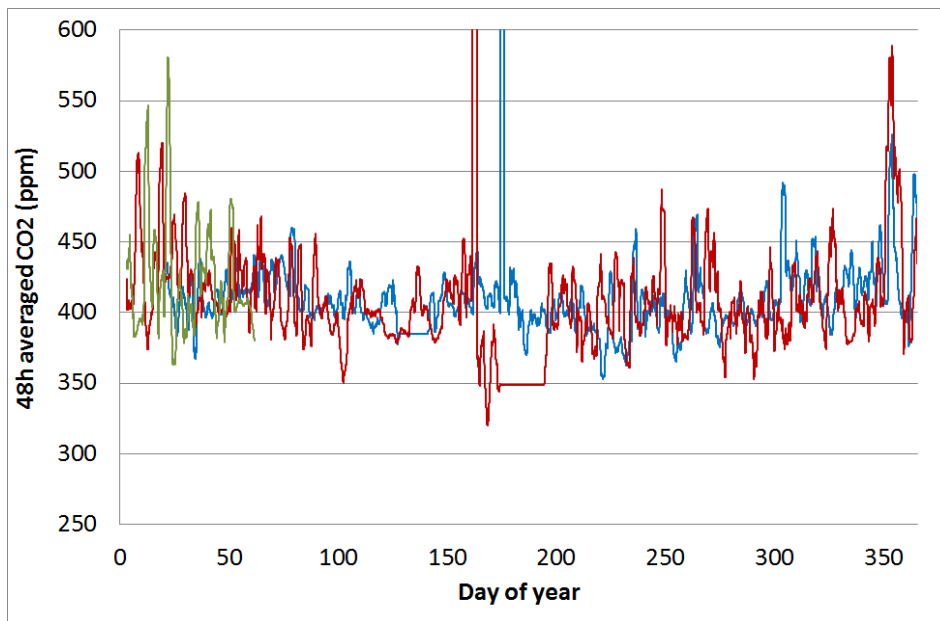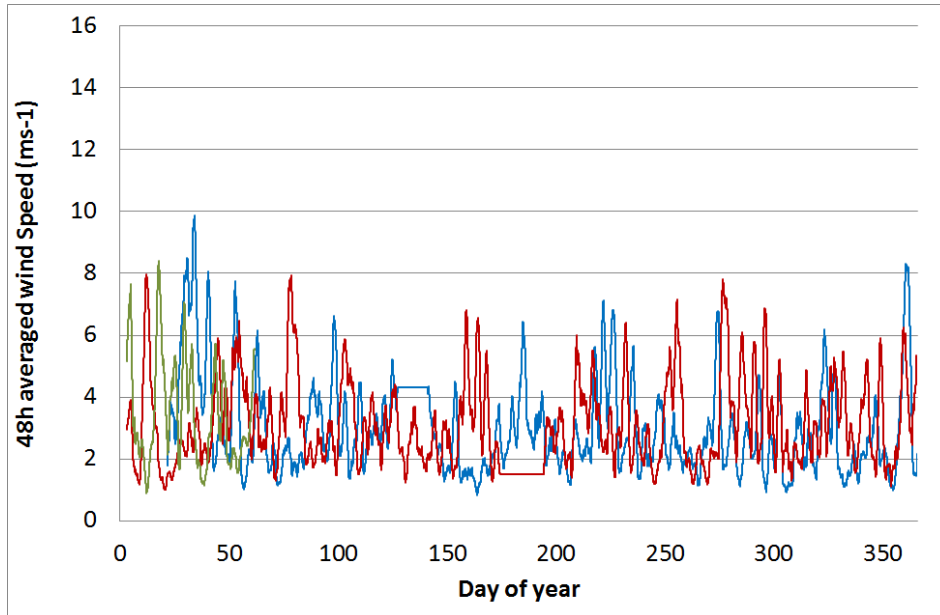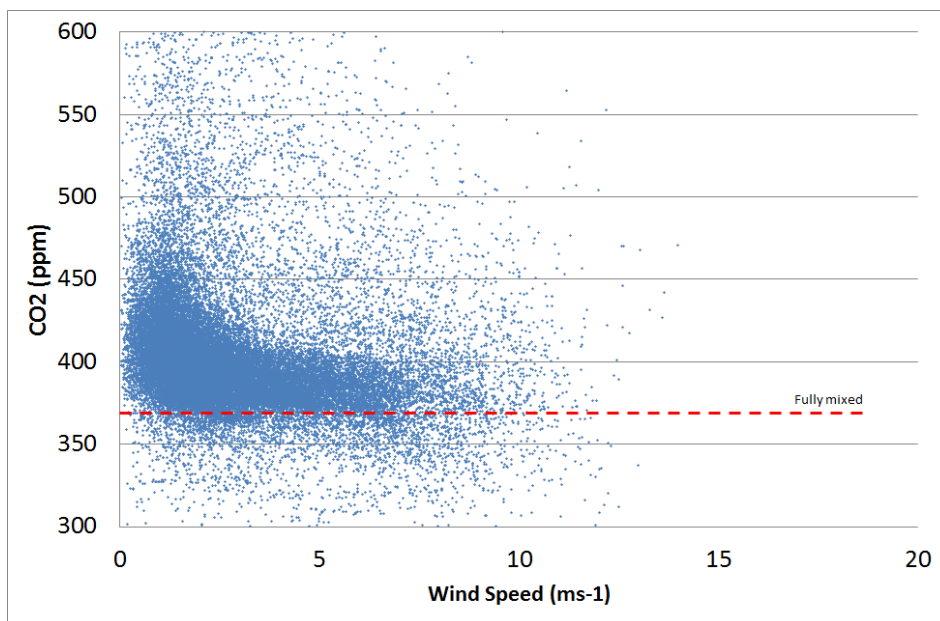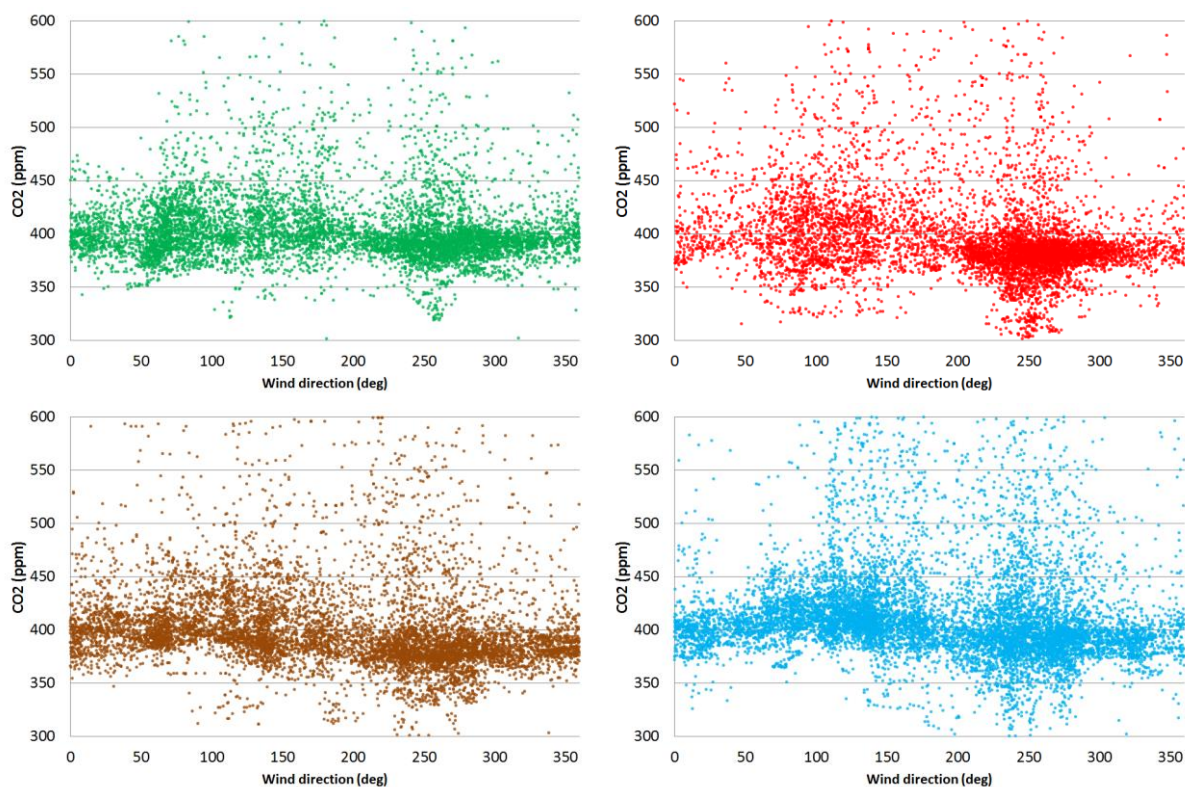

Figure 110. Yearly time series plot of CO_2 concentration for 2016 (blue), 2017 (red) and 2018 (green)

Figure 111. Yearly time series plot of wind speed for 2016 (blue), 2017 (red) and 2018 (green)

Figure 112. CO$_2$ concentration plotted against wind speed. The red line represents the approximate background regional CO$_2$ concentration

120

Figure 113. Seasonal CO$_2$ concentration plotted against wind direction for spring (green), summer (red), autumn (brown) and winter (blue)

6.2.4 Geostatistical analysis of sampling requirements for soil gas measurements

An initial statistical evaluation of soil gas datasets was carried out to examine spatial and temporal variability. The spatial distribution of survey observations was assessed on the basis of a geostatistical model using prior information on likely sources of variation and analysis of the data. The developed model can potentially be used to support decisions on sampling requirements for any future monitoring that is required during baseline and operational phases of shale gas development.

A critical consideration in ongoing monitoring of soil gas concentrations (or equally fluxes) is the number and frequency of measurements (i.e. the sample design) that are required to produce a meaningful estimate of the soil gas status. The accuracy of any estimate of soil gas status will vary according to the number of measurements and the amount of variation in the soil gas concentrations. Now that we have measurements over two years of monitoring, we are in a position to assess the degree of spatial and temporal variation in the observations and the implications for our sampling requirements.

The first stage of such an assessment is to decide the exact spatial and/or temporal scale over which we wish to predict the soil gas concentrations. For instance, we might wish to determine the field scale average concentrations or alternatively we might wish to continuously map the variation of the concentration. Both estimates will be subject to uncertainty. For example, Figure 114 (left) shows a geostatistical prediction of the variation of CO$_2$ flux across a field in November 2015. Note that geostatistical models require that the observations are normally distributed whereas the CO$_2$ fluxes are highly skewed. Therefore, we shifted and log-transformed the data prior to predicting this map. Figure 114 (right) indicates the uncertainty associated with the predictions at each site. It is clear that the expected errors increase as the predictions move away from the measurement sites (although larger errors are also evident at the field edges).

121
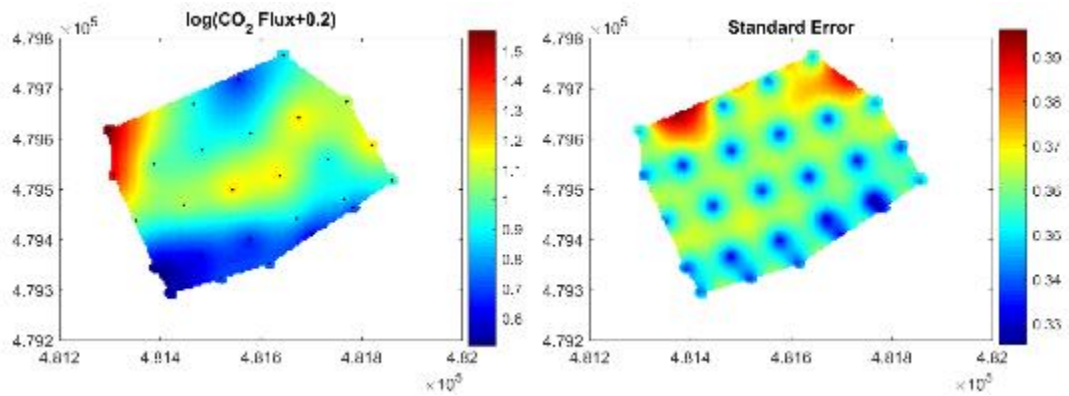
Figure 114. Geostatistical prediction of log (CO$_2$ flux +0.2) with measurement locations denoted by black dots (left) and associated standard errors (right). Units are log(g/m^2/d^1)

Both the predictions and the standard errors shown in Figure 114 depend on the spatial variability or correlation of the flux measurements. This spatial variation can be expressed in terms of a variogram (Webster & Oliver, 2007). The variogram describes how the expected squared difference between two observed values increases as the distance between the two measurements increases. The variograms shown in Figure 115 for log (CO$_2$ flux +0.2) were estimated by residual maximum likelihood (Lark & Cullis, 2006) from the measurements made in each field campaign. Some differences in these variograms from different campaigns are evident. The total variation is largest in the June 2016 and August 2016 campaigns whereas measurements made a small distance apart are most similar for the November 2015 and October 2016 campaigns.
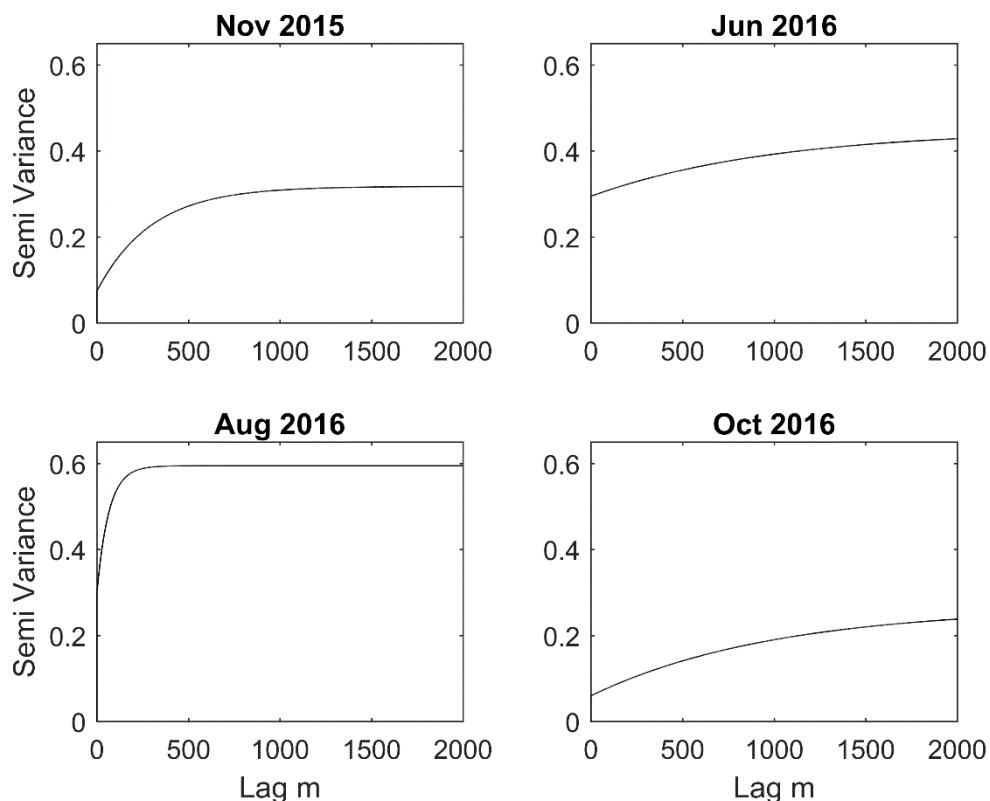
Figure 115. Maximum likelihood estimates of variograms for of log (CO$_2$ flux +0.2)

Once we know the variogram for a particular variable it is possible to use it to calculate the uncertainty associated with spatial predictions of that variable based on any proposed set of measurement sites. For example, we consider 81 soil gas measurements positioned on a regular

square grid and the prediction of the CO_2 flux at the very centre of that grid so that the prediction site is equidistant from the four closest measurements. If we increase the grid-spacing we can explore how the standard errors increase as the measurement intensity decreases (Figure 116).
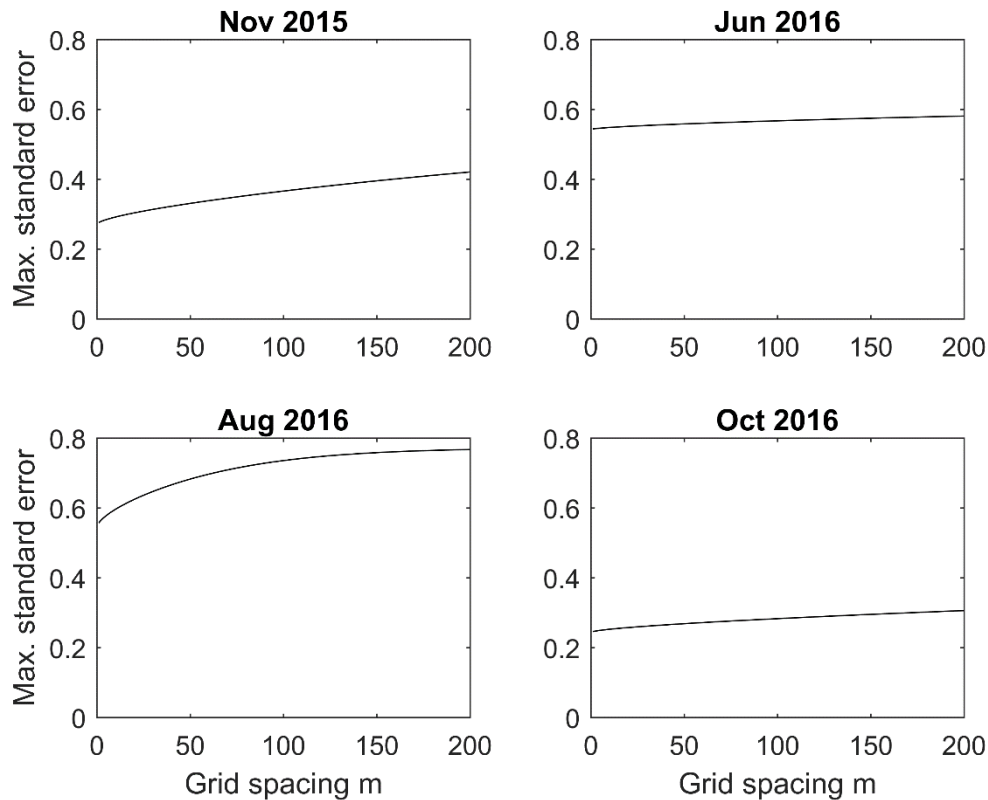
Figure 116. Standard errors for spatial log (CO_2 flux +0.2) predictions at the centre of 81-point regular square grids of different sizes

The rate of increase in errors reflect the variograms shown in Figure 115, with the largest errors occurring in June and August when the fluxes are more variable. Figure 117 shows the results for a similar exercise using CO_2 concentrations.

Although based on a relatively small number of surveys, these results likely reflect the higher biological activity (plant and microbial) in the main spring and summer growing seasons compared with lower levels of activity in the autumn. They support previous studies (e.g. Beaubien et al., 2013) in suggesting that the autumn is the optimal time for detecting any emissions resulting from shale gas (or other) operations as natural background is at its lowest. The variation in error with grid spacing was again more significant for spring and summer surveys. The errors associated with the relatively wide spacing of soil gas and flux measurements (200 m) will be offset by the lower errors arising from more closely spaced mobile laser data (typically 10 m spacing).
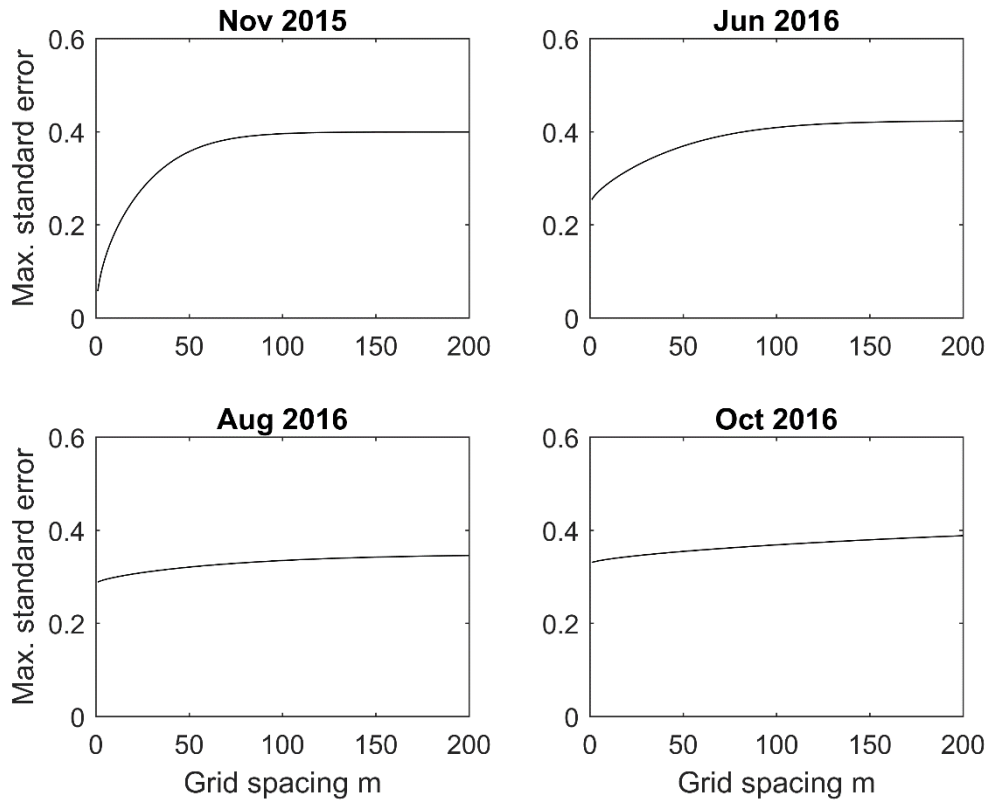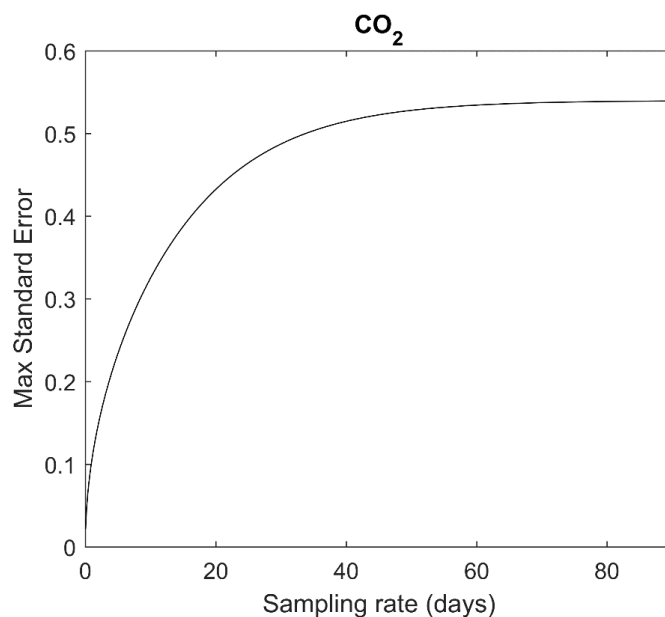
Figure 117. Standard errors for spatial log (CO₂ conc +0.2) predictions at the centre of 81-point regular square grids of different sizes. Units are log (%)

The same approach can also be used to assess the implications of different temporal frequencies of measurements using the data from the continuous CO_2 flux and concentration monitoring stations at KM8 and a farm to the east, respectively. In this case, we predict the gas variable half-way between two measurement times and consider the implications of increasing the gap between measurements (Figure 118 and Figure 119). The benefits of a high frequency of measurements are evident in each case. A very low standard error applies at the 1 hour rate of sampling used for the soil gas and flux measurements and would also be expected for the 30 minute averages derived from the very high (10 Hz) data acquisition rates of the eddy covariance system.
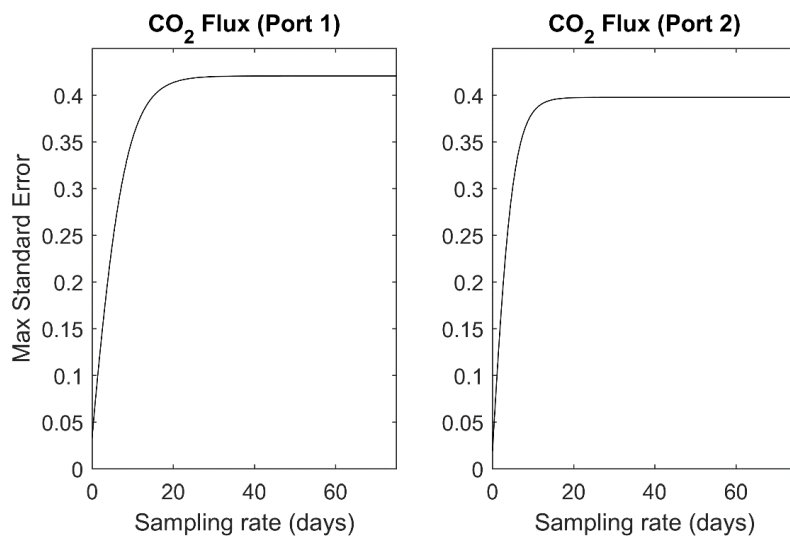
Figure 118. Standard errors for temporal log (CO₂ flux +0.2) predictions at the time midway between two measurements as a function of time between measurements

Figure 119. Standard errors for temporal log (CO$_2$ concentration +0.2) predictions at the time midway between two measurements as a function of time between measurements

In conclusion, now that datasets illustrating the spatial and temporal variation of gas concentrations and fluxes are available we are in a position to use geostatistical techniques to estimate the expected errors that will result from spatial or temporal prediction of these properties over any specified scale under the assumption that these future surveys follow the same patterns of variation. This can be used to guide future surveys or continuous measurements and the analysis can be refined by incorporating the data from that monitoring.

6.2.5 Summary and overall conclusions on baseline monitoring and outcomes

The data collected continue to show the seasonal variability in baseline soil gas and flux values. They also reveal shorter-term diurnal changes and event-driven variations, for example related to the passage of weather systems. The longer time series data and the preliminary geostatistical appraisal of selected data continue to demonstrate that any emissions related to shale gas operations will be easiest to detect in the autumn when baseline biological activity is lower, but the soil remains dry. Saturation of the ground in the winter months precludes free gas measurements.

Earlier survey data from the Vale of Pickering, and other studies (e.g. Beaubien et al, 2013; Romanak et al., 2012), has shown that gas ratios can be useful in separating different source of gas e.g. CO$_2$/O$_2$ and CO$_2$/N$_2$ can distinguish deep gas from shallow biogenic gas and CO$_2$ produced from CH$_4$ oxidation. However, dissolution of CO$_2$ in pore water can blur these distinctions. A very recent paper (Györe et al., 2018) demonstrates the potential value of additional ratios (C1/C2+C3) and stable C isotopes in differentiating deep and shallow gas. Additional measurements and sampling (with laboratory analysis of a wider range of gases and isotope analysis) would help to identify any baseline deep gas present and allow better characterisation of the baseline.

BGS is significantly upgrading its soil-gas monitoring capability. A high precision CH$_4$, CO$_2$, O$_2$ and H$_2$O analyser and upgraded laser CO$_2$ and CH$_4$ analysers are expected for delivery by April 2018. Additional survey measurements using these instruments would further enhance the baseline dataset and allow a direct comparison with measurements with the same equipment during shale gas operations. Further survey data (and continued time series monitoring) could be used to extend and refine geostatistical analysis to optimise future monitoring strategies in the Vale of Pickering, Lancashire or any subsequent areas of shale gas development.

The new lasers can be used in scanning mode for continuous measurements and there is scope to deploy these for periods at KM8, elsewhere in the Vale of Pickering or in Lancashire. The optimal siting would depend on developments at the shale gas sites. For example, the erection of a high sound barrier at KM8 creates very enclosed conditions with turbulent air flows at the site and this can cause serious problems when co-processing gas concentration and 3-D air flow data.

6.3 REFERENCES

Beaubien, S E, Jones, D G, Gal, F, Barkwith, A K A P, Braibant, G, Baubron, J C, Ciotoli, G, Graziani, S, Lister, T R, Lombardi, S, Michel, K, Quattrocchi, F and Strutt, M H. 2013. Monitoring of near-surface gas geochemistry at the Weyburn, Canada, CO2-EOR site, 2001–2011. International Journal of Greenhouse Gas Control, Vol. 16, Supplement 1, S236-S262.

Györe, D, Mckavney, R, Gilfillan, S M V and Stuart, F M. 2018. Fingerprinting coal-derived gases from the UK. Chemical Geology, Vol. 480, 75-85.

Lark, R M, Cullis, B R and Welham S J. 2006. On spatial prediction of soil properties in the presence of a spatial trend: the empirical best linear unbiased predictor (E-BLUP) with REML. European Journal of Soil Science, Vol 57, 787–799.

Romanak, K D, Bennett, P C, Yang, C and Hovorka, S D. 2012. Process-based approach to CO2 leakage detection by vadose zone gas monitoring at geologic CO2 storage sites. Geophysical Research Letters, Vol. 39, L15405.

Smedley, P L, Ward, R S, Allen, G, Baptie, B, Daraktchieva, Z, Jones, D G, Jordan, C J, Purvis, R M and Cigna, F. 2015. Site selection strategy for environmental monitoring in connection with shale-gas exploration: Vale of Pickering, Yorkshire and Fylde, Lancashire. British Geological Survey Open Report, OR/15/067, pp. 22.

Ward, R S, Smedley, P L, Allen, G et al. 2017. Environmental Baseline Monitoring Project: Phase II – Final Report. Report of the British Geological Survey. OR/17/049. http://nora.nerc.ac.uk/id/eprint/517889/.

Webster, R and Oliver, M A. 2007. Geostatistics for Environmental Scientists, 2nd Edition. John Wiley and Sons, Chichester.